Textron Aviation
Raytheon Missile Systems
AIAA Foundation

The 2019-20 AIAA/Textron Aviation/Raytheon Missile Systems Design/Build/Fly Competition was unexpectedly cut short this year due to the COVID-19 pandemic. This was the 24th year for the competition and in spite of the worldwide problems caused by the spread of the virus, the competition received 143 proposals, of which 113 were selected for the competition. Of the 113 teams selected, 101 submitted a formal report. Due to the correct decision to cancel the fly-off, the DBF Organizing Committee along with AIAA and in coordination with the Premier Sponsors Textron Aviation and Raytheon Missile Systems, decided to score the competition based solely on the final report scores. The reports were scored identically as in previous competitions. The results:

First Place ($3,000 and $100 for Best Report Score):   **University of Southern California**

Second Place ($2,000):                                 **Georgia Institute of Technology**

Third Place ($1,500):                                  **University of Nevada, Las Vegas**

In addition to the Best Report Score, the Design Engineering Technical Committee also awards a copy of the AIAA *Aerospace Design Engineers Guide* to the top ten teams.  The top ten teams are:

| Place | Team | Award(s) |
|-------|------|----------|
| 1 | University of Southern California | $3,000 (1st place), $100 (Best Paper Award), Design Guide |
| 2 | Georgia Institute of Technology | $2,000 (2nd place), Design Guide |
| 3 | University Nevada Las Vegas | $1,500 (3rd place), Design Guide |
| 4 | The Pennsylvania State University | Design Guide |
| 5 | The City College of New York (CCNY) | Design Guide |
| 6 | Massachusetts Institute of Technology | Design Guide |
| 7 | Missouri University of Science and Technology | Design Guide |
| 8 | The University of Alabama | Design Guide |
| 9 | Khalifa University | Design Guide |
| 10 | FH JOANNEUM University of Applied Sciences | Design Guide |

The contest theme this year was a Banner Towing Bush Plane. Each aircraft was required to have a 5 foot maximum wing span.  The first mission was a Test Flight with no payload for three laps within five minutes. The second mission was Charter Mission with passengers and luggage.  The mission 2 score was based on the number of passengers (and luggage) flown divided by the time to fly three laps. The final mission was a Banner Flight where teams were to deploy a banner after take-off and release the banner after crossing the finish line during the last lap but before landing. The mission score was based on the size of the banner and number of laps flown in the 10 minute mission window. Teams were also required to complete a timed ground mission demonstrating Mission 2 passenger and luggage loading and Mission 3 banner installation and deployment. More details on the mission requirements can be found at the competition website: http://www.aiaadbf.org.

We owe our thanks for the success of the DBF competition to the efforts of many volunteers from Textron Aviation, Raytheon Missile Systems, and the AIAA sponsoring technical committees: Applied Aerodynamics, Aircraft Design, Flight Test, and Design Engineering. These volunteers

collectively set the rules for the contest, publicize the event, gather entries, judge the written reports, and in all other years, organize the fly-off. Thanks also go to the Premier Sponsors: Textron Aviation and Raytheon Missile Systems, and also to the AIAA Foundation for their enthusiastic and financial support.

Finally, we understand the enormous disappointment of cancelling the fly-off this year. The DBF Organizing Committee expends a large amount of time and effort each year creating the rules and tailoring them to a design competition of this magnitude, scoring proposals and reports and planning and executing the fly-off event. Our reward for this commitment and effort is seeing how the teams implement the rules and create aircraft designs in the reports and at the fly-off with the actual aircraft and payloads. But we also know it is nothing compared to the time and commitment made by the student teams and that this event would not be nearly as successful without the hard work and enthusiasm from all the students and advisors. If it weren't for you, we wouldn't keep doing it.

Russ Althof
For the DBF Organizing Committee

# SCKYFALL

## USCADT 2020

USC presents ARA MAHSEREDJIAN as PROGRAM MANAGER and MICHAEL TAWATA as CHIEF ENGINEER and CHENTAO YU as AERO S&C and NEERAJ UTGIKAR as PERFORMANCE and MICHELLE KARPISHIN as PROPULSION and DREW HUDOCK as STRUCTURES and BEN BOGGS as LANDING GEAR and LAWRENCE GOO as CONFIGURATION and JACKSON MARKOW as PAYLOAD and MUQUN "SUNNY" HU as FLIGHT TEST and JACK AHRENS as CREW CHIEF and DIANA SALCEDO-PIERCE as BUILD and RANDI ARTEAGA as OPERATIONS and CHARLES RADOVICH as ADVISOR and WYATT SADLER as WYATT SADLER

**APRIL 16 - 19**

follow us 🐦 @USCADT

**CESSNA-RAYTHEON-AIAA DESIGN/BUILD/FLY 2020**

## Table of Contents

## ACRONYMS, ABBREVIATIONS, AND SYMBOLS

| | |
|---|---|
| $\alpha$ | Aircraft angle of attack |
| $\delta_e$ | Trimmed elevator deflections |
| $\eta$ | Efficiency factor |
| $\omega_d$ | Damped frequency (rad/s) |
| $\omega_n$ | Natural frequency (rad/s) |
| $\zeta$ | Damping coefficient |
| AIAA | American Institute of Aeronautics and Astronautics |
| AR | Aspect Ratio |
| AVL | Athena Vortex Lattice |
| b | Wingspan |
| $c$ | Wing chord |
| $C_d, C_D$ | Drag coefficient (2D, 3D) |
| $C_{D0}$ | Parasite drag coefficient |
| $C_l, C_L$ | Coefficient of lift (2D, 3D) |
| $C_{L_{max}}$ | Maximum lift coefficient |
| $C_{m_\alpha}$ | Moment coefficient |
| $C_P$ | Coefficient of power |
| $C_T$ | Coefficient of thrust |
| CG | Center of Gravity |
| DBF | Design/Build/Fly |
| $e$ | Oswald efficiency factor |
| ESC | Electronic Speed Controller |
| FEA | Finite Element Analysis |
| FoM | Figures of Merit |
| $L/D$ | Lift to drag ratio |
| $(L/D)_{cruise}$ | Lift to drag ratio in cruise |
| $(L/D)_{max}$ | Maximum lift-to-drag ratio |
| $M_1$ | Mission 1 Flight Score |
| $M_2$ | Mission 2 Flight Score |
| $M_3$ | Mission 3 Flight Score |
| MAC | Mean Aerodynamic Chord (ft, m) |
| MDO | Multidisciplinary design optimization |
| NiCd | Nickel-Cadmium |
| NiMH | Nickel-Metal Hydride |
| LiPo | Lithium-Polymer |
| R/C | Remote-controlled |

| | |
|---|---|
| $S$ | Wing planform area |
| $S_F$ | Flight Score |
| SM | Static Margin |
| TOFL | Take Off Field Length |
| UAV | Unmanned Aerial Vehicle |
| USC | University of Southern California |
| V | Voltage |
| W/S | Wing loading |
| Re | Reynolds number |
| $Re_{cruise}$ | Reynolds number at cruise |
| $Re_b$ | Banner Reynolds Number |
| $AR_b$ | Banner Aspect Ratio |
| $l_b$ | Banner Length |
| $h_b$ | Banner Height |
| PF | Payload Fraction |
| Re | Reynolds number |
| $Re_{cruise}$ | Reynolds number at cruise |
| V | Velocity |
| $V_{stall}$ | Stall velocity |
| $V_{TO}$ | Takeoff velocity |
| LDPE | Low-Density Polyethylene |
| PETG | Polyethylene Terephthalate |

# 1.0 EXECUTIVE SUMMARY

The objective of the 2019-2020 American Institute of Aeronautics and Astronautics (AIAA) Design-Build-Fly (DBF) competition is to design a banner-towing bush plane capable of carrying simulated passengers and luggage [1]. The aircraft must have a maximum wingspan of 5 ft (1.5 m) and take off in 20 ft (6.1 m) when flying without passengers and luggage. Furthermore, it must deploy, fly, and release a banner that must have a minimum length of 10 in. (0.3 m) and a maximum aspect ratio of 5. The aircraft must be capable of completing three flight missions and a Ground Mission.

Mission 1 requires the unloaded aircraft to fly 3 laps in under 5 minutes. Mission 2 requires 3 competition laps in the least time possible while carrying passengers and luggage. Mission 3 requires the aircraft to deploy, tow and release a banner within 10 minutes. The banner must remain vertical during flight and have a depiction of USC's logo that is legible from the ground while the aircraft is airborne. The Ground Mission simulates passengers and luggage loading as well as banner deployment and release.

Score analysis was conducted during the preliminary design phase and indicated that the aircraft needed to balance Mission 2 flight time and passenger count, Mission 3 banner length, and Ground Mission time. Performance trade studies then indicated that flying 39 passengers in 68 seconds would maximize Mission 2 score, and that flying a 300 in. (7.6 m) banner over 12 laps would maximize Mission 3 score.

A taildragger-monoplane configuration was selected during the conceptual design phase because it had fast flight speed on Mission 2, displayed favorable stability characteristics on Mission 3, and maximized lift during takeoff roll due to increased incidence angle relative to a tricycle gear configuration. A balsa-built up conventional tail was selected to allow banner attachment mechanisms to run along the bottom of the aircraft fuselage and connect at the aerodynamic center to minimize moments from the banner. The wing and tail structures were built with a foam core covered with 3-oz. fiberglass skin. Loads going through the wing were transferred through foam with carbon fiber spar caps. The fuselage was built using 1/16 in. balsa wood covered in 3 oz fiberglass. The motor mounting point and fuselage floor were strengthened using plywood and carbon fiber. The fuselage is designed for quick loading and unloading for the Ground Mission.

USC's aircraft, *SCkyfall* (Figure 1), is designed to maximize score by balancing all 3 missions. *SCkyfall* will take off at 26 ft/s (7.9 m/s) before climbing to cruise altitude and velocity. With a top speed of 137 ft/s (42 m/s), *SCkyfall* will complete three laps in 68 s while carrying 39 passengers for Mission 2. For Mission 3, it will fly a 300 in. by 60 in. (7.6 m by 1.5 m) banner constructed of plastic sheeting for 12 laps in 10 minutes. *SCkyfall* will complete the Ground Mission in 100 s. At an empty weight of 6.4 lb (5.7 kg) and with a 60 in. (1.5 m) wingspan, *SCkyfall* will complete all missions with a final score of 537.
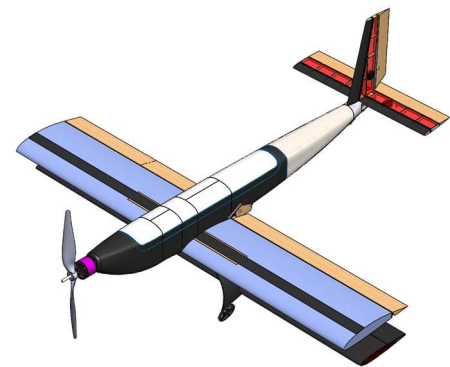


**Figure 1: USC 2019-20 DBF entry.**

## 2.0 MANAGEMENT SUMMARY

The 2019-2020 AeroDesign Team consists of 30 students who contribute on an extracurricular basis. One is a graduate student, five are seniors, and the remainder are underclassmen. The team is student-led but receives guidance from industry advisors, team alumni, and faculty at weekly meetings and design reviews.

## 2.1 TEAM ORGANIZATION

The AeroDesign Team of USC is organized by a matrix leadership structure, similar the management hierarchy employed by most aerospace firms. Team leadership for 2019-2020 is shown in Figure 2.
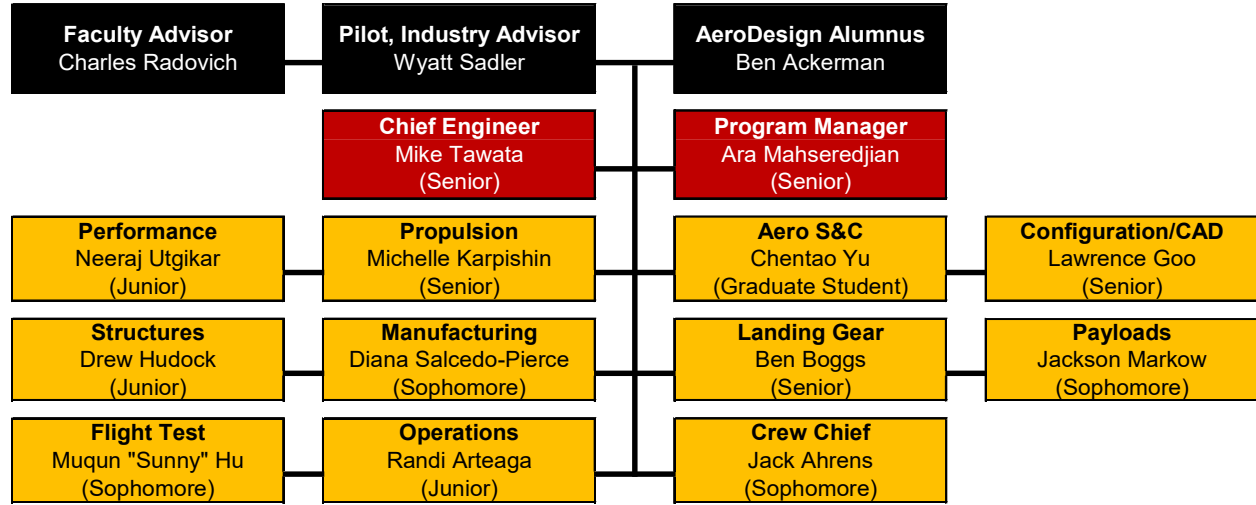
| Faculty Advisor<br>Charles Radovich | Pilot, Industry Advisor<br>Wyatt Sadler | AeroDesign Alumnus<br>Ben Ackerman | |
|---|---|---|---|
| | Chief Engineer<br>Mike Tawata<br>(Senior) | Program Manager<br>Ara Mahseredjian<br>(Senior) | |
| Performance<br>Neeraj Utgikar<br>(Junior) | Propulsion<br>Michelle Karpishin<br>(Senior) | Aero S&C<br>Chentao Yu<br>(Graduate Student) | Configuration/CAD<br>Lawrence Goo<br>(Senior) |
| Structures<br>Drew Hudock<br>(Junior) | Manufacturing<br>Diana Salcedo-Pierce<br>(Sophomore) | Landing Gear<br>Ben Boggs<br>(Senior) | Payloads<br>Jackson Markow<br>(Sophomore) |
| Flight Test<br>Muqun "Sunny" Hu<br>(Sophomore) | Operations<br>Randi Arteaga<br>(Junior) | Crew Chief<br>Jack Ahrens<br>(Sophomore) | |

**Figure 2: AeroDesign Team Organization Chart.**

Two team leaders (**red**) receive suggestions from team advisors (**black**) and coordinate the design effort with 11 sub-team leaders (**gold**). The Chief Engineer leads design, build, test, and analysis efforts. The Program Manager sets major milestones, coordinates documentation efforts and works with the Operations Lead to obtain funding and manage team logistics.

## 2.2 MILESTONE CHART

The Program Manager maintains a schedule, shown in Figure 3, that is used to plan workflow, allocate resources, and track tasks to completion. The manufacturing schedule set at the beginning of the year was updated accordingly as shown by "Actual Timing". Note that actual timing is not shown for future tasks.
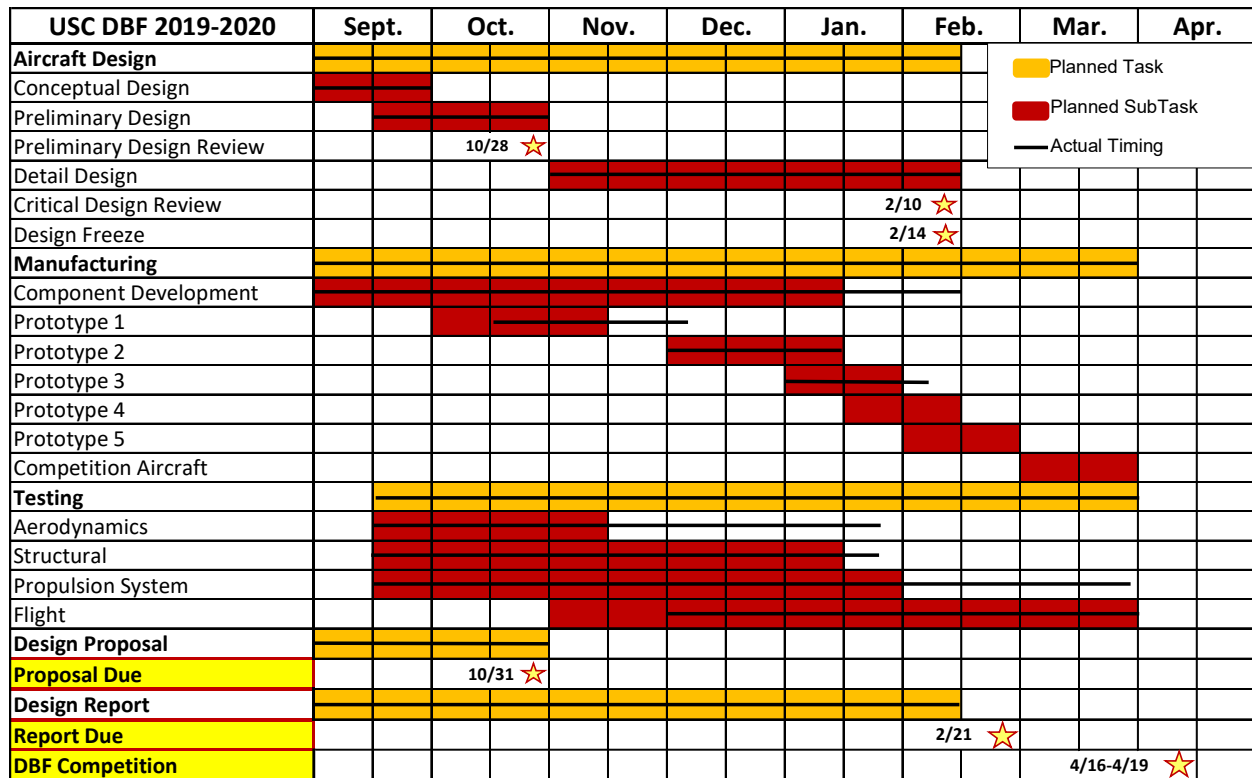
| USC DBF 2019-2020 | Sept. | Oct. | Nov. | Dec. | Jan. | Feb. | Mar. | Apr. |
|---|---|---|---|---|---|---|---|---|
| **Aircraft Design** | | | | | | | Planned Task | |
| Conceptual Design | | | | | | | | |
| Preliminary Design | | | | | | | Planned SubTask | |
| Preliminary Design Review | | 10/28 ☆ | | | | | | |
| Detail Design | | | | | | | Actual Timing | |
| Critical Design Review | | | | | | 2/10 ☆ | | |
| Design Freeze | | | | | | 2/14 ☆ | | |
| **Manufacturing** | | | | | | | | |
| Component Development | | | | | | | | |
| Prototype 1 | | | | | | | | |
| Prototype 2 | | | | | | | | |
| Prototype 3 | | | | | | | | |
| Prototype 4 | | | | | | | | |
| Prototype 5 | | | | | | | | |
| Competition Aircraft | | | | | | | | |
| **Testing** | | | | | | | | |
| Aerodynamics | | | | | | | | |
| Structural | | | | | | | | |
| Propulsion System | | | | | | | | |
| Flight | | | | | | | | |
| **Design Proposal** | | | | | | | | |
| **Proposal Due** | | 10/31 ☆ | | | | | | |
| **Design Report** | | | | | | | | |
| **Report Due** | | | | | | 2/21 ☆ | | |
| **DBF Competition** | | | | | | | | 4/16-4/19 ☆ |

**Figure 3: Master schedule with timing for planned and unplanned tasks.**

## 3.0 CONCEPTUAL DESIGN

During the conceptual design phase, the team analyzed the scoring equation and competition requirements to determine design objectives. Various aircraft configurations were evaluated to identify the highest-scoring configuration. The final conceptual design is presented in Section 3.5.

## 3.1 MISSION REQUIREMENTS

The rules for the 2019-2020 American Institute of Aeronautics and Astronautics (AIAA) Design/Build/Fly (DBF) competition simulate the design of a banner-towing bush plane capable of carrying passengers and luggage, and towing a banner whose minimum length ($l_b$) is 10 in. and maximum aspect ratio ($AR_b$) is 5 [1]. The contest consists of three flight missions and one ground mission, which can be attempted at any time during the competition.

Mission 1 and Mission 3 require the aircraft to take off within 20 ft. Mission 2 has no takeoff field length limitation. Upon taking off, the aircraft will fly competition laps, which consist of two 1,000 ft (300 m) straightaways, two 180° turns, and one 360° turn in the opposite direction of the 180° turns. The flight course requires the aircraft to perform right-hand and left-hand turns and land within the bounds of the runway, demonstrating flight stability and handling characteristics of the aircraft. A schematic of a competition lap is shown in Figure 4. The flight crew will have 5 minutes to load and secure passengers and luggage at the flight line prior to Mission 2. The same time limit applies to banner installation on Mission 3.
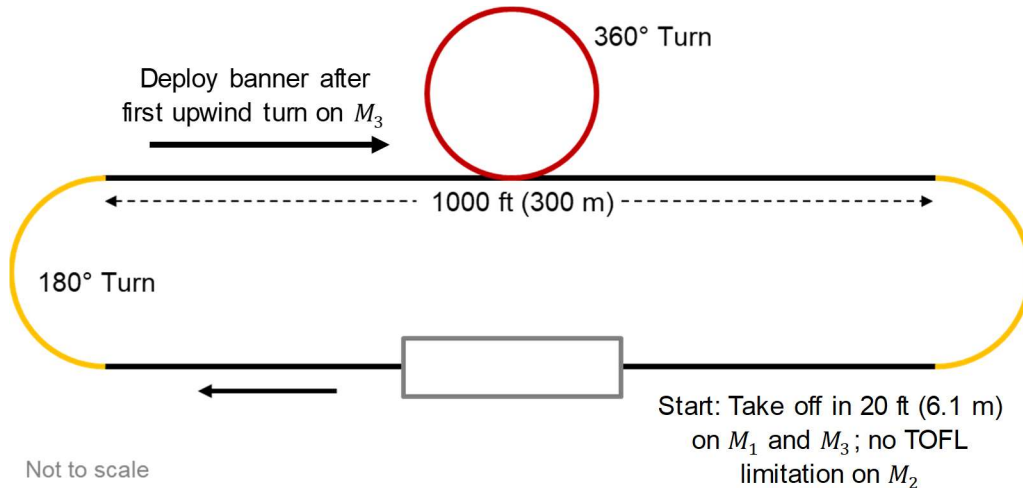
**Figure 4: AIAA DBF lap layout.**

*3.1.1 SCORING SUMMARY*

The overall score for the 2020 AIAA DBF contest is given by Eq. 1.

$$Score = Written\ Report\ Score \cdot Total\ Mission\ Score \qquad \text{Eq. 1}$$

The $Written\ Report\ Score$ is based on the quality of the design report, and the $Total\ Mission\ Score$ is the sum of the scores of each flight mission given by Eq. 2.

$$Total\ Mission\ Score = M_1 + M_2 + M_3 + GM \qquad \text{Eq. 2}$$

$M_1$, $M_2$, $M_3$, and $GM$ denote scores for Mission 1, Mission 2, Mission 3, and Ground Mission respectively.

*3.1.2 MISSION SCORING*

*Flight Mission 1 – Test Flight*

The objective of Mission 1 is to successfully complete 3 competition laps within a 5-minute flight window without any payloads. Timing begins when the throttle is advanced for takeoff. The scoring for this mission is binary: $M_1 = 1.0$ for a successful attempt and $M_1 = 0.0$ for an unsuccessful attempt.

*Flight Mission 2 – Charter Flight*

The objective of Mission 2 is to fly 3 competition laps as quickly as possible while carrying passengers and luggage. Timing begins when the throttle is advanced for takeoff. Scoring for $M_2$ is shown in Eq. 3,

$$M_2 = 1 + \frac{\left(\frac{N_{PAX}}{T_{M2}}\right)_{USC}}{\left(\frac{N_{PAX}}{T_{M2}}\right)_{MAX}} \qquad \text{Eq. 3}$$

where $\left(\frac{N_{PAX}}{T_{M2}}\right)_{USC}$ is USC's ratio of passengers to time completed in Mission 2 and $\left(\frac{N_{PAX}}{T_{M2}}\right)_{MAX}$ is the highest ratio of passengers to time to complete Mission 2 of any team.

*Flight Mission 3 – Banner Flight*

The objective of Mission 3 is to fly as many laps as possible in a 10-minute flight window while towing a rectangular banner. The banner must be at least 10 in. long and its aspect ratio, defined as banner length divided by banner height, must be less than or equal to 5. Scoring for this mission ($M_3$) is given in Eq. 4,

$$M_3 = 2 + \frac{(N_{Laps} l_b)_{USC}}{(N_{Laps} l_b)_{MAX}}$$

Eq. 4

where $(N_{Laps} l_b)_{USC}$ is the maximum product of USC's laps flown and banner length, and $(N_{Laps} l_b)_{MAX}$ is the highest product of laps flown and banner length of any team.

*Ground Mission – Operational Demonstration*

The objective of the Ground Mission is to demonstrate loading and unloading of passengers along with the deployment and release of the banner, which all count towards the GM time. The number of passengers and luggage blocks loaded must be less than or equal to the maximum number declared at Tech Inspection. The scoring equation for this mission ($GM$) is given by Eq. 5,

$$GM = \frac{(T_{GM})_{MIN}}{(T_{GM})_{USC}}$$

Eq. 5

where $(T_{GM})_{USC}$ is USC's Ground Mission time and $(T_{GM})_{MIN}$ is the fastest Ground Mission time of any team.

### 3.1.3 AIRCRAFT CONSTRAINTS

In addition to the requirements outlined in Section 3.1.2, the aircraft must meet the following requirements:

*Configuration*

- The wingspan must be less than or equal to 5 ft (1.5 m).
- The aircraft must have one compartment that carries all passengers in the vertical orientation.
- Passengers must be sufficiently restrained such that they do not move during flight.
- Passengers must weigh at least 4 oz and may not touch while secured in the aircraft.
- Luggage must be stowed in front of and/or behind the passenger compartment.
- Must weigh at least 1 oz and may touch while secured in the aircraft.
- There must be one piece of luggage per passenger flown.

*Takeoff*

- The aircraft must take off on a runway and cannot be held while the motor is spun up for takeoff.
- For Mission 1 and Mission 3, the TOFL limit is 20 ft (6.1 m); there is no limit on Mission 2.

*Propulsion*

- Total stored energy for the propulsion package may not exceed 200 Wh.
- Batteries must be Nickel-Cadmium (NiCd), Nickel-Metal Hydride (NiMH) or Lithium-Polymer (LiPo).
- Only one type of battery may be used for propulsion. If using NiCd or NiMH batteries, only commercially-procured battery packs or cells may be used.

- If using LiPo batteries:
  - Only commercially-available battery packs may be used.
  - All battery packs used must be identical.
  - Each individual pack must cannot exceed 100 Wh.
  - All packs must be parallel; there must be a minimum 0.25 in. gap between packs.
- Components for the propulsion package must be commercially available.

*Payloads – Passengers*

- Passengers must be $3\frac{9}{16}$ in. tall, have a diameter of $1\frac{1}{8}$ in, and weight at least 4 oz.

*Payloads – Luggage*

- There must be one piece of luggage for each passenger.
- Must be a 1.50 in. x 1.00 in. x 0.75 in. rectangular prism and must weigh at least 1 oz.

*Payloads – Banner*

- Must be rectangular with minimum length 10 in. and maximum aspect ratio (length/height) 5.
- Must have the team's university name or logo on both sides.
- Must be compactly stowed externally to the aircraft for takeoff; cannot interfere with flight controls.
- Must be remotely deployed, remain vertical, and remotely released in flight.
- Cannot sustain any damage during flight or upon ground impact after release.

## 3.2 DESIGN REQUIREMENTS

Design requirements were developed from the 2019-2020 DBF scoring equations and competition guidelines to guide the design process. The team determined an aircraft configuration and design approach that would maximize total score by analyzing the scoring equations. Mission requirements and score equations were translated to design parameters, shown in Table 1.

**Table 1: Design parameters.**

| Mission | Objective | Design Parameter |
|---|---|---|
| $M_2$: Charter Flight | Balance passengers flown and flight time to achieve the highest ratio of passengers flown to flight time. | $\left(\frac{N_{PAX}}{T_{M2}}\right)_{USC}$ |
| $M_3$: Banner Flight | Balance banner length with laps flown to achieve the highest product of banner length and laps flown. | $\left(N_{Laps}l_b\right)_{USC}$ |
| GM: Operational Demonstration | Minimize time required to load and unload passengers and luggage. Minimize time required to install and deploy banner. | $\left(T_{GM}\right)_{USC}$ |

*3.2.1 FLIGHT SCORE SENSITIVITY ANALYSIS*

The scoring equations, Eq. 1 – Eq. 5, were analyzed to set design objectives by identifying mission objectives and design parameters, shown in Table 1, that were most important in maximizing total score. Initial score sensitivity analysis revealed that Mission 2, Mission 3, and the Ground Mission were all equally weighted when constant factors were removed, rendering USC's traditional score analysis from past years

insufficient for defining design direction. Instead, the team took a high-level approach, analyzing the costs and benefits of improving each mission's scoring components in order to identify the primary design parameters. Due to the 200 Wh energy limit imposed on the propulsion package, the cost of each component change was weighed against the energy requirement change. This is summarized in Table 2.

**Table 2: Energy costs of various mission component changes.**

| Mission Component Change | Energy Requirement Change |
|---|---|
| Increased $PAX$ | Linear Increase |
| Decreased $T_{M2}$ | Quadratic Increase |
| Increased $L_{Banner}$ | Linear Increase |
| Decreased $T_{M3}$ | Quadratic Increase |
| Decreased $T_{GM}$ | Linear Decrease |

The cost-benefit analysis provided direction for the baseline. However, the Ground Mission's equal scoring weight made establishing a baseline that considered Mission 2, Mission 3, and the Ground Mission difficult.

In order to set a baseline USC competition aircraft, the team created a program called the Brute Force Energy Analysis (BFEA). The program used energy-based models in order to be component-agnostic and remain accurate over a wide variety of power-to-weight ratios and payload fractions, without relying on a database of components such as motors and propellers. The program iterated over a design space that varied the aircraft weight, passenger count, and banner length. Each unique combination within the tested design space was converted into an aircraft with a wing, fuselage, and empennage by using conservative efficiency factors. The wing and empennage were sized using estimated cruise speed and weight, and the fuselage was sized based upon payload requirements. Once the aircraft was created, the lap distance for each mission was determined based upon estimated aircraft performance given cruise velocity, drag, and weight. This lap distance was combined with an estimated energy consumption to determine $N_{Laps}$ for Mission 3 and $T_{M2}$. The final flight score component, $T_{GM}$, was calculated using a simple cost function that utilized team measurements of running to and from the 10 ft line, loading and unloading time for passengers and cargo, and loading time for a banner. Each created aircraft was added to a database that was used to find highest scores for Mission 2 and Mission 3. This database is plotted below in Figure 5.
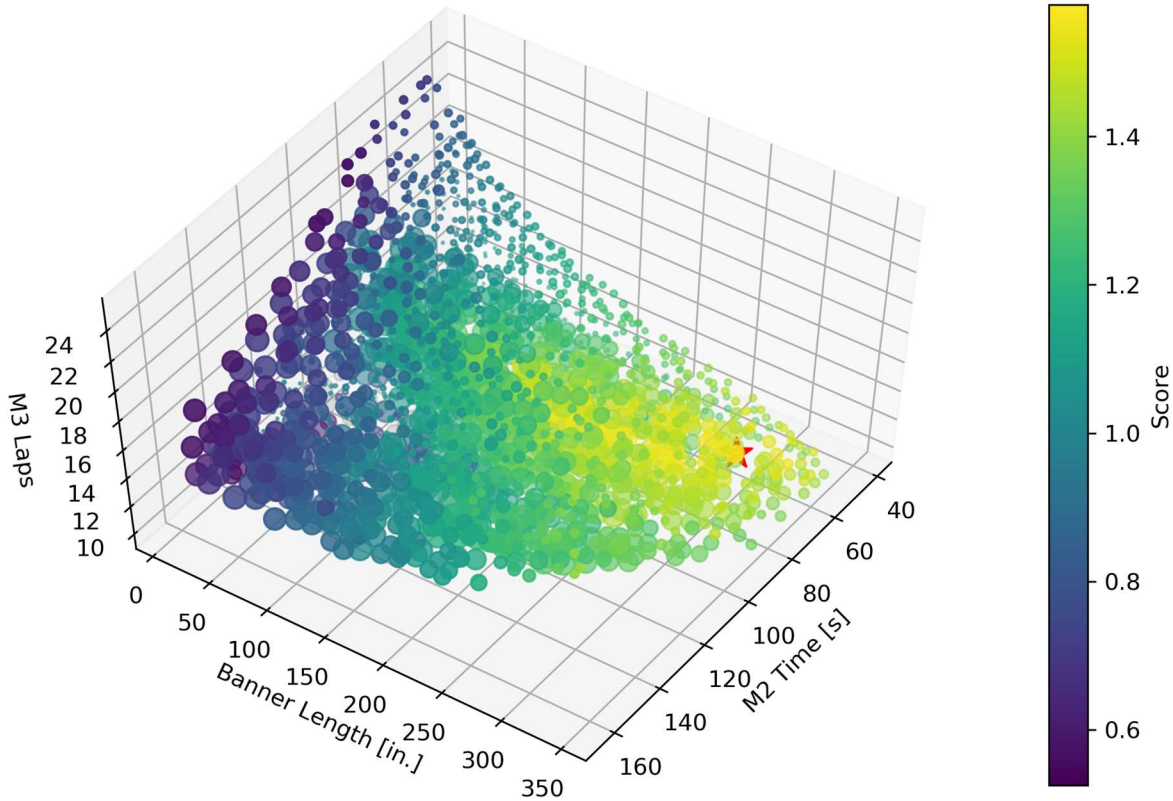
**Figure 5: BFEA results. Circle size corresponds to $N_{PAX}$. Highest score is denoted by the red star.**

The BFEA resulted in a comprehensive, realistic database of 6 million aircraft of different combinations of the mission components. The combination with the highest flight score compared to the entire database was selected as the baseline USC competition aircraft. Key simulation results are shown in Table 3.

**Table 3: BFEA database results.**

| Scoring Parameter | Balanced $M_2$ and $M_3$ | $M_2$ focused | $M_3$ focused |
|---|---|---|---|
| $N_{PAX}$ | 39 | 86 | 16 |
| $T_{M2}$ | 67.7 s | 76.4 s | 63.8 s |
| $l_b$ | 300 in. (7.6 m) | 130 in. (3.3 m) | 334 in. (8.5 m) |
| $N_{Laps}$ | 12 | 12 | 12 |
| $T_{GM}$ | 99.0 s | 189.6 s | 53.7 s |
| Mission Score (out of 3) | 1.58 | 1.48 | 1.54 |

*3.2.2 INTEGRATED PERFORMANCE ANALYSIS*

The BFEA confirms the initial cost-benefit analysis: the highest-scoring planes are more sensitive to $l_b$ as opposed to $N_{Laps}$. The best Mission 2 carries more $N_{PAX}$ as opposed to lower $T_{M2}$. In addition, the BFEA surpasses the initial cost-benefit analysis by showing that while the best Mission 2 flies a high $N_{PAX}$, a better scoring plane flies fewer $N_{PAX}$ to decrease $T_{GM}$ and wing area for Mission 3, resulting in higher $N_{Laps}$ or $l_b$.

The BFEA used conservative assumptions in order to allow for a comprehensive design space to be tested within a reasonable timeframe. Various assumptions, such as battery energy density, energy losses in motor and propeller, turning rates, and payload fraction were varied to validate the results of BFEA. While the results varied with each change as expected, the best overall plane remained at or near the selected baseline aircraft. The most variable assumption was one injected based upon previous experience: an assumed best Ground Mission time. $(T_{GM})_{USC}$ was calculated based upon in-lab testing, but it is highly possible for other teams to have lower values of $T_{GM}$. Considering this, the baseline design still stands if $(T_{GM})_{MIN} \geq 13$ s. Since the $(T_{GM})_{MIN}$ was 12.08 seconds in 2019 and this year's Ground Mission is similar [2], the team concluded that the baseline design was the most competitive design moving forward.

The BFEA indicated that the highest-scoring configuration would fly 39 passengers and luggage in 68 s for Mission 2, and that it would fly 12 laps while towing a 300 in. (7.6 m) banner on Mission 3. BFEA indicates diminishing returns for banner lengths above 300 in. (7.6 m) due to increased energy requirements.

### 3.3 CONFIGURATION SELECTION

After design goals were determined, the team used a configuration downselect to choose a preliminary configuration. Once the configuration was selected, concepts for each individual component were selected.

#### 3.3.1 AIRCRAFT CONFIGURATION

The configuration downselect method used a series of estimates and assumptions that allowed for a quantitative comparison of configurations across various design parameters. Figures of Merit were derived from parameters shown in Table 1. Each Figure of Merit was assigned a Score Factor and was used to identify the most competitive configuration. Score Factors for each Figure of Merit are shown in Table 4.
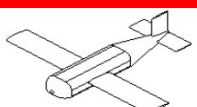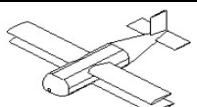
**Table 4: Figures of Merit with corresponding Design Parameters and Score Factors.**

| Figures of Merit | Design Parameters | Score Factor |
|---|---|---|
| Flight Speed | $(T_{M2})_{USC}, (N_{Laps})_{USC}$ | 0.3 |
| Payload Capacity | $(N_{PAX})_{USC}$ | 0.3 |
| Payload Loading/Unloading Time | $(T_{GM})_{USC}$ | 0.2 |
| Stability & Control | $(T_{M2})_{USC}, (N_{Laps})_{USC}$ | 0.2 |

The Score Factor for each Figure of Merit was derived qualitatively by assessing relative importance of each factor based on aircraft design parameters. Score Factors were weighted such that their sum was one. Various aircraft configurations were then scored for each Figure of Merit independently. The monoplane configuration was used as the baseline against which all other configurations were compared, so it was assigned a value of 0 for each Figure of Merit. For all other configurations, a value of 0 implied that the configuration scored the same as a monoplane. A value of -1 indicated a lower score, and a value of 1 indicated a higher score. Each configuration evaluation was multiplied with the corresponding Score Factor and summed. The Total Score for each configuration, shown in the bottom row of Table 5, provided the basis for the quantitative comparison.

The aircraft configuration downselect compared the baseline monoplane configuration to the biplane and blended wing body (BWB) configurations. The biplane configuration was thought to produce more lift while reducing aspect ratio with respect to the monoplane configuration due to the 5 ft (1.5 m) span limitation. The BWB configuration was thought to pack passengers and luggage using internal volume more efficiently than the monoplane configurations. The results of this comparison are shown in Table 5.

**Table 5: Aircraft configuration downselect.**
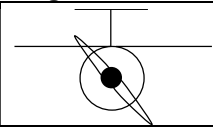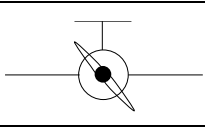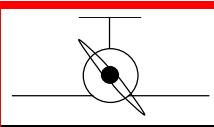
| Figures of Merit | Score Factor | Monoplane | Biplane | BWB |
|---|---|---|---|---|
| Flight Speed | 0.4 | 0 | -1 | -1 |
| Payload Capacity | 0.3 | 0 | 0 | 1 |
| Payload Loading/Unloading Time | 0.2 | 0 | -1 | 0 |
| Stability & Control | 0.1 | 0 | 0 | -1 |
| | Total Score | 0.0 | -0.6 | -0.2 |

As shown in Table 5, biplane and BWB configurations were less competitive than the monoplane configuration. The biplane was less competitive because the additional wing would interfere with passenger loading and unloading, increasing $(T_{GM})_{USC}$. It would also be heavier than the monoplane configuration due to the additional integration weight of the second wing. This additional mass would increase drag, increasing $(T_{M2})_{USC}$ and lowering $(N_{Laps})_{USC}$. The BWB configuration would have a higher $(T_{M2})_{USC}$ and fewer $(N_{Laps})_{USC}$ due to worse stability characteristics, which, in turn, would reduce flight speed.

*3.3.2 WING CONFIGURATION*

The wing configuration downselect compared high-wing, mid-wing, and low-wing configurations. The high-wing configuration was taken as the baseline. The mid-wing configuration was thought to reduce takeoff field length due to increased ground effect. The low-wing configuration was thought to reduce takeoff field length even further than the mid-wing configuration due to increased ground effect relative to the mid-wing configuration. The results of the comparison are shown in Table 6.

**Table 6: Wing configuration downselect.**
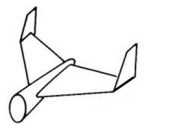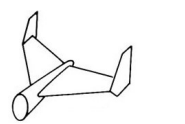
| Figures of Merit | Score Factor | High-Wing | Mid-Wing | Low-Wing |
|---|---|---|---|---|
| Flight Speed | 0.3 | 0 | 0 | 0 |
| Payload Loading Time | 0.3 | 0 | -1 | 1 |
| Takeoff Field Length | 0.3 | 0 | 1 | 1 |
| Stability & Control | 0.1 | 0 | 0 | -1 |
| | Total Score | 0.0 | 0.0 | 0.5 |

*3.3.3 EMPENNAGE CONFIGURATION*

An empennage was required to maintain longitudinal stability of the monoplane configuration. The main factors governing empennage selection were maximizing stability, reducing interference with the banner, and minimizing drag. The conventional configuration was selected as the baseline and the following designs were compared with the downselect shown in Table 7:

- **Conventional:** The conventional design is simple to design and integrate. It provides the stability and control required. The banner must be mounted below the fuselage to avoid interference.

- **U-Tail:** Two vertical stabilizers are attached to the ends of the horizontal stabilizer to minimize interference with the banner. The vertical stabilizers do not extend below the horizontal stabilizer. The U-Tail allows a banner to attach to either the top or bottom of the aircraft without tail interference. The U-Tail configuration maintains similar lateral stability to the conventional tail [3].

- **H-Tail:** Two vertical stabilizers are attached to the ends of the horizontal stabilizer to minimize interference with the banner. The vertical stabilizers extend below and above the horizontal stabilizer. The H-Tail allows a banner to attach to either the top or bottom of the aircraft without tail interference. The H-Tail configuration maintains similar lateral stability to the conventional tail [3].

**Table 7: Empennage downselect.**



| Figures of Merit | Score Factor | Conventional | U-Tail | H-Tail |
|---|---|---|---|---|
| Stability & Control | 0.3 | 0 | 0 | 0 |
| Banner Mount Interference | 0.2 | 0 | 1 | 1 |
| Drag | 0.2 | 0 | 0 | 0 |
| Assembly and Integration | 0.2 | 0 | -1 | -1 |
| Design & Build | 0.1 | 0 | -1 | -1 |
| | Total Score | 0.0 | -0.1 | -0.1 |

As shown in Table 7, the conventional tail was selected due to ease of design, build, assembly, and integration. Although the U-Tail and the H-Tail allow the banner to be mounted to the top surface of the aircraft, the conventional tail was selected because the banner will be mounted to the bottom of the aircraft.

## 3.4 AIRCRAFT COMPONENT SELECTION, PROCESSES AND RESULTS
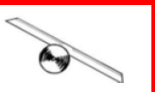
Once aircraft, wing, and tail configurations were selected, payload configuration, propulsion, and landing gear components were chosen. Each decision was quantified using the same downselect process detailed in Sections 3.3.1 and 3.3.3. The highest-scoring components were selected for the final configuration.

### 3.4.1 PROPULSION

The motor configuration was chosen using TOFL, efficiency, weight, and interference with landing gear and banner as Figures of Merit. The tractor configuration was selected as the baseline. The following motor configurations were compared, and downselect results are shown in Table 8.

- **Tractor**: Single motor located at the front of the aircraft
- **Pusher**: Single motor aft of the fuselage
- **Wing-Mounted Twin**: Twin motors mounted on the wings
- **Pull/Push**: Twin motors mounted in-line, fore and aft of the fuselage

**Table 8: Motor configuration downselect.**

| Figures of Merit | Score Factor | Tractor | Pusher | Wing-Mounted Twin | Pull/Push |
|---|---|---|---|---|---|
| TOFL | 0.4 | 0 | -1 | 0 | -1 |
| Efficiency | 0.2 | 0 | -1 | 0 | 0 |
| Weight | 0.2 | 0 | 0 | -1 | -1 |
| Component Interference | 0.2 | 0 | -1 | 1 | -1 |
| Total Score | | 0.0 | -0.8 | 0.0 | -0.8 |

Although the tractor and wing-mounted twin configurations yielded the same score, the wing-mounted twin configuration would pull more current at the same cruise speed, reducing efficiency and endurance.

### 3.4.2 PASSENGER INTERIOR CONFIGURATION

The passenger interior configuration was chosen using $T_{GM}$, fuselage cross-sectional area, and fuselage length as Figures of Merit. $T_{GM}$ is weighted eight times over the remaining Score Factors because the change in aerodynamic drag associated with changing fuselage width and length was found to have a negligible impact on score when compared to the impact of $T_{GM}$. The passenger interior configurations were compared in the downselect shown in Table 9.

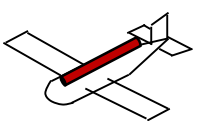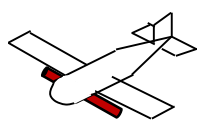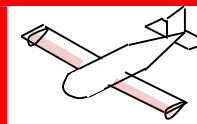**Table 9: Passenger interior configuration downselect.**
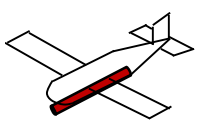
| Figures of Merit | Score Factor | 3-Abreast | 2-Abreast | 3-2-Abreast | 4-Abreast |
|---|---|---|---|---|---|
| $T_{GM}$ | 0.8 | 0 | 0 | -1 | -1 |
| Cross-Section Area | 0.1 | 0 | 1 | 1 | -1 |
| Fuselage Length | 0.1 | 0 | -1 | 0 | 1 |
| Total Score | | 0.0 | 0.0 | -0.7 | -0.8 |

Although the 3-Abreast and 2-Abreast configurations had the same Total Score, the 3-Abreast configuration was chosen to minimize fuselage length, which increases wing incidence angle relative to the horizontal. This allows the wing to sit at a higher angle of attack on takeoff and ensure that the aircraft meets the 20 ft TOFL requirement on Mission 1 and Mission 3.

*3.4.3 BANNER INTEGRATION*

The banner storage configuration was designed to be reliable, easy to assemble and integrate, and minimize drag. Reliability was deemed critical to succeeding in Mission 3, so the reliability Figure of Merit was weighed three times as heavily as the remaining Figures of Merit. In the first configuration, the banner is mounted below the fuselage along the airplane's longitudinal axis. In the second configuration, the banner is mounted longitudinally along the top of the fuselage. In the third configuration, the banner is stored laterally beneath the wing through the aerodynamic center. In the fourth configuration, the banner is stowed in a small wing below the main wing. The banner integration downselect is shown in Table 10.
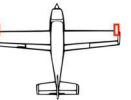
**Table 10: Banner integration downselect.**

| Figures of Merit | Score Factor | Below-Fuse Longitudinal Storage | Above-Fuse Longitudinal Storage | Under-Wing Lateral Storage | Bi-Wing Storage |
|---|---|---|---|---|---|
| Reliability | 0.6 | 0 | -1 | 0 | 1 |
| Assembly, Integration | 0.2 | 0 | 0 | 0 | 0 |
| Drag | 0.2 | 0 | 0 | -1 | 1 |
| Total Score | | 0.0 | -0.6 | -0.2 | 0.8 |

The Bi-Wing configuration was chosen because it would reliably deploy the banner with minimal in-flight moments. It also eliminated the need for a folding banner leading edge, which would have introduced an additional failure mode during deployment. By using leading and trailing edge geometries modeled using the NACA 0012 as a basline, the Bi-Wing configuration reduced drag relative to remaining configurations. Analysis shown in Section 4.4.4 revealed the Bi-Wing configuration increased lift to help meet TOFL limits.

*3.4.4 LANDING GEAR*

The landing gear team was responsible for designing gear to meet takeoff and landing requirements while minimizing weight and drag. Weight, drag, TOFL, integration, and ground handling were emphasized in the downselect to ensure that the aircraft would reliably make the TOFL requirement and fly as fast as possible for the best Mission 2 score. The landing gear downselect is shown in Table 11.

**Table 11: Landing gear downselect.**

| Figures of Merit | Score Factor | Tricycle | Tip Tricycle | Strut Tail Dragger | Bow Tail Dragger | Tip Tail Dragger |
|---|---|---|---|---|---|---|
| Weight, Drag | 0.3 | 0 | 0 | 1 | -1 | 0 |
| TOFL | 0.3 | 0 | -1 | -1 | 1 | 0 |
| Integration | 0.2 | 0 | -1 | 0 | 1 | -1 |
| Ground Handling | 0.2 | 0 | 0 | 0 | 0 | -1 |
| Total Score | | 0.0 | -0.5 | 0.0 | 0.2 | -0.4 |

The Bow Tail Dragger configuration was selected because it would reliably make TOFL even though it was the heaviest option. The bow gear allowed the two main wheels to be mounted slightly forward of the wing, providing greater angle of attack relative to the strut and tip tail dragger configurations [4]. The Bow Tail Dragger features two main wheels forward of the center of gravity (CG) and a tailwheel.

### 3.5 FINAL CONCEPTUAL DESIGN

The final configuration is a single motor, low-wing aircraft with a conventional tail designed to carry 39 passengers and luggage on Mission 2 and a 300 in. (7.6 m) banner on Mission 3 as shown in Figure 1. Passengers are carried 3-abreast. Taildragger gear is used to maximize lift on the takeoff roll.

### 4.0 PRELIMINARY DESIGN

The team designed an aircraft that would meet three design objectives: maximize the $N_{PAX}/(T_{M2})_{USC}$ ratio on Mission 2, maximize the product of $(N_{Laps})_{USC}$ and $(L_{Banner})_{USC}$ on Mission 3, and minimize $(T_{GM})_{USC}$ on the Ground Mission. Additionally, meeting the 20 ft (6.1 m) TOFL requirement was critical to receiving scores for Mission 1 and Mission 3. Numerous trade studies were conducted using software simulations and models to size aircraft components. Computer models and prototypes allowed for further development of aircraft structural elements.

### 4.1 DESIGN METHODOLOGY

The preliminary design was developed through an iterative process that required the input of numerous team members across multiple disciplines. The critical components in the preliminary design phase and their corresponding design requirements are described as follows:

**Wing**

- Wing planform area ($S$): The wing area produces the lift required to support the aircraft and payload. The wing area must meet the 20 ft (6.1 m) TOFL on Mission 1 and Mission 3.

- Aspect Ratio (AR): High AR wings reduce induced drag, offering improved takeoff and cruise performance than low AR wings. AR is limited by the 5 ft (1.5 m) span limitation and wing area $S$ required to meet TOFL limitations.
- Airfoil: The team used a custom airfoil designed to operate efficiently at low Reynolds Numbers ($\text{Re} < 750{,}000$). The airfoil is designed to generate the required lift at takeoff and optimized for the lift to drag ratio at cruise $(L/D)_{Cruise}$ to improve the lifting efficiency and minimize cruise power.
- Ground Mission: The wing must be placed to minimize interference with the fuselage while loading and unloading passengers and luggage to minimize $(T_{GM})_{USC}$.

**Structures**

- Wing core and spar caps: The wing spars were designed to withstand the maximum in-flight and landing loads (2.5 g) expected for the wing. Loads were transferred from the wing foam core to carbon fiber spar caps, and the entire wing was surrounded by cured fiberglass.
- Fuselage: The fuselage connects all aircraft components, requiring efficient load paths from internal components to the ground. The fuselage must be lightweight and aerodynamic. It must efficiently store all passengers, luggage, and critical flight components. Additionally, it must have a mounting point for the banner flown on Mission 3.

**Propulsion**

- Motor, propeller, and battery pack: Components were selected to meet performance goals while minimizing package weight. Performance goals include completing $M_2$ in 68 s, flying 12 laps while towing a 300 in. (7.6 m) banner in 10 min on Mission 3, and achieving TOFL under 20 ft (6.1 m).

**Payloads**

- The passengers and luggage must be designed to meet minimum weight and volume limits prescribed by the AIAA.
- The banner must be designed to minimize drag and have minimal impact on aircraft stability and control on Mission 3.
- Ground Mission: The passengers, luggage, and banner must be designed to be easy to load and unload to minimize $(T_{GM})_{USC}$.

### 4.2 MISSION MODEL

Multidisciplinary design optimization (MDO) was used to determine the highest scoring aircraft design as well as performance during various phases of flight. The MDO and corresponding simulation packages were implemented using PlaneTools, a first-order MATLAB flight model developed by the team. Each program execution simulates flight missions by modeling four phases of the competition course: takeoff, climb, cruise, and turns. Each of the four course segments is detailed in Figure 6.

1. Takeoff – Assumed to be performed at maximum throttle setting using 25° flap deflection. The model varyies $C_L, C_D$, and $C_T$ based on speed. The simulation accounts for runway rolling resistance.

2. Climb – The aircraft was assumed to climb to 25 ft (7.6 m) above the 1300 ft (400 m) altitude (ground level) of Wichita, KS [5]. The rate of climb was estimated by calculating excess power. The model accounts for drag due to the stored banner.

3. Cruise – Assumed steady level flight. The cruise model accounted for banner drag, determined in Section 8.1.1. The simulation also accounted for various cruise throttle settings.

4. Turn – A coordinated level turn with constant speed and radius was assumed for both types of turns (two 180° turns and one 360° turn). Load factor was limited to 7.5 g by structural components.
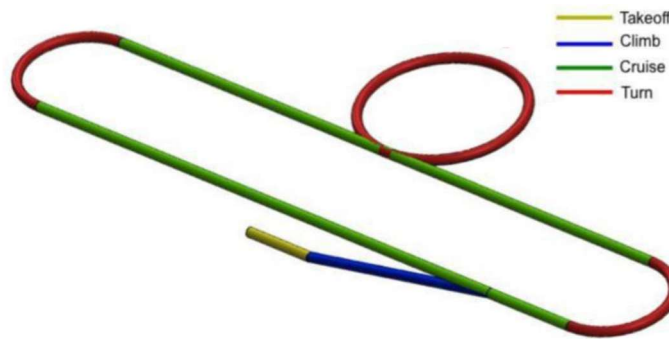


**Figure 6: Flight course model in PlaneTools.**

PlaneTools is an object-oriented mission simulator that allowed the team to isolate each component of the aircraft and perform component- specific trade studies. Uncertainties were propagated throughout the mission model. Figure 7 provides a schematic of the PlaneTools process. The objective of PlaneTools simulations was to determine the initial design parameters with highest scoring impact.

| Plane Components | Misson Model | Flight Attempt | Outputs |
|---|---|---|---|
| • Wing | • Altitude | • Takeoff | • Capacity Required |
| • Empennage | • Headwind | • Climb | • Turning Radius |
| • Fuselage | • Temperature | • Cruise | • Laps Flown |
| • Propeller | • Time Limit | • Turn | • Operating Current |
| • Battery | • Maximum Takeoff | | • Elapsed Time |
| • Motor |   Field Length | | • Score |
| • Payloads | | | |
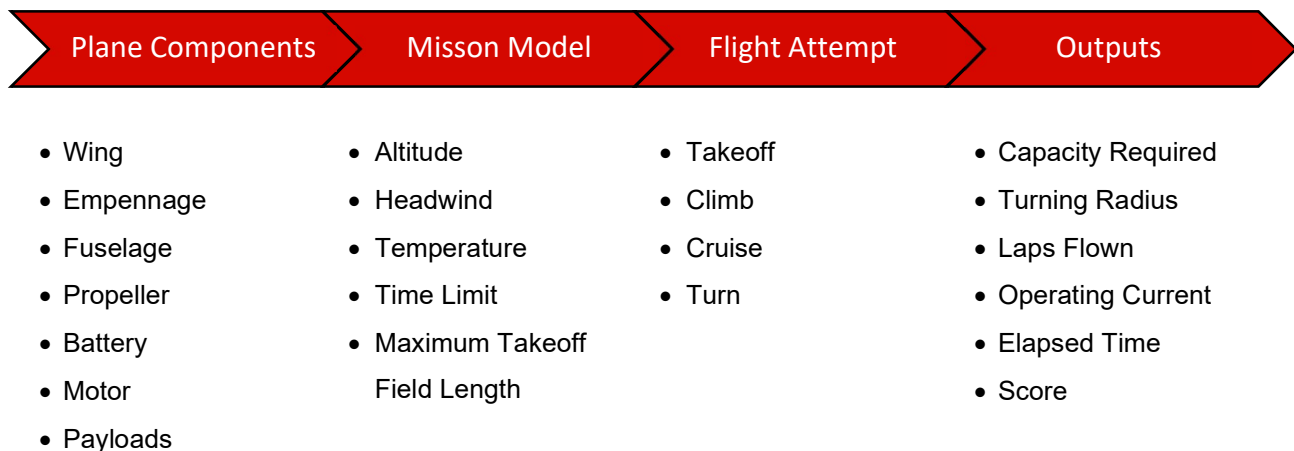
**Figure 7: PlaneTools simulation components.**

Fundamental aircraft performance equations were used to calculate parameters such as rate of climb, cruise speed, and turn radius. The mission model included the following uncertainties and assumptions:

- **Aerodynamic performance** - Lift ($C_L$) and drag ($C_D$) coefficients used in calculations were based on XFLR5 output. The model neglected interference and compressibility.

- **Battery performance** – Battery resistance and capacity were based on in-lab bench tests and flight tests. Battery voltage decay is modeled iteratively and is assumed to drop by 5% each lap. The propulsion model accounted for variations in internal temperature.

- **Propeller performance** – Thrust ($C_T$) and power ($C_p$) coefficients were based manufacturer data and verified via static and flight testing. In cases where yoke twist was present, Eq. 6 was used to determine the effective pitch and diameter. Note that $p$ is propeller pitch, $d$ is propeller diameter, and $\theta$ is yoke twist [6].

$$p_{effective} = \frac{3\pi d}{4} \tan\left[\tan^{-1}\left(\frac{4p}{3\pi d}\right) + \theta\right]$$

Eq. 6

- **Winds** – A headwind of 19 ft/s (5.8 m/s) was assumed for takeoff and cruise based on historical weather patterns during competition weekend (Mid-April) in Wichita, KS [5].

## 4.3 DESIGN TRADE STUDIES

### 4.3.1 WING GEOMETRY

Wing geometry trade studies were performed in PlaneTools to determine the geometry that optimized score. These studies were conducted by varying $S \in [3 \text{ ft}^2, 9 \text{ ft}^2]$, and AR $\in [4, 6]$ and simulating the aircraft at each geometry. PlaneTools results are shown in Figure 8.
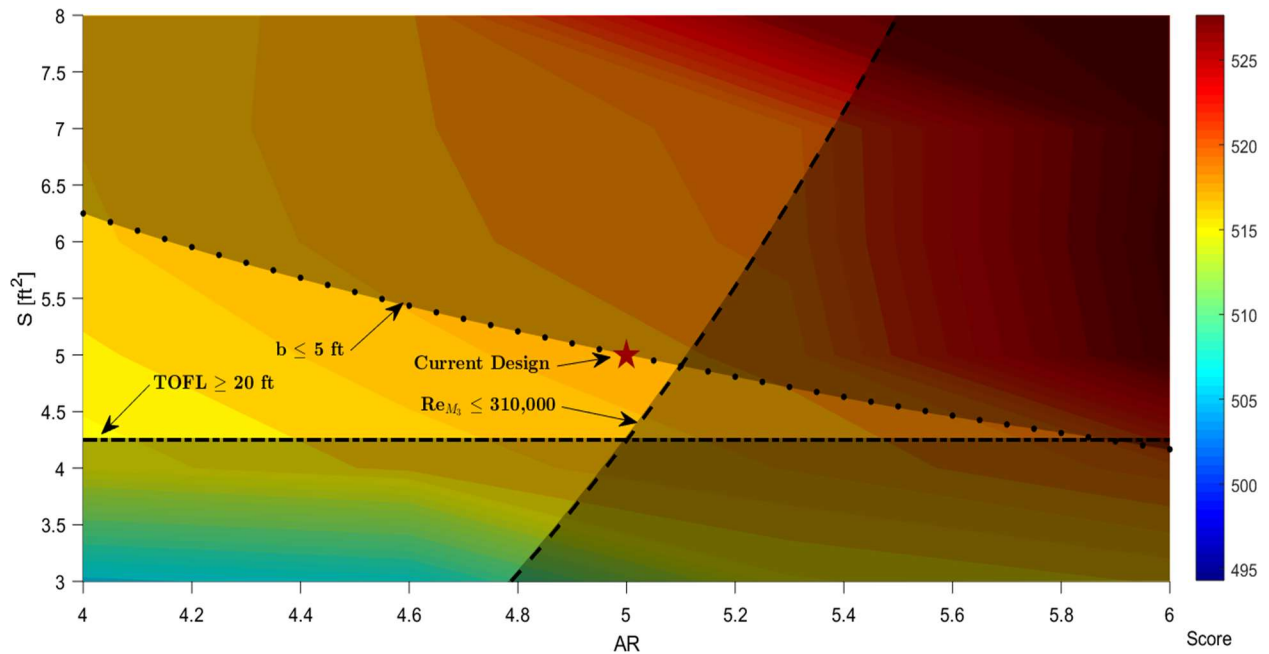


**Figure 8: PlaneTools study varying $S$ and $\mathbf{AR}$. Shaded area is outside the feasible design space.**

The wing design space was restricted by the wingspan requirement of $b \leq 5$ ft (1.5 m) Within the reduced design space, the takeoff field length restriction of 20 ft (6 m) was instituted. The requirements are denoted by the solid line and dashed line, respectively. The current configuration is shown by the red star and corresponds to a wing with wing area $S = 5$ ft$^2$ (0.5 m$^2$) and $AR = 5$. The PlaneTools results are consistent with the findings from the Brute Force Energy Analysis in Section 3.2.1.

### 4.3.2 PROPULSION SIZING

Preliminary propulsion sizing aimed to minimize $T_{M2}$ and maximize $N_{Laps}$ flown during Mission 3. Mission 3 set capacity and endurance requirements. The 20 ft (6.0 m) TOFL requirement set thrust requirements.

Lithium Polymer (LiPo) cells were chosen over NiMH and NiCd cells due to their higher energy and power densities. An additional constraint set by the AIAA limited the power rating of the propulsion system to 100 Wh per battery pack and 200 Wh for the entire propulsion system. Turnigy 2200mAh cells were chosen for Mission 2 and Turnigy 4500mAh for Mission 3 for preliminary testing due to performance measured during static and discharge tests shown in Section 8.1.2. Previous analysis demonstrated that a properly sized propulsion system can achieve at most 80% efficiency, $\eta_b$, calculated by Eq. 7 [2].

$$P = \eta_b P_{battery} = \eta_b VI \qquad \text{Eq. 7}$$

An electrical power loading $P/W$ = 150 W/lb was targeted, which is common for planes seeking high performance capabilities such as basic aerobatics and increased speed. 150 W/lb allows the plane to meet all TOFL requirements while maintaining the endurance needed for a 10 minute Mission 3 and a 68 s Mission 2. The total power required of 1650 W is determined by Eq. 8, using a Mission 3 weight of 9.4 lb.

$$P_R = W_{M_3} * P/W \qquad \text{Eq. 8}$$

The minimum power required from the battery pack is 2060 W, calculated by using Eq. 9

$$P_{battery} = P_R / \eta_b \qquad \text{Eq. 9}$$

The Turnigy LiPo batteries have a nominal voltage $V_C$ of 3.7 volts per cell. The target pack size for both missions is 6S-2P, or $n_c = 12$ cells. The power rating for Mission 2 was 99.7 Wh per pack and 199.8 Wh total; for Mission 3 it was 48 Wh and 96 Wh. Using Eq. 10, maximum static current is 46.4 A.

$$I_{max} = \frac{P_{battery}}{V_C n_{c,M_3}} \qquad \text{Eq. 10}$$

The specifications above were used to determine the required motor $Kv$ [RPM/V]. The Hacker A60-5S V4, with a $Kv$ of 295, was identified as the highest-scoring motor because it balanced $Kv$, power rating, and weight. PlaneTools and online sizing tool eCalc were both used to identify the highest-scoring propeller that would produce enough static thrust to satisfy the TOFL requirement and successfully complete each mission. Additionally, yoke twist was added to the Mission 2 propeller setup to further increase speed by increasing design advance ratio. The preliminary package for each mission is shown in Table 12.

**Table 12: Preliminary propulsion package for each mission.**

| Mission | Motor | Battery Pack | Propeller |
|---------|-------|--------------|-----------|
| 1 & 2 | Hacker A60-5S V4 (295 *Kv*) | 6S2P Turnigy 2200mAh | Aeronaut +5° twist 20x12 |
| 3 | | 6S2P Turnigy 4500mAh | Aeronaut +0° twist 18.5x15 |

### 4.4 AERODYNAMICS

The aerodynamics of the aircraft were designed and analyzed primarily with XFLR5 [7] and Athena Vortex Lattice (AVL) [8]. XFLR5 utilizes the lifting line theory capabilities of XFOIL to predict lift and drag characteristics of an airfoil. AVL employs an extended vortex lattice model to capture aerodynamic characteristics of the full aircraft configuration, allowing for static and dynamic stability to be analyzed. In addition, in-flight and ground testing were conducted to analyze the drag characteristics of the banner so that design spaces and drag models could be determined.

#### 4.4.1 AIRFOIL SELECTION

Several airfoils were analyzed using XFLR5 at the takeoff and cruise Reynolds numbers. $Re_{Cruise}$ for Mission 2 was twice the value of $Re_{Cruise}$ for Mission 3, while $C_L$ required for cruise during Mission 3 was three times greater than the cruise $C_L$ flown on Mission 2. The team determined that a $C_{L_{max}}$ of 1.7 was required to meet the Mission 3 TOFL limit, so the ideal airfoil needed to be highly versatile. Therefore, three categories of airfoils were identified and evaluated: high efficiency for optimal Mission 2 performance, maximizing lift and L/D at high $C_l$ for optimal Mission 3 performance, and balanced lift and drag performance to balance Mission 2 and Mission 3 requirements. Three airfoils for each category were found. The airfoil corresponding to each category respectively were the BA527ls, the FX 63-137, and the la203a. Figure 9 shows lift curves predicted by XFLR5 for each at $Re = 2.5 \times 10^5$, the takeoff Reynolds number.
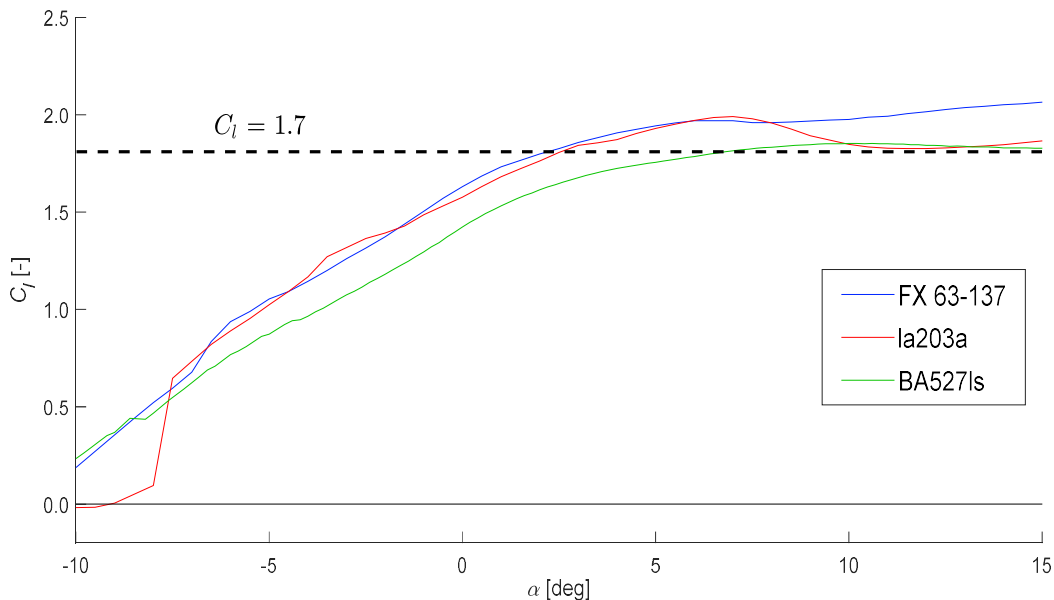


**Figure 9: Lift curves with $\delta_{flap} = 25°$. Each airfoil satisfies the $C_{l_{max}} > 1.7$ TOFL requirement.**

Once airfoils that provided the required $C_l$ were identified, drag polars were used to identify airfoils that provided favorable $L/D$. Drag polars for each airfoil are shown in Figure 10.
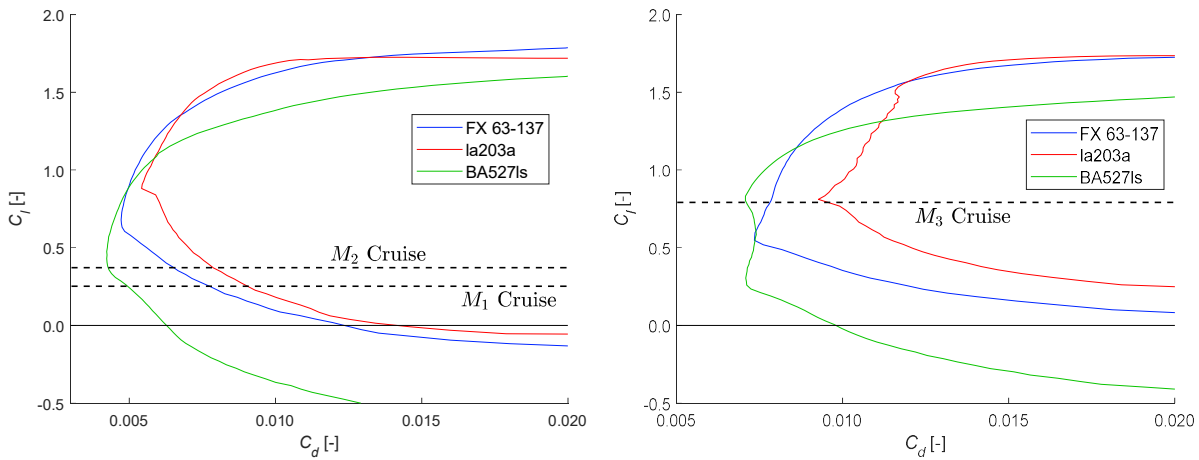


**Figure 10: Drag polars for each airfoil during Mission 2 cruise (left) and Mission 3 cruise (right).**

PlaneTools simulation results indicate that each airfoil would allow the plane to finish all missions in time. However, the BA527ls completed Mission 3 with 6%- and 4%-time margin when compared to the FX 63-137 and la203a, respectively. Although this margin was not enough to yield an extra lap on Mission 3, it was significant enough to make the plane more resilient to uncertainties such as Wichita winds and turn signal delay. In addition, BA527ls was most tolerant to build errors because the other airfoils were thinner and had more camber. Therefore, BA527ls was selected.

### 4.4.2 AERODYNAMIC COMPONENT ANALYSIS

Banner drag was recognized as a priority during preliminary design because it defined the limitations set for score analysis. Banner drag was determined by length $l_b$, aspect ratio $AR_b$, material density, and material rigidity [9]. Tested materials are outlined in Section 5.3.4. Geometry is defined in Figure 11.
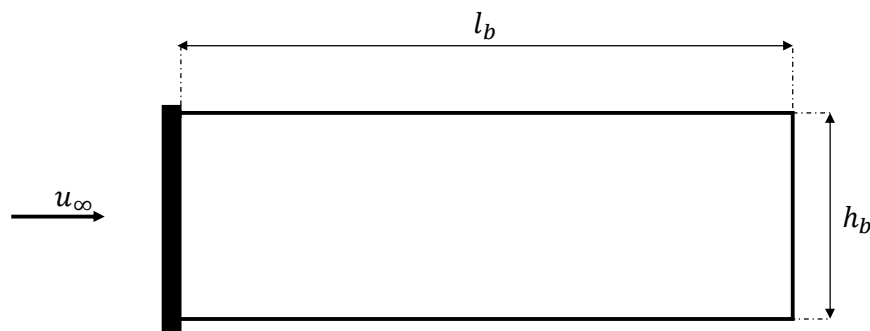


**Figure 11: Banner geometry.**

Using Figure 11, banner aspect ratio $AR_b$ and Reynolds number $Re_b$ are defined in Eq. 11 and Eq. 12 as

$$AR_b = \frac{l_b}{h_b} \qquad \text{Eq. 11}$$

$$\text{Re}_b = \frac{\rho u_\infty l_b}{\mu} \qquad \text{Eq. 12}$$

Banner geometry was varied so that the effect of $\text{AR}_b$ and $\text{Re}_b$ on banner drag could be determined.

The team considered banner placement to ensure the banner would remain vertical. Placing the tow point above the banner center of gravity kept the banner vertical during flight. Banner disturbance was modeled as a pendulum with damping as shown in Figure 12. Observations during flight tests confirmed this analysis.
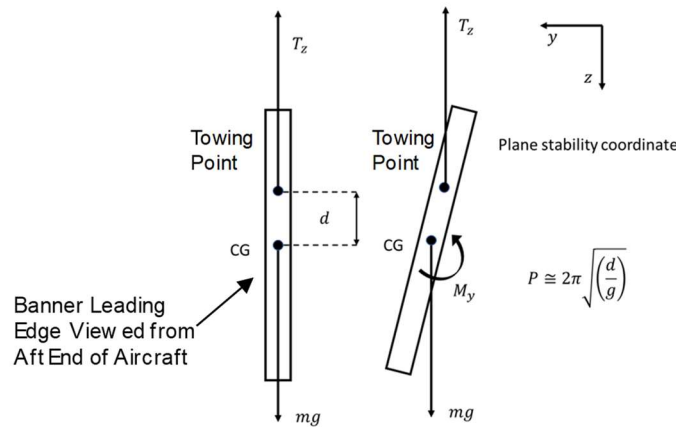


**Figure 12: Banner stability. $T_z$ is tension in the z-direction; $M_y$ is moment about the y-axis.**

Detailed banner testing and results are outlined in Section 7.2.1 and Section 8.1.1.

### 4.4.3 DRAG ANALYSIS

XFLR5 data with 3-D conversions [10] and banner testing data were used to estimate the drag for each component of the aircraft during cruise of each mission, shown in Figure 13.
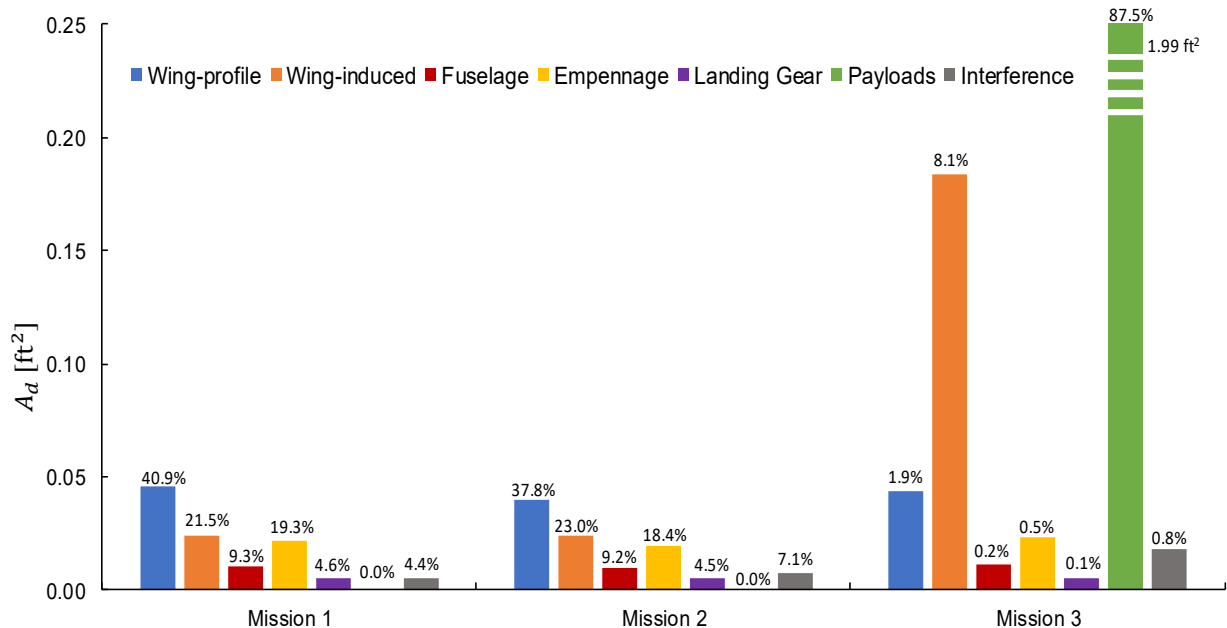


**Figure 13: Aircraft drag breakdown during cruise of each mission.**

The main source of drag on Mission 1 and Mission 2 was wing profile drag. The primary contributors to drag on Mission 3 were the banner and induced drag. Induced drag was increased on Mission 3 because the aircraft flew at a $C_L$ of 0.8 while cruising at 1/3 the flight speed flown on Mission 2. Adding winglets to reduce Mission 3 induced drag was investigated; winglets reduced total drag by only 2% [9]. Therefore, reducing banner drag was a higher priority. Banner drag testing is outlined in Section 7.2.1.

The drag break down shown in Figure 13 was used to create lift to drag ratio ($L/D$) versus coefficient of lift ($C_L$) plots to visualize the efficiency of the aircraft during cruise and turns. The expected $C_L$ values for cruise and turns were obtained through AVL analysis for each mission. Results are shown in Figure 14.
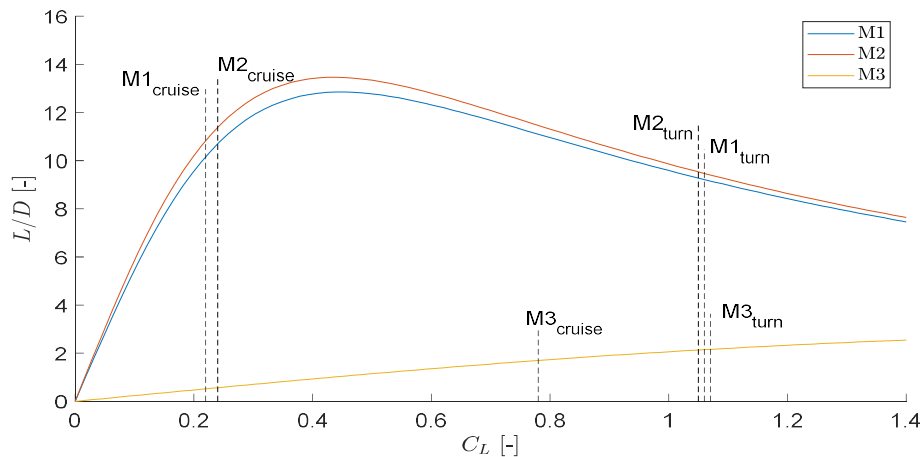


**Figure 14: L/D plot to visualize efficiency. Banner drag was accounted in the Mission 3 curve.**

The aircraft operated at 87% of the maximum lift-to-drag ratio, $(L/D)_{max}$, during Mission 2 cruise. The Mission 3 cruise $L/D$ was 1.7 during cruise and 2.4 in turns.

AVL was used to perform Trefftz plane analysis to determine angle of attack, $\alpha$, and trim elevator deflection, $\delta_e$, and span efficiency, $e$, during all the missions. Results are shown in Table 13 and Figure 15.

**Table 13 (left): Trim deflections with lift and drag coefficients for each mission during cruise.**

| | Mission 1 | Mission 2 | Mission 3 |
|---|---|---|---|
| e [-] | 0.73 | 0.75 | 0.92 |
| $\alpha$ [°] | -1.10 | -1.06 | 4.51 |
| $\delta_e$ [°] | -1.20 | -1.18 | -5.38 |
| $C_L$ [-] | 0.23 | 0.24 | 0.78 |
| $C_D$ [-] | 0.070 | 0.080 | 0.116 (without banner) |
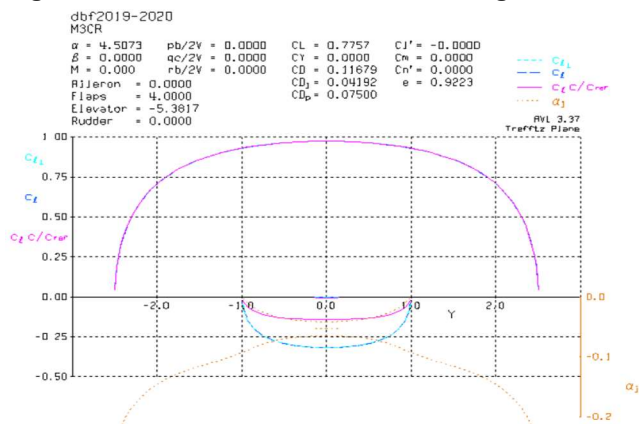


**Figure 15 (right): Trefftz plane analysis of the aircraft during Mission 3 cruise.**

The banner was stowed below the wing to prevent interference. To assist in making the 20 ft (6.0 m) TOFL requirement, banner leading and trailing edges were designed to form the profile of the NACA 0012 airfoil. The stowed banner was placed as far below the wing as possible to minimize flow interaction with the wing, and the wing and banner aerodynamic centers were aligned. AVL was used to investigate lift and stability characteristics imposed by the stowed banner since the vortex lattice model utilized by AVL accounts for interaction between each aerodynamic surface. The configuration and AVL model are shown in Figure 16.
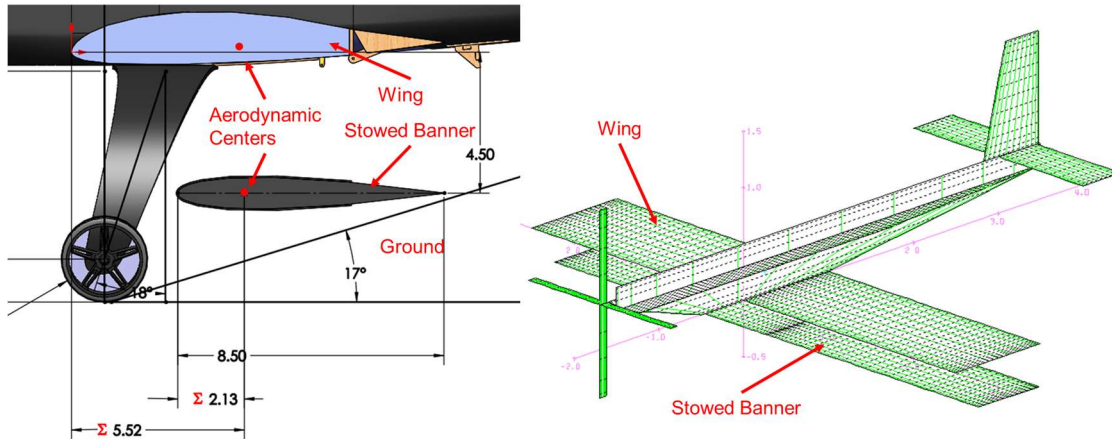


**Figure 16: Banner mounting configuration and corresponding AVL model.**

AVL results showed that when carrying the stowed banner beneath the wing, angle of attack needed to increase from 2.8° in the clean configuration to 5.4° in the Bi-Wing configuration to satisfy the $C_L$ required to meet TOFL on Mission 3 with 25° flap deployed.

## 4.5 STABILITY AND CONTROL

*4.5.1 STATIC STABILITY ANALYSIS*

Sizing of the aircraft for stable flight started by sizing and locating the tail of the aircraft based on a typical horizontal tail volume, $V_H$, of 0.6 and vertical tail volume, $V_V$, of 0.05, using Eq. 13 and Eq. 14 [3].

$$V_H = \frac{l_t * S_{horizontal}}{c * S_w}, \; V_V = \frac{l_t * S_{vertical}}{b * S_w}$$
Eq. 13, Eq. 14

Here, $S_{horizontal}$ and $S_{vertical}$ are the planform areas of each respective surface while $c$, $b$, and $l_t$ are the wing chord, wing span, and tail moment arm, respectively. Tail volume coefficients were used since they are common metrics for tail effectiveness in both longitudinal and lateral-directional stability. Additionally, as a baseline, the center of gravity (CG) of the aircraft was initially placed at the quarter chord of the wing where the center of pressure was located. The tail volumes and CG location were iterated throughout the preliminary design of the aircraft using flight test data and AVL analysis until the aircraft was deemed sufficiently stable by the team and pilot. The final tail had horizontal and vertical tail volumes of 0.52 and

0.07, respectively, while having a CG location that resulted in a static margin of 22%. Static stability derivatives are listed in Table 14 and Table 15.

**Table 14: Static stability derivatives of the aircraft during $M_2$ cruise.**

| $C_{L_\alpha}$ | 4.38 | $C_{m_\alpha}$ | -1.06 | $C_{Y_\beta}$ | -0.380 | $C_{Y_{\delta_r}}$ | -0.004 | $C_{Y_p}$ | -0.031 | $C_{Y_r}$ | 0.375 |
|---|---|---|---|---|---|---|---|---|---|---|---|
| $C_{L_{\delta_e}}$ | 0.009 | $C_{m_{\delta_e}}$ | -0.026 | $C_{l_\beta}$ | -0.064 | $C_{l_{\delta_r}}$ | -0.0006 | $C_{l_p}$ | -0.411 | $C_{l_r}$ | 0.1304 |
| $C_{L_q}$ | 8.46 | $C_{m_q}$ | -11.92 | $C_{n_\beta}$ | 0.129 | $C_{n_{\delta_r}}$ | 0.0024 | $C_{n_p}$ | -0.028 | $C_{n_r}$ | -0.205 |

**Table 15: Static stability derivatives of the aircraft during $M_3$ cruise.**

| $C_{L_\alpha}$ | 4.23 | $C_{m_\alpha}$ | -0.90 | $C_{Y_\beta}$ | -0.382 | $C_{Y_{\delta_r}}$ | -0.004 | $C_{Y_p}$ | -0.188 | $C_{Y_r}$ | 0.359 |
|---|---|---|---|---|---|---|---|---|---|---|---|
| $C_{L_{\delta_e}}$ | 0.009 | $C_{m_{\delta_e}}$ | -0.026 | $C_{l_\beta}$ | -0.120 | $C_{l_{\delta_r}}$ | -0.0006 | $C_{l_p}$ | -0.386 | $C_{l_r}$ | 0.232 |
| $C_{L_q}$ | 8.60 | $C_{m_q}$ | -11.91 | $C_{n_\beta}$ | 0.147 | $C_{n_{\delta_r}}$ | 0.0024 | $C_{n_p}$ | -0.039 | $C_{n_r}$ | -0.229 |

The aircraft was statically stable during Mission 2 and Mission 3 simulations in AVL. From Table 14 and Table 15 it is clear that the pitch control characteristics between Mission 2 and Mission 3 are consistent. Stronger coupling was present in Mission 3 than Mission 2 due to high angle of attack, but the coupling behavior was within the acceptable range according to pilot feedback. Flight tests verified that mounting the banner at the aerodynamic center would cause minimal effect in stability and control during Mission 3.

*4.5.2 DYNAMIC STABILITY ANALYSIS*

The aircraft's dynamic stability characteristics were also analyzed for all flight missions using AVL. A root locus plot was used to analyze the stability of the different dynamic modes of the aircraft, as shown in Figure 17. For a mode to be stable, it must be negative on the horizontal axis. The five dynamic modes of the aircraft are shown both during cruise (CR) and takeoff (TF).
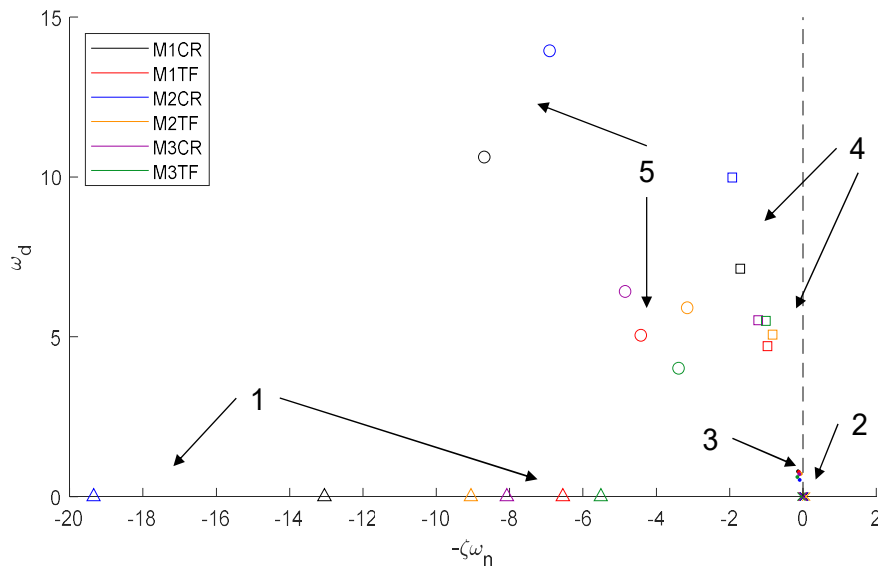


**Figure 17: Root locus plot of the five dynamic stability modes during takeoff and cruise of each mission; roll (1), spiral (2), phugoid (3), dutch roll (4), and short period (5).**

All modes, except spiral during Mission 2, were stable at takeoff and cruise for each mission scenario. The aircraft was designed to satisfy the Level 1 flying qualities of a Class 1 (small and lightweight) aircraft, described in MIL-F-8785C [11]. Characteristic values of the five modes are shown in Table 16 and Table 17, with the MIL-F-8785C requirements in parentheses. Conditions for Mission 2 and Mission 3 were shown because their characteristics were noticeably different due to different cruise speeds. Dynamic stability characteristics of Mission 1 are comparable those of Mission 2, and thus the values are not shown.

**Table 16: Dynamic stability parameters during $M_2$; values are listed as cruise value / takeoff value.**

| | Mode | $\zeta$ [-] | $\omega_n$ [rad/s] | $\zeta\omega_n$ [rad/s] | $\tau$ [s] |
|---|---|---|---|---|---|
| 1 | Roll | - | - | 19.35 / 9.057 | 0.0517 / 0.110 ($\tau < 1.4$) |
| 2 | Spiral | - | - | -0.0196 / -0.0881 | -50.9 / -11.4 |
| 3 | Phugoid | 0.164 / 0.0844 ($\zeta > 0.04$) | 0.531 / 0.718 | 0.0871 / 0.0606 | 11.48 / 16.50 |
| 4 | Dutch Roll | 0.190 / 0.161 ($\zeta > 0.08$) | 10.16 / 5.137 ($\omega_n > 0.4$) | 1.932 / 0.8246 ($\zeta\omega_n > 0.15$) | 0.520 / 1.21 |
| 5 | Short Period | 0.444 / 0.471 ($0.35 < \zeta < 2.00$) | 15.57 / 6.698 | 6.908 / 3.156 | 0.145 / 0.317 |

**Table 17: Dynamic stability parameters during $M_3$; values are listed as cruise value / takeoff value.**

| | Mode | $\zeta$ [-] | $\omega_n$ [rad/s] | $\zeta\omega_n$ [rad/s] | $\tau$ [s] |
|---|---|---|---|---|---|
| 1 | Roll | - | - | 8.077 / 5.514 | 0.118 / 0.124 ($\tau < 1.4$) |
| 2 | Spiral | - | - | 0.00490 / 0.0451 | 204.5 / 22.17 |
| 3 | Phugoid | 0.137 / 0.240 ($\zeta > 0.04$) | 0.709 / 0.634 | 0.0972 / 0.152 | 10.29 / 6.567 |
| 4 | Dutch Roll | 0.216 / 0.182 ($\zeta > 0.08$) | 5.648 / 5.588 ($\omega_n > 0.4$) | 1.222 / 1.015 ($\zeta\omega_n > 0.15$) | 0.818 / 0.985 |
| 5 | Short Period | 0.603 / 0.645 ($0.35 < \zeta < 2.00$) | 8.045 / 5.258 | 4.852 / 3.391 | 0.206 / 0.295 |

The stable modes of the plane all satisfy the MIL-F-8785C requirements. Only the spiral mode during $M_2$ was unstable, while the spiral modes for the rest of missions are stable. Nevertheless, MIL-F-8785C specifies that an unstable spiral mode can still satisfy the requirements if $|\tau| > 5.77$ so further analysis was conducted on the mode [11]. Adding dihedral to the wing would increase the spiral mode's time constant, $|\tau|$, to satisfy MIL-F-8785C for both takeoff and cruise during Mission 2 [11]. However, pilot evaluation from flight test deemed the change unnecessary; thus, dihedral was not added since it would have only increased complexity to the manufacturing process.

## 4.6 PREDICTED AIRCRAFT PERFORMANCE

*SCkyfall*'s performance characteristics based on PlaneTools predictions are shown in Table 18. Each mission was simulated with Wichita winds using assumptions outlined in Section 4.2.

**Table 18: Preliminary design performance characteristics.**

| Performance Parameter | Mission 1 | Mission 2 | Mission 3 |
|---|---|---|---|
| $C_{L_{max}}$ | 1.70 | 1.70 | 1.70 |
| $C_{L_{cruise}}$ | 0.76 | 0.53 | 0.89 |
| $e$ | 0.80 | 0.80 | 0.80 |
| $C_{D_0}$ | 0.06 | 0.06 | 0.06 |
| $(L/D)_{max}$ | 6.97 | 4.54 | 6.77 |
| $(L/D)_{cruise}$ | 3.63 | 7.02 | 1.04 |
| Rate of Climb [ft/s] | 17.54 | 45.91 | 26.23 |
| $W/S$ [lb/ft$^2$] | 1.38 | 5.09 | 2.04 |
| $V_{cruise}$ [ft/s] | 73.83 | 147.58 | 47.84 |
| $V_{stall}$ [ft/s] | 33.02 | 56.47 | 41.74 |
| Gross Weight [lb] | 6.92 | 25.44 | 10.22 |
| Mission Score | 1.00 | 1.48 | 2.86 |

## 5.0 DETAILED DESIGN

Detailed design combined conceptual and preliminary design with detailed testing and analysis of individual components. Structure, weight, and mission performance were considered to refine the competition aircraft.

## 5.1 DIMENSIONAL PARAMETERS TABLE

Table 19 lists characteristic parameters for *SCkyfall*. Each subsystem is highlighted in subsequent sections.

**Table 19: Characteristic component properties for *SCkyfall*.**

| Wing | | Tail | |
|---|---|---|---|
| Airfoil | Ba527ls | Airfoil | NACA 0010 |
| Span | 5.0 ft (1.52 m) | Horizontal Span | 23.9 in. (0.6 m) |
| $MAC$ | 1.0 ft (0.30 m) | Horizontal Chord | 5.4 in. (0.1 m) |
| Planform Area | 5.0 ft$^2$ (0.46 m$^2$) | Vertical Span | 12.0 in. (0.3 m) |
| $AR$ | 5 | Vertical Chord | 6.25 in. (0.2 m) |
| Incidence Angle | 0° | Planform Area | 1.4 ft$^2$ (0.1 m$^2$) |
| Static Margin | 21-24% | Incidence Angle | 0° |
| **Fuselage** | | Tail Arm | 36.0 in. (0.9 m) |
| Total Length | 52.5 in. (1.3 m) | **Controls** | |
| Nose Length | 13.5 in. (0.3 m) | Receiver | Futaba R7008SB |
| Tail Length | 39.0 in. (1.0 m) | Servo | Hitec HS-85MG+ |
| Width | 4.5 in. (0.1 m) | Battery Model | Turnigy Nano-tech 4500mAh |
| Height | 6..0 in. (0.2 m) | Internal Resistance | 0.003 Ω |
| **Motor** | | Cell Count | 6S2P |
| Model | Hacker A60-5S V4-28 Pole | Pack Voltage | 22.2 V |
| Gearbox | N/A [1:1] | Pack Weight | 687g |
| Effective Kv | 295 RPM/Volt | **Propeller** | |
| Power Rating | 2600 W | Manufacturer | Aeronaut Cam Carbon |
| No-Load Current ($I_0$) | 1.7 A | Mission 1 | 20 in. x 12 in. + 0° |
| Internal Resistance | 0.015 Ω | Mission 2 | 18 in. x 15 in. + 5° |
| Weight | 595 g | Mission 3 | 20 in. x 12 in. + 0° |

## 5.2 STRUCTURAL CHARACTERISTICS AND CAPABILITIES

The primary considerations in determining the aircraft structure were weight, aerodynamics, and flight loads. The wing was a solid foam core with embedded carbon spar caps and fiberglass skin sized for a gross weight of 24 lb, 7.5 g turns, and a 1.5 safety factor. This allowed for a maximum bank angle of 82.3°. The fuselage was a semi-monocoque construction consisting of a composite, load-bearing skin and structural bulkheads. This design was chosen to provide space to stow payload and minimize weight. A hatch was built into the top of the fuselage to facilitate passenger and luggage loading. The fuselage was designed to withstand motor thrust and torque, lift force transferred from the wing, and a 2.5 g landing load.

## 5.3 SUB-SYSTEM DESIGN

### 5.3.1 WING

The wing structure was designed to support flight loads and minimize weight. A foam core wing with embedded carbon spar caps and fiberglass skin was chosen. In order to design the wing to have the required bending strength, the optimum spar cap layup was determined. This was done using a MATLAB script written by a former Structures lead. Based on inputs of wing geometry, desired cap width, and expected flight loads, the script generated a plot of the bending moment and the number of plies required at each increment. The spar cap was chosen to be 1.5 in. wide as a compromise between narrow caps which result in high stresses between the cap and core and wide caps which will not be flat due to the chordwise curvature of the airfoil. The spar cap bending moment diagram is shown in Figure 18.
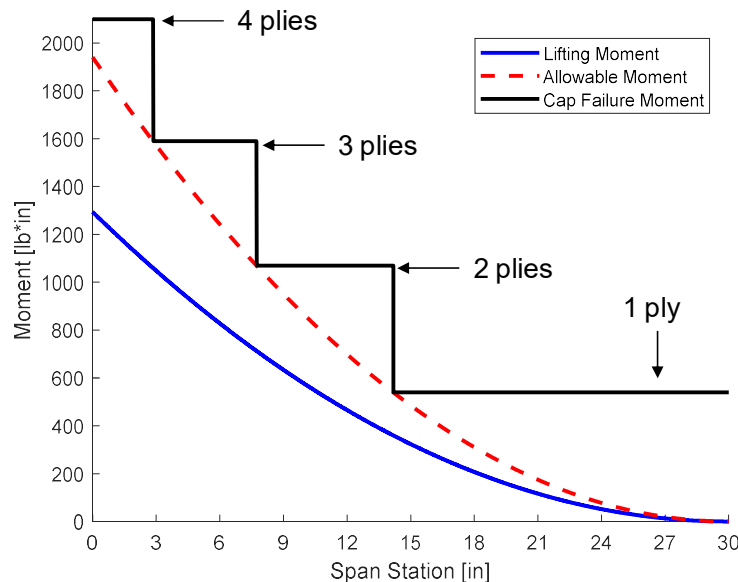


**Figure 18: Cap failure moment is stepped since ply count decreases with span (4 at root; 1 at tip).**

### 5.3.2 TAIL

A balsa built-up construction was used for the tail. The spars for the horizontal and vertical stabilizers were joined together in an upside down "T" structure shown in Figure 19. The spar was made from 1/4 in. balsa

shear web and 3 ply carbon fiber spar caps. 1/16 in. balsa ribs were attached to the spar with 3 in. (8 cm) separation to maintain the shape of the airfoil. The ribs that mounted the servos and the ribs nearest the mounting point with the fuselage were made from 1/16 in. aircraft plywood. A single ply of 45° carbon fiber cloth was used for the D-box to create torsional rigidity. The skin was made of Monokote film. Downward extensions from the innermost plywood ribs fit securely around the aft section of the fuselage, and nylon bolts were used to mount the tail through the fuselage skin. This is shown in Figure 19.
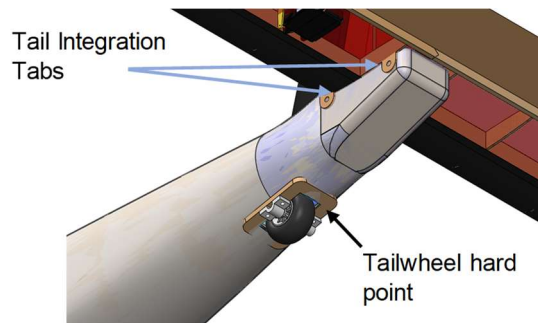


**Figure 19: Tail integration and tailwheel hard point.**

### 5.3.3 LANDING GEAR

The landing gear bow was designed assuming a weight of 24 lb, a 2.5 g load limit, and 5.6 ft/s sink rate, corresponding the mission with highest expected landing loads (Mission 2). The landing gear was positioned forward of the CG at 18° off vertical to prevent nose-over. Mounting the straight-bow gear could obstruct root airflow at the Mission 3 angle of attack. To counteract this, the bow was swept such that the centerline mounted at the aircraft CG, while the bow swept forward to maintain the designed wheel position. To account for the added moment, 2 carbon plies woven at 45° and 1 ply woven at 90° were added to the layup. Finite element analysis was conducted to verify the design and is shown in Figure 20.
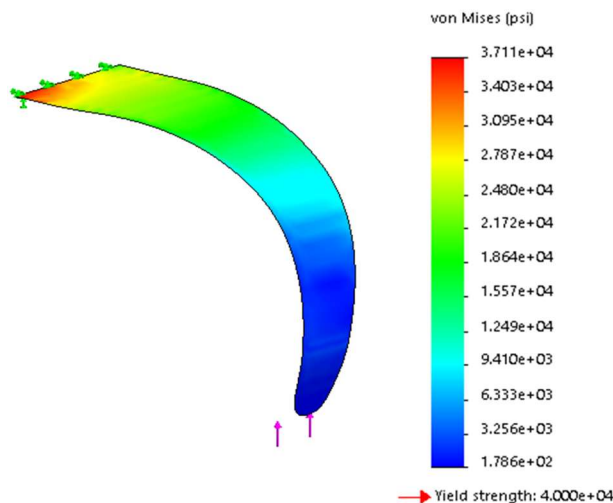


**Figure 20: Von Mises stress at maximum loading, corresponding to maximum deflection of 3.2 in.**

The final landing gear design was tested as outlined in Section 7.2.4.

## 5.3.4 PAYLOADS

### Passengers

The passengers were fabricated from Polyethylene Terephthalate (PETG) using standard additive manufacturing methods with a Flying Bear printer. This process was selected because it allowed the team to efficiently build all 39 passengers and ensure that each weighed no more than 4 oz. The passengers had hollow bases designed to fit 4 stainless steel washers to increase weight to 4 oz. To lower the center of gravity of the passengers, the top 70% of the passenger volume was hollow, with the exterior and "head" fabricated from 2 staggered extrusion-widths. Passenger center of gravity was lowered to ease loading during the Ground Mission and to prevent movement in flight. Passengers are shown in Figure 21.
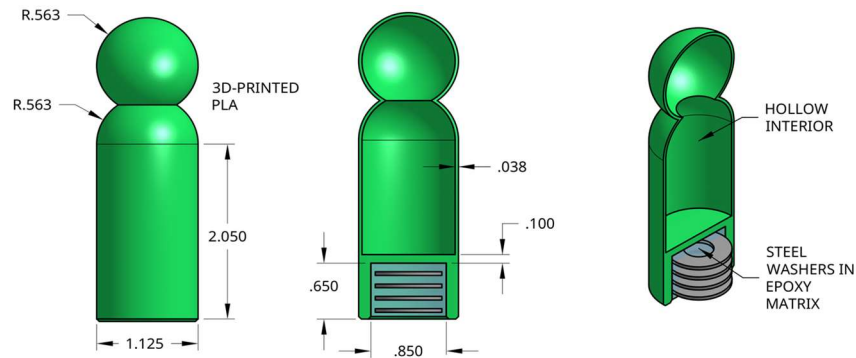


**Figure 21: Detailed passenger design. Dimensions shown are inches.**

### Passenger Restraint

Two passenger restraint systems were considered. The first was a friction fit which held the passengers at the base. The second system considered combined the friction fit with a headplate. The combined design was chosen because it allowed passengers to be held loosely at the base, decreasing $T_{GM}$ and making restraint system damange less likely. Passenger loading time for each system is shown in Figure 22.
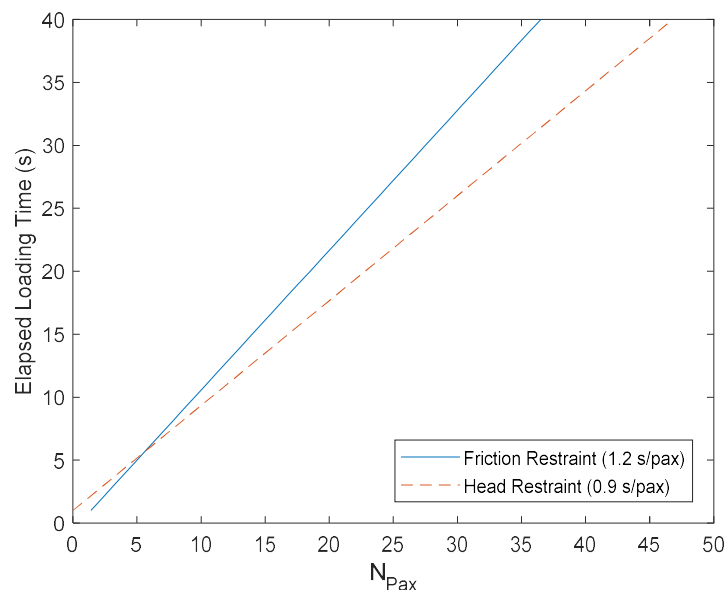


**Figure 22: Experimental loading times of restraint systems. Loading time uncertainty is $\pm$ 0.2 s.**

The passengers were restrained in the aircraft cabin with a friction fit on their bases, achieved with a laser-cut 1/16 in. aircraft plywood structure. This structure comprised interlocking segments, oriented in the beamwise and lengthwise directions, which formed gaps for passengers to be securely inserted. After all the passengers were inserted, they were further secured in position with a head plate. The head plate lowered vertically on the heads of the passenger and was secured by hinges on one side and 2-gram neodymium magnets on the other. The passenger restraint system is shown in Figure 23.
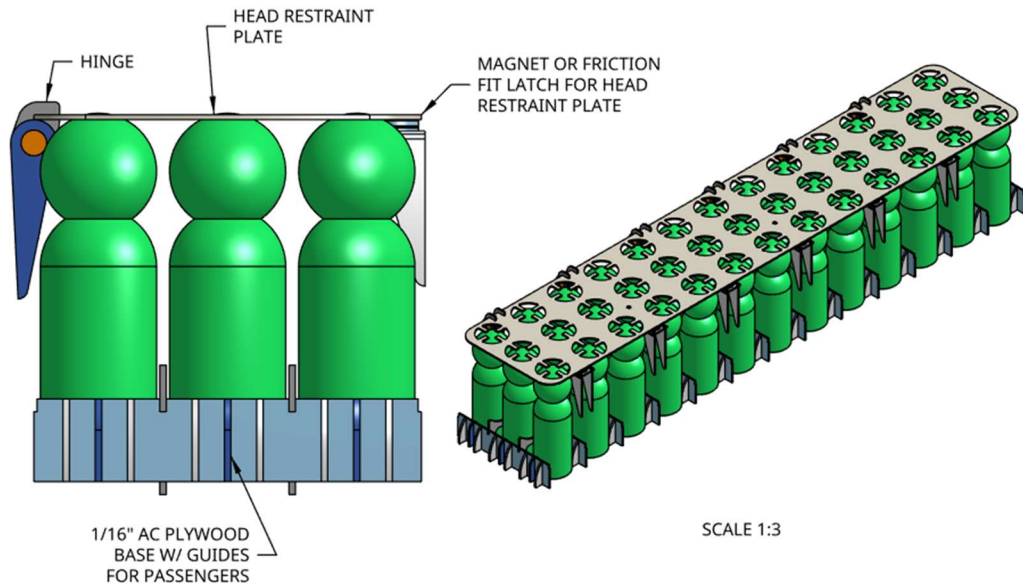


**Figure 23: Passenger restraint system.**

*Luggage*

Luggage was designed to minimize volume and weight. Each block was designed to meet the minimum dimensions and weight prescribed by the AIAA. Each was manufactured using the process used for passengers. Dimensions are shown in Figure 24.
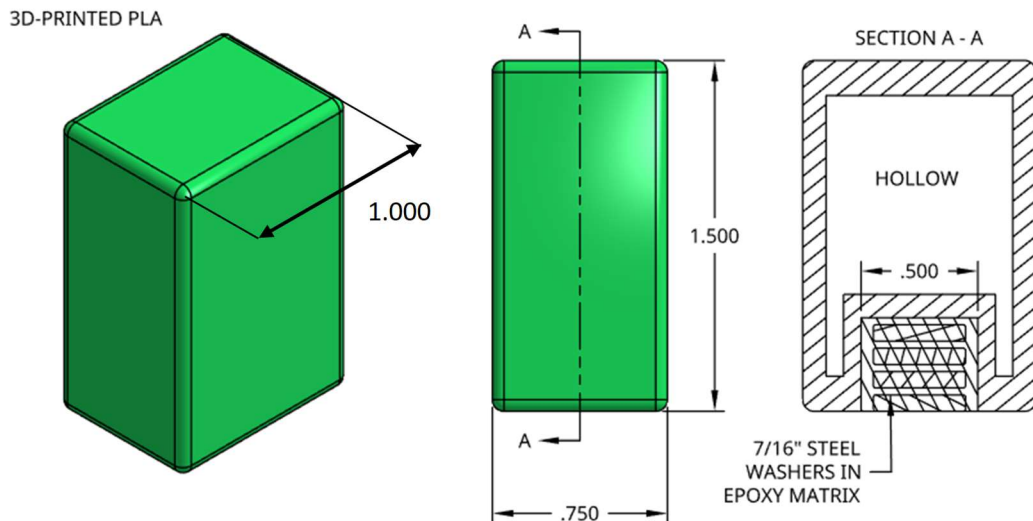


**Figure 24: Luggage design. Dimensions shown are inches.**

*Banner*

Various banner materials were analyzed to identify the lowest-drag configuration possible. Materials considered are shown in Figure 25. Materials were chosen based on material density and rigidity [9].
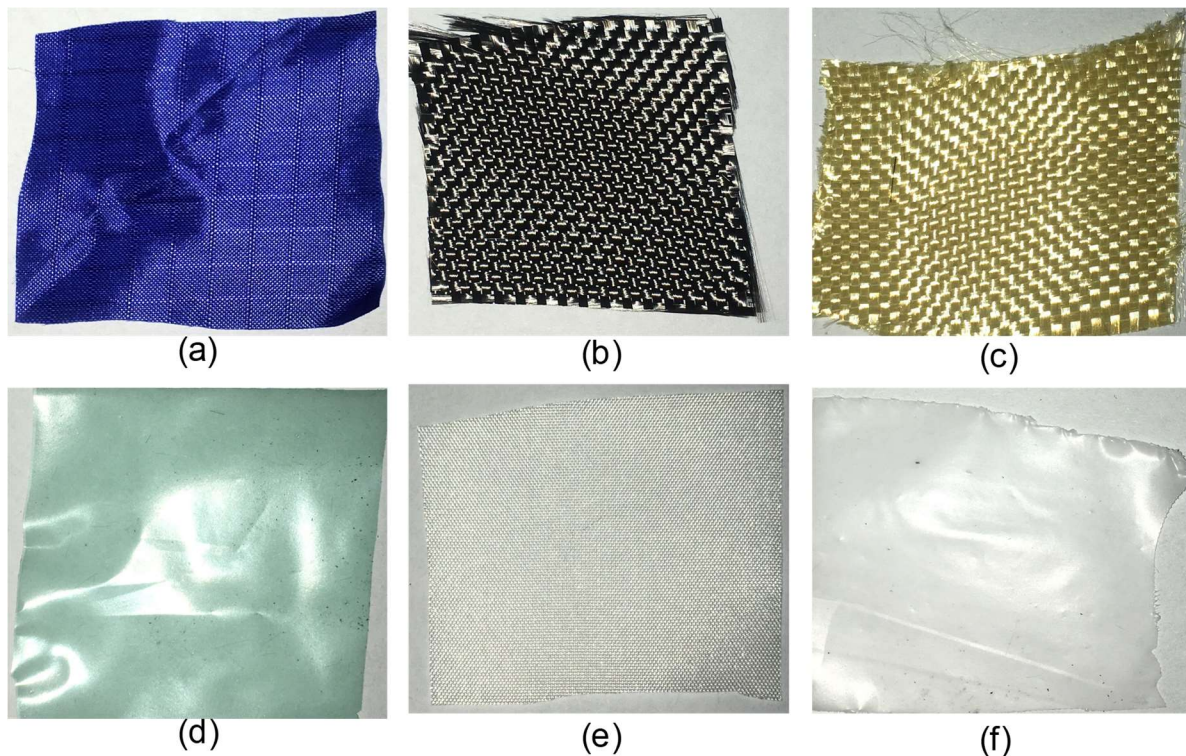


**Figure 25: (a) Icarex polyester, (b) Carbon fiber, (c) Kevlar, (d) Low-Density (0.9 g/cm³) Polyethylene (LDPE), (e) Peel ply, (f) Vacuum bag.**

LDPE was the lowest-drag material identified during flight tests (Section 8.1.1). The banner sheeting was made entirely of LDPE. Carbon was chosen as the leading and trailing edge material because it was the lightest material that would provide required strength. Further tests indicated that $AR_b$ = 5 to minimize drag.

### 5.3.5 FUSELAGE

The fuselage was designed to be lightweight, have efficient load paths between aircraft components, and provide internal space for the payload. The final design was a semi-monocoque construction with a top hatch, as shown in Figure 26. The load-bearing skin was made from thin sandwich panels of 1/16 in. balsa with composite face sheets. 10 plies of carbon fiber were used for the face sheets around the motor mount and extending past the wing to the rear bulkhead. The aft section and top hatch didn't require as much strength, so a single ply of fiberglass was used for each face sheet. Hardpoints made from 1/8 in. aircraft plywood were integrated in the fuselage layup to mount the landing gear, wing, banner release mechanism, and tail structure. Nylon bolts were used for mounting subcomponents to the fuselage, and they were sized to shear upon impact. The motor mount is a thin plate of 10 carbon fiber plies and 1/8 in. aircraft plywood.
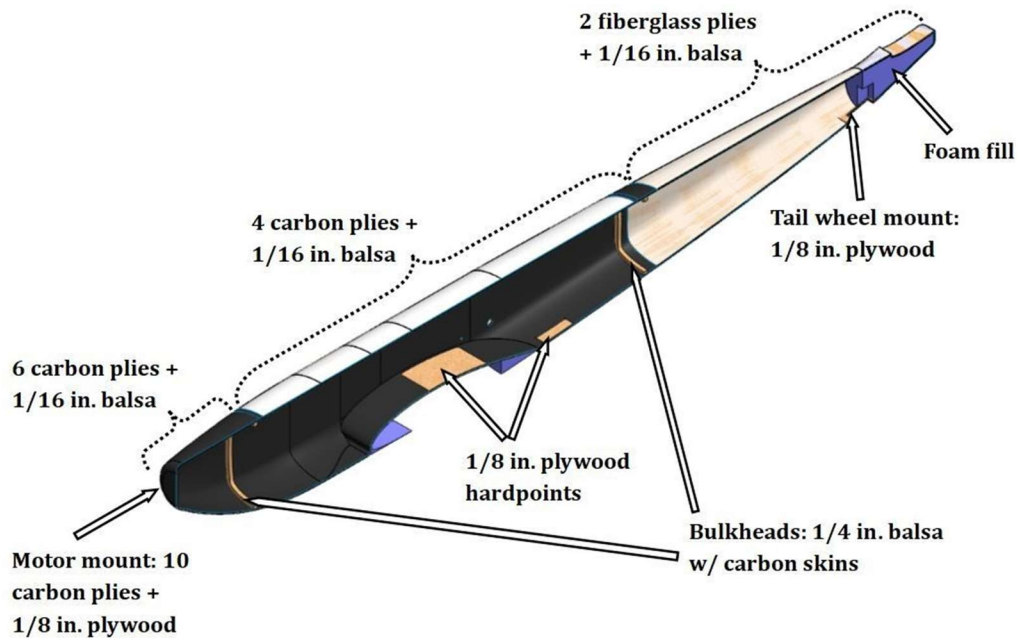
**Figure 26: Number of composite plies and material were varied along the length of the fuselage depending on strength requirements.**

*5.3.6 PROPULSION SYSTEM*

Each propulsion component was tested so that advance ratio $J$ and $N_c$ could be optimized for each mission. Mission 3 endurance and TOFL requirements limited $Kv \leq 500$. Flight testing confirmed that both power and current requirements would be met for each package. Mission components are shown in Table 20.

**Table 20: Package breakdown by mission.**

|  | Mission 1 & 2 | Mission 3 |
|---|---|---|
| **Motor/Gearbox** | Hacker A60-5S V4 (Kv 295) | |
| **Propeller** | Aeronaut +5° twist 20x12 | Aeronaut +0° twist 18.5x15 |
| **Battery** | 6S2P Turnigy 3000 mAh | 6S2P Turnigy 4500 mAh |
| **ESC** | Castle Phoenix Edge 130 A | |
| **Rx** | Futaba R7008SB | |
| **Rx Pack** | 4 x 1/3 AAA 170 mAh | |

## 5.4 WEIGHT AND MASS BALANCE

*SCkyfall*'s empty weight (EW) was 6.4 lb (2.9 kg). Batteries were used as ballast to ensure the center of gravity (CG) was within static margin. The coordinate system used to model the CG is shown in Figure 27.
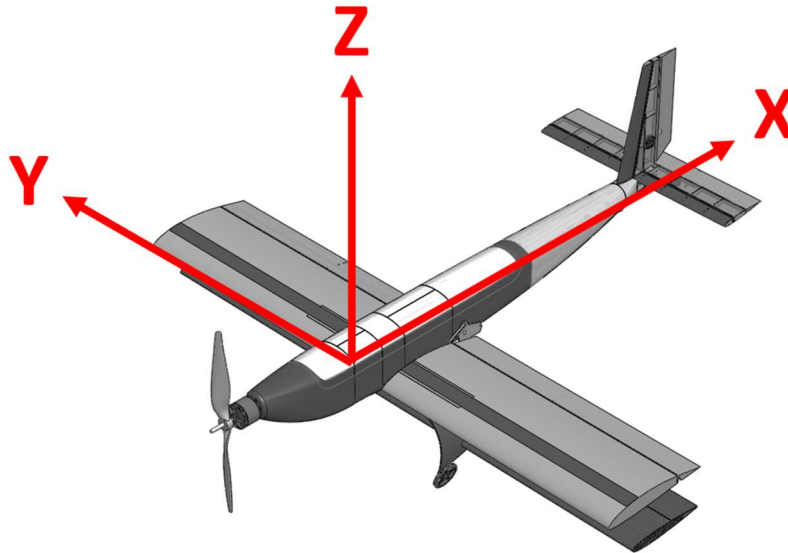
**Figure 27: Aircraft coordinate system with origin placed at the leading edge of the wing.**

Table 21 shows each component's mass and CG location with respect to this coordinate system. In Mission 3 the battery pack was moved aft by 16.5 in. relative to Mission 2. This was due to the lack of passengers and cargo in Mission 3 and the increased weight of battery pack. The banner was stowed near the CG during takeoff to reduce the change in CG when it deployed. The weight of the banner is not included in CG calculations after deployment since it is not rigidly attached to the aircraft.

**Table 21: Mass balance table for all missions.**

| Aircraft Component | Mass | | X | | Y | | Z | |
|---|---|---|---|---|---|---|---|---|
| | (lb) | (g) | (in) | (cm) | (in) | (cm) | (in) | (cm) |
| **General** | | | | | | | | |
| Fuselage | 0.74 | 336 | 9.06 | 23.0 | 0.01 | 0.0 | 3.00 | 7.6 |
| Wing | 2.21 | 1002 | 5.17 | 13.1 | 0.00 | 0.0 | 0.39 | 1.0 |
| Motor | 1.30 | 590 | -14.71 | -37.4 | 0.00 | 0.0 | 4.25 | 10.8 |
| Tail | 0.19 | 84 | 38.65 | 98.2 | 0.00 | 0.0 | 7.79 | 19.8 |
| Landing Gear | 0.31 | 139 | 0.66 | 1.7 | 0.00 | 0.0 | -1.88 | -4.8 |
| $M_1$ | | | | | | | | |
| Battery | 0.80 | 363 | -10.80 | -27.4 | 0.00 | 0.0 | 3.96 | 10.1 |
| Prop | 0.25 | 113 | -17.15 | -43.5 | 0.00 | 0.0 | 4.25 | 10.8 |
| $M_2$ | | | | | | | | |
| Battery | 0.80 | 363 | -10.80 | -27.4 | 0.00 | 0.0 | 3.96 | 10.1 |
| Prop | 0.25 | 113 | -17.15 | -43.5 | 0.00 | 0.0 | 4.25 | 10.8 |
| PAX | 10.40 | 4719 | 2.16 | 5.5 | -0.01 | 0.0 | 2.79 | 7.1 |
| Cargo | 2.63 | 1191 | 16.09 | 40.9 | 0.00 | 0.0 | 3.00 | 7.6 |
| $M_3$ | | | | | | | | |
| Battery | 3.01 | 1365 | 5.70 | 14.5 | 0.00 | 0.0 | 3.15 | 8.0 |
| Prop | 0.25 | 113 | -17.15 | -43.5 | 0.00 | 0.0 | 4.25 | 10.8 |
| Banner | 1.07 | 486 | 6.91 | 17.6 | 0.00 | 0.0 | -0.94 | -2.4 |

## 5.5 FLIGHT AND MISSION PERFORMANCE

The expected flight performance of the final aircraft is listed in Table 22. These figures were calculated using the PlaneTools simulation model.

**Table 22: Predicted aircraft performance parameters for each mission.**

| Performance Parameters | Mission 1 | Mission 2 | Mission 3 |
|---|---|---|---|
| $C_{L_{max}}$ | 1.63 | 1.63 | 1.63 |
| $C_{L_{cruise}}$ | 1.18 | 1.23 | 1.18 |
| $e$ | 0.8 | 0.8 | 0.8 |
| $C_{D0}$ | 0.06 | 0.06 | 0.06 |
| $(L/D)_{max}$ | 7.2 | 7.3 | 7.09 |
| $(L/D)_{cruise}$ | 3.6 | 5.8 | 1.75 |
| Rate of Climb [ft/s] | 6.78 | 10.80 | 4.54 |
| $W/S$ [lb/ft$^2$] | 1.58 | 4.03 | 2.36 |
| $V_{cruise}$ [ft/s] | 77 | 90 | 47 |
| $V_{stall}$ [ft/s] | 29 | 46 | 35 |
| TOFL [ft] | 17 | 89 | 19 |
| Battery Weight [lb] | 1.5 | 1.5 | 2.9 |
| Weight [lb] | 6.4 | 24.0 | 9.4 |

The corresponding mission results and score parameters are listed in Table 23.

**Table 23: Mission-specific PlaneTools scoring predictions.**

| Score Parameters | Mission 1 | Mission 2 | Mission 3 |
|---|---|---|---|
| Completion Score | 1.00 | 1.00 | 2.00 |
| $T_{USC}$ [s] | - | 74.7 | - |
| $T_{Best}$ [s] | - | 77.0 | - |
| $N_{Laps}$ | - | - | 12 |
| *Mission Score* | 1.0 | 1.45 | 2.77 |
| $W$ [lb] | 6.4 | 24.0 | 9.4 |
| *WS* [in] | 60.0 | | |
| *Total Flight Score* | 5.22 | | |
| *Ground Mission Score* | 0.15 | | |
| *Total Score* | 537 | | |

## 5.6 DRAWING PACKAGE

The following drawing package includes a dimensional 3-view, structural arrangements, subassembly detail, and payloads drawings. All drawings were made using SolidWorks [12].

Ø18.50 (M2)   Ø20.00 (M3)

6.00

4.50
18.00

4.70
34.00
12.00
20.00
7.80
6.00
17°
2.00
Ø2.74

36.01
27.56
3.00
12.00
13.50

| | NAME | UNLESS OTHERWISE SPECIFIED:<br>DIMENSIONS ARE IN INCHES | |
|---|---|---|---|
| | | **University of Southern California**<br>Cessna-Raytheon-AIAA Design/Build/Fly 2020 | |
| DRAWN | LG | TITLE: | |
| CONSIDER | | **SCkyfall** | |
| APPV'D | AM | DWG NO. | B |
| MFG | DS | Aircraft 3-View | |
| Q.A | MT | SCALE:1:12   Drawing Package   2/21/2020   SHEET 1 OF 3 | |

| ITEM NO. | COMPONENT | DESCRIPTION | QTY |
|---|---|---|---|
| 1 | Wing | Foam, Carbon Uni, Fiberglass, Balsa, Plywood | 1 |
| 2 | ESC | Castle Pheonix Edge | 1 |
| 3 | Battery Pack | Turnigy Lipo 6S 2P 2200mah/4500mah | 1 |
| 4 | Reciever | R7008SB | 1 |
| 5 | PAX | ABS, Steel Washers | 39 |
| 6 | Cargo Block | ABS, Steel Washers | 39 |
| 7 | Horiontal Stabilizer | Plywood/Balsa Built-up, Carbon D-box, Solite Covering | 1 |
| 8 | Vertical Stabilizer | Plywood/Balsa Built-up, Carbon D-box, Solite Covering | 1 |
| 9 | Fuselage | Carbon fiber/Fiberglass layup, plywood/balsa bulkheads | 1 |
| 10 | Tail Wheel | Rubber/Plastic Wheel | 1 |
| 11 | Banner Clips | Plywood | 1 |
| 12 | Banner (Stowed) | Carbon layup, Low Density Polyethylene Sheeting | 1 |
| 13 | Bow Gear | Carbon Uni layup, Rubber/Plastic Wheel | 1 |
| 14 | Motor | Hacker A60-5S V4 | 1 |
| 15 | Propeller | 18.5x15(5° yoke)/20x12 | 1 |
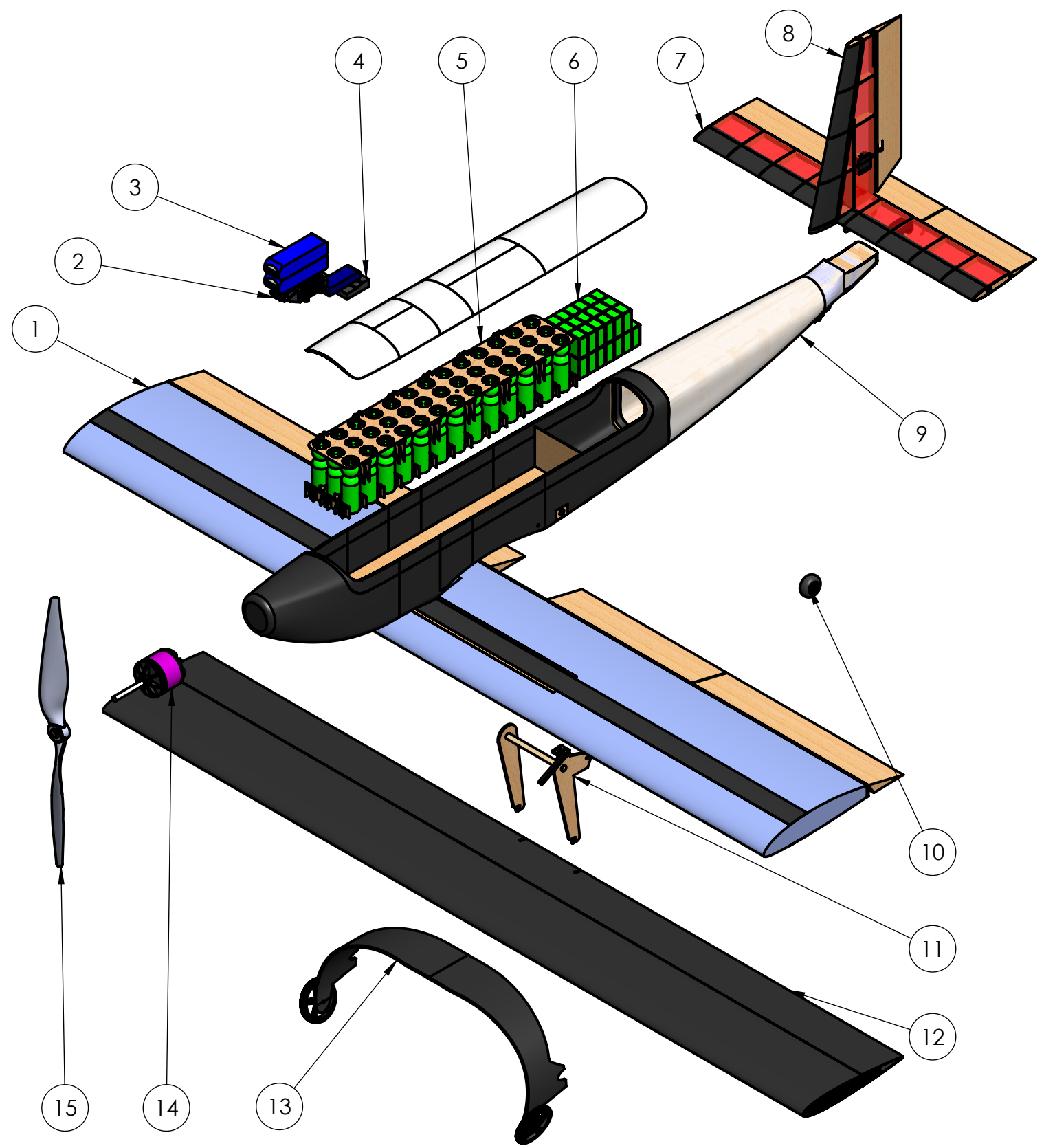
Scale 1:64

300.00

60.00

USC ADT

PAX, Cargo, and Banner are not flown on the same mission.

SOLIDWORKS Educational Product. For Instructional Use Only.

UNLESS OTHERWISE SPECIFIED:
DIMENSIONS ARE IN INCHES

**University of Southern California**
Cessna-Raytheon-AIAA Design/Build/Fly 2020

TITLE:

SCkyfall

Aircraft Overview

| | NAME |
|---|---|
| DRAWN | LG |
| CONSIDER | |
| APPV'D | AM |
| MFG | DS |
| Q.A | MT |

DWG NO.

B

SCALE:1:8   Drawing Package   2/21/2020   SHEET 2 OF 3

# Horizontal Stabilizer



| ITEM NO. | COMPONENT | DESCRIPTION | QTY |
|---|---|---|---|
| 1 | Tab Rib | 1/16" Plywood | 2 |
| 2 | Rib | 1/16" Balsa | 7 |
| 3 | Aft Spar | 1/8" Balsa | 1 |
| 4 | Elevator | Balsa | 1 |
| 5 | Servo Rib | 1/16" Plywood | 1 |
| 6 | Control Horn | 1/16" Plywood | 1 |
| 7 | Spar Cap | Carbon Uni | 1 |
| 8 | Front Spar | 1/8" Balsa | 1 |
| 9 | Servo | Hitec HS-85 MG | 1 |
| 10 | D-Box | 45° Carbon | 1 |

# Vertical Stabilizer
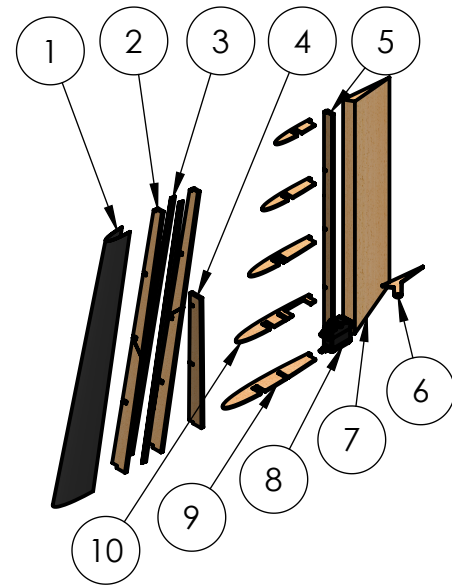


| ITEM NO. | COMPONENT | DESCRIPTION | QTY |
|---|---|---|---|
| 1 | D-Box | 45° Carbon | 1 |
| 2 | Front Spar | 1/8" Balsa | 1 |
| 3 | Spar Cap | Carbon Uni | 1 |
| 4 | Mid Spar | 1/8" Balsa | 1 |
| 5 | Aft Spar | 1/8" Balsa | 1 |
| 6 | Control Horn | 1/16" Plywood | 1 |
| 7 | Rudder | Balsa | 1 |
| 8 | Servo | Hitec HS-85 MG | 1 |
| 9 | Rib | 1/16" Balsa | 4 |
| 10 | Servo Rib | 1/16" Plywood | 1 |

# Passengers
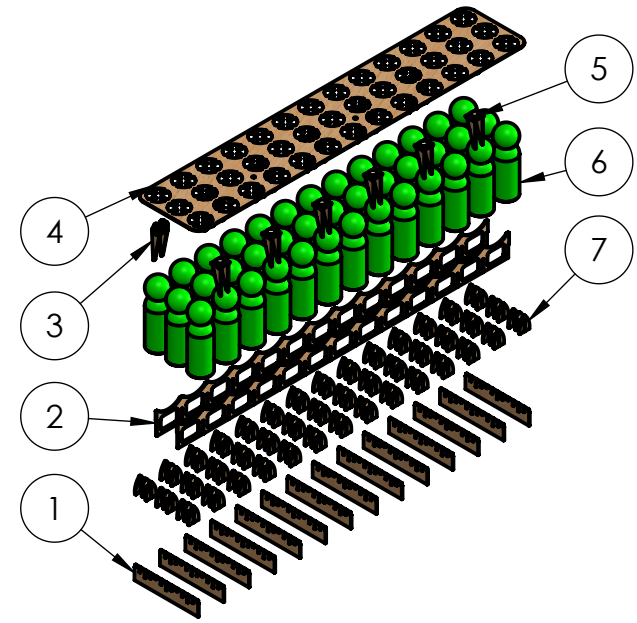


| ITEM NO. | COMPONENT | DESCRIPTION | QTY |
|---|---|---|---|
| 1 | Cross Piece | 1/16" Plywood | 15 |
| 2 | Connector | 1/16" Plywood | 2 |
| 3 | Hinge | 1/16" Plywood, Spruce Dowel | 6 |
| 4 | Plate | Balsa, 1/16" Plywood | 1 |
| 5 | Magnet Latch | 1/16" Plywood, Neodynium Magnets | 6 |
| 6 | PAX | ABS, Steel Washers | 39 |
| 7 | Friction Hold | 1/16" Plywood | 135 |

# Fuselage
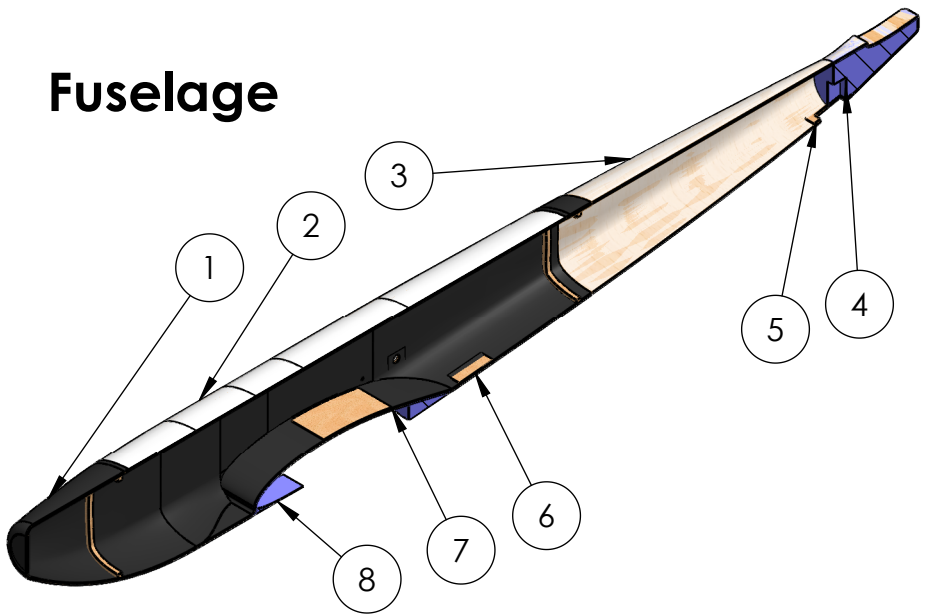


| ITEM NO. | COMPONENT | DESCRIPTION | QTY |
|---|---|---|---|
| 1 | Nose Section | Carbon Fiber, 1/16" Balsa, Plywood | 1 |
| 2 | Hatch | Fiberglass, 1/16" Balsa | 1 |
| 3 | Tail Section | Fiberglass, 1/16" Balsa | 1 |
| 4 | Tail Filler | 2PCF Foam | 1 |
| 5 | Tail Wheel Hard Point | 1/8" Plywood | 1 |
| 6 | Banner Hard Point | 1/8" Plywood | 1 |
| 7 | Wing Hard Point | 1/8" Plywood | 1 |
| 8 | Fairing | 2PCF Foam | 2 |

# Banner
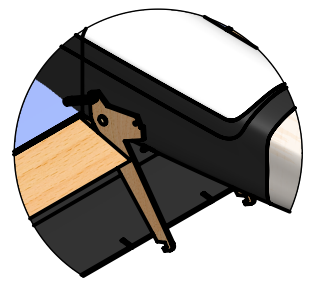


## 1) Clip into servo
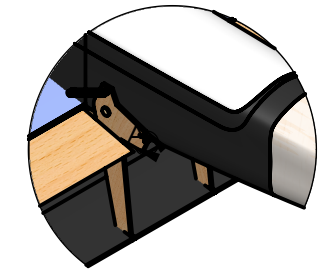
## 2) Hold during takeoff
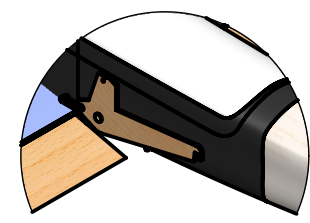


## 3) Deploy Banner

## 4) Release Banner



NiChrome Wire
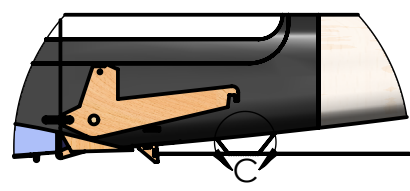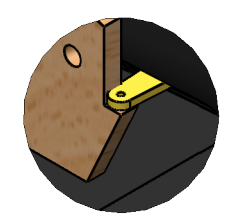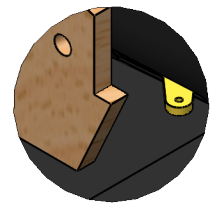
DETAIL A
SCALE 1 : 1

DETAIL B
SCALE 1 : 1
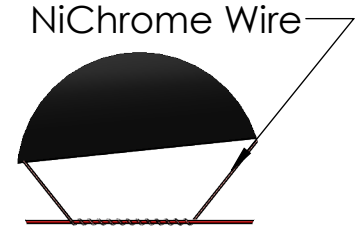
DETAIL C
SCALE 1 : 2

UNLESS OTHERWISE SPECIFIED:
DIMENSIONS ARE IN INCHES

**University of Southern California**
Cessna-Raytheon-AIAA Design/Build/Fly 2020

TITLE:
## SCkyfall

| | NAME |
|---|---|
| DRAWN | LG |
| CONSIDER | |
| APPV'D | AM |
| MFG | DS |
| Q.A | MT |

DWG NO.
Subassembly Detail

B

SCALE:1:8 | Drawing Package | 2/21/2020 | SHEET 3 OF 3

## 6.0 MANUFACTURING PLAN

Numerous manufacturing processes were evaluated for each component including the wing, fuselage, tail, landing gear, and payload mechanisms. The fabrication of each component was evaluated and selected as detailed in the following subsections.

### 6.1 MANUFACTURING PROCESSES INVESTIGATED

#### 6.1.1 FOAM

Foam is relatively cheap and can be easily shaped using a hotwire foam cutter and sanding. Foam structures are often heavier than balsa and composites structures [2]. The team has extensive experience building with foam to validate sizing of prototype aircraft. Although in previous years the team has used balsa and composites in lieu of foam for final competition components, the team elected to use foam in combination with composites for the wing because of the magnitude of the expected loads on Mission 2.

#### 6.1.2 BALSA BUILD UP

Balsa is the lowest-density material used for construction of aircraft structures [2]. Well-designed balsa structures are often lighter than composite structures for smaller aircraft, as demonstrated by the historical success of balsa aircraft in previous AIAA DBF competitions [5]. However, balsa is not as strong as composites. The accessibility of CAD and laser cutters make balsa-built structures more precise.

#### 6.1.3 3D PRINTING

Additive manufacturing allows for the design of complex forms that would be otherwise difficult to build. The team has access to a Markforged Mark Two 3D printer that creates high precision ($\pm 0.005 \text{ in.}$) parts reinforced with fiberglass, carbon fiber, or Kevlar [13]. 3D printing was especially useful this year because it allowed the team to print passengers and luggage blocks simultaneously, reducing build time and allowing the team to focus time on more build-intensive processes such as wing and fuselage layups.

#### 6.1.4 COMPOSITES

Composites have high semi-isotropic strength-to-weight ratios [2]. Additionally, composites are more durable than other materials because they are more likely to bend than break. The team has a strong composite build skillset which will be used to build the final wing and fuselage sections. Building composites is expensive because of material costs and requires lead times as long as four weeks.

### 6.2 MANUFACTURING PROCESSES SELECTED

#### 6.2.1 WING AND TAIL STRUCTURE

The foam core for the wing was cut from a large block using a hotwire device that was passed over plywood templates in the shape of the airfoil.  Shallow recesses were hollowed out of the foam core to insert the plywood hardpoints for mounting the wing and servos. This allowed the plywood to sit flush with the surface

of the wing. 3 oz/yd$^2$ fiberglass skins were cut at 45-degree angles to provide maximum torsional strength. The fiberglass skin and uni-directional carbon fiber spar caps were wet-out on a sheet of mylar and then draped over the foam core. After the wing was vacuumed and cured, the control surfaces were attached, holes were drilled for mounting, and servos were installed. The wing is detailed in Figure 28.
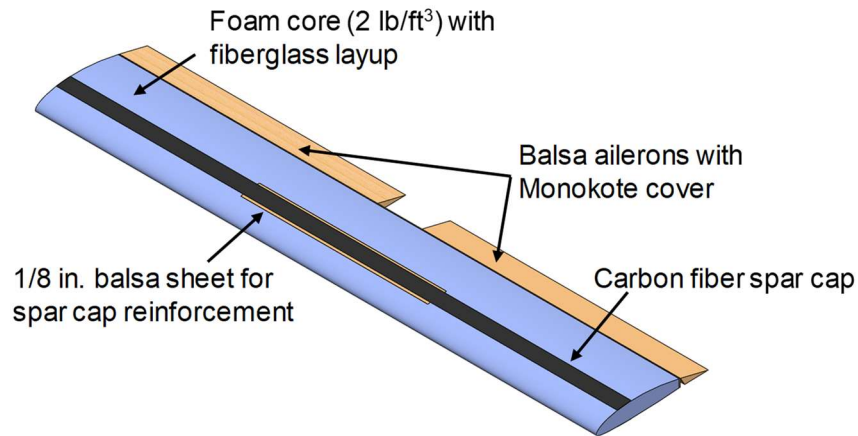


**Figure 28: Foam-core wing structure.**

The horizontal and vertical stabilizers shared an upside down "T"-shaped spar. This spar was made from 1/4 in. balsa pieces epoxied together and 3 plies of uni-directional carbon fiber for the caps. 1/8 in. balsa and plywood ribs were laser cut and joined to the spars with CA glue. D-boxes for the vertical and horizontal stabilizers were each made from a single layer of 45° carbon fiber that was laid-up separately and attached to the balsa structure with epoxy. Lastly, the servos were installed, control surfaces were attached, and Monokote skin was applied. The tail structure is shown in Figure 29.
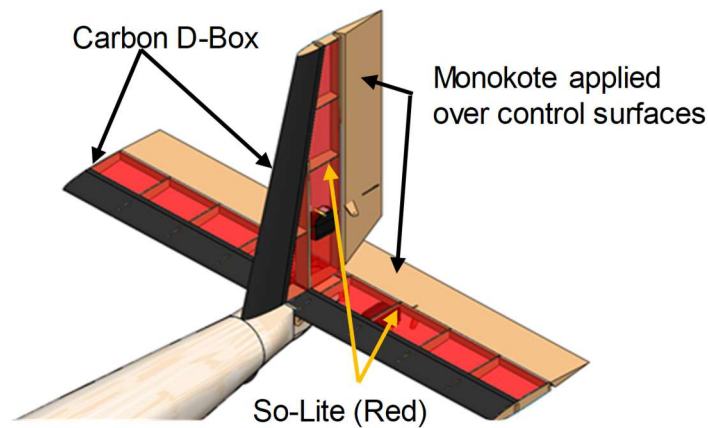


**Figure 29: Balsa built-up tail and mounting ribs.**

### 6.2.2 FUSELAGE STRUCTURE

A foam buck was manufactured by hotwiring out the general shape of the fuselage and then sanding it down to the correct geometry. The buck was then cut along the vertical centerline and the two halves were used to make female molds. The female molds were created by using flash breaker tape to cover the foam, thoroughly waxing the taped surface, and then applying many layers of fiberglass over the buck. Once

cured, the female molds were sanded to have a uniformly smooth surface. The fuselage was made in two halves then joined once they cured. For each half of the fuselage layup, the outer composite face sheets were placed in the female mold and then 1/16 in. sheets of balsa core material were placed over it. Next, plywood hardpoints were mounted using epoxy and the inner composite face sheets were placed in the molds, vacuumed, and left to cure. The halves were taken out of the mold, trimmed, and joined together using two plies of carbon fiber at the seam. The motor mount was then installed with epoxy and additional carbon plies were laid up around it. Lastly, the top hatch was fixed into place and holes were drilled through the skin to mount the wing, banner release mechanism, and tail. A prototype is shown in Figure 30.
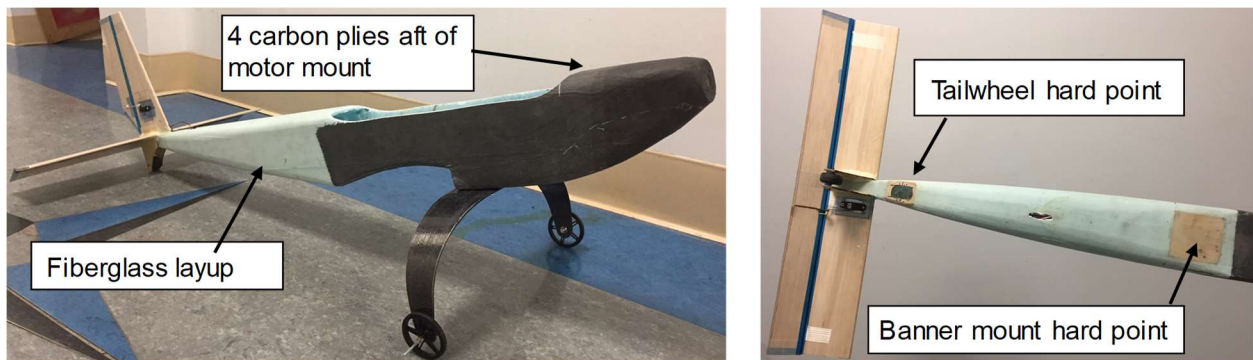


**Figure 30: Prototype fuselage.**

*6.2.3 LANDING GEAR*

The landing gear was manufactured using a carbon fiber wet layup. A mold was cut from foam using a hotwire and laser-cut templates. 14 unidirectional, 1 strip woven at 90°, and 4 strips woven at 45° were laid up onto the mold and cured under vacuum. Once cured, the desired shape was cut with a rotary tool and sanded to shape. Finally, axle and mounting holes were drilled. The axles were held in place with locking hex nuts, and the wheels were held on the axles with collars. The bow bolted to a plywood bulkhead under the fuselage with 1/4 in. nylon bolts designed to shear off on a "crash landing" where greater than 50% of the load is perpendicular to the bow strut. The bow is shown in Figure 31.
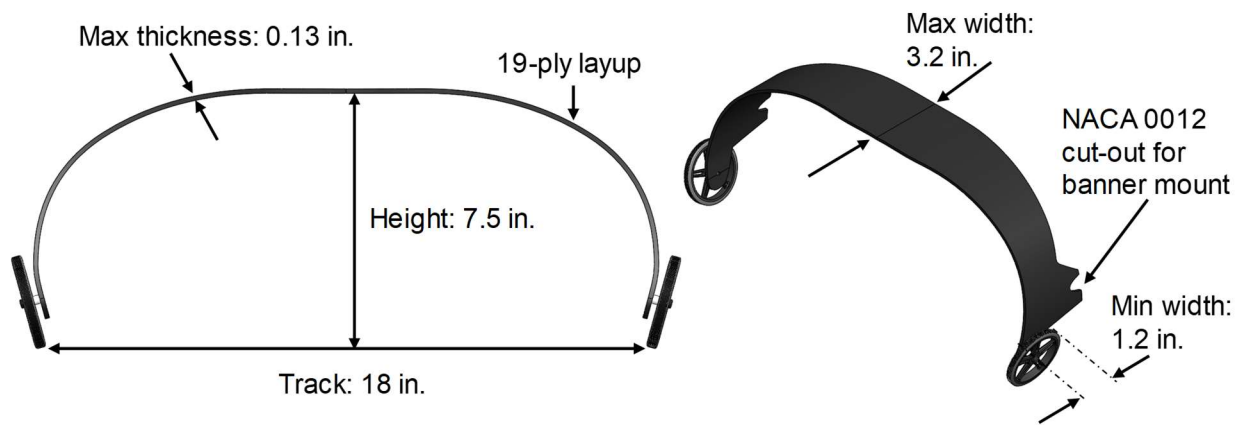


**Figure 31: Bow gear dimensions.**

### 6.2.4 PASSENGERS

The passengers were 3D printed using PETG plastic. Steel washers were epoxied into the base to increase weight to 4 oz. The same process was used with luggage. A prototype passenger is shown in Figure 32.
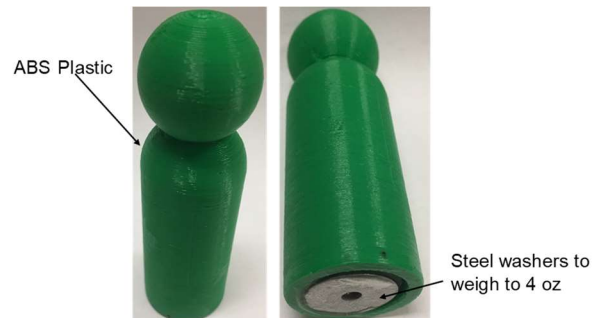


**Figure 32: Prototype passengers. Luggage blocks were manufactured using the same techniques.**

### 6.2.5 PASSENGER RESTRAINT SYSTEM

The restraint system had two components and was made of laser-cut 1/16 in. aircraft plywood. The first component was a grid-like system that restrained each passenger at the base. The second component was a laser-cut head restraint that connected to the fuselage hatch. The restraint is shown in Figure 23.

### 6.2.6 BANNER AND DEPLOY-RELEASE MECHANISM

The banner was made of low-density (0.9 g/cm$^3$) polyethylene sheeting (LDPE) and was mounted between carbon leading and trailing edges. LDPE was found to produce the lowest drag when compared to other tested materials as shown in Section 8.1.1. The banner leading and trailing edges were made of carbon fiber and combined to form a NACA 0012 profile. The banner leading edge was designed to rest in the aft portion of the carbon bow gear as shown in Figure 31, and the banner trailing edge was secured in the stowed position by two 1/8 inch aircraft plywood arms that swung back when the banner was released with a servo. The banner trailing edge was designed to serve as a drag element to reduce banner flapping, which in turn would reduce total drag. The deploy-release mechanism is shown in Figure 33.
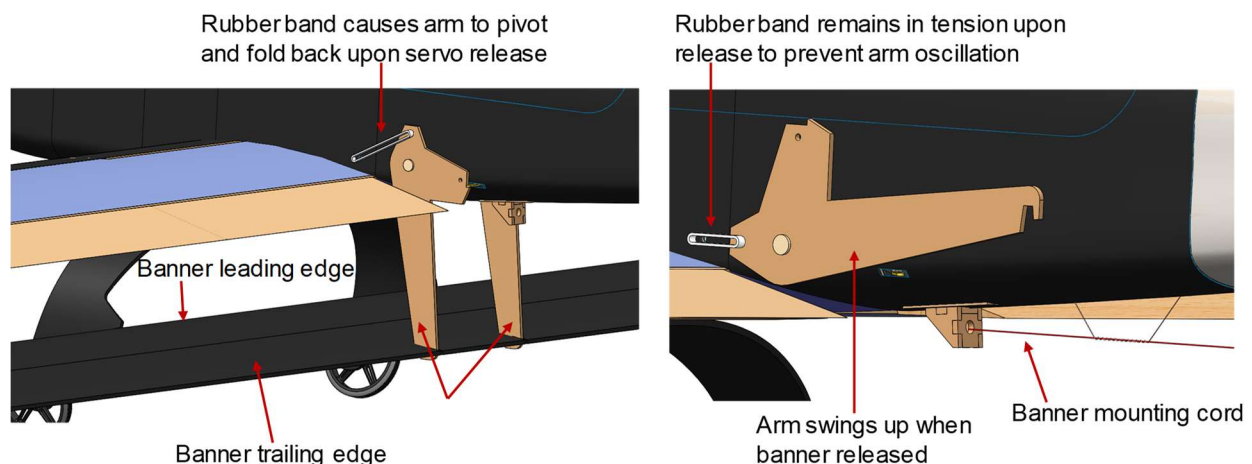


**Figure 33: Banner deploy-release mechanism.**

## 6.3 MANUFACTURING MILESTONES

A manufacturing milestone chart was prepared so the team would remain on schedule and coordinate build between different sub-teams. Although the plan in Figure 34 only depicts the schedule for aircraft prototype #2, the same scheduling was implemented for the construction of other prototype airplanes and the competition aircraft. Lessons learned in the development of this aircraft were incorporated into the schedule for the competition build. As shown, build and assembly required upwards of four weeks so that high quality parts could be produced. Simultaneous lab testing was conducted on the wing, tail, and fuselage, as detailed in Section 7.0 to ensure the aircraft would meet all load requirements once fully integrated.
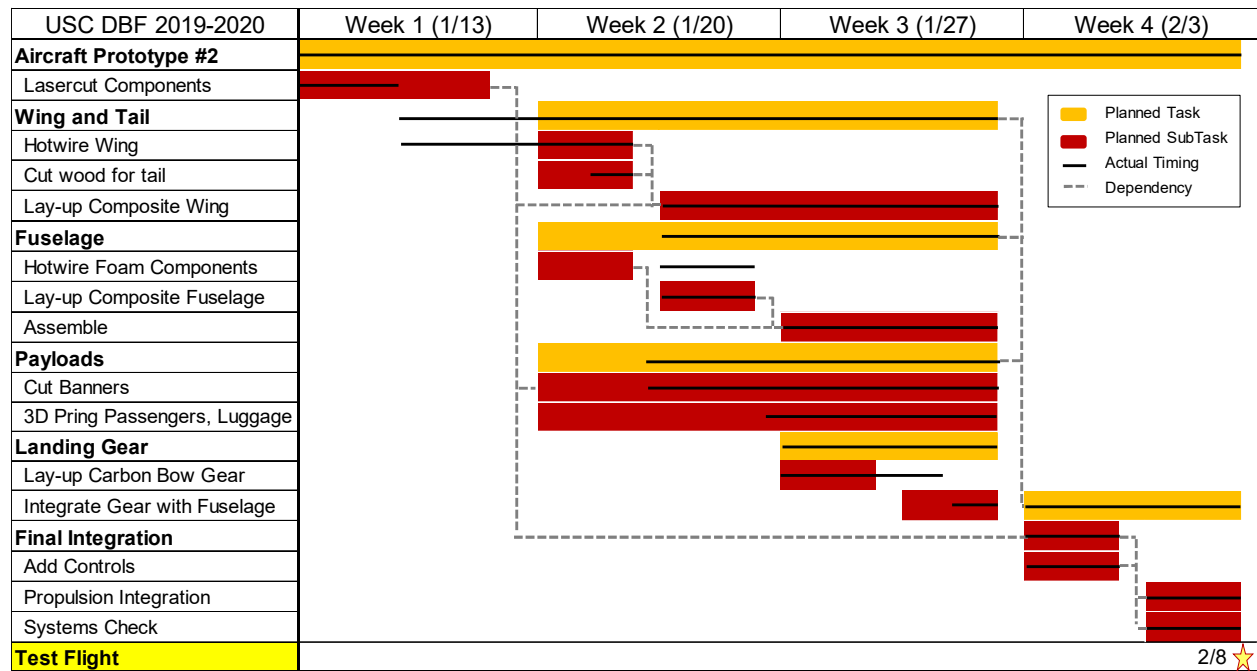


**Figure 34: Aircraft manufacturing milestone chart. Note that planned and actual timing is shown.**

## 7.0 TESTING PLAN

A test plan was implemented to verify aerodynamics, stability and control, structures, landing gear, and payloads predictions and inform future design decisions. The team took experimental data in the laboratory and at test flights. Testing began during the conceptual design phase and continued into the preliminary and critical design phases. The test schedule is presented in Figure 35 and detailed in Sections 7.1 – 7.4.

| Test Plan 2019-2020 | Sept. | Oct. | Nov. | Dec. | Jan. | Feb. | Mar. | Apr. |
|---|---|---|---|---|---|---|---|---|
| **Subsystem Testing** | | | | | | | | |
| Banner Drag | | | | | | | | |
| Battery Pack | | | | | | | | |
| Motor/Propeller | | | | | | | | |
| Wing Load | | | | | | | | |
| Fuselage | | | | | | | | |
| Payload Storage, Banner | | | | | | | | |
| **Flight Testing** | | | | | | | | |
| Proof of Concept Flight | | | | | | | | |
| Preliminary Design Flight | | | | | | | | |
| Detailed Design Flight | | | | | | | | |
| Competition Trim | | | | | | | | |
| **Competition** | | | | | | | | 4/16-4/19 ⭐ |

Legend: 🟨 Planned Task  🟥 Planned Subtask  — Actual Timing
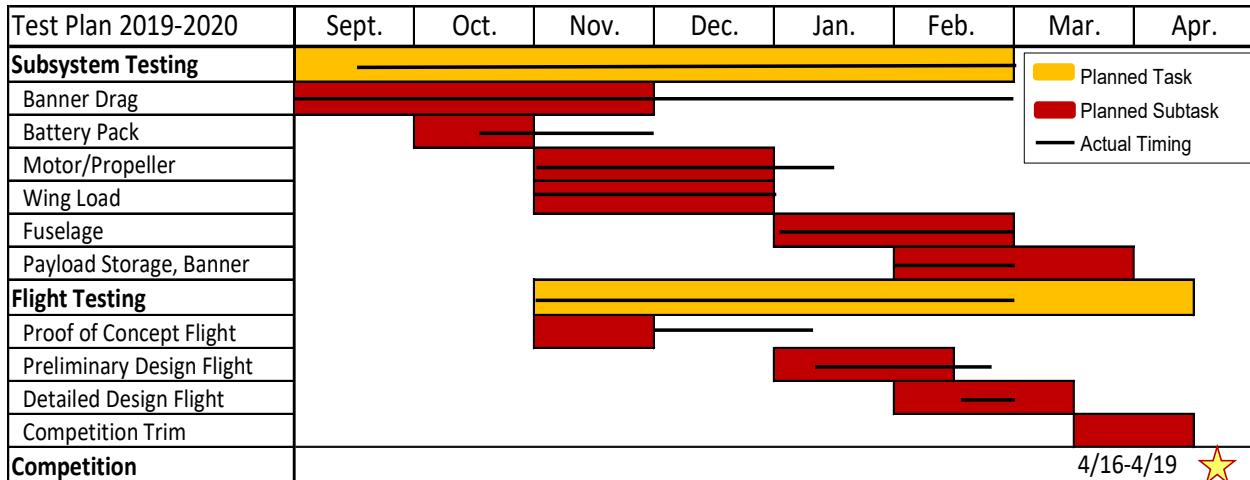
**Figure 35: Test plan for the 2019-2020 competition year.**

## 7.1 TEST OBJECTIVES

Tests for each sub-team were conducted to ensure that the designed components met all competition and design requirements.

Aerodynamics

- Banner testing (both on-ground and in-flight) was used to determine the geometries and drag reduction techniques that minimized banner drag. On-ground testing consisted of tugging a banner outside the wake of a pickup truck. In-flight testing consisted of flying a banner behind the aircraft.
- Flight tests confirmed AVL and XFLR5 predictions for aircraft lift, drag, and stability characteristics.
- Pilot feedback was used to verify that aircraft stability characteristics were acceptable.

Propulsion

- Lab testing was conducted using a battery tester to characterize battery discharge performance.
- Static and dynamic tests were used to verify expected current, voltage, thrust, and endurance.

Performance

- Flight tests were conducted to validate performance predictions provided by PlaneTools including takeoff field length, cruise speed, lap times, and endurance.

Payloads

- The ground crew tested passengers, luggage, and their restraints that would minimize loading and unloading times. Banner loading and release were also tested to minimize loading time.
- The banner storage mechanism was tested in flight to ensure the banner would not release until commanded by the pilot.
- The banner deploy-and-release mechanism was first tested in lab. Once the system worked as expected, it was tested in-flight to ensure it still functioned in flight.

Structures

- Wingtip tests were performed at maximum takeoff weight to simulate technical inspection.

- Failure points and deflections predicted in SparSizer were validated through wing loading tests.

- In-lab load testing was conducted to ensure the fuselage could withstand maximum design loads.

Landing Gear

- Drop tests with high-speed video were conducted to simulate a 2.5 g landing.

- Ground handling tests ensured that the aircraft would track straight for takeoff and landing.

## 7.2 SUBSYSTEM TESTING

### 7.2.1 AERODYNAMIC TESTING

*Banner Drag – Truck Testing*

Aerodynamic testing was conducted to measure and understand banner drag. Test variables included the banner length ($l_b$), banner aspect ratio ($\mathrm{AR}_b$), and freestream velocity ($V_\infty$). This data was processed into a model for the banner drag coefficient vs. banner Reynolds number, $C_d$ vs. $\mathrm{Re}_b$, as shown in Figure 43 in Section 8.1.1. This model was then implemented into PlaneTools for mission simulation and sizing efforts. Additional test variables included banner material density and rigidity, and various drag reduction methods such as attaching streamers to the end of the banner.

Testing began with a pickup truck that towed a banner while driving on a dry lakebed (El Mirage, CA). Truck testing was used instead of a wind tunnel so that the banner Reynolds number would be representative of expected flight conditions. The pickup truck test setup is shown in Figure 36; a load cell was used to measure the drag force directly while the truck maintained constant speed.



**Figure 36: Banner test setup. The testing rig is shown on the left, and a representative data run is shown on the right. The rig was mounted one truck width away to be isolated from the truck wake.**

Inviscid steady-state computational fluid dynamic (CFD) analysis was also conducted to ensure the banner and test rig would be isolated from the truck wake during testing; these results are shown in Figure 37.
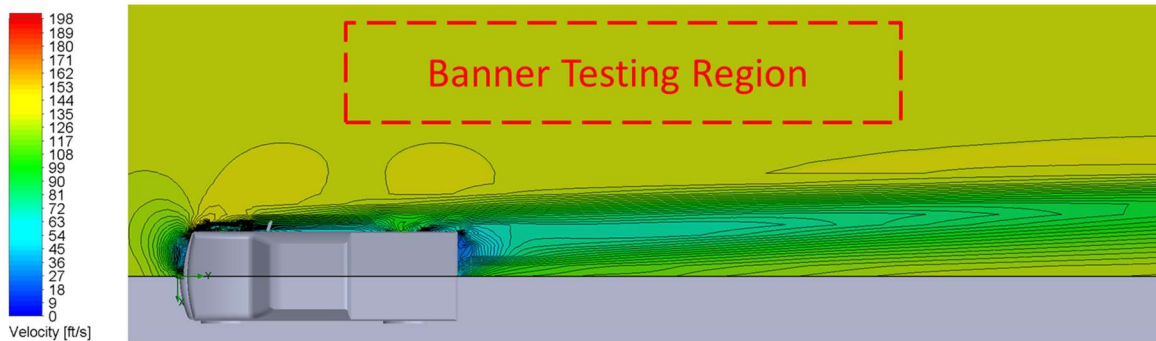
**Figure 37: CFD analysis of the truck wake. The banner was tested in the red boxed region.**

*Banner Drag – Flight Testing*

Flight tests with the banner attached to an aircraft were conducted to determine how in-flight banner drag measurements differed compared to the truck testing environment. These tests allowed the team to confirm there were no adverse effects on flight dynamics due to the banner, and to validate propulsion performance estimates with the additional drag due to the banner. A test aircraft was used to tow banners while early *SCkyfall* prototypes were still being manufactured. Drag was measured using an S-Cell strain gauge, shown in Figure 38. Test variables included cruise speed, banner length, and with/without streamers attached to the end of the banner. Flight test results ($C_d$ vs. $\mathrm{Re}_b$) are presented and compared to the truck test data in Figure 45 and Figure 46 (Section 8.1.1).



**Figure 38: Strain gauge mounted on the test aircraft for banner flight tests.**

*7.2.2 PROPULSION TESTING*

Propulsion testing had two primary objectives. The first objective was to characterize the performance of the selected batteries. The second objective was to validate PlaneTools predictions of each propulsion package to select the highest scoring configuration. Battery testing was conducted using the West Mountain Radio Battery Tester, which draws user-specified currents and logs the voltage of the battery packs throughout the test [14]. The propulsion sub-team built, charged, and discharged various battery packs to test at the expected cruise currents. This was to ensure that the capacities of the selected batteries were sufficient for each mission's objectives. Plots of voltage versus time and current versus time allowed the team to determine an expected flight time for each package and its respective mission. Testing was also

conducted at currents of 100 A to account for the maximum static current draw experienced at takeoff. While the expected static currents were approximately 85 A, this testing was conducted to ensure that there were no significant voltage drops or damage to the batteries at the expected current range of 80-100 A. Testing demonstrated that the batteries could withstand 80 A current. There were no losses in voltage or capacity, so the team concluded that the battery packs could endure the maximum expected current draw. However, thicker wires and higher-current connecters were needed compared to wires and connectors of past years. The testing apparatus is shown in Figure 39.
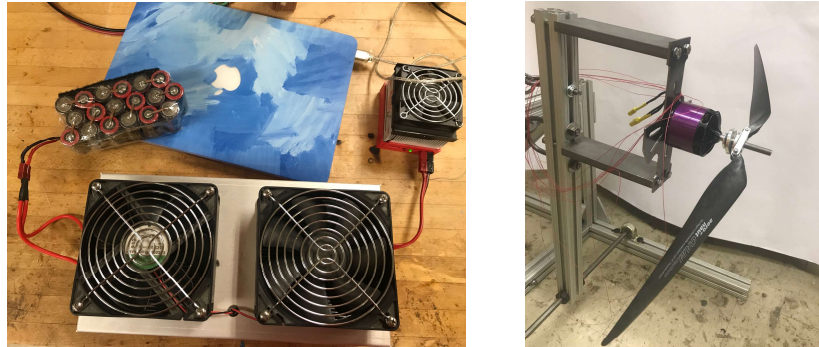


**Figure 39: Battery tester (left) and lab-built thrust stand for propulsion system testing (right).**

Static motor testing was done using a team – built thrust stand, shown in Figure 39, designed to handle loads up to 100lb. The thrust stand allowed the team to test the full-scale propulsion system and confirm battery output, current, and thrust predictions. A secondary objective of motor testing was to compare measured performance to theoretical PlaneTools and eCalc predictions.

### 7.2.3 STRUCTURAL TESTING

Structural testing was conducted to validate the analysis performed in the detailed design phase. To test the wing strength, the wing root was firmly mounted to a representative fuselage section and then clamped to the edge of a tabletop. Weights were then placed on the wing surface to model an elliptical lift distribution. The test was carried out until structural failure. The test setup and results are shown in Figure 40.



The foam core crushed, causing carbon spar cap to collapse. The spar cap did not delaminate

Wing was modelled as a cantilevered beam. Weights used to simulate elliptical loading
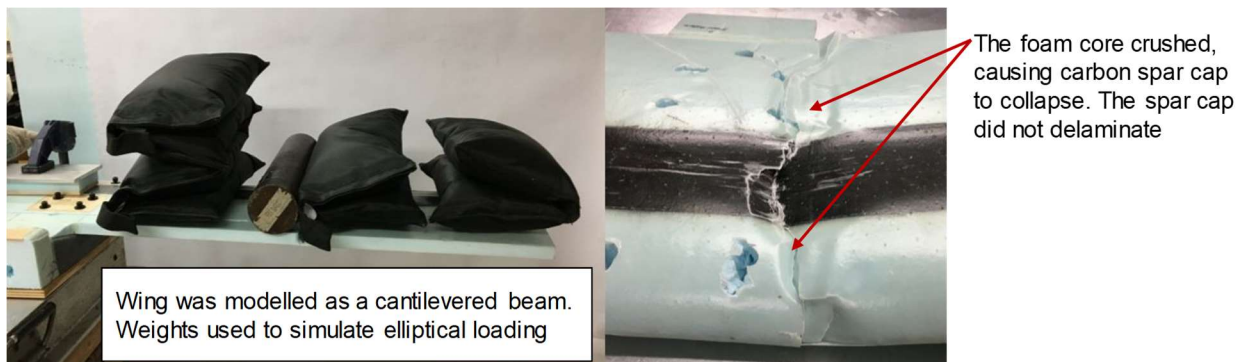
**Figure 40: Elliptical wing loading testing.**

The fuselage was tested to withstand the expected motor thrust and torque loads. To simulate thrust from the motor, a fish scale was attached to the motor shaft and a pulling force of 33 lb, equivalent to the expected maximum static thrust with a 1.5 safety factor, was applied. The expected motor torque of 24.5 lb-in. with an additional 1.5 safety factor was simulated by attaching a plywood plate and rod to the motor mount and hanging weights from the end of the rod to generate a torque. These tests are shown in Figure 41.



**Figure 41: Simulated testing of motor thrust (left) and torque (right).**

### 7.2.4 LANDING GEAR TESTING

The landing gear was tested for taxiing and landing loads. With a proper CG, a test mule fitted with the gear was run up to $V_{stall}$ to ensure the gear tracked straight enough to take off without nosing over. To test the landing load condition, a drop test was performed. A drop height of 3 in. was determined to be equivalent to a 2.5 g landing at maximum weight. The landing test setup is shown in Figure 42.
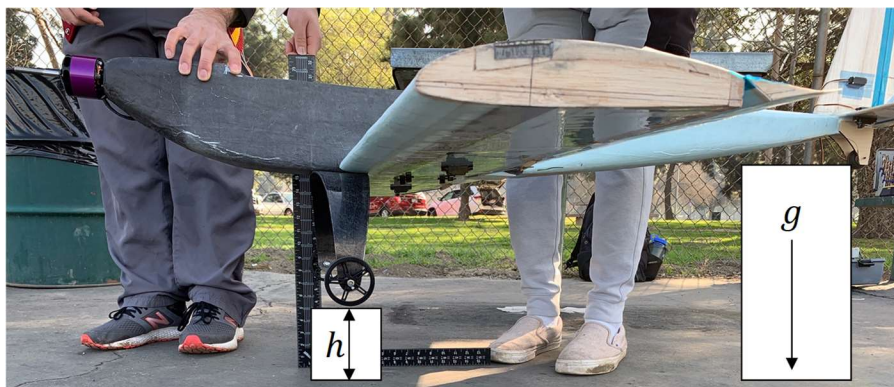


**Figure 42: Landing drop test setup.**

## 7.3 FLIGHT TEST SCHEDULE AND FLIGHT PLAN

Tests flights played an important role to validate our design of the aircraft. Post-flight pilot comments allowed to team to determine the aircraft stability, pilot workload, and flight performance at various throttle settings, control inputs, payload amounts, banner sizes and materials, and battery capacities. Flight data was collected through an integrated sensor package that measured airspeed, altitude, g-loads, rotation

rates, ground speed, position, and heading. Propulsion data was collected through a data logging ESC that measured voltage, current, RPM, and throttle position.

The flight test schedule and objectives are displayed in Table 24. Each flight test had explicit design objectives that were used to incrementally validate the effectiveness of all aircraft subsystems. Flight test objectives that were not met were reattempted in subsequent tests. Note that there are upcoming flight tests planned for February 23, March 1, March 8, and April 5.

**Table 24: Flight Test Schedule.**

| Date | Location | Objectives |
|---|---|---|
| Dec 14, 2019 | Whittier Narrows, South El Monte, CA | Determine stability effects of banner, measure drag on banners of various sizes, test banner release mechanism in flight |
| Jan 26, 2020 | Whittier Narrows, South El Monte, CA | Simulate effect of M2 payloads, measure drag of various banners, determine in-flight performance, validate propulsion |
| Feb 1, 2020 | Whittier Narrows, South El Monte, CA | Measure drag on various banners |
| Feb 8, 2020 | Whittier Narrows, South El Monte, CA | Measure drag on various banners |
| Feb 16, 2020 | Sepulveda Basin, Van Nuys, CA | Test performance at various throttle settings |
| Feb 23, 2020 | Sepulveda Basin, Van Nuys, CA | M3 simulation, test banner deploy/release mechanism |
| Mar 1, 2020 | Sepulveda Basin, Van Nuys, CA | M2/M3 Simulation |
| Mar 8, 2020 | Sepulveda Basin, Van Nuys, CA | M2/M3 simulation, validate improvements |
| Apr 5, 2020 | Sepulveda Basin, Van Nuys, CA | Trim competition aircraft |

Each flight test was separated into specific objectives, which included the acceptance criteria to ensure all objectives were met. A sample plan from the Dec. 14, 2019 flight test is shown in Table 25.

**Table 25: Dec. 14, 2019 flight test plan.**

| Flight # | Flight Name | Payloads | Objectives | Acceptance Criteria |
|---|---|---|---|---|
| 1 | Trim Flight | None | Trim aircraft | Aircraft trimmed for level flight; nominal data from sensor package |
| 2 | Banner #5 | Banner #5 (Length: 93 in.) | Assess banner drag, stability characteristics | Banner remains vertical and fully deployed; banner is cutoff before landing |
| 3 | Banner #15 | Banner #15 (Length: 75 in.) | Assess banner drag, stability characteristics | Banner remains vertical and fully deployed; banner is cutoff before landing |
| 4 | Banner #27 | Banner #27 (Length 139 in.) | Assess banner drag, stability characteristics | Banner remains vertical and fully deployed; banner is cutoff before landing |

## 7.4 FLIGHT CHECKLISTS

The team adhered to a pre-flight checklist (Table 26) before each flight to ensure efficiency, proper data acquisition, and team safety. It also served as a final flight go or no-go evaluation criterion from the pilot.

The on-site inspections checklist (Table 27) was used before and after each flight to ensure aircraft and crew safety. The inspection of each category of components allowed for the systematic division of duties for aircraft inspection, discrepancy noting, and maintenance if necessary.

**Table 26: Pre-flight checklist.**

| Component | Task |
|---|---|
| **Fuselage (Internal)** | ☐ Secure and connect the fully charged battery<br>☐ Receiver has all connections plugged in and secured<br>☐ CG aircraft<br>☐ Load passengers and cargo (if applicable) |
| **Fuselage (External)** | ☐ Close and secure all external hatches<br>☐ Arm banner deploy and release mechanisms (if applicable) |
| **Pilot's Checks** | ☐ Check all control surfaces with receiver<br>☐ Motor run-up<br>☐ Go/No-Go decision |

**Table 27: Aircraft inspection checklist.**

| Component | Task | Discrepancies |
|---|---|---|
| **Motor** | ☐ Secure motor mount and fasteners<br>☐ Fuselage around motor mount is free of cracks or fractures<br>☐ Motor is free of damage and debris<br>☐ Propeller is fastened to shaft properly<br>☐ Propeller is free of damage and balanced | |
| **Fuselage** | ☐ Battery is secured to fuselage and connected properly<br>☐ Speed controller is secure and connected<br>☐ Receiver is secure and has all servos connected properly<br>☐ Servo wires are all secure<br>☐ Fuselage is secured and free of debris<br>☐ Fuse connectors secured (internal and external)<br>☐ Banner deploy and release mechanism operational (M3)<br>☐ Banner deploy and release mechanism armed (M3) | |
| **Wing** | ☐ Wings are free of tears, cracks, and fractures<br>☐ Servo arms are secure with minimal play<br>☐ Control surfaces are secure and free of obstructions<br>☐ Fuselage around wing mount is free of cracks and fractures<br>☐ Wing is securely mounted to fuselage | |
| **Landing Gear** | ☐ Wheels spin freely and are secure<br>☐ Torsional rigidity of gear<br>☐ Landing gear mounted securely<br>☐ Fuselage is free of cracks and fractures around mount | |
| **Tail** | ☐ Servo arms are secure<br>☐ Tail is free of tears, cracks, and fractures<br>☐ Tail is securely mounted to tail boom | |
| **Control Surfaces** | ☐ Check all control surface motion using transmitter<br>☐ Control surfaces move freely without obstruction | |

## 8.0 PERFORMANCE RESULTS

Predictions made during the Detailed Design phase were compared to aircraft subsystem performance. Key systems were tested in lab and during flight tests to ensure each component performed as predicted.

### 8.1 DEMONSTRATED PERFORMANCE OF KEY SUBSYSTEMS

#### 8.1.1 AERODYNAMICS

*Banner Drag – Truck Testing*

A banner drag test matrix was developed to evaluate the effects of banner length, aspect ratio, banner material on the drag force produced. Truck test results using a LDPE plastic sheet (Figure 43) show that banner drag coefficient ($C_d$) decreases with increasing banner Reynolds number ($\text{Re}_b$), as expected based on literature from [15]. A wide range of Reynolds numbers were tested since a target banner length had not been established at the time; however, the current target "Design Region" ($\text{Re}_b \sim 10^7$) is highlighted on the chart. A sample of uncertainty estimates ($\Delta C_d$) based on the raw data are presented across the range of Reynolds numbers tested, showing a trend of reduced uncertainty magnitude with increasing $\text{Re}_b$. A turbulent boundary layer "flat plate" drag coefficient model is also displayed [16]. This represents the ideal banner drag scenario and was used to anchor the truck testing model at sufficiently high $\text{Re}_b$ ($\sim 10^7$).
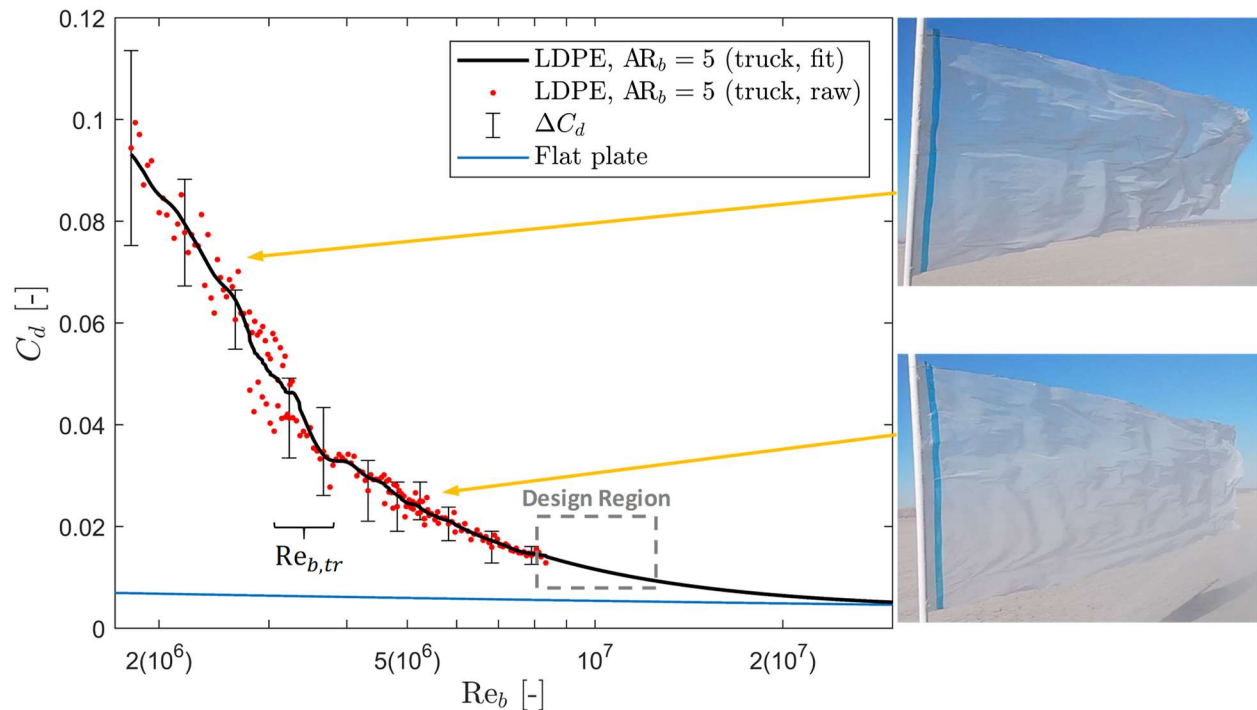


**Figure 43: Banner drag measured during truck testing using a plastic (LDPE) material, $\text{AR}_b = 5$.**

In the Design Region, the predicted banner $C_d$ is on the order of $0.02 - 0.1$ while Prandtl's flat plate skin friction model predicts $C_d$ on the order of ~0.005. The higher $C_d$ for an LDPE plastic sheet is a result of the banner flapping, which can be seen in the images included with Figure 43. For this material, a steep

transition in $C_d$ exists near $\text{Re}_{b,tr} \approx 3 * 10^5$. For $\text{Re}_b < \text{Re}_{b,tr}$, the banner oscillations were observed to have relatively lower frequency but higher amplitude, while $\text{Re}_b > \text{Re}_{b,tr}$ oscillations were higher in frequency but lower in amplitude. The higher amplitude motions correspond to more energy dissipation and thus more drag, while lower amplitudes correspond to lower energy dissipation and drag [15]. This trend indicates the banner should be designed for the highest possible banner Reynolds number ($\text{Re}_b$).

Further testing was conducted to determine the effect of varying $\text{AR}_b$ and banner material. The leftmost plot in Figure 44 shows there is no significant difference in $C_d$ at the same $\text{Re}_b$ when $\text{AR}_b$ was varied between 3 and 5; LDPE plastic sheeting was used for both tests. However, $\text{AR}_b = 5$ was selected for the design since this minimized the banner area for a given length, which in turn minimized banner drag.
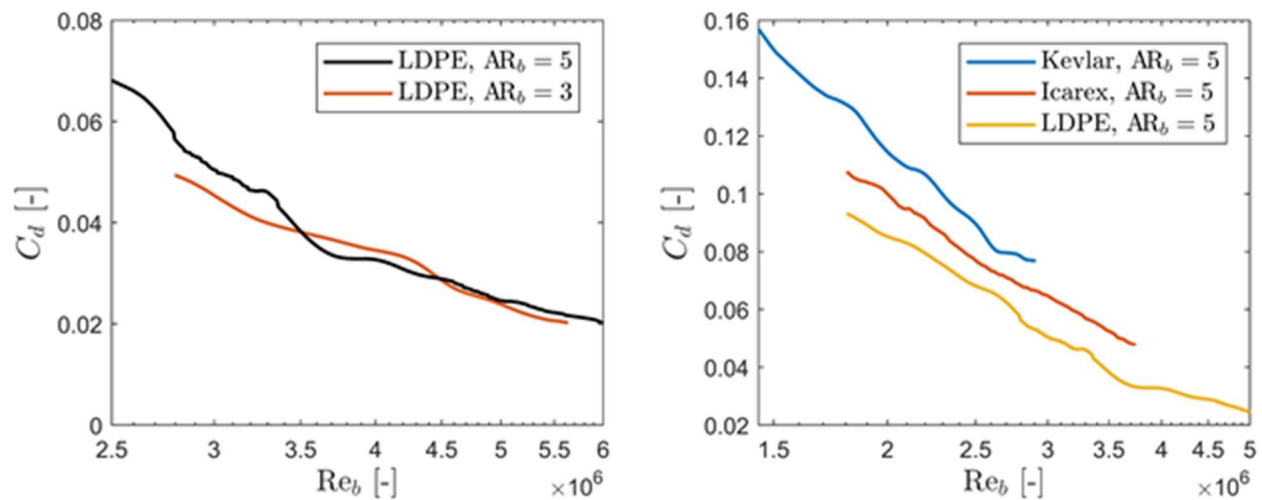


**Figure 44: Banner drag as a function of $\text{AR}_b$ (left) and material (right; for constant area and $\text{AR}_b$).**

The rightmost plot in Figure 44 shows the LDPE plastic sheeting resulted in the lowest $C_d$ of the three materials tested: LDPE, Kevlar and Icarex (airtight polyester). LDPE plastic sheeting also showed no signs of damage due to aerodynamic loads during the test, so this material was selected for the final design and used during subsequent flight tests.

*Banner Drag – Flight Testing*

Analysis done during the truck testing phase indicated that the optimal $\text{Re}_b$ was out of the bounds tested. Flight tests were performed to determine the optimal banner length, validate in-flight propulsion estimates with the banner attached, and to ensure there were no adverse effects on stability and control. In addition, tests were performed to include the current Design Region since truck testing did not cover this $\text{Re}_b$ range. A slightly over-powered aircraft was assembled and used for these test flights while this year's aircraft (*SCkyfall*) was being designed and manufactured.

Results from flight testing are shown in Figure 45 along with the $C_d$ vs. $\text{Re}_b$ model produced after the truck tests. Flight tests were conducted using five LDPE plastic banners with lengths ($l_b$) ranging from 140 in. to

410 in., all with $AR_b = 5$. A range of cruise speeds were used which provided $C_d$ measurements across the range $Re_b \approx 4 * 10^6$ to $12 * 10^6$. The flight and truck tests data sets show a similar trend and magnitudes near the current Design Region. Flight test data showed the transition Reynolds number increased to nearly $Re_{b,tr} \approx 5 * 10^6$, but fortunately this occurred before the Design Region.
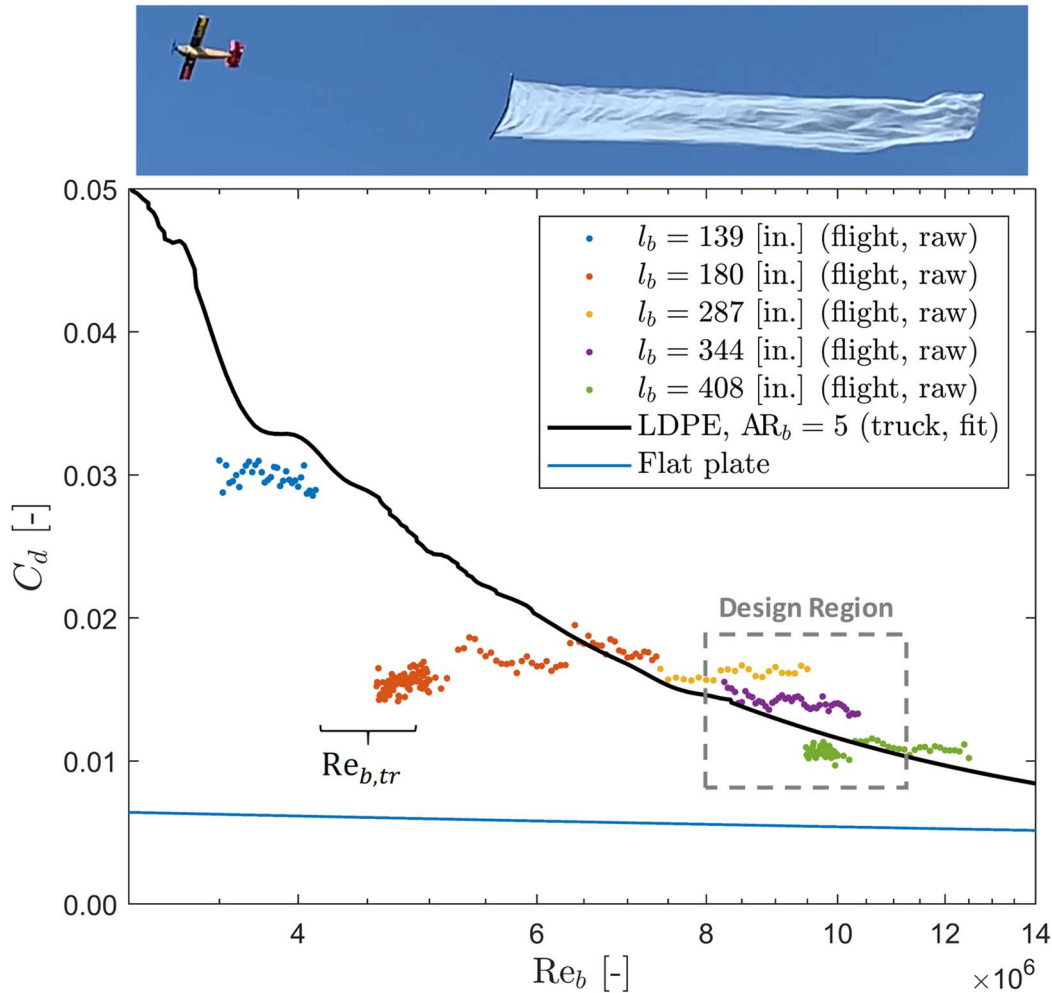


**Figure 45: Banner drag measured during flight test.**

As a final investigation, trailing-edge streamers were added to a banner to see if $C_d$ could be further reduced in flight. One $AR_b = 5$ LDPE banner was tested at a fixed $Re_b$; results presented in Figure 46 show a 15% reduction in $C_d$ with streamers. This test program will be expanded to cover $Re_b$ values in the current Design Region and additional banner drag reduction techniques will be explored before the competition.
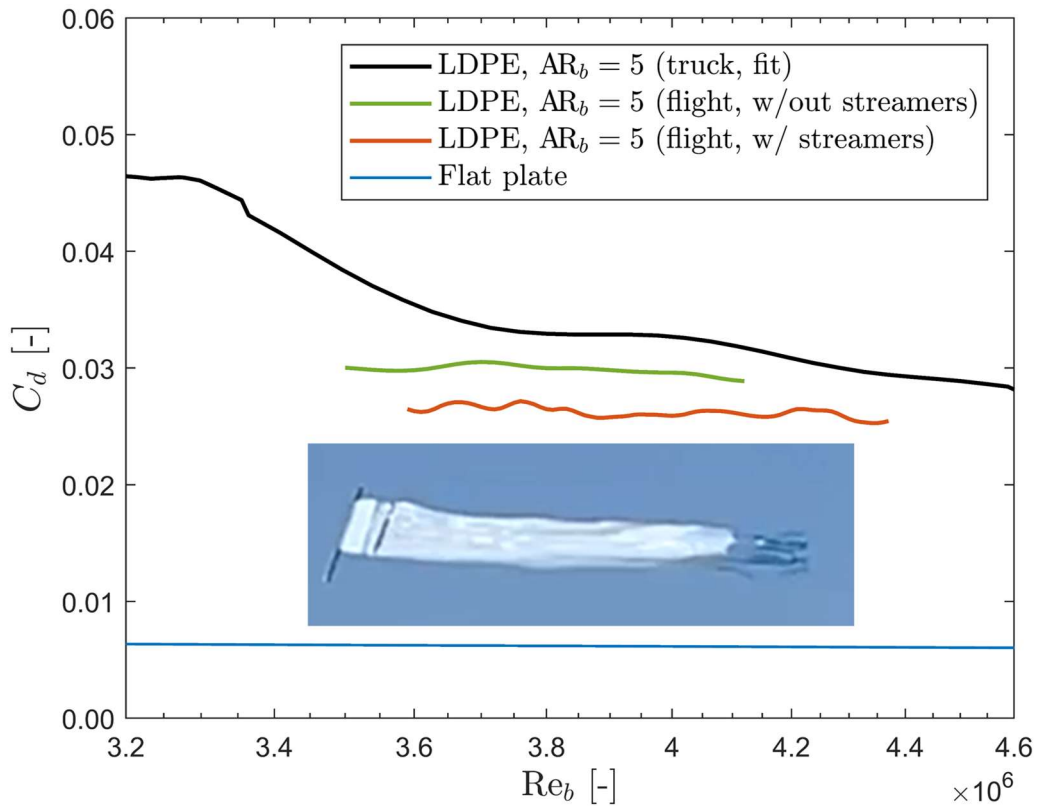
**Figure 46: Trailing-edge streamers reduce banner drag by 15%.**

The test results demonstrated that adding streamers reduced banner drag by 15%. More banner drag reduction techniques will be explored before the competition date in April.

*8.1.2 PROPULSION*

*Discharge Testing*

Battery testing was conducted to characterize the performance of each battery pack to ensure the propulsion system would be capable of completing each mission at the expected cruise current. Turnigy LiPo 2200 mAh cells were used on Mission 2 for a flight duration of 2.5 min while Turnigy LiPo 4500 mAh batteries were used for Mission 3 with a flight duration of 10 min. The battery discharge was performed at 4 A, which was comparable to the current calculated by eCalc. Test results are shown in Figure 47.
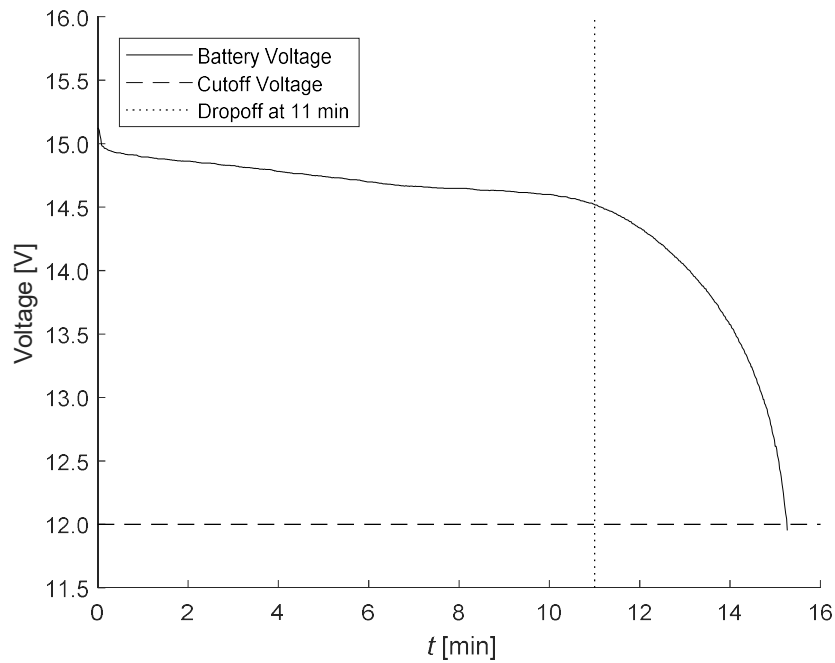
**Figure 47: Battery dropoff testing at 4 A.**

Preliminary battery analysis compared measured Turnigy battery voltage decay to dropoff estimates from eCalc. The voltage began to drop off at 11 min, while eCalc predicted the same dropoff at 10.4 min. The Mission 3 propulsion system was therefore shown to have more conservative endurance.

*Static Testing*

Static tests were conducted with Mission 1, Mission 2 and Mission 3 propulsion packages. Results, displayed in Table 28 and Table 29, show that the LiPo batteries produced more voltage than predicted.

**Table 28: Static thrust testing results.**

| Value | Turnigy 3000 mAh eCalc Prediction | Turnigy 3000 mAh Static Test | Turnigy 4500 mAh eCalc Prediction | Turnigy 4500 mAh Static Test |
|---|---|---|---|---|
| RPM | 5530 | 5600 | 5700 | 6100 |
| Thrust [lb] | 12.0 | 10.5 | 17.6 | 16.3 |
| Current [A] | 89.0 | 110.2 | 80.0 | 79.6 |
| Voltage [V] | 25.2 | 24.2 | 25.2 | 24.4 |

**Table 29: Turnigy 3000 mAh and Turnigy 4500 mAh flight test result.**

| Hacker A60-5S V4 | Turnigy 3000 mAh (6S2P) | Turnigy 4500 mAh (6S2P) |
|---|---|---|
| Propeller | Aeronaut 18.5x15 in. 5° twist | Aeronaut 20x12 in. |
| Static Curent, $I_{max}$[A] | 88.4 | 80.0 |
| Static Thrust [lbf] | 22.0 | 18.3 |
| Cruise Current, $I_{crz}$ [A] | 80.2 | 76.2 |
| Dynamic RPM | 5400 | 5600 |
| Cruise Speed [ft/s] | 140 | 60 |
| Battery Pack Weight [lb] | 2.2 | 3.3 |

*Flight Testing*

Propulsion data acquired during flight testing of various banners was used to correlate $N_{Laps}$ on Mission 3 with $l_b$. This data was used to plot $Score_{M_3}$ against $N_{Laps}$. Results are shown in Figure 48.
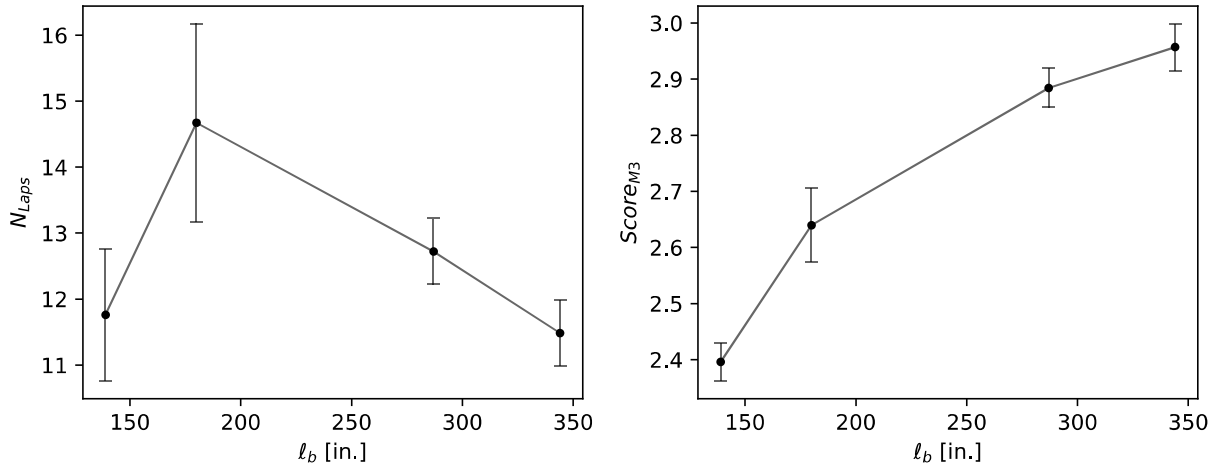


**Figure 48: $N_{Laps}$ and $Score_{M_3}$ as functions of $l_b$ using flight test data.**

Flight test results indicated that increased $l_b$ was a higher priority than increased $N_{Laps}$ on Mission 3. These results are consistent with BFEA findings in Section 3.2.1. However, flight testing indicated that flying a 344 in. (8.7 m) banner would yield a higher score than the 300 in. (7.6 m) banner identified by BFEA. Longer banner lengths will be explored in flight tests leading up to the competition date in April.

*8.1.3 STRUCTURES*

The results of the structural tests performed in Section 7.2.3 are shown in Table 30. Each component failed at a load greater than it was designed to withstand.

**Table 30: Results of structural testing.**

|  | Designed Load | Tested Load |
|---|---|---|
| **Wing Bending Moment [lb-in.]** | 2025 | 2210 |
| **Motor Thrust [lb]** | 33 | 33 |
| **Motor Torque [lb-in.]** | 36.8 | 36.8 |

## 8.2 DEMONSTRATED FLIGHT PERFORMANCE OF COMPLETED AIRCRAFT

Flight tests were used to validate aircraft performance predictions. The goal was to evaluate performance and capabilities of the detailed design aircraft. Each flight test had its own set of performance objectives. Table 31 summarizes flights to date and future test plans.

**Table 31: Aircraft performance evaluation.**

| Date | Description | Problems | Solutions |
|---|---|---|---|
| December 14, 2020 | Measure banner drag | Motor gearbox failure | Replace gearbox |
| January 26, 2020 | Simulate Mission 1-3; measure banner drag | High-speed elevator flutter; crash | Larger control horns; robust control surfaces |
| February 1, 2020 | Measure banner drag, validate TOFL | Motor gearbox failure | Switch to motor without gearbox |
| February 9, 2020 | Measure banner drag | - | - |

The primary purpose of previous flight tests was to measure banner drag and identify drag reduction techniques. A repeated issue with the overpowered test-plane was that the motor torque that resulted from flying the banner caused damage to multiple gearboxes. This was resolved on the February 9 test flight, when the motor sized for this year's competition, the Hacker A60-5S V4, was used. Upcoming test flights will be used for mission simulations and to evaluate performance predictions from PlaneTools. Performance data from previous test flights is compared to PlaneTools predictions in Table 32.

**Table 32: Comparison of predicted and in-flight performance parameters.**

| | Parameter | Predicted | Flown | Δ% |
|---|---|---|---|---|
| **Mission 1** | Flight Speed | 60 ft/s (18 m/s) | 75 ft/s (20 m/s) | +25 % |
| | Cruise Current | 14 A | 22 A | +57 % |
| **Mission 2** | Flight Speed | 140 ft/s (43 m/s) | 161 ft/s (49 m/s | +15 % |
| | Cruise Current | 88 A | 110 A | + 25 % |
| | $(T_{M2})_{USC}$ | 68 s | 73 s | + 7 % |
| **Mission 3** | Flight Speed | 50 ft/s (15 m/s) | 45 ft/ (14 m/s) | -10 % |
| | Cruise Current | 48 A | 55 A | +15 % |
| | $(N_{Laps})_{USC}$ | 12 | 10 | -17 % |
| **Ground Mission** | $(T_{GM})_{USC}$ | 100 | 110 | +10 % |

As shown in Table 32, flight speeds for Mission 1 and Mission 2 were approximately 25% faster than predicted, while the flight speed for Mission 3 was 10% lower than predicted, leading to a 17% reduction in $N_{Laps}$. Flight speed for Mission 3 is expected to increase as banner drag reduction techniques are improved in the weeks leading up to the competition date in April. Cruise currents are higher for all Missions by an average of 30%. This presents no issue on Mission 1 and Mission 2 since endurance is not an issue; cruise current is expected to drop on Mission 3 once banner drag is reduced. The Ground Mission time is expected to drop as the team gains more experience loading and unloading passengers with the prototype aircraft. The prototype aircraft will be flown on the February 22nd test flight.



**Figure 49: A *SCkyfall* prototype during Mission 2 simulation on the January 26, 2020 flight test.**

## 9.0 BIBLIOGRAPHY

[1]  AIAA, "2019-2020 DBF Rules," Reston, VA, 2019.

[2]  USC AeroDesign Team, "Aircraft Design Report, 2019 AIAA DBF Competition," 2019.

[3]  T. Yechout, Introduction to Aircraft Flight Mechanics, Reston, VA: AIAA, 2014.

[4]  D. Raymer, Aircraft Design: A Conceptual Aproach, Reston, VA: AIAA, 1999.

[5]  USC AeroDesign Team, "Aircraft Design Report, 2018 AIAA DBF Competition," 2018.

[6]  "Aeronaut Twisted Yokes and Effective Pitch," 2004. [Online]. Available:
https://www.rcgroups.com/forums/showthread.php?229672-Aeronaut-twisted-yokes-and-effective-
pitch/page2.

[7]  M. Drela, "XFOIL," MIT, 2013. [Online]. Available: http://web.mit.edu/drela/Public/web/xfoil.
[Accessed 13 Gebruary 2017].

[8]  M. Drela and H. Youngren, "AVL," web.mit.edu, 2017. [Online]. Available:
http://web.mit.edu/drela/Public/web/avl/.

[9]  S. Hoerner, "Fluid Dynamic Drag," Bakersfield, CA, 1965.

[10] "XFLR5," [Online]. Available: http://www.xflr5.com/xflr5.htm. [Accessed 2020].

[11] MIL-F-8785C, Flying Qualities of Piloted Planes, Military Specification, 1980.

[12] "SolidWorks," Dassault Systemes, [Online]. Available: https://www.solidworks.com/.

[13] Markforged, Inc., "THE MARK TWO," 2017. [Online]. Available: https://markforged.com/mark-two/.
[Accessed 13 January 2017].

[14] West Mountain Radio, "CBA IV - Computerized Battery Analyzer," 2017. [Online]. Available:
http://www.westmountainradio.com/product_info.php?products_id=cba4. [Accessed 20 January
2017].

[15] A. Carruthers and A. Fillipone, "Aerodynamic Drag of Streamers and Flags," AIAA, Reston, VA,
2012.

[16] F. M. White, Fluid Mechanics, 7th ed., New York: McGraw-Hill, 2011.

# TABLE OF CONTENTS

# LIST OF FIGURES

## LIST OF TABLES

# ACRONYMS AND NOMENCLATURE

| | | | | | |
|---|---|---|---|---|---|
| AIAA | – | American Institute of Aeronautics and Astronautics | S | – | Reference Area (ft$^2$) |
| DBF | – | Design Build Fly | $S_{wet_f}$ | – | Wetted Area of the Fuselage |
| CAD | – | Computer Aided Design | $A_{max}$ | – | Max Cross-Sectional Area |
| FON | – | Figure of Merit | $C_L$ | – | Coefficient of Lift |
| TMS | – | Total Mission Score | $\alpha$ | – | Angle of Attack (degrees) |
| LiPo | – | Lithium Polymer | $\beta$ | – | Sideslip Angle (degrees) |
| NiMH | – | Nickel Metal Hydride | $C_m$ | – | Aircraft Pitching Moment Coefficient |
| M1 | – | Mission 1 | $C_n$ | – | Aircraft Yawing Moment Coefficient |
| M2 | – | Mission 2 | L.E. | – | Leading Edge |
| M3 | – | Mission 3 | g | – | Gravitational Acceleration |
| GM | – | Ground Mission | $V_{NE}$ | – | Never Exceed Speed |
| psf | – | Pounds per Square Foot | ESC | – | Electronic Speed Controller |
| C.G. | – | Center of Gravity | ID | – | Inside Diameter |
| T.O. | – | Take Off | OD | – | Outside Diameter |
| $V_{max}$ | – | Max Velocity | FEA | – | Finite Element Analysis |
| Wh | – | Watt-hour | W | – | Weight (lb) |
| mAh | – | Milli-Amp-hour | $V_{min}$ | – | Minimum Velocity |
| Kv | – | Motor Velocity Constant | $V_{max}$ | – | Maximum Velocity |
| $c_l$ | – | Sectional Coefficient of Lift | fps | – | Feet per Second |
| $R_e$ | – | Reynolds Number | CA | – | Cyanoacrylate |
| AVL | – | Athena Vortex-Lattice | FRP | – | Fiber Reinforced Plastic |
| $C_{L, max}$ | – | Maximum Coefficient of Lift | CNC | – | Computer Numeric Control |
| OpenVSP | – | Open Vehicle Sketch Pad | RPM | – | Revolutions per Minute |
| $C_{D,0}$ | – | Zero-Lift Coefficient of Drag | GPS | – | Global Positioning System |
| $R_{wf}$ | – | Wing Fuselage Interference Factor | L' | – | Airfoil Thickness Location Factor |
| $S_{wet_w}$ | – | Wetted Area of the Wing | $t/c$ | – | Thickness to Chord Ratio |

# 1 EXECUTIVE SUMMARY

This report details the design, testing, and manufacturing of the Georgia Institute of Technology's entry in the 2019-2020 AIAA Design/Build/Fly (DBF) competition, *F-104 Buzzfighter*. Over the course of the competition year, the team designed, manufactured, and tested multiple prototypes to develop an aircraft that would successfully complete the four missions described by the rules.

## 1.1 Design Process

Conceptual design of the aircraft began with development of requirements through analysis of key mission requirements and scoring criteria. In the preliminary design phase, the aircraft dimensions and propulsion system were sized using constraint analysis of critical flight phases. In the detail design phase, aircraft dimensions were finalized, propulsion system components were selected, and the banner mechanism subsystem was integrated. This design was then prototyped and flight tested to determine design improvements that were incorporated in successive iterations. The final design was tested to verify that it meets the system requirements.

## 1.2 Key Performance Parameters and Design Features

Competition rules and the scoring functions were analyzed to determine key mission requirements, including high maximum cruise speed, high efficiency at low cruise speed, internal payload capacity, internal payload containment, banner deployment mechanism, and takeoff roll. These requirements influenced the subsequent design choices.

## 1.3 System Performance Capabilities

The design requirements and goals to maximize the performance of the aircraft system can be summarized by the parameters shown in Table 1.1.

*Table 1.1: System performance capabilities*

| Parameter | Value |
|---|---|
| Empty Weight | 4.46 lb |
| Minimum Flyable Weight | 8.27 lb |
| Maximum Takeoff Weight | 20.77 lb |
| Takeoff Roll for Mission 1 and Mission 3 | < 20 ft |
| Mission 1 Lap Time | 28.2 s |
| Mission 2 Lap Time | 33.7 s |
| Mission 3 Lap Time | 66.3 s |
| Mission 2 Payload | 40 Passengers and Luggage (12.5 lb) |
| Banner Length | Up to 12 ft long |
| Ground Mission Completion Time | ~45 s |

The final design is a conventional aircraft with a propulsion system with enough power for the ambitious takeoff and cruise targets and a structure designed for the high load factors during aggressive maneuvers. The team has completed 59 successful flight tests of three different prototypes and is continuing to improve the current aircraft based on pilot feedback and flight test results.

# 2 MANAGEMENT

## 2.1 Team Organization

A project of this scale must be divided up in order to achieve maximum quality and efficiency. The team chose to divide into five main sub-teams: Structures and Computer Aided Design (CAD), Subsystems, Aerodynamics, Propulsion, and Manufacturing. The team uses a hierarchical structure to establish leadership among its senior members, with responsibilities flowing down to the team's newer members. This hierarchy serves as an outline only, as all team members collaborate extensively to meet deadlines, share ideas, learn various disciplines, and produce a more successful aircraft. All team members were taught basic manufacturing skills and aircraft concepts at the beginning of the competition year. Each sub-team was taught the skills that would be required for that particular area, such as MotoCalc for propulsion analysis and SolidWorks for CAD work. Members can move between different sub-teams based on prior expertise, interest, or need. During construction, testing, and report writing, all team members participated fully. Figure 2.1 shows the organizational chart for the 2019-2020 team. A major point of emphasis is cross-collaboration between sub-teams, as shown by the horizontal arrows, within the organizational structure.
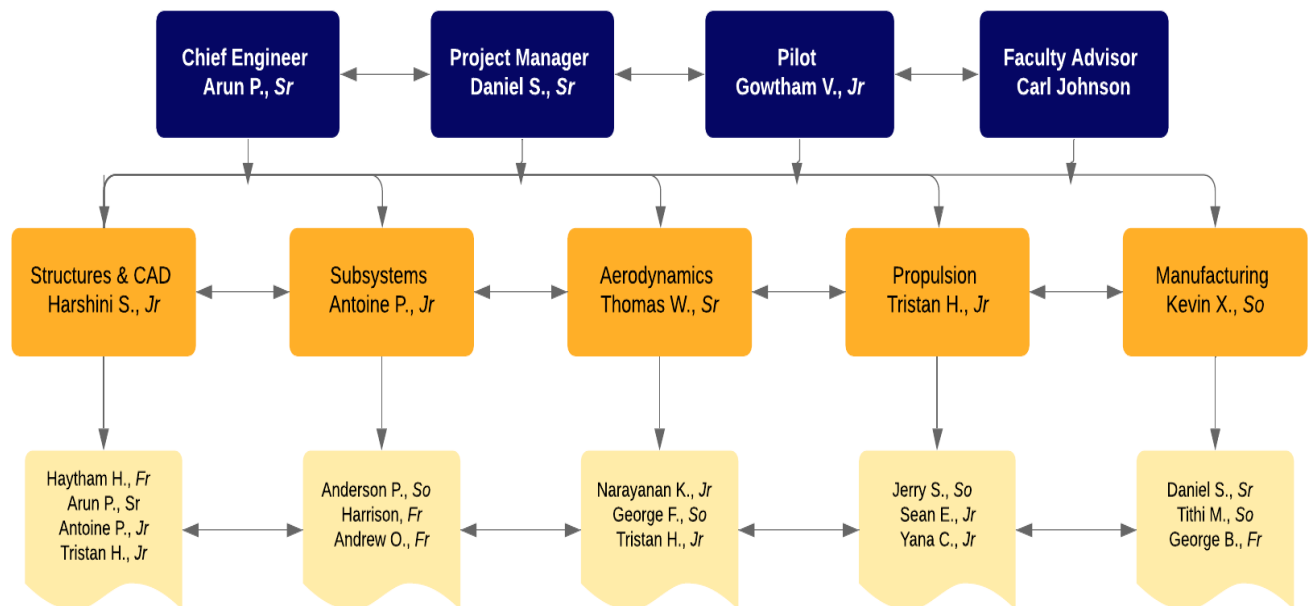


Figure 2.1: Team organization chart

## 2.2 Milestones

A schedule was established at the beginning of the school year by the project manager with assistance from the sub-team leaders and the faculty advisor. The schedule captures major deadlines and keeps the team on track for major milestones. The team also uses Trello, a project management tool, to assign tasks to members and track their progress. Another key factor in effective project management is the use of parallel development, which allowed the team to more efficiently use all its members to design, construct prototypes, and test them simultaneously. Figure 2.2 shows the team Gantt chart, with planned and actual

progress, as well as important milestones. The planned progress is shown in yellow, while the actual progress for completed items is shown in blue. The planned progress also includes any buffer time that was budgeted at the beginning of the year. The team met most of the design targets early on and completed the detail design only two weeks late. Subsystem testing started on schedule, but took longer than planned due to changes and improvements made during the system integration process.
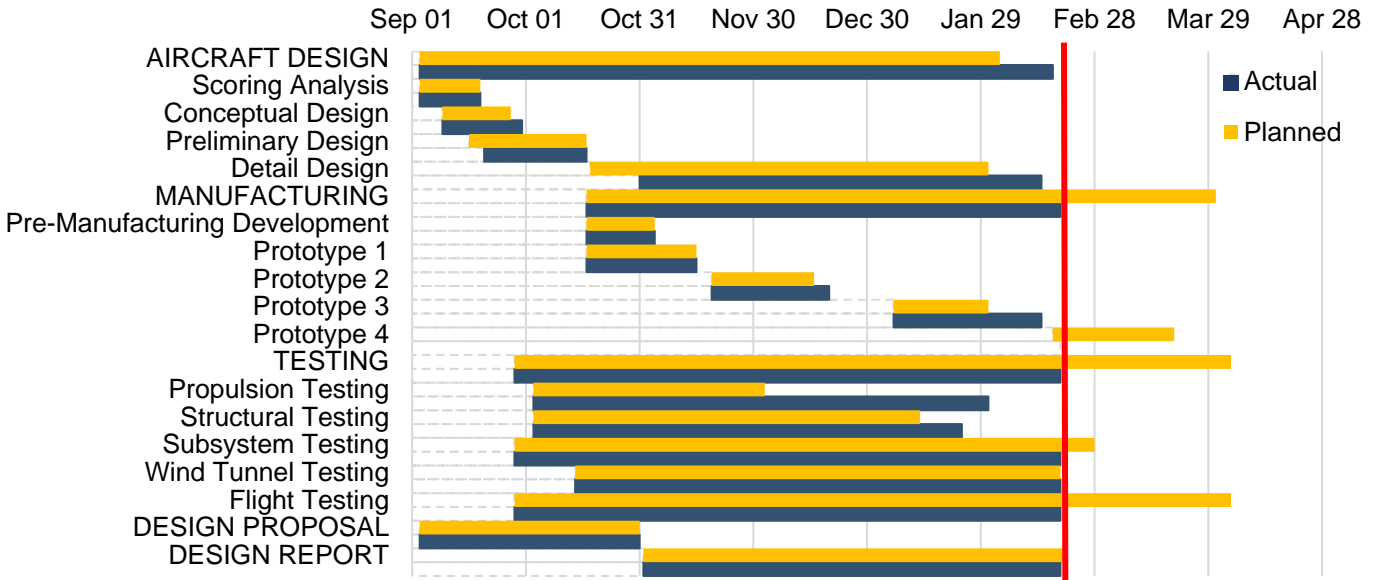


*Figure 2.2: Aircraft design milestone chart showing planned progress (shown in yellow) and actual progress (shown in blue). Major sections within the schedule are listed in all caps*

# 3  CONCEPTUAL DESIGN

The team analyzed the competition rules to identify performance characteristics that maximize the potential flight score in conceptual design. The rules were translated into design requirements and scoring factors that were used in Figures of Merit (FOM). The FOM were used to evaluate the four most promising design alternatives. The best scoring alternative was selected as the final configuration.

## 3.1  Rule Analysis

### 3.1.1  Scoring Analysis

The AIAA Design/Build/Fly 2019-2020 competition score consists of three flight missions, a ground mission, and a design report. The total score function is shown in Equation 1. The total mission score is shown in Equation 2.

$$SCORE = Written\ Report\ Score \ \times Total\ Mission\ Score \tag{1}$$

$$TMS = Mission\ 1\ Score + Mission\ 2\ Score + Mission\ 3\ Score + Ground\ Mission\ Score \tag{2}$$

### 3.1.2    Aircraft Requirements from Rules

The competition rules stipulate specific requirements on the aircraft dimensions, takeoff distance, payload, and propulsion system, as described below.

Aircraft Geometry: The aircraft must have a maximum wingspan of 5 feet.

Takeoff Distance: For flight missions 1 and 3, the aircraft must takeoff in less than 20 ft.

Passengers and Luggage: The aircraft must carry at least one 4 oz passenger of specific dimensions and its 1 oz luggage of specific dimensions.

Banners: The aircraft must take off with a stowed banner, deploy the banner in flight, and release the banner before landing. The banner must have a maximum aspect ratio of 5 and a minimum length of 10 in.

Propulsion System: The aircraft must be propeller-driven and electrically powered with commercially available components. These include the motor, propeller, speed controllers, receivers, and batteries. The battery selection is limited to LiPo or NiMH, but may be of any cell count, voltage, or capacity, as long as the energy stored is less than 200 Wh. There is no limit on the weight of the battery packs. The entire propulsion system must be armed by an external safety plug or fuse. The safety plug or fuse must be mounted on the exterior of the aircraft and be accessible from behind in a tractor propeller configuration.

### 3.1.3    Flight Missions

Flight missions begin from the runway. The aircraft must takeoff and then complete laps, as shown in Figure 3.1. A complete lap is defined as crossing the finish line, completing the defined pattern, and then crossing the finish line while still in the air.

1. Successful takeoff from runway
2. Climb to safe altitude
3. 180⁰ turn 500 ft upwind from the finish line
4. 1000 ft downwind leg
5. 360⁰ turn during the downwind leg
6. 180⁰ turn
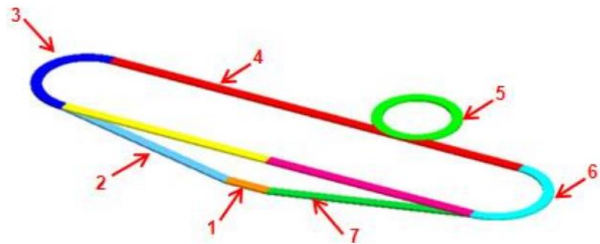7. 500 ft final with a successful landing



*Figure 3.1: Flight mission course*

Each mission has specified constraints and scoring objectives that are described in greater detail below.

Mission 1 (Test Flight): The empty aircraft must take off from the runway in less than 20 feet and complete three laps within a five-minute flight window. Time begins once the aircraft throttle is advanced for the first time and ends once the aircraft passes over the finish line in the air at the end of the third lap. The aircraft must complete a successful landing to receive a score. The scoring formula is shown below in Table 3.1.

*Table 3.1: Flight Mission 1 scoring*

| Mission | Description | Score |
|---------|-------------|-------|
| M1 | Aircraft completes the mission with a successful landing | 1.0 |
| | Aircraft does not attempt or complete a successful flight | 0.0 |

Mission 2 (Charter Flight): The aircraft must carry passengers and luggage as payload, take off from the runway, and complete three laps within a five-minute window. There must be an equal number of passengers and luggage, and the total payload cannot exceed the number given at technical inspection. The mission score is a function of the number of passengers flown divided by the time to complete the laps, not including the landing, as shown in Table 3.2.

*Table 3.2: Flight Mission 2 scoring*

| Mission | Description | Score |
|---------|-------------|-------|
| M2 | Aircraft completes the mission with a successful landing | $1.0 + \dfrac{\left(\dfrac{\#\ of\ Passengers}{Time}\right)_{Buzzfighter}}{\left(\dfrac{\#\ of\ Passengers}{Time}\right)_{Max,all\ teams}}$ |
| | Aircraft does not attempt or complete a successful flight | 0.0 |

Mission 3 (Banner Flight): The empty aircraft must carry an externally stowed banner, take off from the runway in 20 feet, and complete laps within a ten-minute window, which begins when the throttle is advanced. After the first turn, the banner must be deployed remotely and remain deployed for the duration of the scoring laps. When the aircraft crosses the finish line on the final lap, the banner must be released remotely. The aircraft must pass over the start/finish line to successfully count a lap. The landing does not have to be completed within the prescribed time limit. The scoring formula is shown in Table 3.3.

*Table 3.3: Flight Mission 3 scoring*

| Mission | Description | Score |
|---------|-------------|-------|
| M3 | Aircraft completes the mission with a successful landing | $2.0 + \dfrac{(Laps\ x\ Banner\ Length)_{Buzzfighter}}{(Laps\ x\ Banner\ Length)_{Max,all\ teams}}$ |
| | Aircraft does not attempt or complete a successful flight | 0.0 |

Ground Mission (Operational Demonstration): The passengers, luggage, and the banner must be installed in a timed ground mission. The time starts at the mission official's command after the aircraft is placed in the mission box. The assembly crew member will first load the passengers and luggage then run back to the start line. Time stops when they cross the line, after which the pilot will demonstrate the flight controls are active. Time will resume when the mission official indicates, and the assembly crew member will return to the mission box, unload the passengers and luggage, and load the banner in the stowed configuration. Time will stop when the crew member crosses the start/finish line. The pilot will again demonstrate that the

flight controls are active, before a final demonstration of the banner being deployed and released with the aircraft held in a tail-down, vertical position. The scoring formula appear in Table 3.4.

*Table 3.4: Ground Mission scoring*

| Mission | Description | Score |
|---|---|---|
| GM | Aircraft completes the mission | $\dfrac{Time_{min,all\ teams}}{Time_{Buzzfighter}}$ |
| | Aircraft does not attempt or complete the mission | 0.0 |

## 3.2  Scoring Analysis

A sensitivity analysis on the scoring functions were performed to determine the design parameters and mission objectives that maximize the total mission score. Each mission scoring function was analyzed individually, and missions with scoring trades were identified. Individual analyses were combined to determine the most important design drivers.

### 3.2.1  Mission Analysis

The missions are first considered individually. The Ground Mission score requires minimizing the time to load the aircraft, meaning that loading the passengers, luggage, and banner must be as efficient as possible. The time to load is assumed to be linear with respect to the number of passengers and constant with the size of the banner. The Mission 1 score is binary; the team will receive one point after a successful mission. For this analysis, the team will assume Mission 1 is always successfully completed.

The Mission 2 score is a function of the number of passengers and how fast the aircraft flies with the passengers. There is a trade between these two parameters, in that increasing the number of payloads increases payload weight, which increases induced drag and decreases velocity. Mission 3 score is a function of banner length and how many laps the aircraft can fly in ten minutes. There are two significant trades in this mission. First, increasing the length of the banner increases a component of the scoring function, but also increases parasite drag, which decreases velocity and the number of laps the aircraft can fly. Second, if the constraint on battery energy is active, the aircraft can increase banner length but will run out of energy before the time runs out. Missions with trades, as well as missions that are coupled together require more detailed analysis.

The Ground Mission and Mission 2 are coupled as the number of passengers and luggage factors into both mission scoring functions. The Ground Mission score decreases with the number of passengers, while the Mission 2 score increases. For Mission 2, increasing the number of passengers was assumed to increase the weight of the aircraft by the weight of the passenger and their luggage, plus a structural multiplier for the additional payload. A plot of score versus number of passengers is shown in Figure 3.2. The score was normalized based on an assumption of a competitive performance score from other teams.
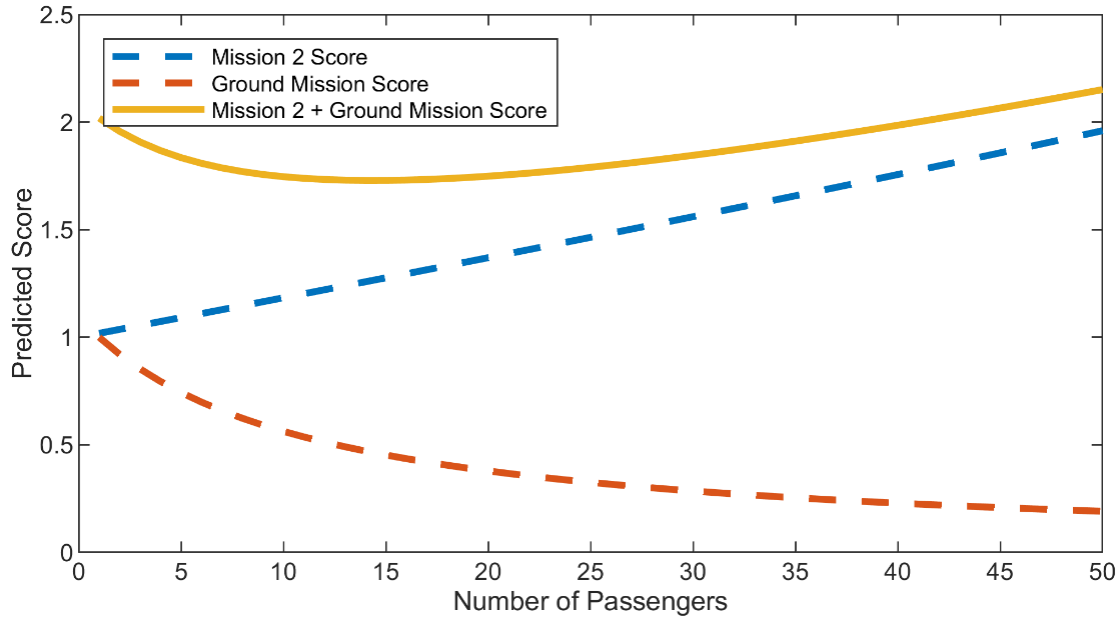
*Figure 3.2: Score versus number of passengers*

The graph shows two directions for locally maximizing score. First is a small aircraft, with the minimum number of passengers and minimum size of banner. Second is a large aircraft, maximizing the number of passengers and size of banner. The analysis indicates that a large aircraft is likely to score more overall, and that a small aircraft's score is more sensitive to the performance of other teams. Although this analysis shows that payload should be maximized, the exact design point needs to be determined using other constraints.

For Mission 3, there is a trade between the length of banners and the number of laps that the aircraft can fly. Given that Missions 1 and 2 scores are independent of Mission 3, and the ground Mission score does not change with banner length, it makes sense to analyze Mission 3 individually. The trade was analyzed looking at varying two flight parameters: current draw and velocity. The files outputted from MotoCalc, a commercially available motor analysis tool, for a notional propulsion combination were used to create a 2D polynomial fit of thrust as a function of current and velocity. Aircraft drag was calculated using an assumed drag polar and weight. The maximum banner length was calculated using excess thrust and a simple model for banner drag [1]. The mission laps were simulated assuming the aircraft flies one upwind and one downwind stretch at a constant velocity. Additionally, the number of laps completed was constrained by velocity and energy. The contour plots of Mission 3 score and banner length were overlaid, as shown in Figure 3.3, to find the optimal banner length.
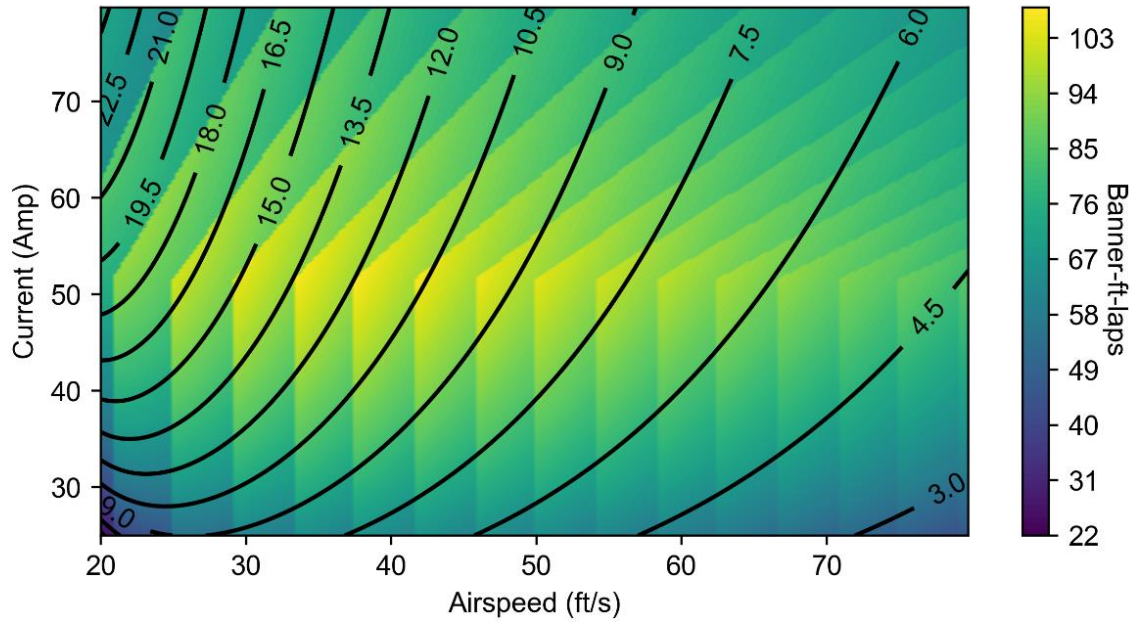
*Figure 3.3: Mission 3 score (shaded sontours) and banner length (contour lines) versus airspeed and motor current, with no wind*

Assuming no wind, the maximum score is achieved with a banner length of 12 ft, a current draw of 51.5 A, and an airspeed of 37.5 ft/s, where the aircraft is predicted to fly 9 laps and achieve a score of 107 banner-ft-laps. Although this case is ideal, there is a high probability of wind in Kansas.  Assuming a wind speed of 20 ft/s parallel to the runway, the aircraft needs to fly with a banner of 7.4 ft, a current draw of 51.5 A, and an airspeed of 57.3 ft/s. In this case the aircraft is predicted to achieve a score of 88 banner-ft-laps, which is a significant decrease in score. Given the sensitivity to wind speed, multiple banners will be required at competition to maximize the flight score for given conditions.

### 3.2.2    Translation into Design Requirements

Based on results from scoring analysis, the targets were set for payload and mission timing. Preliminary scoring targets are given in Table 3.5.

*Table 3.5: Scoring targets for Buzzfighter*

| Target | Value |
|---|---|
| Number of Passengers and Luggage | 40 |
| Mission 2 Lap Time | 30 s |
| Banner Length | 10 ft |
| Mission 3 Lap Time | 60 s |
| Ground Mission Time | 30 s |

These targets imply the following requirements on aircraft performance:

High Maximum Cruise Speed: Increasing aircraft velocity increases Mission 2 and Mission 3 score, all else being equal. Increasing velocity requires a propulsion system with a high thrust at speed, as well as a configuration with low drag.

High Efficiency at Low Cruise Speed: Mission 3 is an endurance flight, and the energy limit of the batteries is an active constraint on what current the motor can draw. Scoring analysis shows that carrying a large banner is beneficial to the score, but the velocity of the aircraft should still be maximized for the constrained current draw by producing thrust with high efficiency.

In addition, several other requirements impact configuration selection and aircraft design:

Internal Payload Capacity: Increasing the number of passengers and luggage increases Mission 2 score, all else being equal. High payload capacity requires a propeller-motor combination with a high power output and sufficient structure to withstand the high aerodynamic and landing forces.

Internal Payload Containment: The large amount of payload requires payload bays that are sufficiently large to contain the passengers. The payload must be safely secured to prevent movement of the C.G., while also being easily and quickly loadable to minimize the Ground Mission time.

Banner Deployment Mechanism: Because the banner also needs to be loaded during the Ground Mission, it must be easily mounted on the mechanism. However, given that the mechanism is mounted externally, the stowed configuration must minimize the drag produced by the banner

Takeoff Roll: Takeoff roll is a constraint for Mission 1 and Mission 3. The takeoff roll is reduced with either increasing thrust to weight ratio or decreasing wing loading. In addition, flaps or flaperons can be used for takeoff to increase the lift coefficient.

## 3.3 Configurations Explored

The mission requirements and constraints translated to five figures of merit that were used to assess the design alternatives. A weight of five means the figure of merit was the most important to consider in configuration selection, whereas a one was the least important. These figures appear in Table 3.6.

*Table 3.6: Figures of merit and their respective weights*

| Figure of Merit | Weight |
|---|---|
| Drag | 5 |
| Payload Integration | 4 |
| Simplicity | 3 |
| Weight | 2 |
| Stability | 1 |

Low drag received the maximum weight of 5 because it is essential to improve flight speed, which must be maximized to improve Mission 2 and Mission 3 scores. Payload Integration receives a weight of 4 because the loading speed factors heavily into the Ground Mission Score. Simplicity receives a 3 because it is important to be able to quickly and consistently build prototype aircraft with reliable performance. However,

simplicity may still be outweighed by significant increases in performance. From the sensitivity analysis, weight has an indirect effect on the aircraft's performance via induced drag. Finally, stability is given the lowest priority. While the aircraft should be stable, it should also be maneuverable to minimize turning time. A matrix of alternatives was developed to identify potential configurations seen in Table 3.7. The components considered include the wing, empennage, motor, fuselage, and payload attachment.

*Table 3.7: Matrix of alternatives for Buzzfighter configuration selection*

| Component | Configuration Options | | | | |
|---|---|---|---|---|---|
| Wing | Conventional | Biplane | Blended Wing Body | Tandem | Canard |
| Empennage | Conventional | V-Tail | H-Tail | T-Tail | Cruciform |
| Motor | Single Puller | Twin Puller | Single Pusher | Twin Pusher | Pusher-Puller |
| Fuselage | Tube | Blended Wing Body | Double Bubble | | |
| Landing Gear | Tricycle | Taildragger | Bicycle | Quadricycle | Retracting |
| Banner Attachment | Tow line | Rod | Under Fuselage | Under Tail | Behind Tail |

Four design alternatives were generated by selecting combinations of configuration options that were compatible with each other, shown in Figure 3.4. The first design is a conventional design with a single motor, straight wings, and T-tail attached to a simple fuselage. The second design is a biplane with a single motor, and a T-tail. The third design is a blended wing body with a V-tail to reduce drag. The fourth alternative is a tandem wing design with two wings and a T-tail attached to a simple fuselage. In all configurations, the banner is notionally attached to the bottom of the fuselage; the exact banner attachment location is considered in the preliminary and detailed design phases.
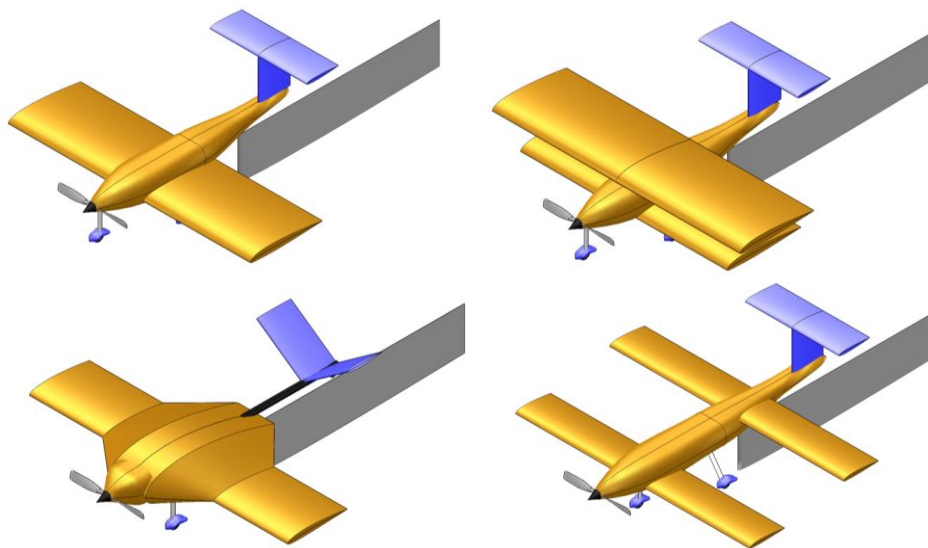


*Figure 3.4: Four identified design alternatives, clockwise from top right: conventional, biplane, blended wing body, and tandem wing*

The performance of each configuration with respect to the FOMs were evaluated from a scale of 1 to 5, with 5 being most effective, in the weighted Pugh Matrix shown in Table 3.8. The weighted scores were summed for each configuration to determine the best design.

The conventional design is relatively simple, making analysis, design, and manufacturing tasks easier. The T-tail reduces the chance of banner interference with the control surfaces.

The biplane design allows for a higher aspect ratio for the same area, which reduces induced drag and decreases takeoff distance. However, two surfaces will likely result in more interference drag, as well as increased structural complexity and difficulty loading passengers. Furthermore, there is increased uncertainty in predicting the up- and downwash interactions between the two surfaces.

The blended wing body design creates a much smoother transition between the wing and fuselage, which reduces interference drag. The V-tail further reduces parasite drag. However, there is increased design and construction complexity, and much of the transition volume in the body cannot be used to fit payload.

The tandem wing, like the biplane, allows for a larger effective aspect ratio for the same wing area, but presents challenges with analysis, stability, and control. Having the wing structure forward and aft allows for a larger continuous passenger cabin, but also increases the complexity of the design.

*Table 3.8: Weighted Pugh matrix for Buzzfighter configuration selection*

| FOM | Weight | Conventional | Biplane | Blended Wing Body | Tandem |
|---|---|---|---|---|---|
| Drag | 5 | 4 | 2 | 5 | 4 |
| Payload Integration | 4 | 4 | 1 | 4 | 4 |
| Simplicity | 3 | 5 | 4 | 2 | 3 |
| Weight | 2 | 4 | 3 | 4 | 4 |
| Stability | 1 | 5 | 2 | 4 | 3 |
| TOTAL | | 64 | 34 | 59 | 56 |

Based on the results of the weighted Pugh matrix, the conventional design was selected as the final configuration for this year's competition aircraft. A three-view and isometric sketch of this design appears in Figure 3.5. Passengers and luggage are carried inside the fuselage, and banner is carried externally under the fuselage.
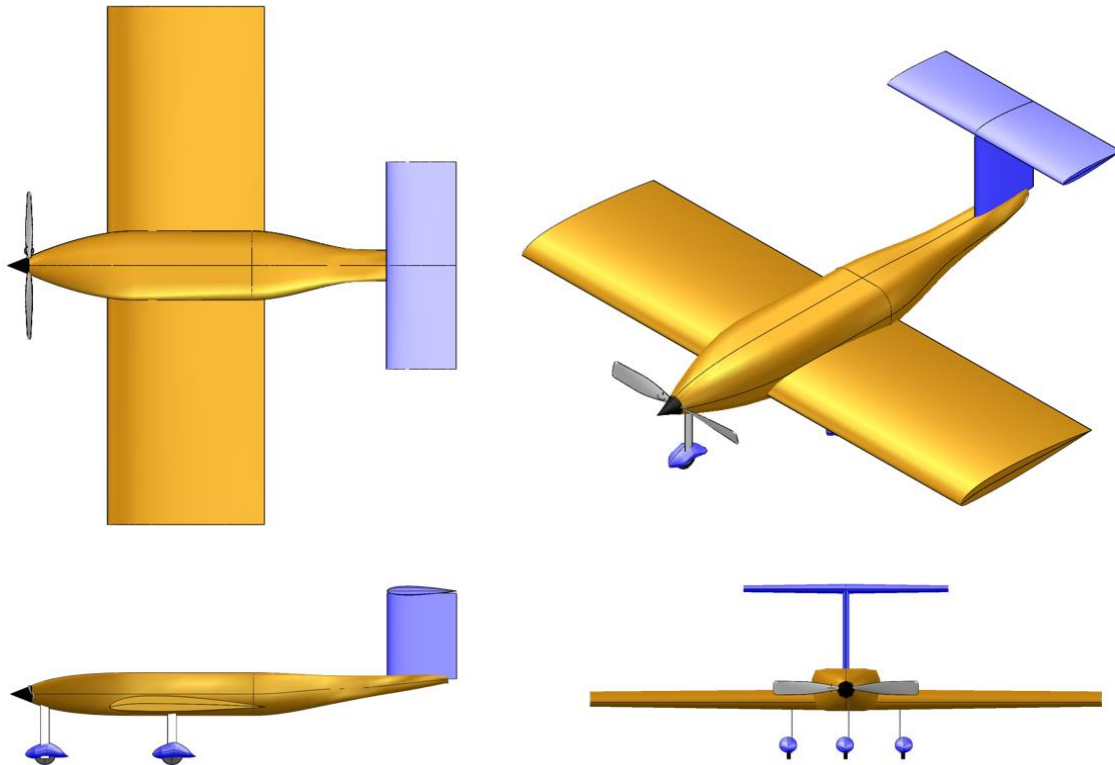
*Figure 3.5: Three view and isometric view of the selected configuration*

# 4 PRELIMINARY DESIGN

## 4.1 Design Methodology

The team followed an aircraft design process that has been developed based on faculty advisor guidelines and previous team experience. The rules and scoring functions were analyzed to determine requirements that will drive aircraft design. Configuration alternatives were evaluated and the most promising was selected for further development. These requirements were used to perform a constraint analysis and estimate a maximum takeoff weight and wing area to size the aircraft. A variety of propulsion systems were analyzed and tested, and the best was selected based on the mission requirements. Mission models were developed to simulate mission performance. The mission models also allow for refinement of prior analyses. The preliminary design was analyzed to determine if mission performance requirements were met and to ensure stability. The components and subsystems were then designed in detail. Systems and subsystems were manufactured and flight tested to evaluate performance.

Although the design process is presented above as linear, it is highly iterative as seen in Figure 4.1. Results from analyses and testing were applied to improve previous analyses and reevaluate design choices. Intermediate results such as performance predictions, aerodynamic characteristics, and manufacturing issues were used to improve the design, leading to a higher scoring aircraft.
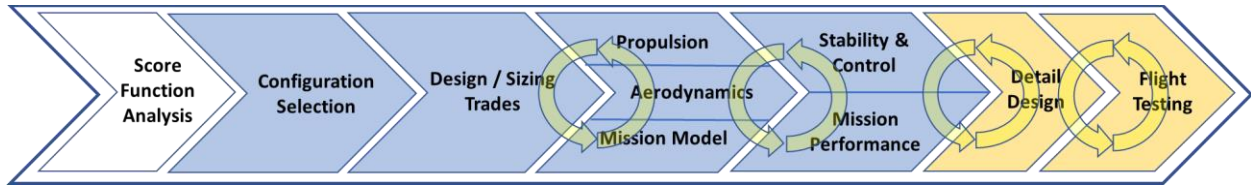


*Figure 4.1: The team's preliminary design methodology highlighting the multidisciplinary iterations*

## 4.2 Design Trades

### 4.2.1 Constraint Sizing

Using assumptions from scoring analysis, requirements, and historical aircraft data, a constraint analysis was conducted to determine the power-to-weight ratio and wing loading. The constraint curves were calculated using an energy-based constraint analysis from [2]. Target values for M2 cruise velocity, M3 cruise velocity, and M3 takeoff distance are shown in Figure 4.2, as well as the selected design point. This design point minimizes the thrust required and the wing loading, which translates to a smaller, lighter aircraft.
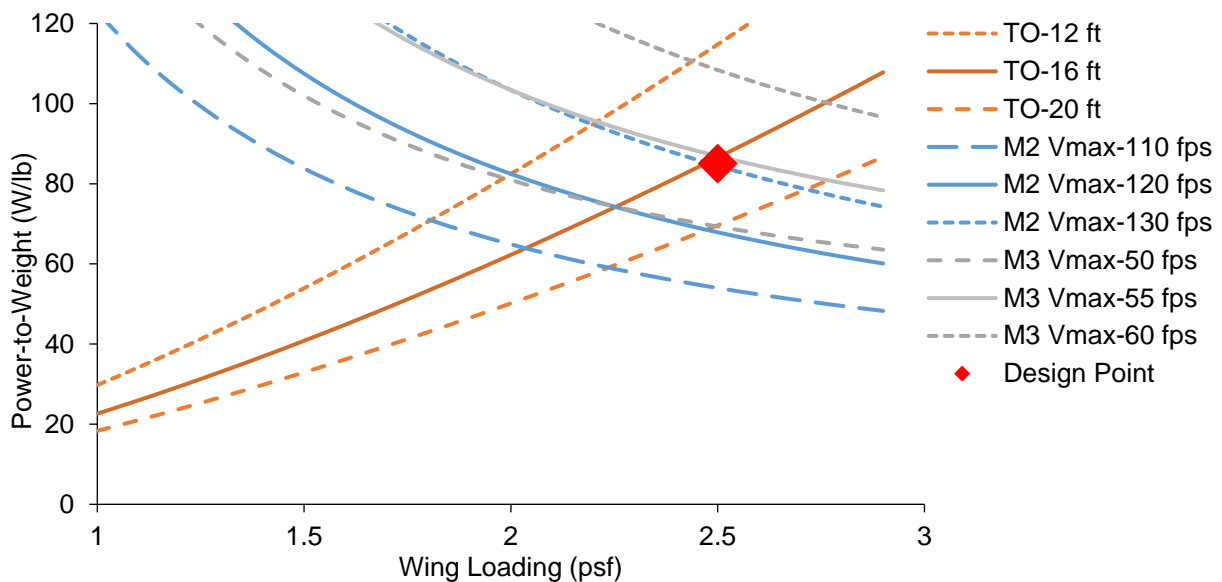


*Figure 4.2: Constraint diagram*

The weight is estimated using data from historical Georgia Tech DBF Aircraft. As described in Section 4.2.2, the selected batteries had a weight of 1.7 lb. For Mission 2, which is relatively short, the team elected to use only one battery to save weight. The payload of 40 passengers targeted in Section 3.2.2 weighs 12.5

lb, totaling 14.3 lb of payload and battery weight. Assuming an empty weigh fraction of approximately 0.3, based on prior team experience, the maximum takeoff weight for the aircraft is 20.7 lb. Based on these results and constraints sizing, the target design point for this aircraft is shown in Table 4.1.

*Table 4.1: Target design parameters for Buzzfighter*

| Parameter | Target |
|---|---|
| Maximum Takeoff Weight | 20.7 lb |
| Empty Flyable Weight | 8.27 lb |
| Payload Capacity | 12.8 lb (40 passengers and luggage) |
| Propulsion System Power | 1800 W |

### 4.2.2 Propulsion System Selection

LiPo batteries were chosen over NiMH because of their higher power density and energy density. The rules state that the energy limit for LiPo batteries must be no more than 100 Wh per pack, with a maximum of two packs connected in parallel equaling 200 Wh. By extension, pack voltage and pack capacity are constrained. For this scale of propulsion system, 6 cell and 8 cell batteries were considered as possible candidates. Using high capacity cells is preferable, since combining many smaller cells can result in too much internal resistance, therefore 6 cell batteries were chosen. Two Scorpion 6s 4500 mAh LiPo battery packs were selected and connected in parallel. Given the corresponding battery voltage, 4500 mAh is the maximum possible cell capacity so that two identical battery packs connected in parallel have a total stored energy below the limit of 200 watt-hours. These batteries have a nominal energy capacity of 99.90 Wh each, which is close to the limit. Drawing upon a compiled database of motors, propellers, and batteries, MotoCalc was used to estimate the thrust and current produced for 20 different propulsion systems at varying airspeeds. These propulsion systems were evaluated based on their ability to provide the power required per constraint sizing in Section 4.2.1. The static thrust estimates were verified with in-house static thrust testing and deemed acceptable for use in down-selection. Furthermore, battery current draw was estimated for the top three propulsion systems with varying airspeed and throttle setting in order to predict the maximum cruise speed at which 10 minutes of endurance for Mission 3 is achievable. The tested combinations, shown in Table 4.2, were based on previous experience and available components.

*Table 4.2: Propulsion systems considered for MotoCalc analysis*

| Motor | Kv | Battery (cells) | Current (Amps) | Propeller | Static Thrust (lb) | Propulsion System Weight (lb) |
|---|---|---|---|---|---|---|
| Hacker A60-5XS | 420 | 6 (4500 mAh) | 96.7 | 17x12 | 15.26 | 4.44 |
| Hacker A60-6XS | 370 | 8 (3300 mAh) | 99.5 | 16x12 | 18.06 | 4.38 |
| Hacker A50-16s | 365 | 6 (4500 mAh) | 67.4 | 16x12 | 12.18 | 4.14 |

Table 4.2 shows the final motor-battery-propeller combinations and their respective produced static thrust the team considered. In the end, the Hacker A60-5XS with an APC 17x12E propeller was chosen based

on its balance between static thrust and thrust at high speed. The validation of the chosen propulsion system with static thrust testing is described in Section 8.1.1.

## 4.3    Aerodynamic Characteristics

### 4.3.1    Airfoil Selection

Selecting an appropriate airfoil for the aircraft is important to achieve the desired aerodynamic characteristics in order to meet the design requirements. A variety of airfoils were compared based on XFOIL [3] analysis and validated using wind tunnel results [4]. There are several factors used to select candidate airfoils.

Manufacturing: Airfoil geometries such as thin trailing edges and high camber can present difficulties during manufacturing, especially at a small scale. Overly complex airfoil geometries may also lead to manufacturing imperfections, which will cause the aerodynamic characteristics to differ from the design.

Thickness: The airfoil selected must have enough thickness in order to accommodate internal structure. Thin airfoils also tend to have sharp leading edges which cause abrupt stall behavior. Abrupt stall characteristics are especially problematic in Mission 2, where the high wing loading can lead to an unrecoverable state.

Aerodynamic Properties: The airfoil should have a high lift-drag ratio for cruising efficiently. An additional consideration that is especially important for this year's competition is the maximum lift coefficient; a higher lift coefficient aids in takeoff and turning. A third consideration is the zero-angle of attack lift coefficient. Using the maximum sustained speed provided by the propulsion system and a desired wing loading for Mission 3, the target wing lift coefficient for level flight was calculated to be between 0.25 and 0.5. An ideal candidate airfoil should therefore have a section lift coefficient at zero angle of attack that is slightly above this value.

Based on maximum section lift to drag ratio and the criteria described above, four airfoils from the UIUC airfoil database were considered for the wing. One candidate airfoil is the SD 7062, a 14% thick airfoil that has been used on numerous prior DBF aircraft because of its high maximum lift to drag ratio, moderate thickness to allow for structure, and gradual stall characteristics. Other airfoils selected for more detailed analysis include the NACA 2410, NACA 64A410, and RG 14, which were selected because of their low thickness (≤10%) and low camber. These characteristics contribute to low drag at cruise. The lift and drag characteristics were analyzed using XFOIL, and the results are shown in Figure 4.3.
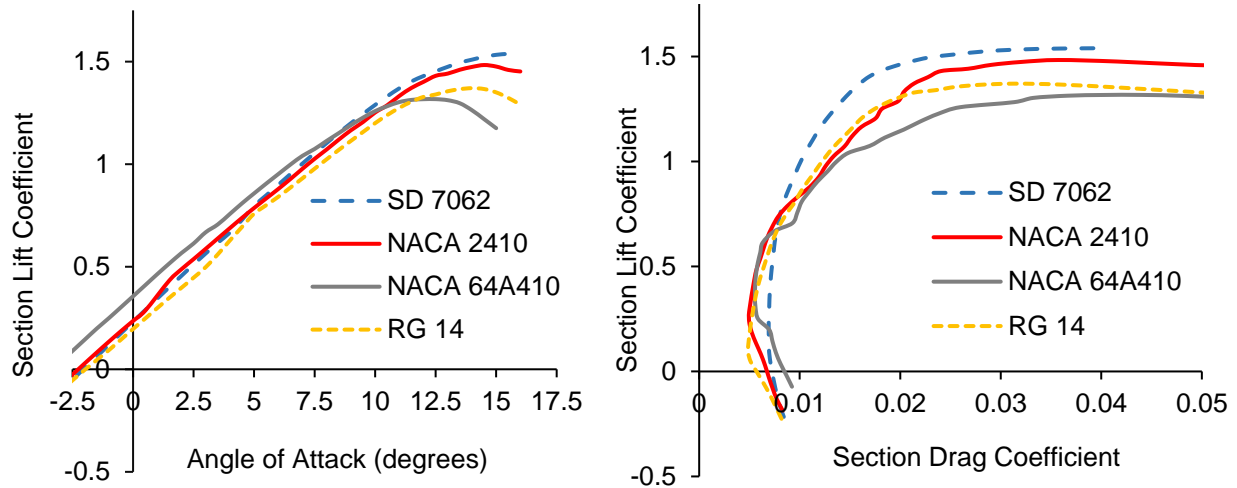
*Figure 4.3: XFOIL lift and drag characteristics for several airfoils under consideration*

The first property of interest is the drag coefficient at lift coefficients in the range of 0.25-0.5, where *Buzzfighter* will be cruising. Examination of the drag polar shows that the NACA 2410 and RG 14 both have a relatively low and consistent drag coefficient over this range of $c_l$. The NACA 64A410 has a similar drag coefficient, but this increases abruptly outside of a small range. The SD 7062 has a higher drag coefficient for this entire range. Another property of interest is a high maximum lift coefficient, which is important for short takeoff, high turn rate, and short landings. The SD 7062 reaches the highest lift coefficient, with the NACA 2410 only slightly lower. The NACA 64A410 and RG 14 both reach a significantly lower lift coefficient. A final consideration is the steepness of the stall, which affects how quickly the pilot can respond. Based on XFOIL's predictions, all of the selected airfoils appear to have reasonable stall characteristics, though the SD 7062 has the smoothest.

Based on these considerations, the NACA 2410 was selected and the analyzed using XFOIL at a Reynolds number of 500,000, as this is the approximate Reynolds number for cruise conditions. The XFOIL analysis was also run at a Reynolds number of 3,000,000 and compared with experimental data [4] to validate XFOIL. The result is shown in Figure 4.4. The XFOIL results for a Reynolds number of 3,000,000 has a slightly higher lift coefficient than the experiment conducted at the same Reynolds number. The difference increases at higher angles of attack. Furthermore, the lift coefficient falls off much more quickly in the experiment, which means that stall will occur more abruptly than XFOIL would predict. These discrepancies are likely due in part to inaccuracies in XFOIL's boundary layer model. The difference in the stall behavior is not surprising, due to the complexities of separated flow.
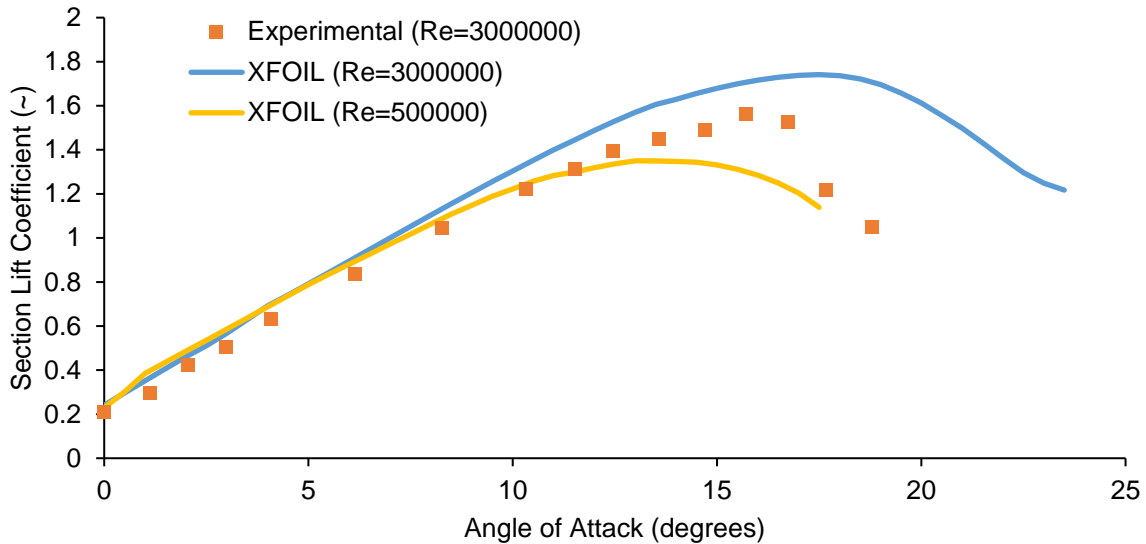
*Figure 4.4: Wind tunnel test data for NACA 2410 [4] compared to XFOIL*

For the horizontal and vertical tails, a NACA 0010 was selected for its simple geometry, moderate thickness, and symmetry.

### 4.3.2 Lifting Surface Analysis

Lifting surfaces including the wing and tail were analyzed using Athena Vortex Lattice (AVL) developed by Dr. Mark Drela [5]. AVL models lifting surfaces as infinitely thin vortex sheets and calculates aerodynamic characteristics including lift and drag coefficients, as well as stability derivatives and control surface deflections for trim.

A major driver for the planform geometry is manufacturing. Rectangular wings with right angles are the easiest to manufacture, but more complex planform geometries can also improve performance. For this competition, takeoff and turning require a high wing lift coefficient, and the low aspect ratio makes having a high spanwise efficiency factor important.

Increased span efficiency and wing lift coefficient can be achieved by modifying the planform to keep the section lift coefficient as close to constant as possible across the wing. To allow for a good balance between design freedom and ease of manufacturing, the wing geometry was parametrized to be defined by two variables: the break point where the wing would begin to taper and a taper ratio. The span was constrained to 5 ft based on the rules, and the area was constrained to 8.5 ft$^2$ based on the preliminary design. In addition, the team chose to sweep the leading edge in order to make the design and manufacture of control surfaces simpler. The wing geometry was then optimized based on these two design variables using an AVL wrapper in Python to find the maximum lift coefficient that a planform could achieve before stall. A contour plot of the wing lift coefficient versus the two design variables is shown in Figure 4.5.

22
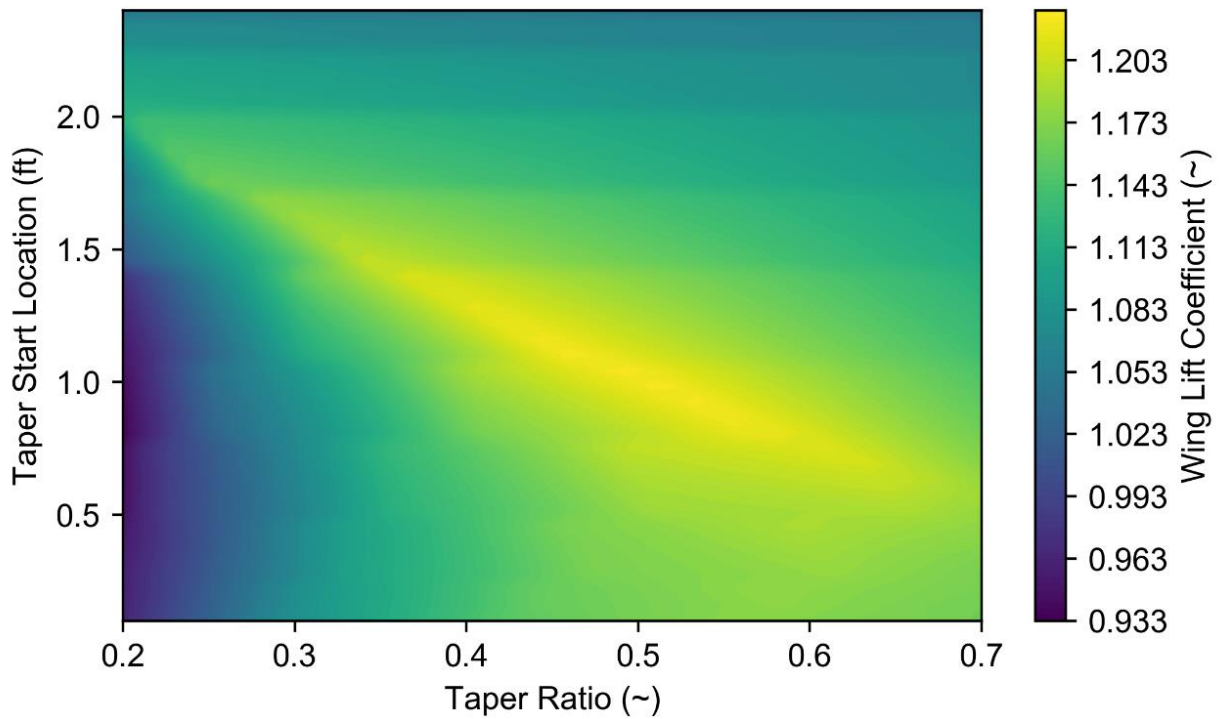
*Figure 4.5: Plot of wing lift coefficient versus taper start location and taper ratio*

Selecting the optimal point in this design space results in a planform with a maximum lift coefficient of 94% of the airfoil section maximum lift coefficient, which is a 12% improvement over a straight wing. The higher maximum lift will improve short field and turning performance.

The aircraft horizontal and vertical stabilizers were sized using AVL to achieve the static stability and controllability requirements derived from past experience with previous competition aircraft. Figure 4.6 shows the lift distribution of the lifting surfaces with the angle of attack close to stall and the elevator set to maintain trim. In this condition, the elevator deflection is −12.4°, which is well within the limits of the elevator hinge design.
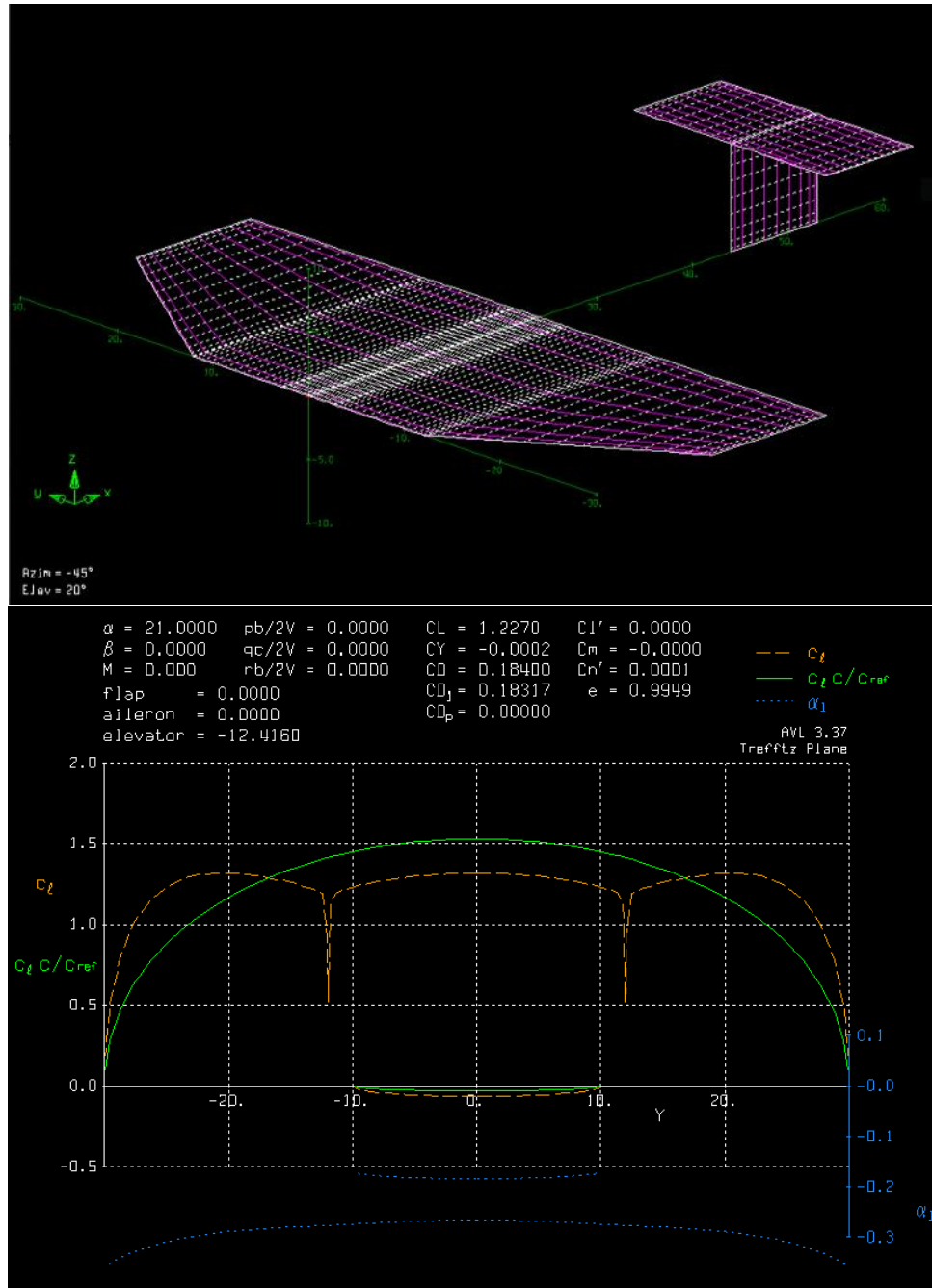
*Figure 4.6: Model of the aircraft in AVL (top) and the resultant Trefftz plot at $C_{Lmax}$ (bottom)*

### 4.3.3    Drag Analysis

Preliminary parasitic drag estimates, as well as the model shown in Figure 4.7 for all components except the banner, were obtained from OpenVSP's Parasite Drag analysis tool [6], using the form factor relationships from Hoerner's *Fluid Dynamic Drag* [7] and normalizing each component according to the wing reference area. The parasite drag for the banner was calculated using an empirical model [1].
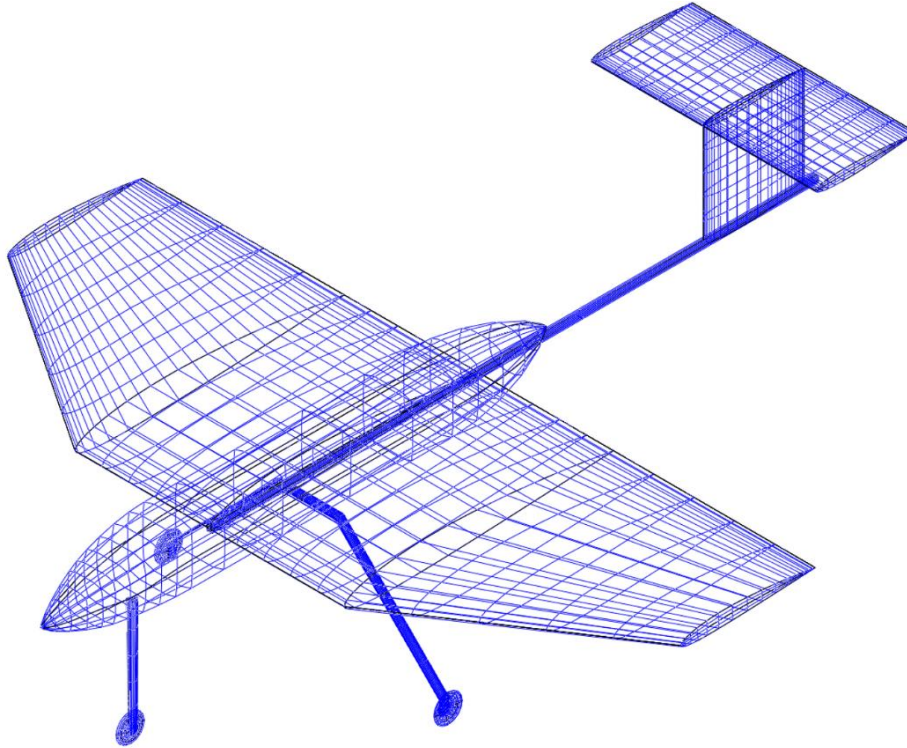
*Figure 4.7: OpenVSP model of Buzzfighter*

<u>Wing</u>: The parasite drag coefficient of the wing was found using the semi-empirical Hoerner's method for lifting surfaces.

<u>Fuselage</u>: The parasite drag coefficient for the fuselage was found using the semi-empirical Hoerner's method for streamlined bodies.

<u>Empennage</u>: The horizontal and vertical stabilizers were modeled as wings, and their drag was determined using Hoerner's method for lifting surfaces.

<u>Landing Gear</u>: The main gear and nose gear drag contributions were calculated separately, but both were modeled as a wheel and a flat plate.

<u>Banner:</u> The drag of the banners was calculated using an empirical model [1], which shows that the parasite drag coefficient for a banner is 0.16 when normalized by the area of the banner, for a banner that is five times longer than its width. This value was corroborated during flight tests by measuring the decrease in velocity of the aircraft with the addition of a banner.

The large increase in parasite drag for Mission 3 is due to the large size of the banner. Figure 4.8 shows the data as a percentage breakdown for each different configuration of the aircraft. In the clean configuration for Mission 1 and Mission 2, the wing and fuselage contribute the most significant portion of the parasite

drag. The landing gear also contributes a significant portion of the drag. For Mission 3, the banner is by far the most significant source of drag.

| Component | $C_{D,0}$ |
|---|---|
| Wing | 0.0081 |
| Fuselage | 0.0031 |
| Empennage | 0.0028 |
| Landing Gear | 0.0078 |
| **Clean Configuration (M1 & M2)** | **0.0302** |
| Banner (Max. Size) | 0.542 |
| **Banner Towing Configuration (M3)** | **0.572** |

13.4%
33.6%
41.0%
12.0%

■ Fuselage ■ Wing ■ Empennage ■ Landing Gear
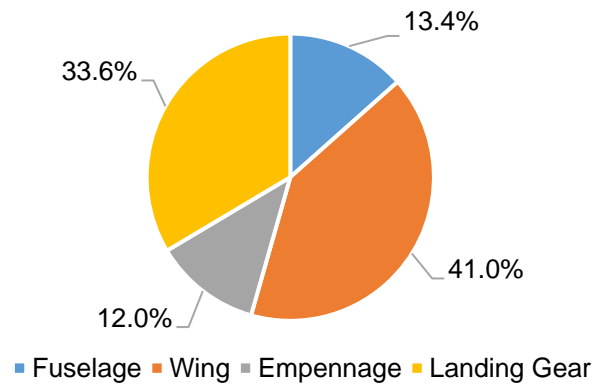
*Figure 4.8: Breakdown of various sources of drag*

The parasite drag estimates were combined with induced drag estimates from AVL to create a drag polar shown in Figure 4.9. The large contribution of the banner to parasite drag can be seen to dominate in the Mission 3 configuration.
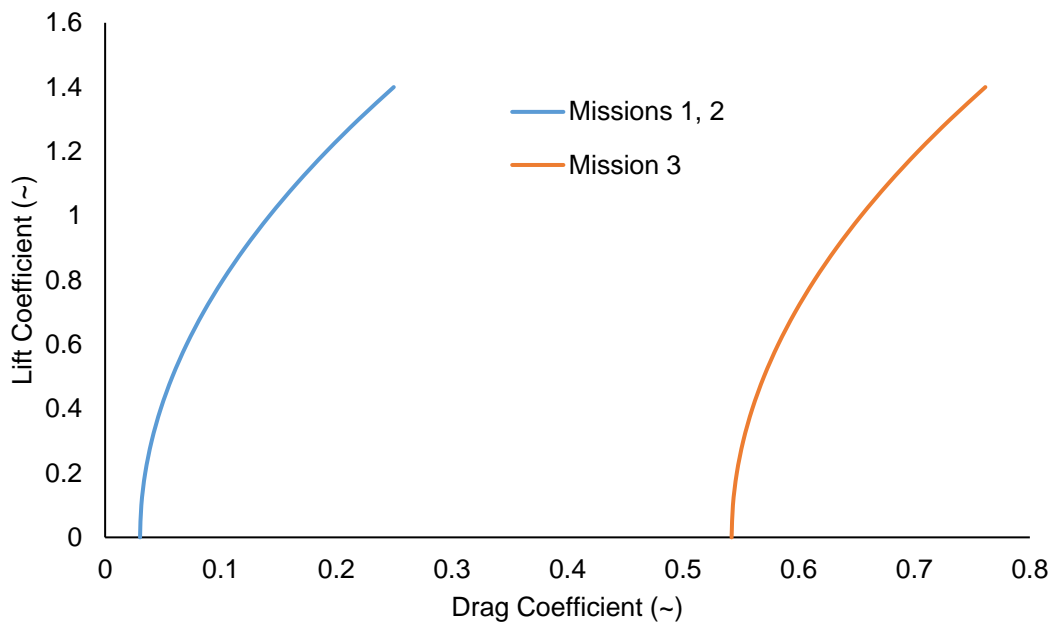
*Figure 4.9: Drag polar of the aircraft for the three different missions*

## 4.4 Stability and Control

### 4.4.1 Static Stability Analysis

Static stability was evaluated using the vortex lattice method implemented in AVL. The most demanding flight condition for trim was at the highest weight and lowest speed, for which stability derivatives are given in Table 4.3. The aircraft is trimmed at this condition with an elevator deflection of -12.4°. All cases indicate the aircraft is longitudinally, statically stable with a static margin of 9.5% at 0° angle of attack and 12.9% at 21° angle of attack. All pitch, roll, and yaw derivatives are stable and within the acceptable range based on previous aircraft and pilot feedback.

*Table 4.3: Relevant stability coefficients and derivatives for static stability*

| Parameter | AVL Results | |
|---|---|---|
| **Aerodynamic Parameters** | $C_L$ | 1.23 |
| | $\alpha$ (deg.) | 21 |
| | $\beta$ (deg.) | 0.0 |
| **Stability Derivatives** | $C_{l,\beta}$ (rad$^{-1}$) | 0.0 |
| | $C_{L,\alpha}$ (rad$^{-1}$) | 2.62 |
| | $C_{m,\alpha}$ (rad$^{-1}$) | -0.34 |
| | $C_{n,\beta}$ (rad$^{-1}$) | 0.17 |
| **Damping Derivatives** | $C_{l,p}$ (rad$^{-1}$) | -0.21 |
| | $C_{m,q}$ (rad$^{-1}$) | -3.5 |
| | $C_{n,r}$ (rad$^{-1}$) | -0.11 |
| **Static Margin ($\alpha$=0°)** | % Chord | 9.5 |
| **Static Margin ($\alpha$=21°)** | % Chord | 12.9 |

### 4.4.2 Dynamic Stability Analysis

Having found the trim conditions as a part of the static stability analysis, the next step was to take the aerodynamic derivatives about the trim conditions described earlier and investigate the dynamic behavior of the airplane. The stability and control derivatives were obtained from AVL, the mass properties from the CAD file, and the stability characteristics calculated from the full 12×12 6-DOF linearized differential equations found in Phillips's *Mechanics of Flight,* Section 9.8 [8]. The eigenvalues and eigenvectors of the matrix showed the stability of each of the five dynamic modes, showing that the aircraft is stable in all dynamic modes except spiral. However, all values are reasonable based on previous Georgia Tech DBF aircraft. The flight conditions used were the same as those used in the static stability section, listed in Table 4.3. The dynamic stability characteristics are tabulated in Table 4.4.

*Table 4.4: Dynamic stability characteristics*

| Mode | Longitudinal Modes | | Lateral Modes | | |
|---|---|---|---|---|---|
| | Short Period | Phugoid | Dutch Roll | Roll | Spiral |
| Damping Rate (s$^{-1}$) | 3.16 | 0.00627 | 0.590 | 3.26 | -0.127 |
| Time to double/half (s) | 0.219 | 110 | 1.17 | 0.213 | 5.44 |
| Damping Ratio (~) | 0.607 | 0.00647 | 0.118 | - | - |
| Damped Natural Frequency (s$^{-1}$) | 4.14 | 0.968 | 4.56 | - | - |
| Undamped Natural Frequency (s$^{-1}$) | 5.21 | 0.968 | 4.99 | - | - |

## 4.5    Mission Performance

### 4.5.1    Mission Model

The aircraft performance for all three missions was predicted using a mission model. The model allows for sensitivity exploration, comparison between predicted performance and flight test data, and evaluation of assumptions. The model simulates the aircraft with one degree of freedom. Thrust and current are interpolated from MotoCalc data, which assumes a fixed throttle setting for the entire flight. Drag is calculated as a function of velocity and load factor using aerodynamic results from Section 4.3. The course is segmented into turns and straight sections. For each segment, velocity, acceleration, and linear/angular position are tracked over finite time steps to calculate the time to complete each segment. Battery current draw is also integrated over time to determine the state of charge and energy used. Turns are modeled as being at constant altitude and at the highest load factor allowable by stall and structure. The velocity in turns is not sustained.

Individual segments are then connected and aircraft parameters are varied to simulate entire missions. A score for each mission can be predicted, as well as specific performance capabilities such as time to complete a 360° turn. Parameters such as velocity over the course of the missions can also be tracked to show the dynamics of the aircraft over the course of a mission. The velocity trajectories for the first lap of Mission 2 and the first lap of Mission 3 are shown in Figure 4.10.
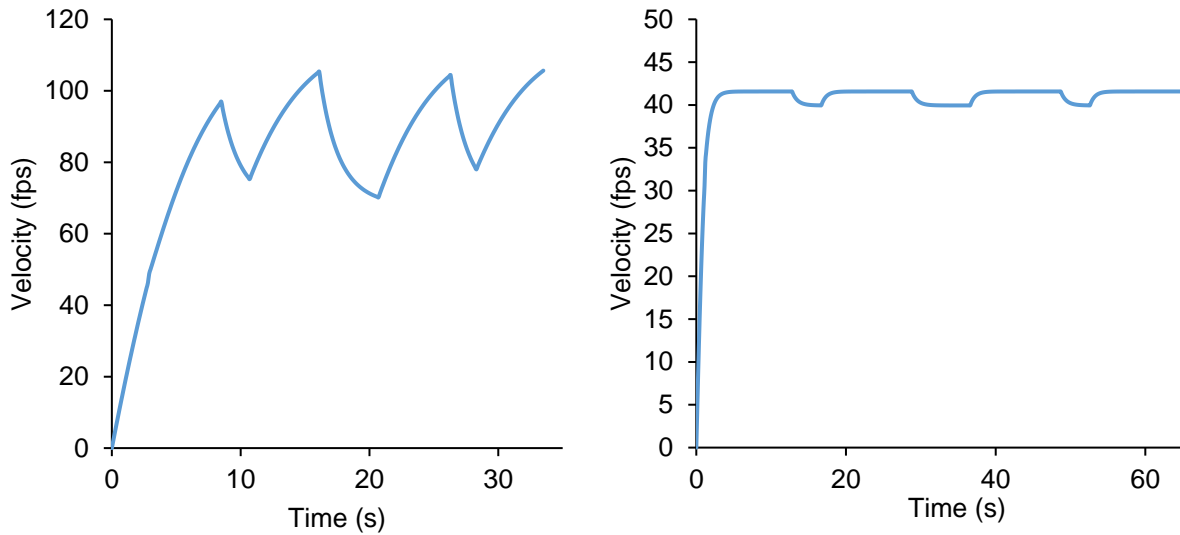
*Figure 4.10: Simulated trajectory for first lap of Mission 2 (left) and the first lap of Mission 3 (right)*

Analyzing results from the mission model highlights phenomena warranting further analysis, such as the loss of speed and slow acceleration seen in the Mission 2 trajectory.

### 4.5.2　Operating Condition Considerations

It is important to be aware of and consider the conditions in which the aircraft will be operating in the system design. Based on previous years' experience, wind in Kansas significantly affects flight performance. Flying upwind decreases ground speed and increases overall lap time, so the aircraft needs to maintain a higher airspeed. The distribution of average wind speeds in Kansas from 2010 to 2019 is shown in Figure 4.11, with an overall average of 13.7 mph [9].
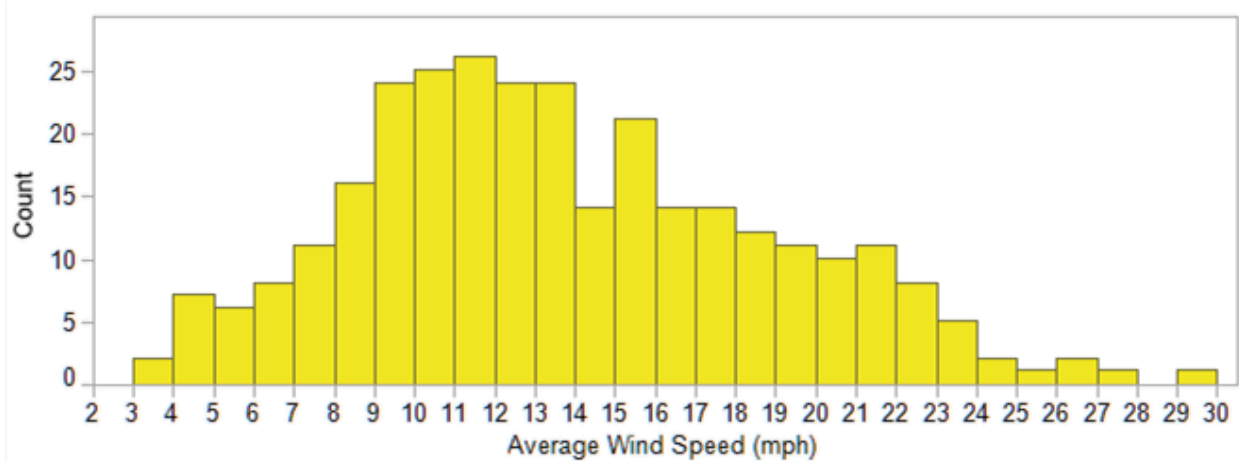


*Figure 4.11: Average wind speed in Wichita, Kansas from 2010 to 2019 [9]*

To ensure the aircraft can perform in the competition conditions, wind speed was incorporated in the performance and banner sizing models. Wind speed was an important factor in determining optimal banner size, so the analysis from Section 3.2.1 was refined to include data from the selected propulsion system and aerodynamic data from the selected configuration. The model was used to determine optimal banner sizes for a number of wind speeds. The team elected to create four banners, each of which are optimized for 10 mph wind intervals, as shown in Table 4.5.

*Table 4.5: Optimal banner length for a given wind speed*

| Wind Speed (mph) | Banner Length (ft) | No. of Laps | Banner-ft-laps |
|---|---|---|---|
| 0-10 | 10.1 | 10 | 101 |
| 11-20 | 5.9 | 13 | 76.6 |
| 21-30 | 4.2 | 14 | 59.2 |
| 30+ | 2.5 | 15 | 43.9 |

### 4.5.3 Uncertainties

As with any model, simplifying assumptions can lead to inaccurate results. Turning is one uncertainty, as the pilot cannot reliably recreate the conditions assumed in the model. There will be changes in altitude, roll, and thrust that are not modeled, and the turns will not be performed as close to stall as the model assumes. Another uncertainty is the propulsion data from MotoCalc. Although the static thrust and current data was validated, the data for the real system at speed could not be validated. As with the propulsion model, the aircraft aerodynamic model includes assumptions that lead to uncertainties. However, by selecting models that are most appropriate for the given aircraft and flight conditions, uncertainties were reduced as much as possible to obtain useful results from the models.

# 5 DETAIL DESIGN

## 5.1 Final Design – Aircraft

The aircraft dimensions did not vary much between the preliminary and detailed design stages because the structural analysis, component selection, and weight-balance calculations did not indicate major changes were needed. The final dimensional parameters are listed in Table 5.1. All wing and control surface chords were chosen to allow sufficient thickness for structure, embedded servos, and providing stability. Overall, the final aircraft is designed for stability, simplicity, and efficiency.

*Table 5.1: Final Aircraft Dimensions*

| Overall Dimensions | | | Wing Dimensions | | |
|---|---|---|---|---|---|
| Length | 69.0 | in | Span | 60.0 | in |
| L.E. X-Location | 10.0 | in | Mean Chord | 20.4 | in |
| C. G. X-Location | 18.0 | in | Aspect Ratio | 3 | ~ |
| Static Margin | 9.5% | chord | Area | 8.5 | ft$^2$ |
| Vertical Tail Dimensions | | | Horizontal Tail Dimensions | | |
| Height | 9.0 | in | Span | 20.0 | in |
| Chord | 9.0 | in | Chord | 9.0 | in |
| L.E. X-Location | 54.0 | in | L.E. X-Location | 54.0 | in |

## 5.2    Structural Characteristics

### 5.2.1    Layout and Design

The structural layout was designed to support all loads and provide an adequate load path to the major load-bearing components. The loads can be categorized and sized as follows:

Motor Loads: These include motor thrust, torque, and sustained vibrations at maximum thrust condition. These loads are primarily handled by the fuselage structure.

Aerodynamic Loads: These include wing and banner lift, drag, and moment. These loads are handled primarily by the wing structure, including spars, D-box, and shear webbing.

Ground Loads: These are impact loads when landing at maximum aircraft weight. These loads are handled primarily by the landing gear structure.

These loads transfer to the major load bearing components, which include the center fuselage spar, main and rear wing spars, and landing gear, as shown in Figure 5.1.
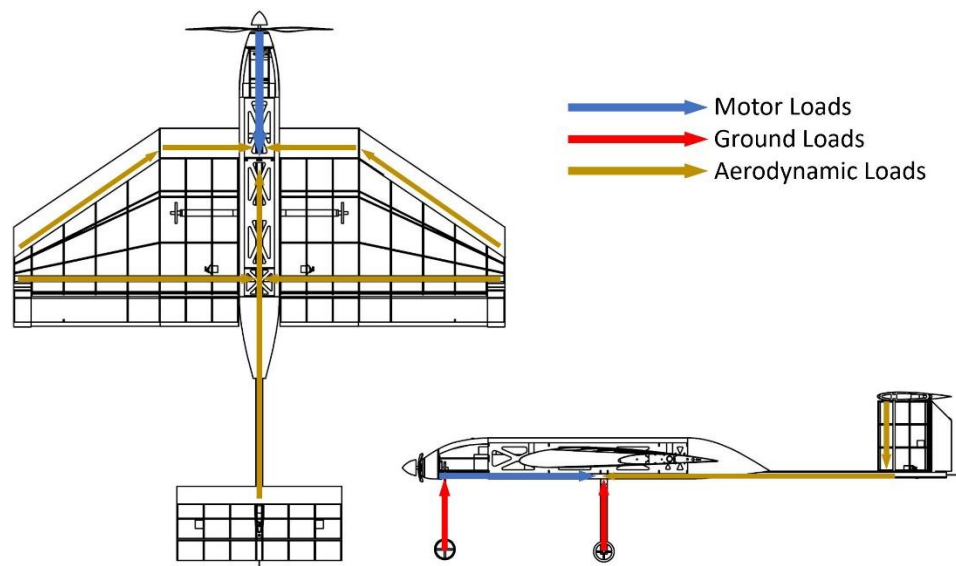


*Figure 5.1 Load paths of major forces*

The operating limits of the aircraft are defined by its aerodynamic and structural characteristics. Figure 5.2 displays these limits in a V-n diagram. The maximum allowable load factor is limited by either the maximum $C_L$ to prevent stall or by the structural load limit of 9g. The never-exceed velocity, $V_{NE}$, is set to 10% higher than the maximum cruise velocity to avoid flutter and buffeting. While the aircraft does not have enough thrust to reach $V_{NE}$ in level cruise, it could possibly do so in a dive.
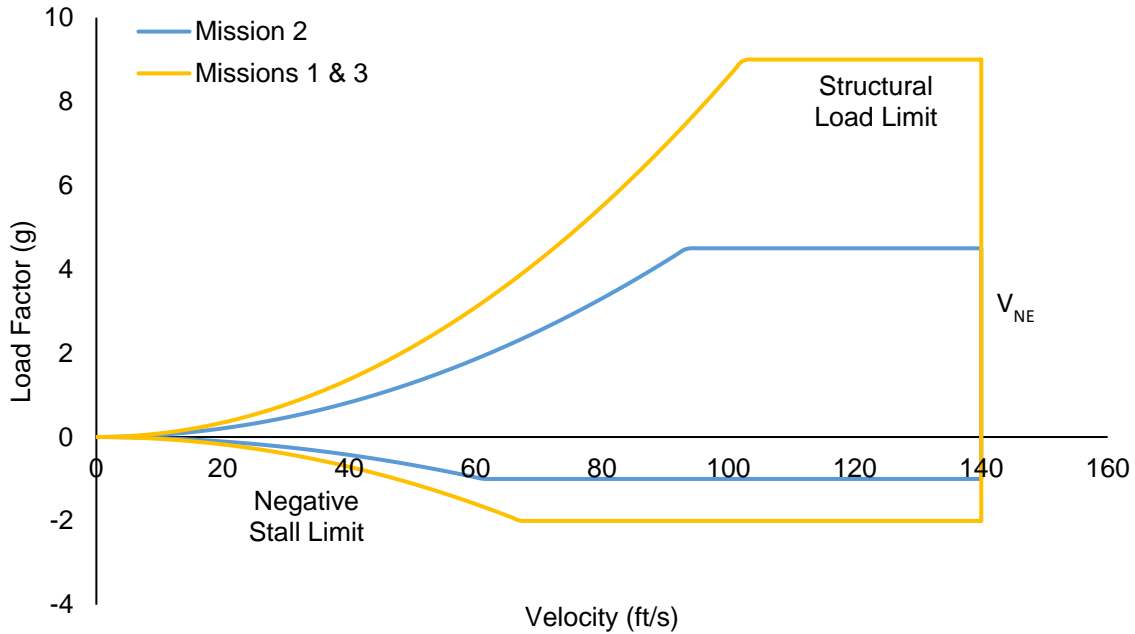


*Figure 5.2: V-n diagram showing loading as a function of velocity for all flight missions*

## 5.3   System and Subsystem Design and Implementation

The subsystems and components that make up *Buzzfighter* include the propulsion system, fuselage central spine, motor mount, fuselage, wing, empennage, banner release mechanism, landing gear, and avionics. While individually meeting performance requirements, these subsystems must also interface without hindering overall aircraft performance. This section details each subsystem and how it works in tandem with other subsystems.

### 5.3.1    Central spine

The central spine is the primary load-bearing member of the aircraft, extending from the motor mount through the fuselage and wing back to the empennage. As such, it is vital that this component does not fail under various flight loads. Based on aerodynamic analysis in Section 4.3, the lift distribution at the most strenuous flight condition is recorded and used to size the central spine. A square carbon fiber tube 0.83 inches in width and with a wall thickness of 0.034 was selected for its minimal deflection under maximum

flight loads. Euler-Bernoulli beam analysis was used to find the maximum deflection under worst case scenario loading conditions. The deflection and moment of across the spine are shown in Figure 5.3. The deflection of 0.22 in is 0.5%, which is within team's threshold for 5% of the distance from the C.G. This small deflection ensures that aeroelastic effects will not affect aircraft dynamics.
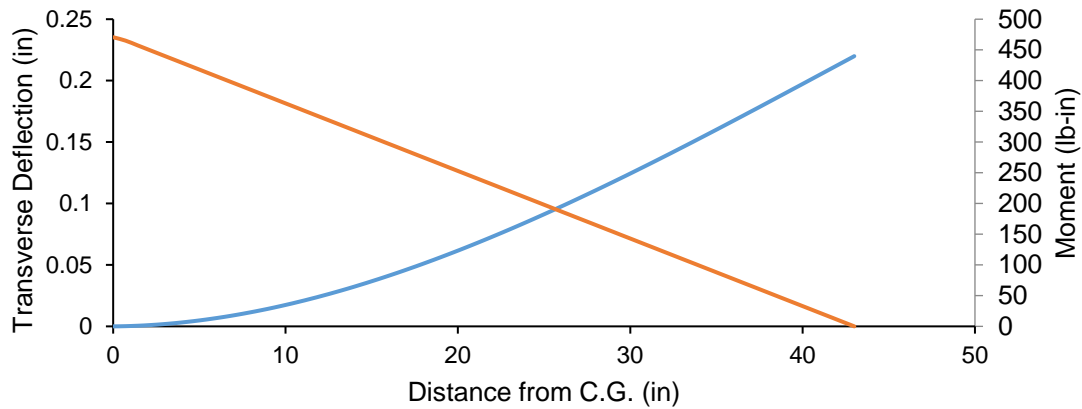


*Figure 5.3: Tail deflection and moment under maximum load*

### 5.3.2    Motor Mount

The motor mount shown in Figure 5.4 consists of two quarter inch thick plywood plates glued together with epoxy resin. Both plates have four holes each to accommodate fasteners used to mount the motor, which fits onto these plates and distributes the loads from the motor to a larger area on the spar. This design provides sufficient load transfer across the plates to the central spine for both the axial load which transfers across the epoxy joint and the torque load which transfers through friction between the plates and square spine. Some extra balsa wood stringers extend from the first fuselage bulkhead to the motor mount to add stiffness. Two collars attach the nose gear to the motor mount plate and spar via four bolts so that the moment from the long nose gear is effectively transferred into load bearing components.
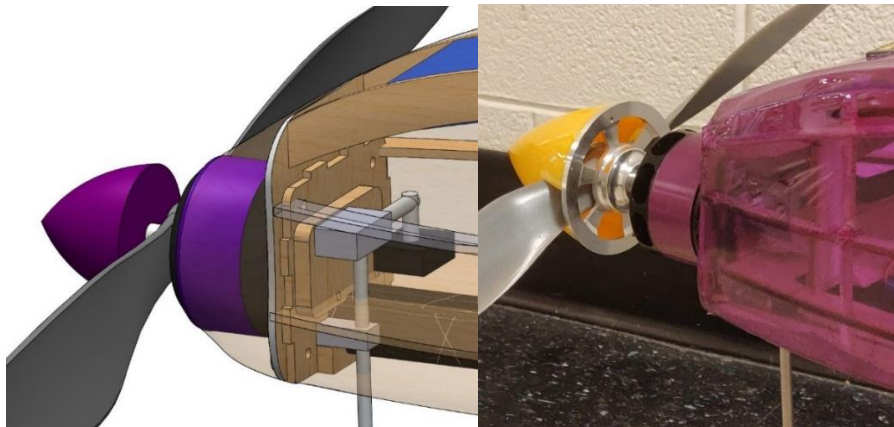


*Figure 5.4: CAD motor mount assembly (left) and real motor mount (right)*

### 5.3.3    Fuselage

The fuselage is designed to accommodate the passengers and luggage, as well as the battery, ESC, and receiver. To reduce form drag, the forward and aft sections are faired, and sharp exterior corners are rounded, as shown in Figure 5.5. All loads transfer to the main load bearing fuselage component (the central spine) through several plywood bulkheads glued onto the spine with epoxy resin. Additionally, there are vertical slots through the front and rear sections of the fuselage for the wing spars, allowing the aircraft to be disassembled for transportation.
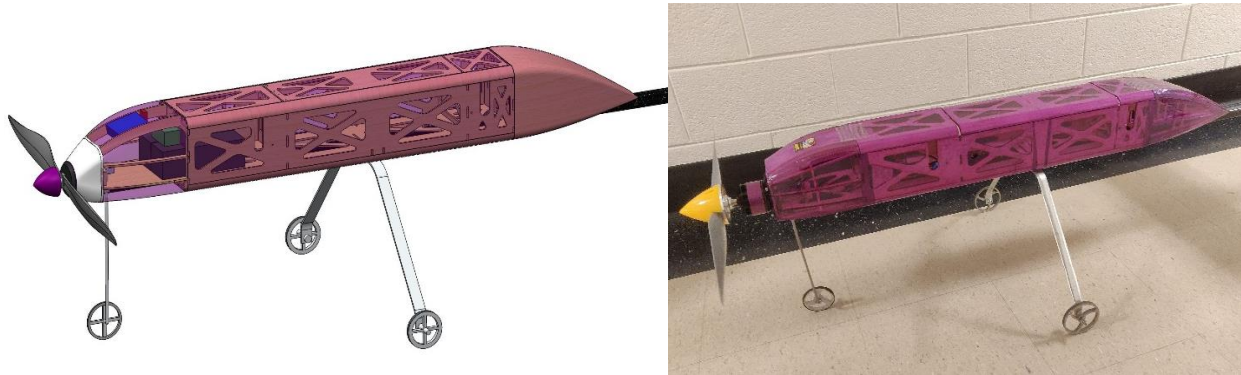


*Figure 5.5: Fuselage assembly*

### 5.3.4    Wing

The wing transfers aerodynamic loads of up to 5g at the maximum weight through two unidirectional carbon fiber spars. A 0.545" ID 0.631" OD forward spar runs through the front of the wing across the straight section, and 0.625" ID 0.713" OD aft spar runs across the entire wingspan as displayed in Figure 5.6. The wing slides into vertical slots in the fuselage and fastens with four bolts that transfer shear loads between the wing and the fuselage. The ailerons have balance tabs to reduce aerodynamic loads and to reduce the risk of flutter at high speeds. The usual external servo linkage on the ailerons was eliminated by mounting the servos inside the balance tabs, reducing drag from excrescence. In addition to ailerons, inboard flaps increase lift for takeoff and landing, decreasing takeoff distance and landing speed. The inboard section of the wing is constructed with eighth inch thick balsa and plywood ribs and stringers with a gap in the center to accommodate the fuselage box. The outboard sections use the same construction method, but taper toward the tips, as shown in Figure 5.6.
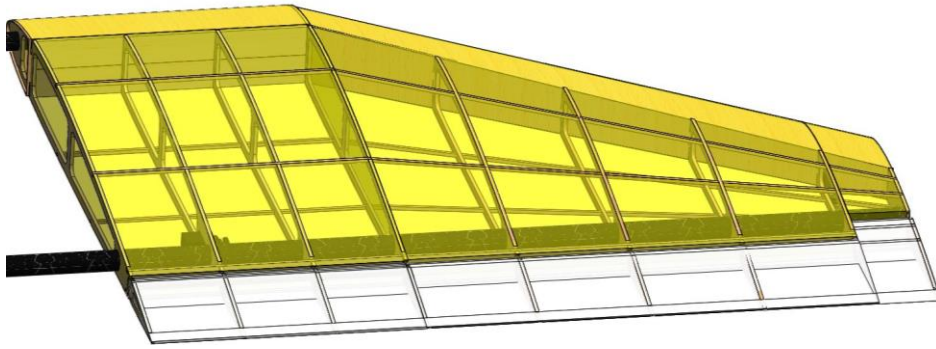
*Figure 5.6: Wing*

These tubes were sized to withstand the maximum aerodynamic load with a tip deflection of 10% of the wing semi-span. From the team's experience with previous competition aircraft, this requirement prevents control surface binding, overstretching of the plastic covering material, and other aeroelastic problems. The analysis was performed using the lift distribution calculated by AVL, and Euler-Bernoulli beam bending theory [10]. Using the resulting spar spanwise shear, bending moment, and deflection, the graphs displayed in Figure 5.7 and Figure 5.8 were generated.
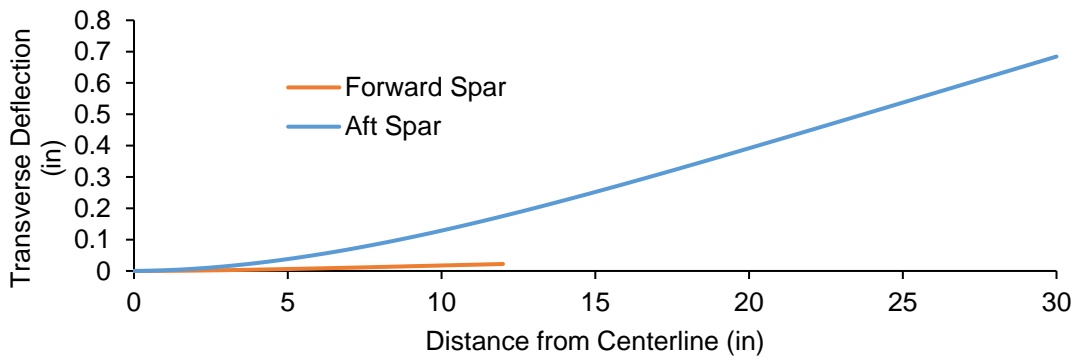


*Figure 5.7: Wing deflection distribution under maximum loading*
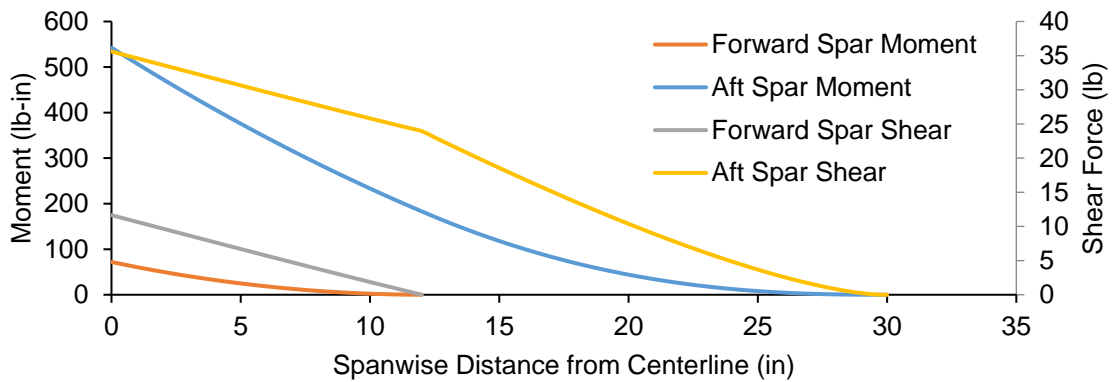


*Figure 5.8 Moment and shear distribution under maximum loading*

The aircraft experiences 0.7 inches of deflection at the tip under the maximum load of 94.5 lb for the 21 lb airplane at a load factor of 4.5. This deflection is 2.3% of the semi-span, lower than the 10% threshold used for safety. From Figure 5.7, the deflection on the aft spar is much greater, because the aft spar extends farther from the centerline and is subjected to greater forces farther from the root. The root bending moment and shear force can be seen to be far greater for the aft spar in Figure 5.8 as well, indicating that the forward spar is oversized.

### 5.3.5    Empennage

The empennage consists of a vertical tail mounted onto the rear of the carbon fiber central spine and a horizontal tail mounted atop the vertical in a T-Tail configuration, as shown in Figure 5.9. Both components are constructed in a similar fashion to the wings, with primarily balsa structure strengthened with plywood in areas with high stress concentrations. The horizontal tail is reinforced with carbon fiber strips that are bonded to the surface across the top and bottom of the quarter-chord to transfer moment loads. The primary structure in the vertical tail is the front and rear spars, which are 0.25 in diameter carbon fiber tubes that transfer loads from the horizontal and vertical tail to the fuselage spar. The elevator is split to provide redundancy in control, and both halves have balance tabs with integrated servos, similar to the ailerons.



*Figure 5.9: Empennage assembly*

### 5.3.6    Banner Deployment and Release Mechanism

The banner subsystem shown in Figure 5.10 is composed of two parts: a mechanism to hold the banner in place and deploy it on command, and a mechanism to tow the banner and release it on command. The banner is securely stowed underneath the aircraft with rubber bands at two locations to prevent rotation, which are held in place and released by pins attached to servos. The banner release mechanism consists of a pin that goes through a loop in the banner string. When commanded to release, the pin is pulled, and the banner falls from the aircraft.
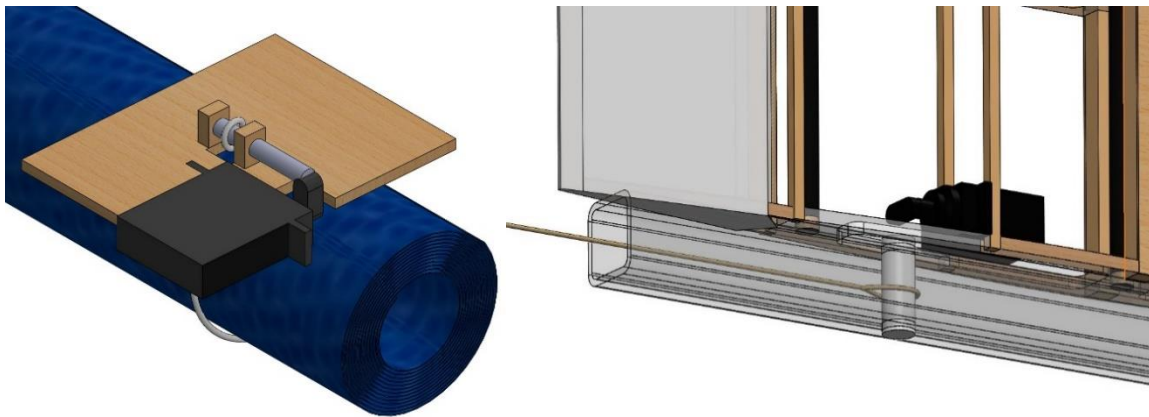
*Figure 5.10: Banner deployment mechanism with banner attached (left) and release mechanism (right)*

### 5.3.7    Landing Gear

A tricycle landing gear configuration was selected to provide enough clearance to mount and deploy the banner beneath the aircraft. The main landing gear is formed out of a strip of 5/16 inch thick, 3/4 inch wide aluminum, which was selected both to withstand the impact loads upon landing and save weight (compared to steel). The U-bend of the landing gear also acts as a spring, absorbing the landing impulse and reducing the forces on the fuselage. The front landing gear is steerable to control the aircraft during takeoff and landing rolls. The wheel is mounted on a 5/16 inch steel rod that extends into the nose of the aircraft and is actuated by a servo linkage. The wheels are made of water jetted aluminum, and are thin to reduce frontal area and thus drag. The height of the gear was geometrically determined to allow a roughly 14 degree tip-back angle, mitigating the risk of a tail strike on takeoff or landing.

The landing gear was analyzed to ensure that it can withstand landing forces using a SolidWorks FEA tool. Similar wheels have been in the past on heavier aircraft without showing any signs of fatigue, so only the aluminum U-shaped strip was considered in the analysis. A total force of 42 lb was applied evenly between the two wheel axles to simulate a 2g landing at full weight. The landing gear is mounted to the fuselage through four screws, so the screw holes and the area in contact with the fuselage can be simulated as fixed. To reduce the risk of gear failure, the thickness of the aluminum strip was increased until the maximum stress exceeded the yield stress of 6061 aluminum with a safety factor of 1.5. As can be seen in Figure 5.11, stress was evaluated using the von Mises stress criterion, which is a method for calculating local stress. After this analysis, a thickness of 5/16 inch was chosen for the gear, as this is the minimum thickness that can safely withstand landing loads and also be readily purchased.
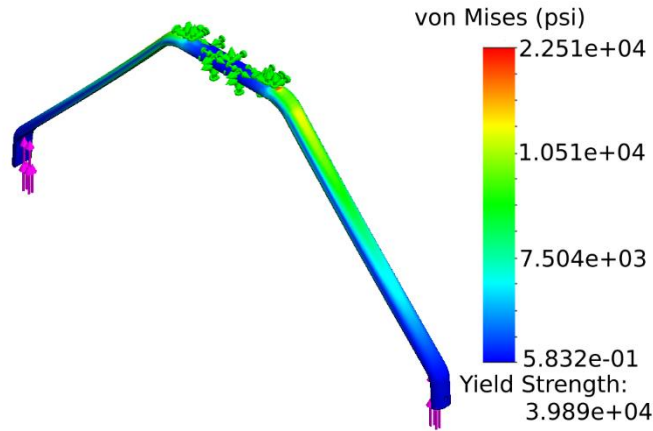
*Figure 5.11 FEA of landing gear subject to 2g loading*

### 5.3.8 Passenger Restraint System

As can be seen in Figure 5.12, the cabin floor is covered with evenly spaced wooden dowels to both restrain and separate the passengers. These dowels are also chamfered so as to make loading of the passengers easier when they are dropped into the payload bay. In order to secure the passengers and maintain their separation, a restraint attached to the bay lid is placed over top of them, constraining vertical motion and sideways motion.
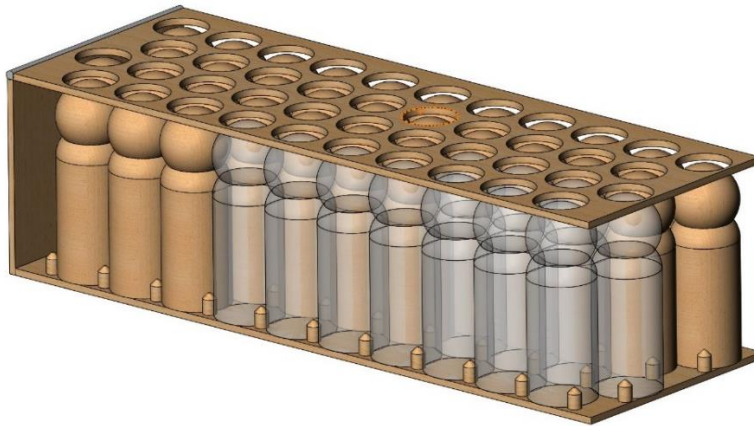


*Figure 5.12: Passenger restraint system*

### 5.3.9 Propulsion System

A combination of two 6S 4500 mAh Scorpion Competition Powerpack LiPo batteries connected in parallel was selected to provide necessary capacity for Mission 3's required power draw, as explained in Section 4.2.2. A Castle Lite 100 Amp ESC was selected to handle the maximum current draw expected for Mission 2. A variety of motors and propeller combinations were analyzed using the MotoCalc program with this battery choice, as described in Section 4.2.2, from which the Hacker A60 5XS motor and APC 17x12E propeller were chosen to balance low speed thrust for a short takeoff and thrust at higher velocities for cruise. The final selected propulsion system is listed in Table 5.2.

*Table 5.2: Propulsion system components*

| Components | Description |
|---|---|
| Motor | Hacker A60-5XS 420 Kv |
| Battery | 2 x Scorpion 6S 4500 mAh LiPo |
| Speed Controller | Castle Phoenix Edge Lite 100 |

### 5.3.10   Avionics

The aircraft has a total of 11 servos that are used to actuate control surfaces, landing gear, and various mechanisms. Servo selection involves four main considerations: torque, form, response time, and weight. For this aircraft, torque, form, and response considerations outweighed weight considerations. The servos on the ailerons should provide sufficient torque to actuate the ailerons, and have a relatively short response time to increase maneuverability. They also must be small enough to fit inside the aileron balance tab while leaving enough space for wood structure. For the flaps, response time is not as important, but the servos need to be strong enough to hold the flaps against aerodynamic loads. Similarly to the ailerons, quick response time and high strength are both required in the elevator servos to increase maneuverability. The servos and throttle are controlled using a Futaba R7014SB receiver, which is in turn commanded by a Futaba T14FG transmitter from the pilot. The final selected components are shown in Table 5.3

*Table 5.3: Selected electronics components*

| Components | Description | Servo Torque (kg-cm) |
|---|---|---|
| Receiver | Futaba R7014SB | ~ |
| Transmitter | Futaba T14FG | ~ |
| Elevator Servos | Turnigy TGY-811 | 8.2 |
| Rudder and Gear Servos | Corona DS-236MG | 6.0 |
| Aileron and Flap Servos | Corona DS-236MG | 6.0 |
| Banner Mechanism Servos | Turnigy TGY-811 | 8.2 |

## 5.4   Weight and Balance

A correct center of gravity (C.G.) location is critical for longitudinal control and stability. All C.G. analysis was performed in SolidWorks using models for each component with proper weights and densities, and then validated with the physical vehicle. The results for all three missions are displayed in Table 5.4. The X locations are measured aft positive from the front of the motor mount.

Since Mission 2 requires carrying 40 passengers and their luggage, amounting to 12.5 lb of payload, the passengers and luggage C.G. must be close to the empty C.G. location in order to maintain longitudinal stability. Having two luggage compartments and having space to adjust battery location allows the C.G. to be adjusted if necessary.

*Table 5.4: Weight and balance table*

| Category | Components | Weight (lb) | X-CG location (in) |
|---|---|---|---|
| Structure | Nose Landing Gear | 0.25 | 2.08 |
| | Main Landing Gear | 0.54 | 19.64 |
| | Tail | 0.60 | 58.38 |
| | Wing | 1.80 | 19.68 |
| | Fuselage Spar | 0.36 | 29.08 |
| | Fuselage | 0.60 | 17.23 |
| | Aileron/Flap Servos | 0.18 | 56.88 |
| | Rudder/Elevator Servos | 0.13 | 17.88 |
| | Banner Mech. Servos (2) | 0.12 | 17.88 |
| **Empty Aircraft Structure** | **Structure** | **4.46** | **25.73** |
| Propulsion | Prop Spinner | 0.12 | -1.99 |
| | APC 17x12E | 0.11 | -1.99 |
| | Hacker A60-5XS | 1.31 | 0.28 |
| | Castle Phoenix Edge Lite 100 | 0.24 | 4.28 |
| | Receiver | 0.04 | 7.18 |
| | Wiring and Connectors | 0.21 | 29.08 |
| | Main Battery | 1.70 | 14.50 |
| | Receiver Battery | 0.07 | 7.32 |
| **Mission 1** | **Propulsion + Structure** | **8.27** | **16.3** |
| M2 Propulsion | Main Battery | 1.70 | 7.28 |
| Mission 2 Subsystems | Passengers (40) | 10.00 (M2) | 18.58 |
| | Luggage (40) | 2.50 (M2) | 20.88 |
| **Mission 2** | **M2 Propulsion + Structure + M2 Subsystems** | **20.77** | **18.0** |
| M3 Propulsion | Main Batteries | 3.40 | 16.88 |
| Mission 3 Subsystems | Banner | 0.91 (M3) | 17.88 |
| **Mission 3 (Stowed/Released)** | **M3 Propulsion + Structure + M3 Subsystem** | **10.87 / 10.87** | **18.1 / 21.5** |

The static margin for all 3 missions ranges between 8.1% and 9.1%, making it sufficiently stable while also allowing the pilot to maneuver as necessary.

## 5.5   Performance

### 5.5.1   Flight Performance

Analysis was conducted to assess the aircraft's performance on different sections of the flight course. Point performance parameters for each mission are shown in Table 5.5. The wing loading and stall speed were calculated at a load factor of one for the gross takeoff weight of each mission using an estimation of $C_{L,max}$ from AVL modeling and section lift data. Then, the load factor was calculated by dividing the maximum design load of 108 pounds by each mission's gross takeoff weight. The turn radius was calculated using

the maximum allowable load factor in a level turn in the equation for turn radius from *Aircraft Performance and Design* [11].

$$R = \frac{V_\infty^2}{g\sqrt{n^2 - 1}}$$

(5.1)

Time for 360 was calculated using the equation for turn rate from *Aircraft Performance and Design* [11].

$$\omega = \frac{g\sqrt{n^2 - 1}}{V_\infty}$$

(5.2)

*Table 5.5: Aircraft flight performance parameters for each mission*

| Parameter | Mission 1 | Mission 2 | Mission 3 |
|---|---|---|---|
| Weight (lb) | 8.3 | 20.7 | 10.9 |
| W/S (psf) | 0.98 | 2.44 | 1.28 |
| $V_{min}$ (fps) | 25.9 | 41.0 | 29.7 |
| $V_{max}$ (fps) | 123 | 121 | 48 |
| Turn Load Factor | 9.0 | 4.5 | 3.0 |
| Turn Radius (ft) | 52.8 | 103.2 | 25.3 |
| Time for 360 (s) | 2.7 | 5.4 | 3.3 |

MotoCalc was used to provide a thrust available curve with respect to velocity for the selected propulsion system. This was then co-plotted with required thrust curves for the aircraft configuration in each mission and can be seen in Figure 5.13: Thrust available and thrust required curves for each flight mission. The maximum velocity is determined by finding the intersection between these curves and the minimum velocity is determined by stall. In Mission 1, the aircraft has the lowest weight and the lowest drag, which results in the highest cruise velocity. In Mission 2, the aircraft is heavily loaded with payload, which causes a large increase in induced drag at lower velocities, but only leads to a decrease in maximum velocity of 2 fps. In Mission 3, the large banner contributes to a large increase in parasite drag, limiting the maximum velocity to 48 fps.
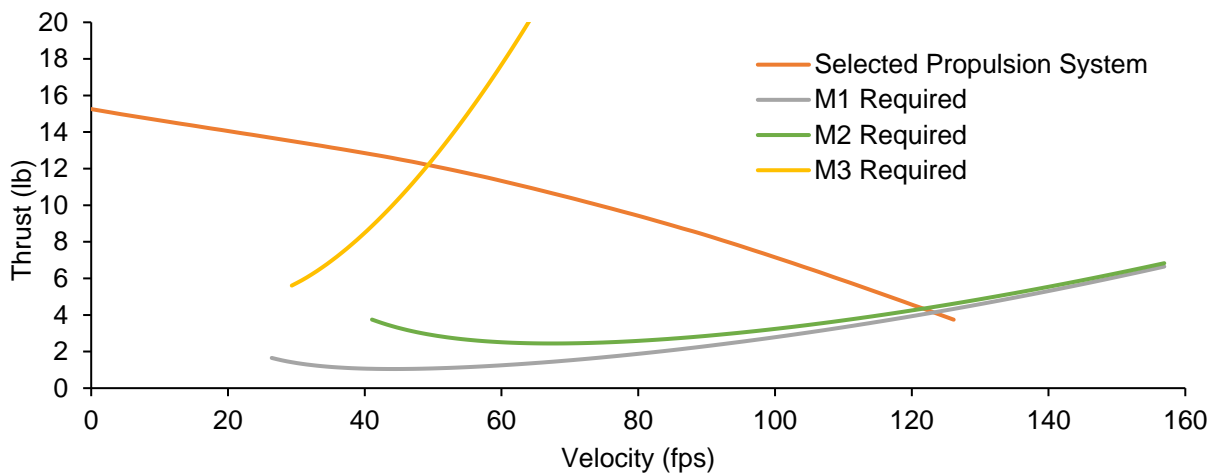


*Figure 5.13: Thrust available and thrust required curves for each flight mission*

### 5.5.2    Mission Performance

The mission model described in Section 4.5 was used to estimate the overall mission performance of the aircraft, along with lift and drag values from AVL confirmed by flight testing. Figure 5.14: Simulated trajectory for the first lap of Mission 2 (left) and the first lap of Mission 3 shows velocity trajectories of the first lap of Mission 2, which is representative of all three of its laps (apart from the slow start after takeoff). The velocity trajectory for the first lap of Mission 3 shown in Figure 5.14 exhibits fewer fluctuations as the aircraft can accelerate more quickly and performs turns with a much lower load factor. The first Mission 2 lap lasts 33.7 seconds while the second and third laps each last 29.3 seconds.
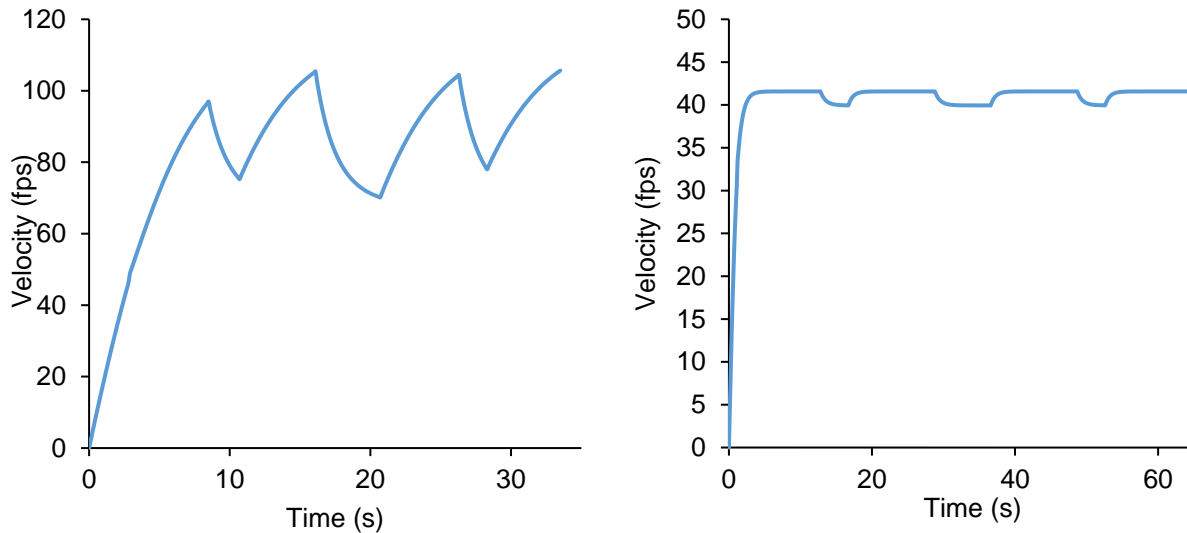


*Figure 5.14: Simulated trajectory for the first lap of Mission 2 (left) and the first lap of Mission 3 (right)*

## 5.6   Drawing Package

The following four pages illustrate the detailed CAD of the *Buzzfighter* system. The first sheet contains the three-view diagram with relevant dimensions. The second sheet contains the structural arrangement of all major components. The third sheet shows the system layout of electronics and subsystems. The fourth sheet displays the payload accommodation.
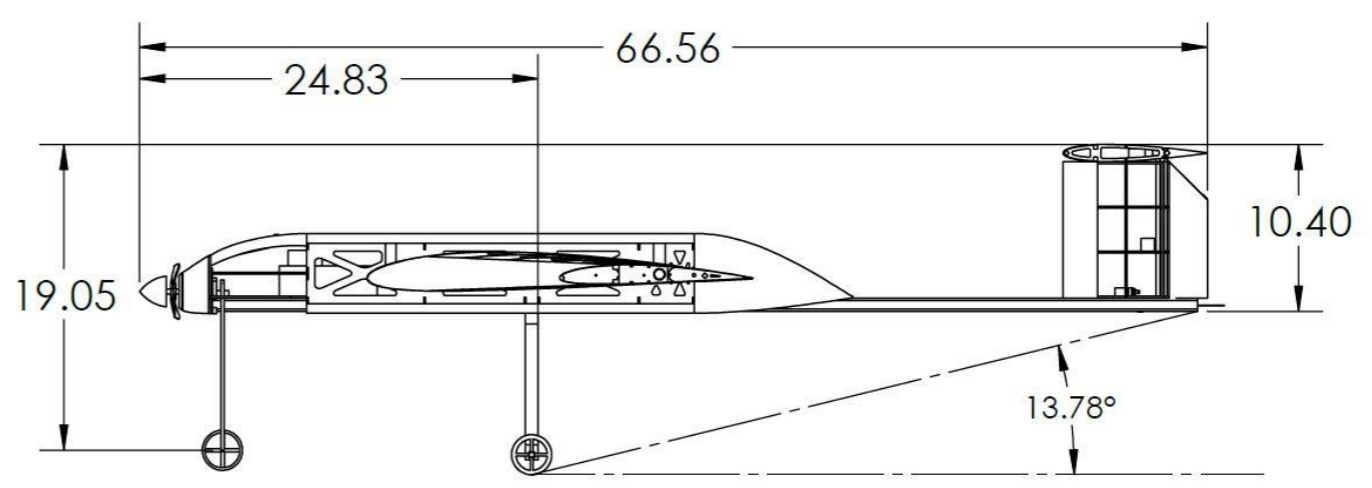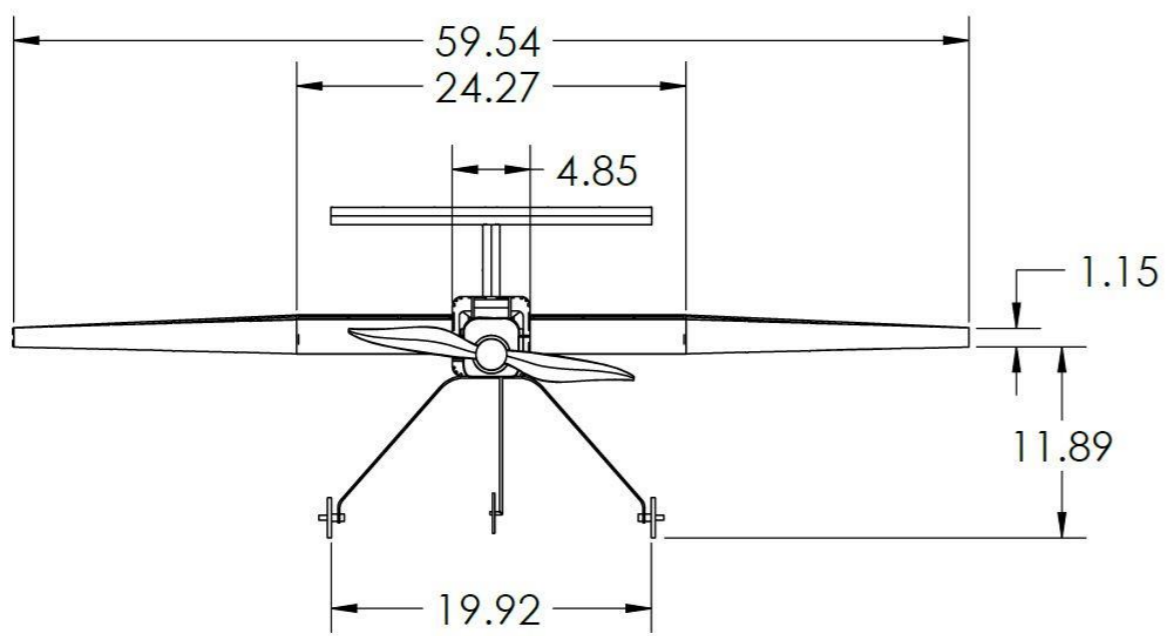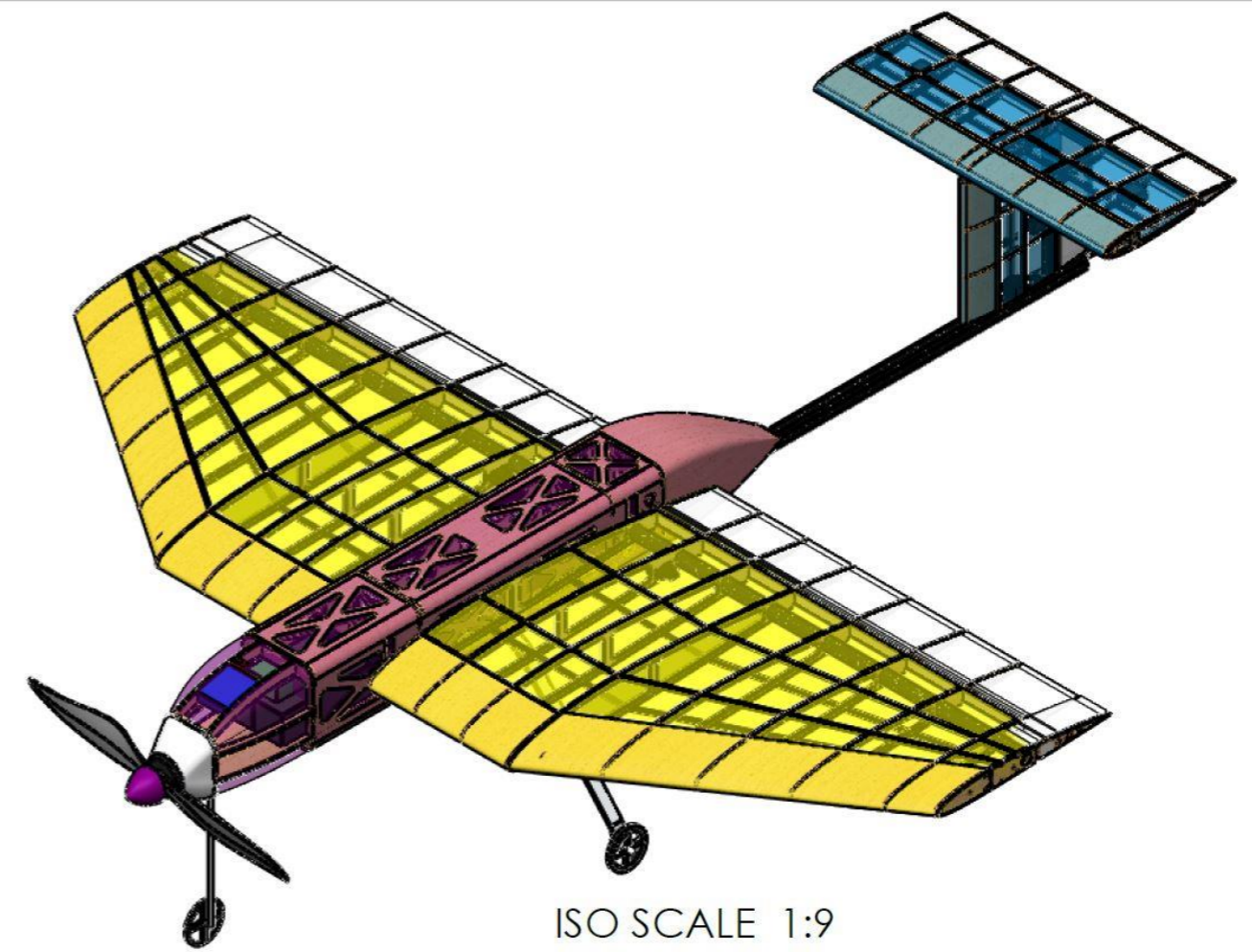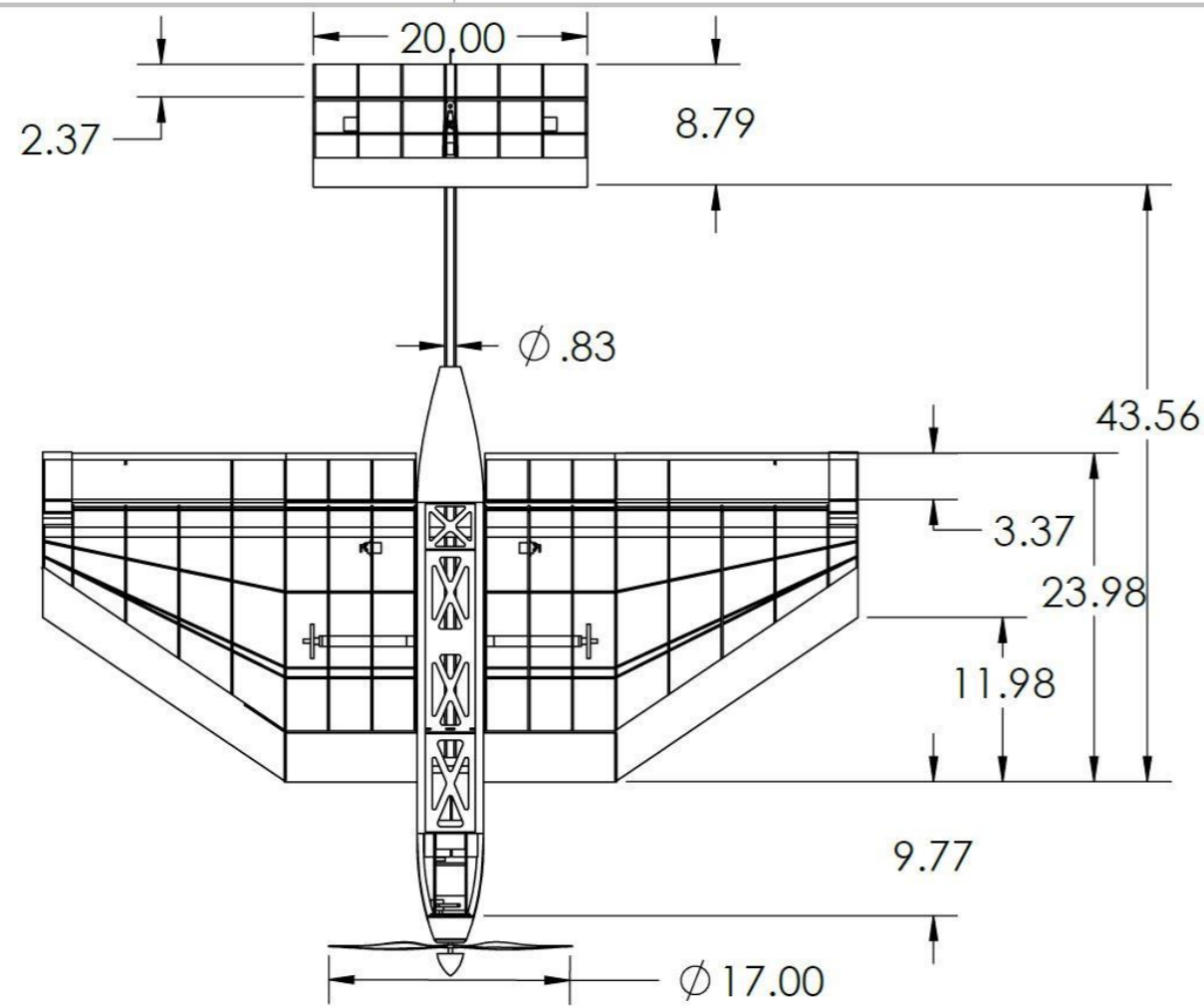
ISO SCALE 1:9

| 2/20/2020 | Georgia Institute of Technology | |
|---|---|---|
| Drawn by: Antoine Paletta | Buzzfighter | |
| Checked by: George P. Burdell | Size B | Aircraft Three-View with Dimensions |
| Scale 1:12 | All Dimensions in Inches | Sheet 1 of 4 |

Dimensions (top view): 20.00, 2.37, 8.79, ⌀.83, 43.56, 3.37, 23.98, 11.98, 9.77, ⌀17.00

Dimensions (front view): 59.54, 24.27, 4.85, 1.15, 11.89, 19.92

Dimensions (side view): 66.56, 24.83, 19.05, 10.40, 13.78°

| PARTS LIST | | | |
|---|---|---|---|
| ITEM | QTY. | ITEM NAME | MATERIAL |
| 1 | 2 | Motor Mount | Plywood |
| 2 | 1 | Front Wing Spar | Carbon Fiber |
| 3 | 18 | Wing Rib | Plywood and Balsa |
| 4 | 1 | Aft Wing Spar | Carbon Fiber |
| 5 | 2 | Balance Tab | Plywood |
| 6 | 2 | Flaperon | Balsa |
| 7 | 2 | Aileron | Balsa |
| 8 | 1 | Tail Boom | Carbon Fiber |
| 9 | 1 | Vertical Tail | Balsa |
| 10 | 1 | Horizontal Tail | Balsa |
| 11 | 2 | Elevator | Balsa |
| 12 | 1 | Rudder | Balsa |
| 13 | 2 | Tail Spar | Carbon Fiber |
| 14 | 1 | Payload Bay | Plywood |
| 15 | 1 | Main Landing Gear | Aluminum |
| 16 | 2 | Main Wheel | Aluminum |
| 17 | 1 | Fuselage | Plywood and Balsa |
| 18 | 1 | Nose Fairing | 3D Printed PLA |
| 19 | 1 | Nose Landing Gear | Aluminum |
| 20 | 1 | Nose Wheel | Aluminum |
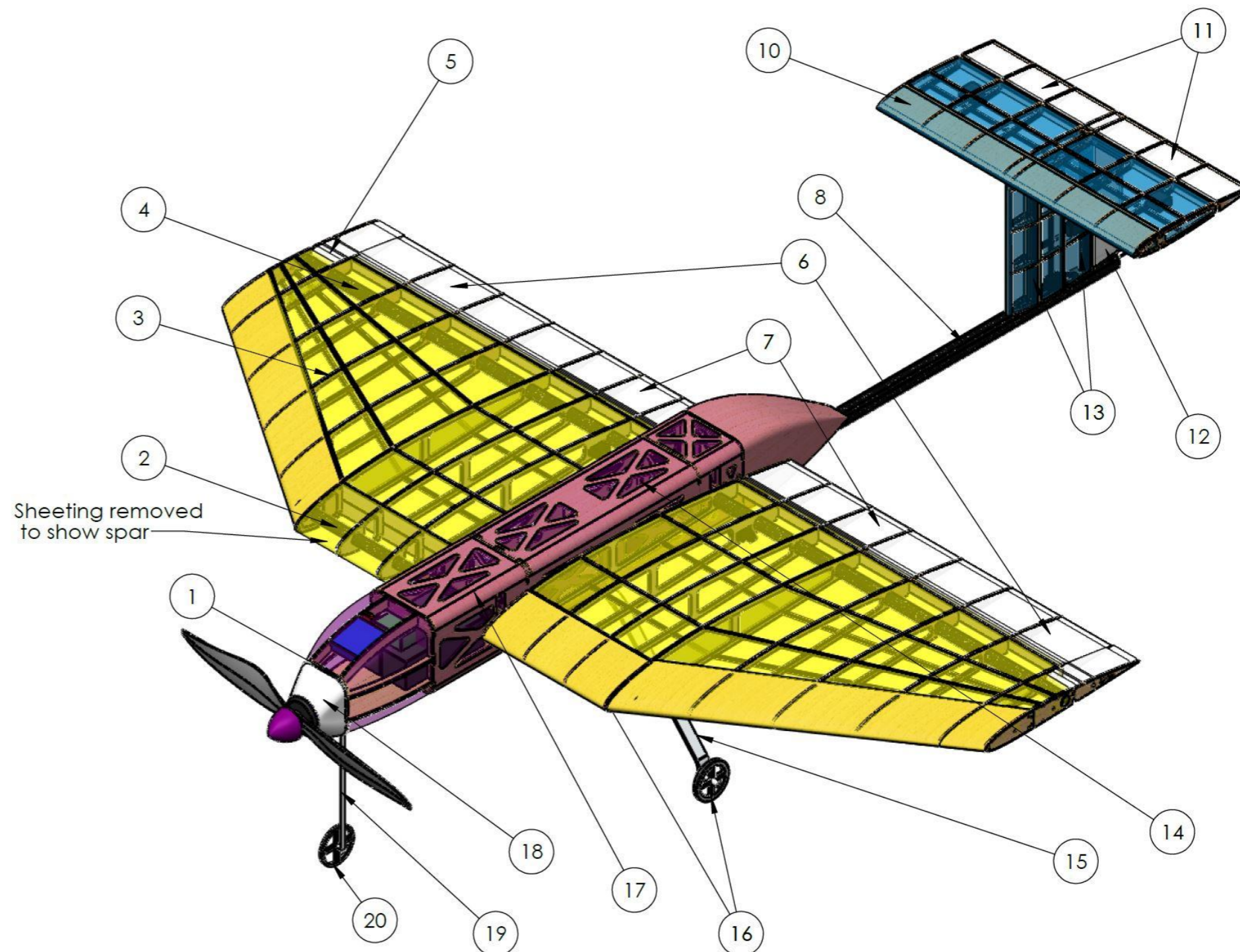
Sheeting removed to show spar



| | 2/20/2020 | Georgia Institute of Technology | |
|---|---|---|---|
| | Drawn by: Antoine Paletta | Buzzfighter | |
| | Checked by: George P. Burdell | Size B | Aircraft Structural Arrangement |
| | Scale 1:7 | All Dimensions in Inches | Sheet 2 of 4 |

| SYSTEMS LIST | | | |
|---|---|---|---|
| ITEM | QTY. | ITEM NAME | DESCRIPTION |
| 1 | 2 | Propeller | APC 17 x 12E |
| 2 | 1 | Motor | Hacker A60-5XS |
| 3 | 1 | Speed Controller | Castle Phoenix Edge Lite 100 A |
| 4 | 1 | Fuse | 100 A |
| 5 | 2 | Aileron Servo | Corona DS-236MG |
| 6 | 2 | Flaperon Servo | Corona DS-236MG |
| 7 | 1 | Rudder Servo | Corona DS-236MG |
| 8 | 2 | Elevator Servo | Turnigy TGY-811 |
| 9 | 1 | Banner Release Servo | Turnigy TGY-811 |
| 10 | 1 | Banner Deploy Servo | Turnigy TGY-811 |
| 11 | 2 | Battery | 6S 4500mAh LiPo |
| 12 | 1 | Receiver | Futaba R7014SB |

| 2/20/2020 | Georgia Institute of Technology | |
|---|---|---|
| Drawn by: Antoine Paletta | Buzzfighter | |
| Checked by: George P. Burdell | Size B | Aircraft Systems Layout |
| Scale 1:7 | All Dimensions in Inches | Sheet 3 of 4 |
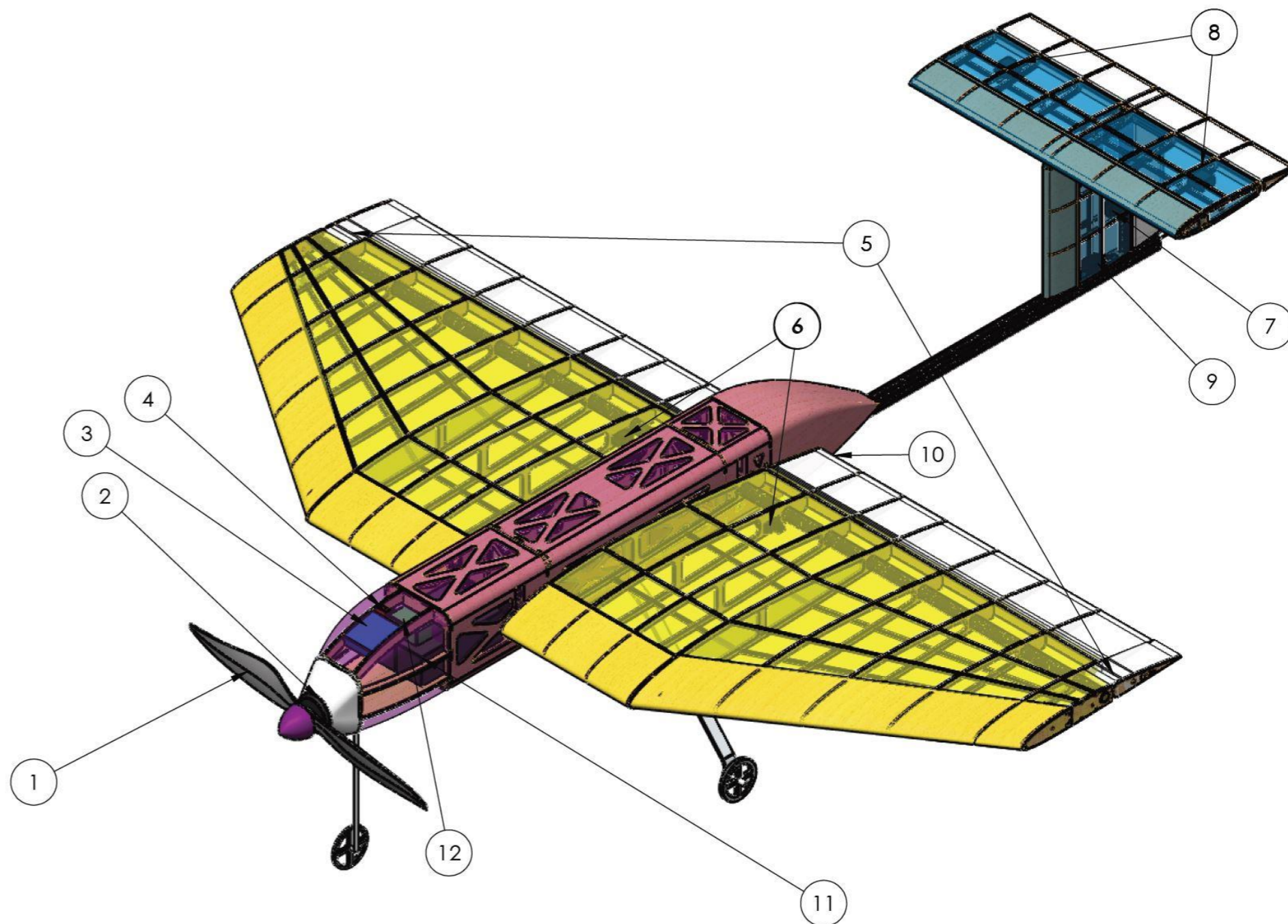
Deploy servo pulls pin which releases rubber band and deploys banner

Detail A
Scale 1:1
Section View
Isometric
Deploy Servo

Top restraint attached to lid
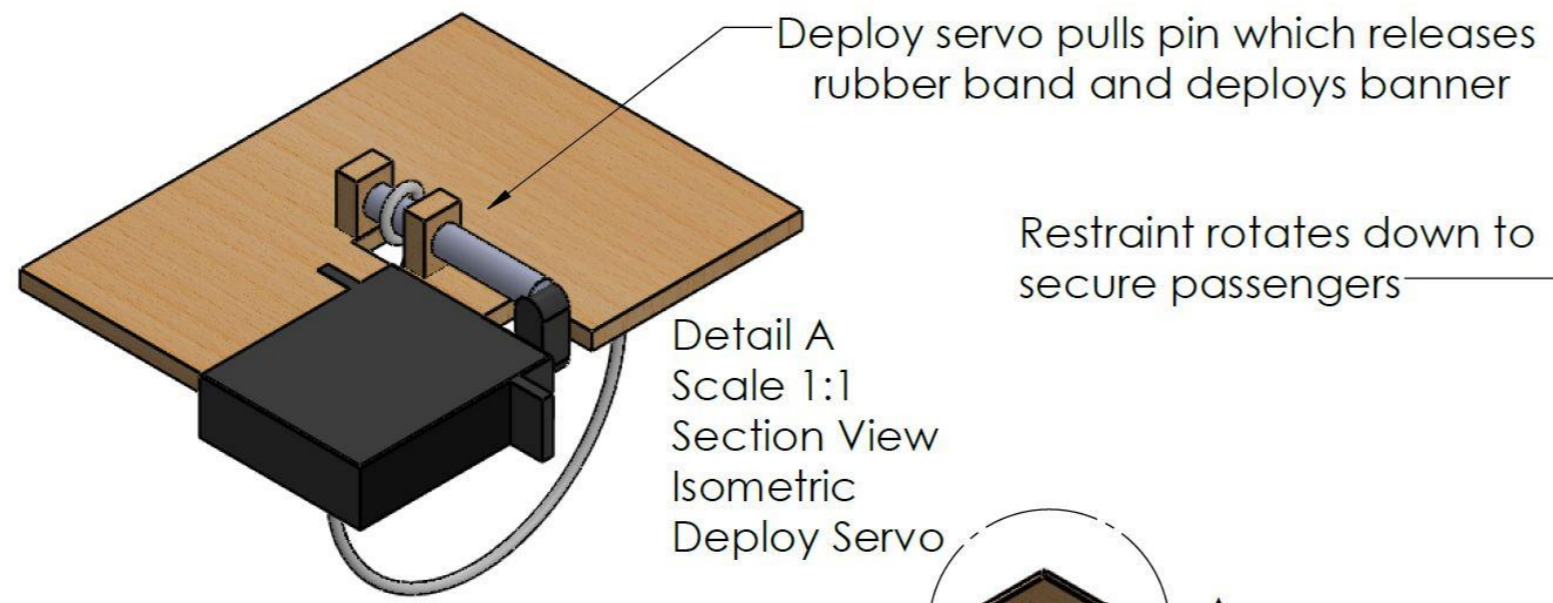
Restraint rotates down to secure passengers

A

Deploy Servo

Banner

Rubber Band

Passengers

Floor Restraint
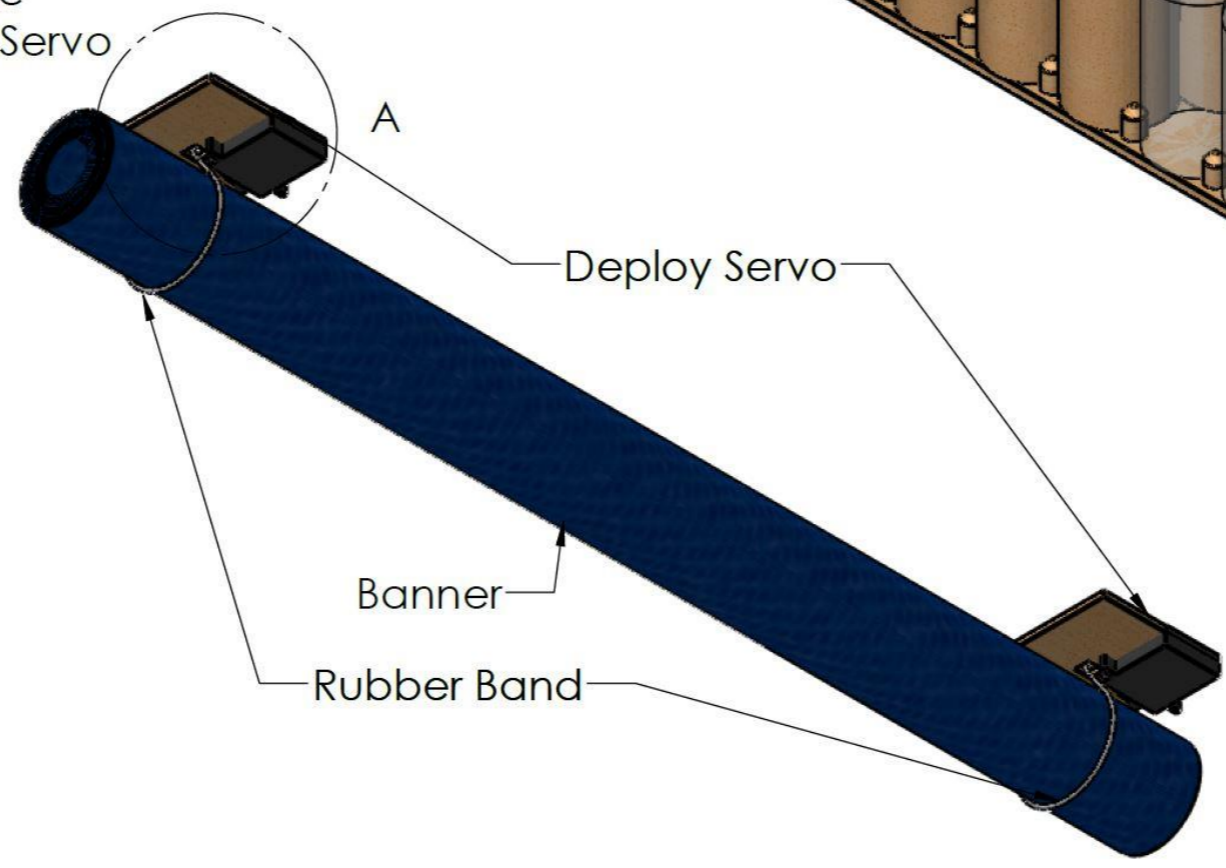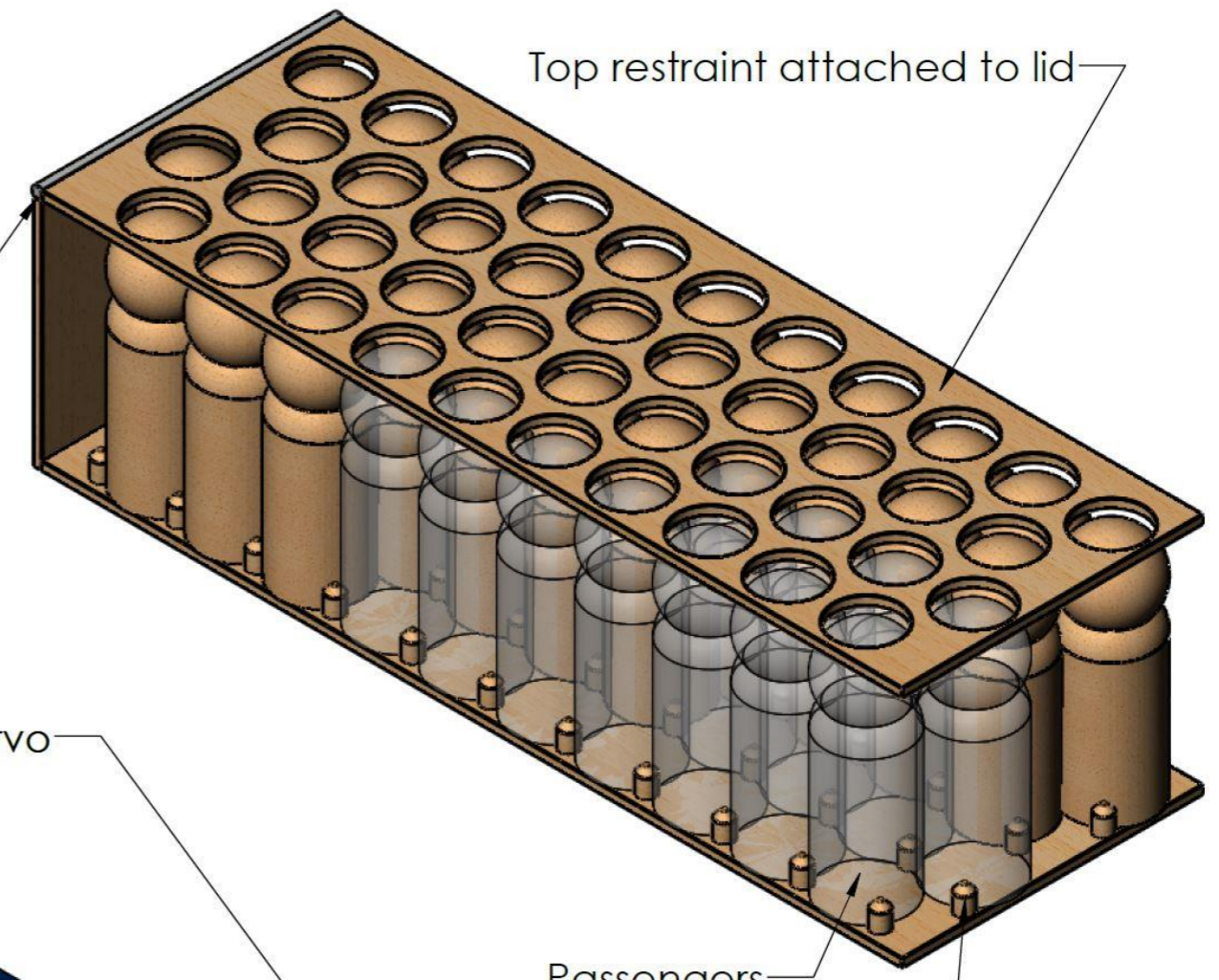
To Banner

Release servo pulls pin which releases string attached to banner

Attachment Pin
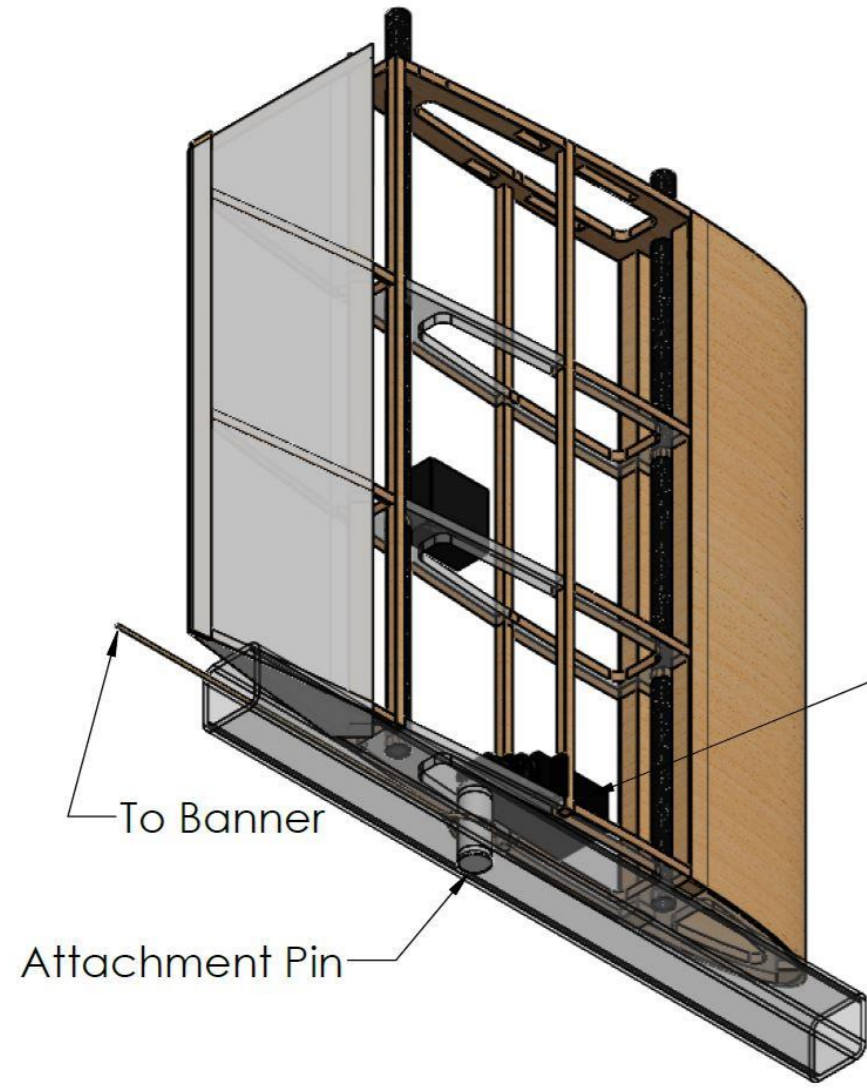
Tail Scale 1:4

| 2/20/2020 | Georgia Institute of Technology | |
|---|---|---|
| Drawn by: Antoine Paletta | Buzzfighter | |
| Checked by: George P. Burdell | Size B | Aircraft Payload Accommodation |
| Scale 1:2 | All Dimensions in Inches | Sheet 4 of 4 |

# 6  MANUFACTURING

The team considered various manufacturing processes and materials to construct the aircraft. The manufacturing process selected represented the best combination of weight, ease of repair, speed of manufacturing, team experience with the process, and cost.

## 6.1  Processes Investigated

The team had extensive experience using the built-up balsa wood manufacturing technique. However, there were viable alternative processes which could have been superior and thus were worth investigating. To evaluate alternatives, figures of merit were chosen that reflected important considerations in the manufacturing process.

Ease of Manufacture: The ability to quickly produce aircraft to specification is critical for rapid prototyping to meet important deadlines. Thus, it was assigned a weight of 3.

Weight: Weight factors into flight performance and is critical for efficient flying at low speeds. The effect of manufacturing materials and techniques on aircraft weight were assigned a weight of 5.

Experience: The team's knowledge was given some weight because it relates to the ability of team members to produce quality results, as well as to refine existing techniques. Experience also contributes to relative ease of manufacture. However, the team is always open to learning new techniques, so experience was given a weight of 2.

Ease of Repair: Minor damage is an inevitable part of testing, so the ability to repair components quickly should be considered. This was deemed to be of moderate importance and was thus assigned a weight of 2.

Cost: It should be kept in mind that the team has limited resources, thus cost is also a factor. However, if budgeting allows, the team should be willing to pay for higher performance materials and parts if they contribute to the success of the aircraft. Cost was therefore assigned a weight of 1.

Based on these Figures of Merit, several manufacturing processes and materials common to remote control aircraft construction were investigated.

Built-up Balsa: Pieces made of aerospace grade balsa wood are laser cut from CAD models and glued together using cyanoacrylate (CA) adhesive to form the airframe and tail surfaces of the aircraft. Carbon Fiber and plywood are used when required to reinforce specific parts of the aircraft, after which it is then covered with Monokote heat shrink film.

Fiber Reinforced Plastic (FRP): Foam molds are created based on the outer-mold line of the aircraft. A fiberglass-epoxy layup or carbon fiber-epoxy layup is then made within a vacuum bag, and the system is sealed for 24 hours to allow for a full cure. The molds are then removed so that the reinforced plastic acts as the primary structure.

3D Printing: CAD models are printed using professional grade 3D printers. Print time increases proportionally with the volume of the aircraft.

Foam Core Composite: Large blocks of foam are cut with a hot-wire or CNC router to form the basic shape of the aircraft. Structural reinforcements are locally added if needed, and the entire foam-core is coated in fiberglass or carbon fiber, adding strength as a monocoque.

The processes were evaluated against each other by assigning each one a FOM score, with a score of five indicating a superior choice, three an average choice, and one equaling an inferior choice. All methods were assumed to result in an aircraft designed for an identical load. The results of the comparison are summarized in Table 6.1: Weighted Pugh matrix for manufacturing process selection.

*Table 6.1: Weighted Pugh matrix for manufacturing process selection*

| FOM | Value | Manufacturing Process | | | |
|---|---|---|---|---|---|
| | | Built-up Balsa and Ply | Fiberglass | 3D Printing | Foam Core Composites |
| Weight | 5 | 5 | 4 | 2 | 3 |
| Ease of Manufacture | 3 | 3 | 2 | 4 | 3 |
| Reparability | 2 | 3 | 4 | 1 | 1 |
| Experience | 2 | 5 | 2 | 4 | 3 |
| Cost | 1 | 5 | 3 | 2 | 3 |
| Total | 13 | 60 | 41 | 34 | 35 |

Based on the Figures of Merit, built-up balsa was considered the best method for the major airframe and empennage structure. However, the team determined that different elements of the design could use different manufacturing processes, such as 3D Printing or Foam Core Composites, to create an aircraft that emphasized the priorities listed in Table 6.1.

## 6.2   Processes Selected

The team used the above comparison to optimize the built-up balsa and ply technique to achieve the most competitive aircraft by prioritizing speed and weight without sacrificing structural integrity. Of the many ways to apply built-up balsa and ply, the team chose specific techniques that are as follows.

Selective Material Use: Since wood can vary significantly in density and strength, it is sorted by weight. Heavy pieces are used for prototypes, and small components that need to be stronger. Lighter pieces are used for large aircraft components, such as ribs, and the lightest pieces are reserved for the competition aircraft.

Local Reinforcements: Sharp internal corners, structural joints, and hinges can be locations of stress concentrations that would be potential failure points. Rather than overbuild the entire structure, these locations are reinforced with carbon fiber, additional balsa wood, or plywood to increase strength with minimal weight penalty.

Lightening Holes: The efficiency of the built-up structural design comes from the distribution of loads over the structural members. This means there are areas where stresses are relatively low, and material can be removed without significant losses in stiffness or strength.

Covering: The aircraft is covered with Monokote, a heat shrinking, adhesive-backed plastic covering material designed for skinning model aircraft. This material is readily available, easy to use, and skins the aircraft with minimal additional weight.

### 6.2.1 Lifting Surfaces

The lifting surfaces are primarily constructed using the built-up balsa method, with two carbon fiber spars for load transfer. Balsa ribs are laser cut with jigs, which slot together with a base piece to properly align them. The structure is then built up with balsa stringers and sticks to reinforce the structure and maintain the outer mold line. The leading edge is sheeted in 1/32 in balsa wood to maintain the shape of the airfoil, and shear webbing is added to stiffen the wing. The electronics are then installed, and the lifting surfaces are covered in Monokote.

### 6.2.2 Control Surfaces

The control surfaces are cut and built up with the main lifting surfaces, but are detached and manufactured separately with a similar process. They are then reattached to the lifting surfaces using point hinges.

### 6.2.3 Fuselage

The fuselage is made of slotted and fingered components that jig together around the fuselage spar. They are laser cut out of balsa or plywood, depending on what loads each part is expected see. Stringers are used to maintain the outer mold line, which is then covered with Monokote.

### 6.2.4 Landing Gear

The main landing gear is manufactured out of a 5/16 in thick, 3/4 in wide strip of 6061 aluminum that is bent into the correct shape. The leading edge is rounded and the trailing edge is sharpened to reduce drag. The wheels are cut from a 1/4 in thick sheet of 6061 aluminum using a water jet.

## 6.3 Manufacturing Milestones

A production schedule containing manufacturing milestones was established prior to initial prototype manufacturing to ensure a logical, consistent order is followed during construction. Progress is recorded and monitored by the manufacturing lead to ensure all major milestones were met. The Gantt chart that represents this is shown in Figure 6.1, capturing the planned and actual timing of manufacturing steps. While most of the time required for different processes remained the same, some parts, such as the construction of the wings, takes longer due to the tapered planform. The team is planning to have constructed four aircraft by competition, each of which follows a timeline similar to that in Figure 6.1 describes the typical manufacturing timeline for a single aircraft.
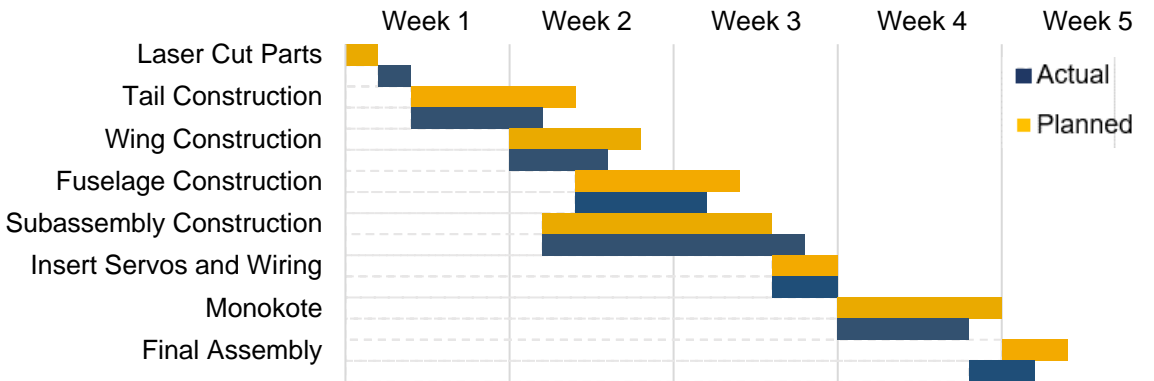
*Figure 6.1: Aircraft manufacturing milestone chart showing planned and actual timing of a prototype*

# 7 TESTING PLAN

An extensive testing campaign to validate the aircraft and its components was created to ensure functionality and to minimize risks of malfunction during flight tests and competition. Testing culminates in test flying a full set of competition flights on the final competition airframe.

## 7.1 Objectives

Testing is broken up into four main categories: propulsion, structural, subsystems, and flight performance. Propulsion testing is done to verify the performance of the combination of motor, propeller, and batteries chosen in Section 4.2.2. The objective of the structural testing is to ensure that the airframe can withstand the shear, bending and torsion loads seen in operation. Subsystem testing, which includes the banner deployment and release mechanism, requires a variety of testing procedures to prove readiness for flight. Finally, flight performance is tested to ensure successful integration of all systems and provide verification of performance models.

### 7.1.1 Propulsion Testing

The propulsion system combination selected in Section 4.2.2 is assembled and tested on a static thrust test stand. Static thrust, current, and power draw are measured and compared against MotoCalc results for validation.

Static propulsion testing utilizes a rig that includes a scale to measure thrust as well as an electric motor measurement system. The team uses the rig to perform static thrust tests and uses the data obtained to compare with MotoCalc predictions. The electric motor parameters are monitored with an EagleTree system that records the RPM, voltage, and current draw of the motor. Custom written software is used to collect the torque and thrust values as well as to remotely control the motor for 30-second intervals with 10-second full thrust intervals and 10-second acceleration and deceleration intervals.

### 7.1.2 Structural Testing

A wing tip test is done to simulate the loading the wings would experience in flight by loading the maximum expected payload weight into the fuselage and lifting at the wing tips. The wing tip test simulates approximately a 2g maneuver, which is well within the design limits of the structure.

A drop test is also performed to simulate the impact forces experienced during touchdown upon landing. This test verifies the integrity of the landing gear attachment points in the fuselage, the tailwheel attachment structure at the rudder, and the fuselage structure supporting the passengers and luggage.

### 7.1.3 Subsystem Testing

Banner Material and Design: Several different materials and designs are considered for the banners, and each are tested to determine which has the most desirable characteristics. Optimally, the banner will have low weight, low drag, stows/deploys well, and not easily fray. The size of each test banner is much smaller than the size that will be incorporated into the aircraft for ease of manufacture and comparison. A banner of each material and design is attached to a mockup of the banner mechanism, and the deployment, cruise, and release are tested in the wind tunnel. The mechanism is moved around in the flow to simulate aircraft maneuvers. The banner responses are recorded using slow-motion video recording, and the banners with the qualitatively lowest flutter response amplitude are chosen since these will have the lowest drag and will be the least likely to be prematurely released. Of these, the material with the lowest likelihood of fraying is chosen. This selected banner is then attached to a load cell to measure the drag force to validate and correct the team's conceptual drag models.

### 7.1.4 Flight Testing

Flight testing is the culminating point of the iterative design and manufacturing process. It allows the team to compare the estimated aircraft performance against the performance of the prototype. The results can then be used to evaluate the feasibility of the performance targets and identify areas for improvement. Each subsystem is tested thoroughly on the ground before being put on the plane, and then the aircraft and subsystems are tested together to ensure every component worked well together. Based on the achieved performance, improved designs are suggested and implemented, and the process continues until the final iteration.

The team takes a conservative approach to flight testing to avoid damaging or crashing the prototype aircraft during flight testing. The first prototype aircraft is flown without any payload or subsystems attached, and takeoff is not performed at immediate full throttle. The aim of the first flight is to verify the function of the propulsion system and aircraft controls, as well as to determine the trim of the aircraft. Once the first flight is completed, subsequent iterations with subsystems and payload can be performed. Weight was gradually added to the aircraft to minimize the risk of exceeding the aircraft performance limits. Testing Mission 2 begins with minimal passengers and luggage loaded onto the aircraft and with each subsequent flight, more passengers/luggage are added and the aircraft is flown more aggressively. This gradual

envelope expansion minimizes the risk of overloading the aircraft and prematurely depleting the batteries in flight.

Intermediate iterations are currently being used as testing platforms, with changes being implemented based on feedback from assembly teams and the pilot. This form of testing is low risk because the aircraft will not be used in competition, so preliminary tests can be done to see if the change being made is worth being added to the final aircraft.

The current iteration of *Buzzfighter* is being used to verify the required battery size to complete M3. Experience and data gained from all iterations will be used to generate a final design that will go to competition. The final iteration will fly simulations of the flight missions to verify and validate the aircraft's capabilities as well as train the pilot for competition.

## 7.2   Schedule

A testing schedule was established that mirrored the aircraft design milestones to monitor the success of the propulsion, structure, and subsystem designs. Progress is monitored by the project manager to ensure all tests are conducted in a timely manner. A Gantt chart representing important testing milestones is shown in Figure 7.1.
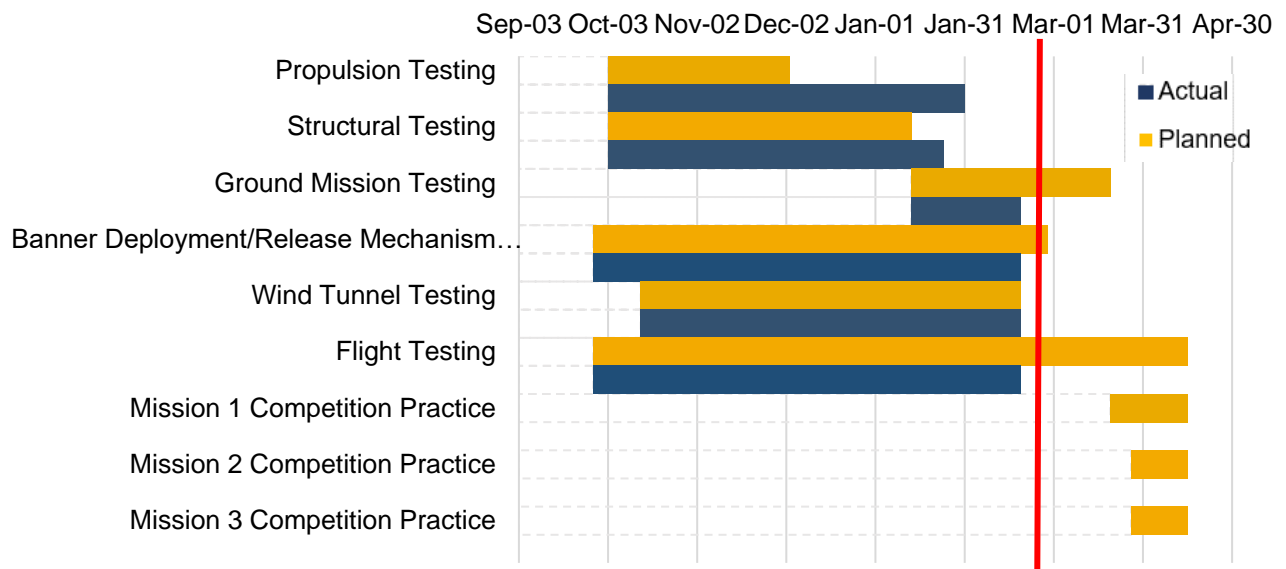


*Figure 7.1: Aircraft testing milestone chart showing planned and actual progress*

## 7.3   Checklists

Various tests have specific procedures which must be followed accurately to produce the desired objectives and to ensure safety. This section contains the checklists utilized for *Buzzfighter* when conducting tests that required a significant number of steps, such as propulsion and flight testing.

The propulsion test checklist was created to ensure the team's safety while working with propellers and electrical equipment on the ground and in flight. In addition, the checklist helps make sure the test is not

wasted due to a mistake in preparation. This checklist is used in the testing of all motor, battery, and propeller combinations.

The flight test checklist was created with the important goal of preventing any system from malfunctioning, which could lead to the in-flight failure of the aircraft and/or subsystems. Its thorough execution is paramount to the team's success, and it will be used at the fly-off as well.

The testing checklist for the banner deployment and release mechanism allows the team to decide whether a mechanism is operational or needs modification. If any of the above success criteria are not met, the mechanism will be modified or redesigned to resolve the deficiencies, and the above testing cycle repeated. The final checklists are shown in Figure 7.2.

| Propulsion Test Checklist | Flight Test Checklist |
|---|---|
| **Before Test** | **Before Flight** |
| ☐ Propeller Secure | ☐ Propeller Secure |
| ☐ Motor Mount Secure | ☐ Fasteners Tightened |
| ☐ Connections Secure | ☐ Connections Secure |
| ☐ Batteries Peaked | ☐ Primary Battery Secure/Charged |
| ☐ Throttle Down | ☐ Control Surfaces Free/Correct |
| ☐ Data System On | ☐ Receiver Pack Plugged In |
| ☐ Custom Code Running | ☐ Receiver BatterySecure/Charged |
| ☐ Testing Rig All Clear | ☐ Passengers Secure |
| | ☐ Luggage Secure |
| **During Test** | ☐ Banners Secure |
| ☐ Aircraft Restrained | ☐ Banner Mechanisms Stowed |
| ☐ Throttle Full | ☐ Runway All Clear |
| ☐ Current and Voltage Checking | |
| | **During Flight** |
| | ☐ Banner Fully Deployed when Commanded |
| | ☐ Banner was Vertical During Duration of Flight |
| | ☐ Banner was Released When Commanded |
| | ☐ Banner Mechanism Withstood Aerodynamic Loads |
| **After Test** | **After Test** |
| ☐ Throttle Idle | ☐ Throttle Idle |
| ☐ Battery Disconnected | ☐ Battery Disconnected |

*Figure 7.2: Propulsion, Flight Test and Banner Mechanism checklists*

# 8 PERFORMANCE RESULTS

## 8.1 Component and Subsystem Performance

### 8.1.1 Propulsion Tests

Static thrust testing was performed to better measure the available thrust for short takeoff and determine the propeller size that provides the optimal balance of static thrust and high-power draw in this situation. The combination of an A60 5XS motor with a 17x12E propeller and two 6s 4300 mAh scorpion batteries was chosen as the propulsion system using MotoCalc with the method described in Section 4.2.2. This data was verified against data gathered from static test stand testing. Figure 8.1 gives the comparison between the static thrust and current draw data with the chosen propeller system and varying propeller sizes from these tests and the corresponding predicted values from MotoCalc.
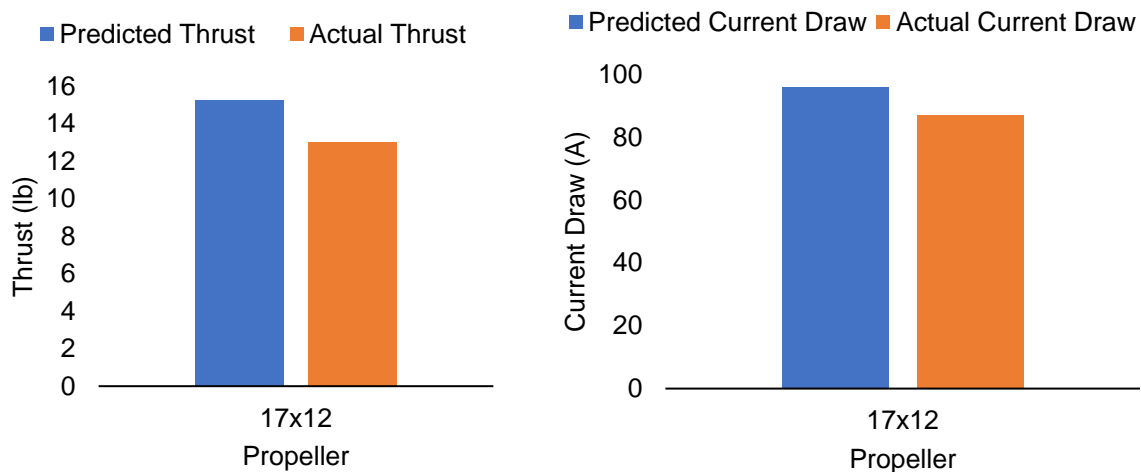


*Figure 8.1: Static thrust (left) and current draw (right) predicted by MotoCalc vs tested static thrust and current draw.*

Figure 8.1 shows that the static thrust values predicted by MotoCalc are largely validated by the test stand data. The results indicate the model is reasonably accurate however, it still does not account for various factors such as manufacturing tolerances for the various components and prop blockage caused by the stand.

### 8.1.2 Structural Tests

The full-size airplane was subjected to the required wingtip test specified in the rules as a part of the technical inspection process. The wingtip test was conducted for Mission 2, the heaviest aircraft configuration, and the aircraft was loaded with 40 passengers and their luggage. The successful wingtip test is shown in Figure 8.2.

*Figure 8.2: Wingtip test of fully loaded aircraft*

### 8.1.3   Subsystem Tests

The banner deployment and release mechanism underwent a three-phase testing process that included ground, wind tunnel and flight testing to ensure that it could hold on to the banner until the moment of deployment and keep the banner attached until the moment of release. The banner was also tested in order to find the material and the modifications that would result in the least drag. In the end, the banner was found to lack stiffness in the back half, so carbon fiber stiffener rods were added to remedy this. The material used was a rip-stop nylon, which allowed for a light yet durable banner. Another issue found in testing was that the end of the banner tended to fray even in the wind tunnel. Therefore, the entire banner was hemmed and pockets for the carbon fiber stiffeners were sewn in to prevent wear and tear from aerodynamic loads in flight.


*Figure 8.3: Banner wind tunnel testing*

## 8.2 System Performance

A practice Ground Mission was performed according to the rules. The time required to complete the Ground Mission was ~45 seconds, compared to the estimated 30 seconds. The team believes with further improvements to the aircraft and more practice, the Ground Mission time will be improved.

Takeoff tests were completed as a part of flight testing. The aircraft was able to takeoff reliably in the 20 feet distance required for Mission 1 and 3 without headwind. Figure 8.4 shows the aircraft successfully taking off in the 20 foot distance while completing a practice Mission 1 scenario.



*Figure 8.4: Aircraft completing short takeoff for Mission 1*

The team equipped the aircraft with a data collection system that could capture GPS data in order to compare the actual trajectory to the estimated mission trajectory outlined in Section 4.5. Competition length laps were flown with team members signaling turns visually in accordance with competition rules. Figure 8.5 shows the recorded flight path of a single lap.

*Figure 8.5: Recorded flight path of a single competition lap*

Table 8 shows the aggregated system performance from various flight tests of the current iteration. The results indicate the performance predictions were realistic. The team hopes to improve system performance with further improvements of the aircraft such as weight and drag reduction and increasing pilot familiarity to improve on current performance.

*Table 8.1: Predicted vs. flight test performance results*

|  | 1st Lap Time (s) | | Time for 360 (s) | | Laps Flown | | Max. Speed (fps) | |
|---|---|---|---|---|---|---|---|---|
|  | Pred. | Act. | Pred. | Act. | Pred. | Act. | Pred. | Act. |
| M1 | 28.2 | 28 | 2.7 | 4.4 | 1 | 1 | 123 | 126.1 |
| M2 | 33.7 | ~ | 11.9 | ~ | 3 | ~ | 121 | ~ |
| M3 | 66.3 | 45 | 3.3 | 7.6 | 9 | ~ | 48 | 62.8 |

The team has been able to collect performance data for several missions or mission segments. The aircraft has flown empty multiple times to prove airworthiness, trim, and test capabilities. The actual and predicted lap time and max speed match well for Mission 1, showing that the models are reasonably accurate. However, for the time to perform a 360, the actual time is much greater than the predicted time. This is most likely due to differences in how the turn was modeled and how it was performed. The model assumes the turn is performed at maximum load factor, and the pilot was likely at a lower load factor. Also, the model assumes the aircraft has enough power to sustain the load factor, which is not the case for the actual aircraft.

The aircraft has not been flown at full Mission 2 weight, but is currently undergoing envelope expansion. For Mission 3, as in Mission 1, the predicted turn time is much lower than the actual. Again, this can be explained by the pilot turning at a lower load factor and insufficient thrust.

Comparing the actual and predicted first lap times and velocities for Mission 3, the actual aircraft flies more quickly and completes laps in less time than is predicted. This is in part due to the fact that in the mission model, the aircraft current is constrained to increase endurance, whereas in the test flight the current is limited by the ESC. Limiting the current on the actual aircraft to a level sustainable for the full 10 minutes will be explored in future flight tests.

The GPS ground speed for a Mission 1 practice lap was collected and co-plotted with the predicted lap speed over a single lap shown in Figure 8.6. The lap data shown is the same used to generate the ground path shown in Figure 8.5.
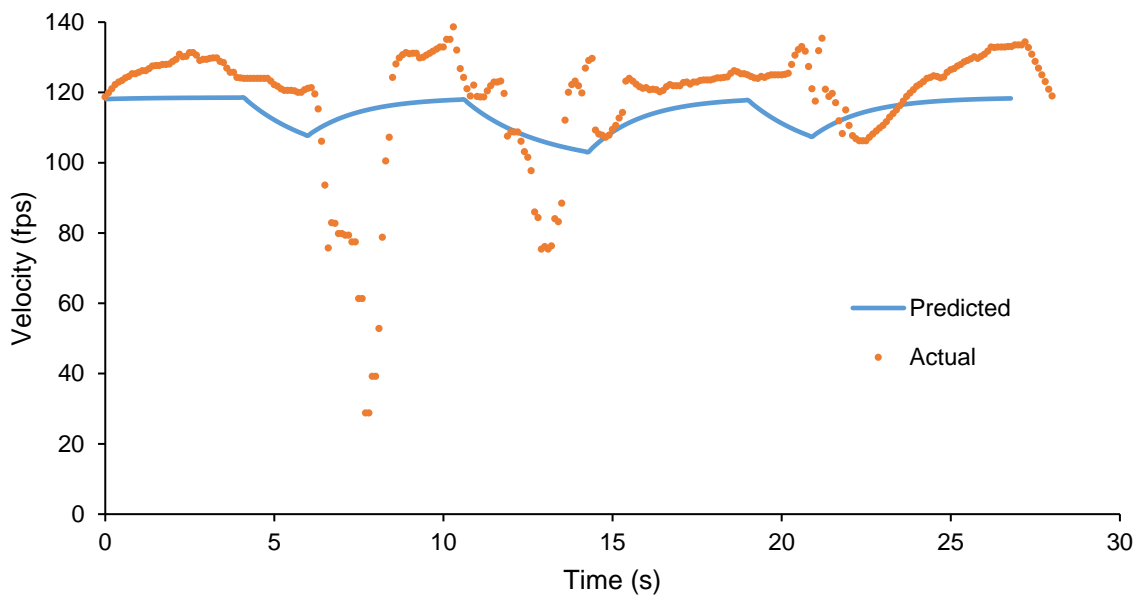


*Figure 8.6: Comparison between predicted and actual Mission 1 trajectory*

The predicted speed is lower than in the actual flight speed, possibly because the propulsion system produced more thrust at speed than the predicted. In the actual lap, the aircraft loses more speed in turns and appears to be turning for longer. The pilot was not turning as aggressively as the model assumes, meaning the aircraft spent more time in turns, and that the overall lap time was longer than predicted. Uncertainties such as wind speed, variations in altitude, and variations in how the laps were flown also likely contributed to differences, but cannot be quantified from the data the team collected.

As the pilot gains more experience with the aircraft dynamics and limitations, the lap times are expected to improve. Concurrently, pilot feedback will be integrated to improve flight characteristics and further efforts will be made to improve performance. As of the report submission, the team has completed 59 flights of prototype aircraft and tested numerous subsystem prototypes. The current prototype is shown in Figure 8.7. The team is awaiting more testing opportunities before the competition to make further improvements on the aircraft and meet the target mission performance. The concept of a single-engine mono-wing conventional aircraft proved to be capable of meeting the aircraft requirements and completing all missions. The team is confident that the overall configuration for *Buzzfighter* will be a competitive entry in Wichita.



*Figure 8.7: Buzzfighter in flight*

# 9  BIBLIOGRAPHY

[1] Carruthers, A. C., and Filippone, A., "Aerodynamic Drag of Streamers and Flags," *Journal of Aircraft*,

vol. 42, 2005, pp. 976–982.

[2] Mattingly, J. D., Heiser, W. H., and Daley, G. H., *Aircraft Engine Design, Third Edition | AIAA*

*Education Series* Available: https://arc.aiaa.org/doi/book/10.2514/4.105173.

[3] Drela, M., and Youngren, H., "XFOIL", *Massachusetts Institute of Technology* [online], 2013,

https://web.mit.edu/drela/Public/web/xfoil/ [retrieved 21 February 2018]

[4] Koftin, L.K., Cohen, K.S., "Aerodynamic Characteristics of a Number of Modified NACA Four-Digit-

Series Airfoil Sections", NACA TN 1591, 1948.

[5] Drela, M., and Youngren, H., "AVL Overview", *Massachusetts Institute of Technology* [online], 2008,

http://web.mit.edu/drela/Public/web/avl/. [retrieved 21 February 2018],

[6] *Parasite Drag Tool*. Available: http://openvsp.org/wiki/doku.php?id=parasitedrag. [retrieved 15 October

2019].

[7] Hoerner, S. F., *Fluid Dynamic Drag*, 2nd ed., Published by author, 1992.

[8] Phillips, W. F., *Mechanics of Flight*, 1st ed., Wiley, Hoboken, NJ, 2004.

[9] *Wichita, KS Weather History*. Available:

https://www.wunderground.com/history/monthly/us/ks/wichita/KICT/date/2010-4. [retrieved 12

February 2020].

[10] Bauchau, O. A. Craig, J. I, *Structural Analysis: with applications to aerospace structures*, SPRINGER,

2009.

[11] Anderson, John D., *Aircraft Performance and Design*, 1st ed., Boston, MA: McGraw-Hill, 1999.

HOWARD R. HUGHES
College of
ENGINEERING

## List of Figures

## List of Tables

## List of Variables and Acronyms

| | |
|---|---|
| A | Area |
| α, AOA | Angle of Attack |
| AR | Aspect Ratio |
| AVL | Athena Vortex Lattice Software |
| b | Wingspan |
| c | Chord length |
| CAD | Computer Aided Design |
| CFD | Computational Fluid Dynamics |
| CNC | Computer Numerical Control machine |
| CG | Center of Gravity |

| | |
|---|---|
| D, Cd | Drag, Coefficient of drag |
| E | Modulus of Elasticity |
| ESC | Electronic Speed Controller |
| FEA | Finite Element Analysis |
| FoM | Figure of Merit |
| g | Acceleration due to gravity |
| GPS | Global Positioning System |
| l | Moment arm |
| L, Cl | Lift, Coefficient of lift |
| LiPo | Lithium Potassium battery |
| m | Mass |
| MAC | Mean Aerodynamic Chord |
| MDF | Medium Density Fiberboard |
| MPH | Miles per hour |
| n | Load factor |
| P | Load |
| pcf | Pounds Per Cubic Foot |
| psf | Pounds Per Square Foot |
| PVA | Polyvinyl Acetate |
| RANS | Reynolds Averaged Navier-Stokes |
| ρ | Density |
| S | Wing Area |
| s | Wingspan or second |
| SST | Shear Stress Transport |
| σ | Stress |
| UNLV | University of Nevada, Las Vegas |
| UTS | Ultimate Tensile Strength |
| v | Cruising Speed of *Bullitt*- $v_1$ for Mission 1, $v_2$ for Mission 2, $v_3$ for Mission 3 |
| V | Volume |
| W | Weight of *Bullitt* |

## 1.0 Executive Summary

This report describes the design, manufacturing, and testing processes of the University of Nevada, Las Vegas (UNLV) *Bullitt* aircraft (shown below) for the 2019-2020 AIAA Design Build Fly (DBF) Competition.
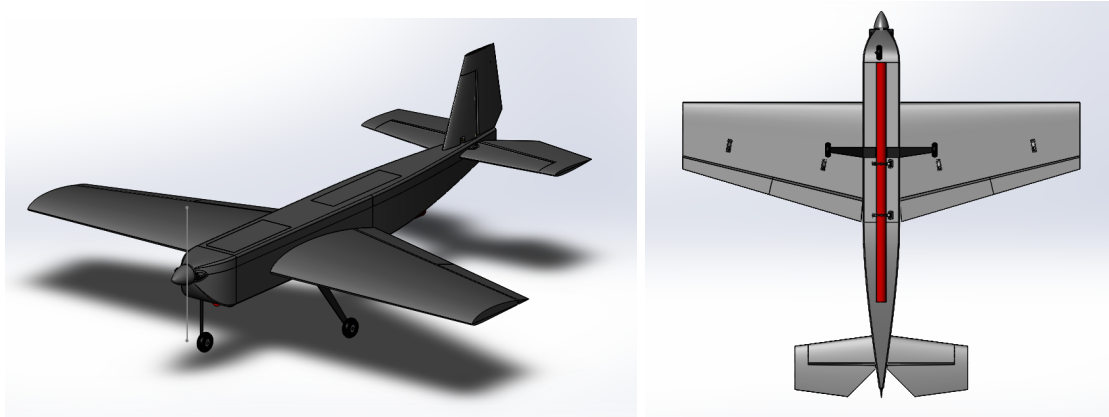


**Figure 1.1 Competition Aircraft**

The AIAA DBF Organizing Committee has specified the need for a passenger/advertisement fixed-wing aircraft with a maximum wingspan of 5 feet. The plane must carry secured passengers and their luggage and also store, deploy, and release an advertisement banner in mid-flight. *Bullitt* is a single-motor, composite airframe, mono-wing aircraft which can carry 24 passengers and luggage and tow various ripstop Nylon banners with a maximum length of 25 feet and a minimum length of 5 feet. The aircraft will compete in the following missions:

- Mission 1: Demonstration Flight
- Mission 2: Passengers & Luggage Flight
- Mission 3: Banner Flight
- Ground Mission: Aircraft Assembly and Reconfiguration

The main mission requirements are speed, lift capability, low weight, power from the motor, and capacity of the batteries. Scoring sensitivity analysis was performed to determine which design parameters have the highest effect on the overall score. From the sensitivity analysis, the team identified speed as the primary design goal. The design is heavily focused on decreasing weight and maximizing the speed while meeting the design and component requirements of each mission. The *Bullitt* aircraft is designed to meet all the mission requirements and perform competitively. The performance of the aircraft for each mission can be summarized by the following:

- ➢ Mission 1: Weight: 8 lbs, Maximum speed: 80 MPH, Takeoff distance: 12 ft
- ➢ Mission 2: Weight: 14 lbs, Maximum speed: 78 MPH, Takeoff distance: 20+ ft
- ➢ Mission 3: Weight: 9 lbs, Maximum speed: 45 MPH, Takeoff distance: 13 ft

The team is organized into six subteams which conduct their respective research and analysis and are led by team leads supervised by the Project Lead. All groups worked together to design, manufacture, and test the aircraft per the plans laid out in this design report.

# 2.0 Management Summary

## 2.1 Team Organization

The project team was organized into six sub-teams shown in Figure 2.1. Led by managerial and technical project heads, the smaller working groups focused on particular aspects of the project. Each student in the project chose the area(s) which piqued their interest and proceeded to research their respective topics. Six group leaders were designated to lead each sub-team in their tasks; they were selected based on prior experience and skills.
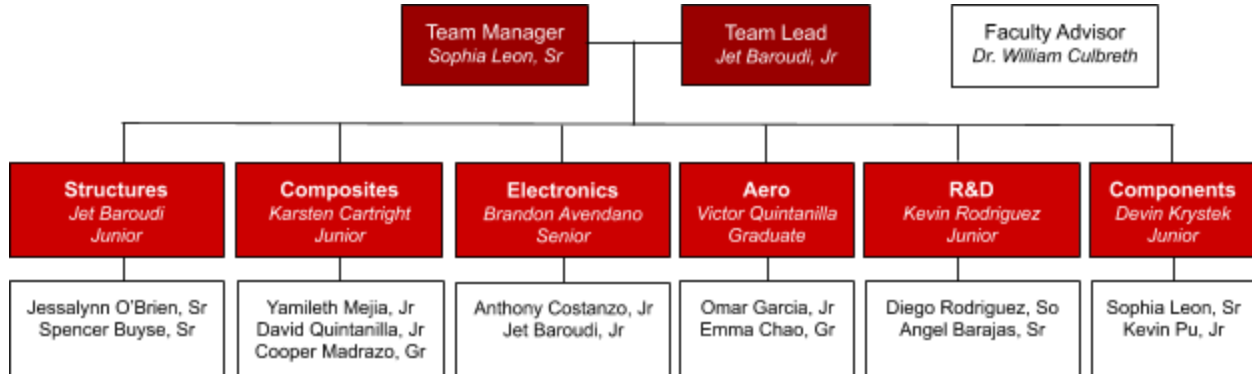


**Figure 2.1 Organization Chart**

The tasks and responsibilities of each of the sub-teams shown in the organization chart above are outlined in the following table. Most of the students on the project were underclassmen studying Mechanical Engineering and had a basic understanding of SolidWorks CAD software.

**Table 2.1 Sub Team Responsibilities**

| Sub Team | Responsibilities |
|---|---|
| Structures | ● Study existing aircraft to design airframe <br> ● Use CAD to model designs in SolidWorks and analyze on Hyperworks suite |
| Composites | ● Research, practice, and test different manufacturing techniques and materials <br> ● Use laminate theory and Altair software to obtain stress properties of structure |
| Electronics | ● Design, program, and integrate electronic components to achieve and collect flight test data <br> ● Choose and test propeller, motor, and battery |
| Aerodynamics | ● Conduct analysis of designs for optimal aerodynamic performance and stability <br> ● Identify aerodynamic tradeoffs and determine aircraft characteristics of each mission <br> ● Use ANSYS Fluent and Altair AcuSolve to model aerodynamic design |
| R&D | ● Design and build test planes and components |
| Components | ● Design banner, passengers, luggage, and passenger/luggage holder <br> ● Test and manufacture each component |

| Team Lead | • Guide working groups to make realistic decisions and support research and manufacturing<br>• Oversee final assembly and testing of aircraft |
|---|---|
| Team Manager | • Handle interaction with AIAA HQ, compile and submit reports, question, and organize finances and travel |

## *2.2 Project Timeline*

Below is a milestone chart showing planned and actual timing of major elements. Everything has been accomplished as planned up to the date of the report submission including a complete design and functional test plane. Due to setbacks in supplier deliveries, manufacturing of the final competition aircraft has not yet been completed at the time of the report submission. In the months following the report submission and leading up to the competition, one or more composite aircrafts will be constructed and tested in a similar fashion to the testing that was accomplished on the foam prototype.
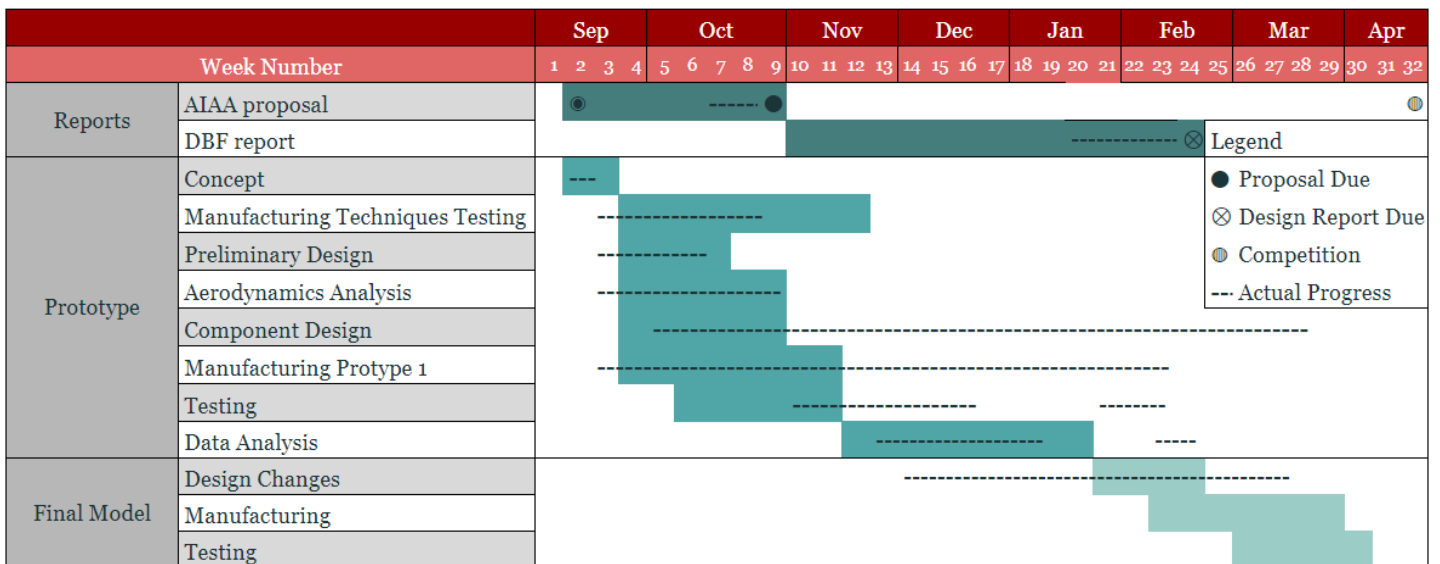


**Figure 2.2 Gantt Chart**

## 3.0 Conceptual Design

## *3.1 Mission and Design Requirements*

### 3.1.1 Mission 1

This is the demonstration flight which requires the aircraft to successfully complete three laps within 5 minutes. Upon completion, the aircraft will score 1.0 point. The plane must take off without a payload in 20 feet.

$$Score\_Mission\_1 = 1 \text{ or } 0$$

For this mission, the design requirements stipulate the aircraft must be able to get off the ground in 20 feet. The airfoil must have a positive coefficient of lift upon takeoff and the motor and propeller must generate enough thrust so that the

aircraft can take off. This mission requirement of a short takeoff distance indicates that the design should include flaps. Flaps assist the aircraft in short takeoff and slower landings, by altering the airfoil to generate more lift. In general, the aircraft should not weigh too much or present too much drag so it should be designed with that in mind, having an aerodynamic outer mold line and maintaining the requirement of a maximum 5 foot wingspan.
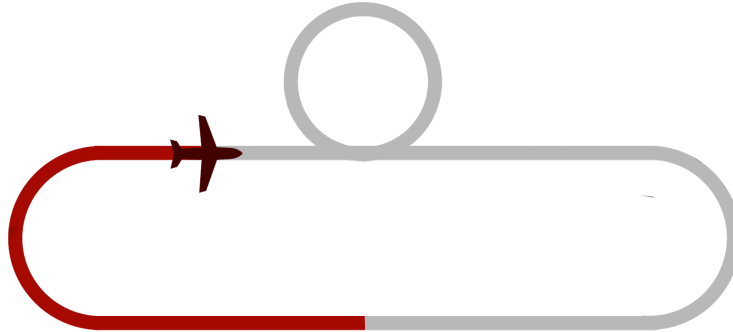


**Figure 3.1 Mission 1**

### 3.1.2 Mission 2

The goal of this mission is to carry as many passengers as possible and complete three laps in as little time as possible. The number of laps, time frame, and landing requirements are the same as Mission 1, but there is no takeoff requirement. The score is shown by the equation below. The scoring shows that the plane must have the greatest ratio of passengers to speed.

$$Score\_Mission\_2 = 1 + (Passengers \ / \ flight \ time) \ / \ (Max)$$

To design the aircraft to carry many passengers while still going fast, the fuselage must have ample volume while still being sleek and aerodynamic. A long, skinny fuselage and a strong motor and propeller combination are required to maximize *Bullitt*'s performance in Mission 2.
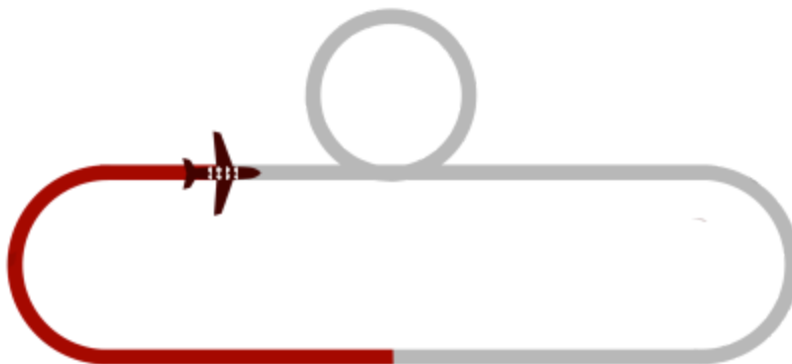


**Figure 3.2 Mission 2**

### 3.1.3 Mission 3

The goal of this mission is to tow a banner as large as possible (while maintaining an aspect ratio of 5:1) as far as possible. The plane must take off in 20 feet with the banner stowed in freeflow air. The banner is deployed after the first turn and released after crossing the finish line. The time allotted for the mission is 10 minutes. The score is determined by the number of laps multiplied by the banner length (see the equation below). As with all missions, the aircraft must successfully land in order to receive the score.

$$Score\_Mission\_3 = 2 + (banner\ length * laps) / (Max)$$

Based on the mission requirements, the design requirements for Mission 3 are to reduce drag from the plane and the banner and increase the thrust power from the motor by increasing the battery amperage. Because it is expected that a flapping banner will produce a significant amount of drag, a balance between speed and banner size must be found through optimization techniques. It is also necessary that the banner remains upright and readable, so a weight and other methods must be implemented to meet this requirement.
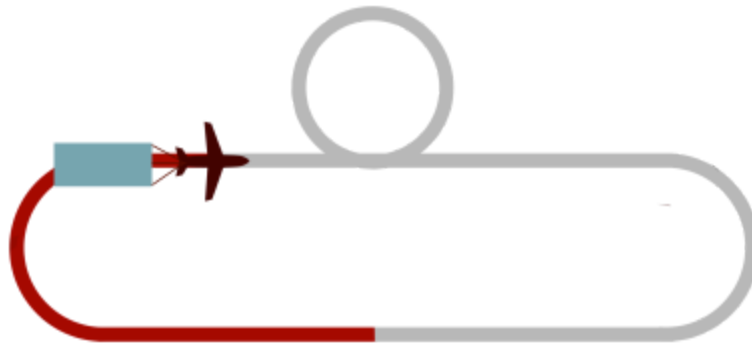


**Figure 3.3 Mission 3**

### 3.1.4 Ground Mission

The plane and payloads must be placed within the mission box, a 10' x 10' area outlined on the ground with tape. A runner stands outside the box, enters and loads the passenger payload, then unloads it while the banner payload is rolled up and attached to the plane. The banner must then be deployed and the runner will leave the mission box.

$$Score\_Ground\_Mission = UNLV's\ speed / Fastest\ speed$$

The design requirements for the ground mission are speed and ergonomics. As a result, the passenger compartment and the banner attachment mechanism must be designed not only for functionality during the flight missions but also for rapid assembly and disassembly during the ground mission.

### 3.2 Scoring Sensitivity

The sensitivity analysis shows that the total score is most sensitive to the speed variable. The following figure uses three variables; banner length, number of passengers, and speed at which each mission is performed. These three variables were normalized from a scale of 0 to 1, a score of 1 being the highest possible score. Then these variables were put into the scoring rubric for each mission. Note that all mentions for lap times or flight times were lumped into the variable for speed.  For each presented graph, two variables were held fixed at an average score and the remaining score was set to a variable value between 0 to 1. The plots then show what the total score, excluding the report score, would be.
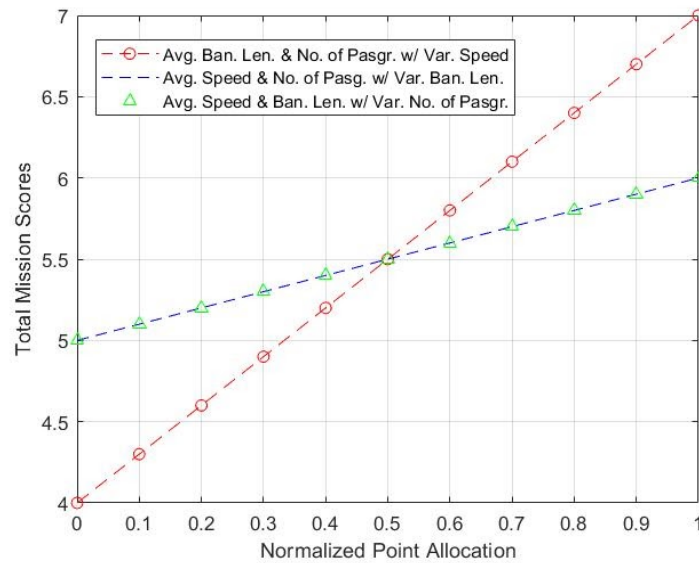


**Figure 3.4 Sensitivity Analysis**

Notice in figure 3.4, that the red dashed line with circles has a steeper slope than the other two lines. This shows that if the team has an average number of passengers and an average size banner relative to the other teams, the overall score is more easily impacted by the speed at which the missions are performed. In the above figure, if the team is the slowest of all competing teams and average amongst banner size and passenger count, a minimum score multiplier of 4 will be achieved. However, even if the team is in the upper quarter percentile in speed, such as lap times, the achievable score surpasses the maximum achievable score under the other two scenarios.

### 3.3 Concepts and Configurations Considered

3.3.1 Concept Weighting / Selection Process

For several characteristics of the aircraft and subsystems designs including fuselage shape, banner attachment method, etc., design matrices were created to value each configuration considered against several factors of merit. The primary factors considered are given in table 3.1. Simplicity indicates the manufacturability of the configuration; higher scores correspond to designs that would be easier to manufacture and replicate. Weight is valued higher if the aircraft is lighter. Speed & Drag incorporates how quickly the aircraft can take off and how well it will fly. Stability indicates the configuration

or component's effect on the aircraft's stability and maneuverability. Finally, certain components are valued higher for having a lower Space / Volume consumption. These factors are weighted as shown in the table below.
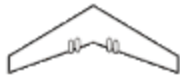
**Table 3.1 Design Matrix Factors**

| Factor of Merit | Importance |
|---|---|
| Simplicity | 2 |
| Weight | 4 |
| Speed & Drag | 5 |
| Stability | 3 |
| Space/Volume Consumption | 3 |

### 3.3.2 Aircraft Design

The first design matrix describes the selection of the general aircraft design. Three classic configurations were considered based on historical or existing aircraft. Between the conventional acrobatic design, the twin fuselage design, and the flying wing design, an acrobatic configuration was selected for its highest score. The *Bullitt* aircraft's design was inspired by the Funtana RC aircraft with which the student pilot is very experienced flying.
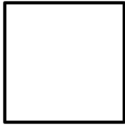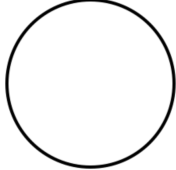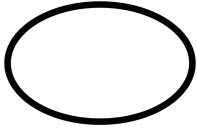
**Table 3.2 Early Conceptual Designs**

| General Design | | | | |
|---|---|---|---|---|
| Figures of Merit (FoM) | Weight | Acrobatic | Twin Boom | Flying Wing |
| Simplicity | 2 | 3 | 1 | 1 |
| Speed & Drag | 5 | 2 | 0 | 3 |
| Volume Availability | 3 | 2 | 2 | 0 |
| Weight | 4 | 2 | 0 | 3 |
| Stability | 3 | 2 | 1 | 0 |
| Total Score | | **36** | 11 | 29 |

The second design matrix was used to determine the cross-sectional shape of the fuselage. A circular and elliptical cross-section were considered because round shapes are structurally stronger as they do not have weak points at corners. However, because the square cross sectional shape allows for the maximization of space consumed by the passengers and luggage inside the fuselage, this shape was selected. The corners will be filleted for a stronger and more aerodynamic design resulting in an oblong square fuselage cross-section.
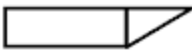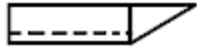
**Table 3.3 Fuselage Cross Section Shape**

| Fuselage Cross Section Shape | | | | |
|---|---|---|---|---|
| **Figures of Merit (FoM)** | **Weight** | **Square** | **Circle** | **Ellipse** |
| **Simplicity** | 2 | 3 | 1 | 1 |
| **Speed & Drag** | 5 | 2 | 0 | 3 |
| **Volume Availability** | 3 | 2 | 3 | 0 |
| **Weight** | 4 | 2 | 0 | 3 |
| **Stability** | 3 | 1 | 1 | 0 |
| **Total Score** | | **33** | 14 | 29 |

The third design matrix helped to decide whether or not to incorporate a semi-circular recess on the bottom surface of the fuselage. The benefit of the recess was better storage of the rolled-up banner during flight in the stowed position for a more aerodynamic, streamlined design during Mission 3. However, because most of the flight time will be spent without a stowed banner under the fuselage, the addition of this feature creates more work than benefit and is deemed less favorable than a flat-bottomed fuselage.

**Table 3.4 Fuselage Bottom**

| Fuselage Bottom | | | |
|---|---|---|---|
| **Figures of Merit (FoM)** | **Weight** | **Flat Bottom** | **Banner Recess** |
| **Simplicity** | 2 | 1 | 0 |
| **Speed & Drag** | 5 | 0 | 1 |
| **Volume Availability** | 3 | 1 | 0 |
| **Weight** | 4 | 1 | 0 |
| **Stability** | 3 | 1 | 1 |
| **Total Score** | | 12 | 8 |

The final design matrix used to characterize the aircraft design was a general selection of the type of airfoil that would be needed to meet the design requirements stipulated by Section 3.1. A low camber airfoil was selected for its more favorable lift to drag ratio as the symmetrical airfoil would not provide enough lift for a short takeoff and a deep camber

airfoil would create too much drag during Missions 2 and 3 during which it is essential the aircraft fly quickly. Further investigation of this decision is included in Section 4.2.2 in which specific airfoils were compared.
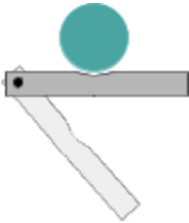
**Table 3.5 Airfoil Camber**

| Airfoil Camber | | | | |
|---|---|---|---|---|
| **Figures of Merit (FoM)** | **Weight** | **Symmetrical** | **Low Camber** | **Deep Camber** |
| **Lift** | 4 | 0 | 2 | 1 |
| **Drag** | 5 | 2 | 0 | 1 |
| **Manufacturability** | 2 | 1 | 1 | 0 |
| **Stall Characteristics** | 4 | 0 | 2 | 1 |
| **AoA** | 2 | 1 | 2 | 0 |
| **Total Score** | | 14 | **22** | 13 |

### 3.3.3 Component Design

Component design matrices in the following section focus on the optimization of the banner and passenger design to improve mission performance.

The first matrix describes the selection of the mechanism that holds the banner in its towed configuration at the base of the fuselage. The latch/hook system was selected because it is very easy to manufacture and control with a servo for secure containment of the banner during flight and reliable deployment of the banner during Mission 3.
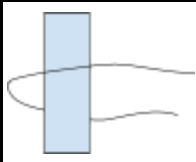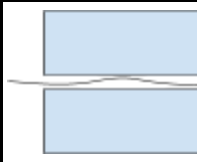
**Table 3.6 Stowed Banner Holding Mechanism**

| Stowed Banner Holding Mechanism | | | | |
|---|---|---|---|---|
| **Figures of Merit (FoM)** | **Weight** | **Latch / Hook System** | **Rubber Band** | **Hair Claw** |
| **Simplicity** | 2 | 2 | 1 | 1 |
| **Loading Speed** | 4 | 1 | 1 | 2 |
| **Modularity** | 3 | 1 | 1 | 2 |
| **Volume Consumption** | 3 | 2 | 1 | 0 |
| **Total Score** | | **17** | 12 | 16 |

The following design matrix demonstrates the deliberation between two ways to attach the banner to the tail of the aircraft that could also be undone for the release of the banner from the aircraft during Mission 3. One method would simply use friction to press against the string attached to the banner to prevent it from slipping. The other method has the string looped around a device that opens up to release the string when the banner is released to the ground.

**Table 3.7 Deployed Banner Attachment Mechanism**

| Deployed Banner Attachment Mechanism | |  |  |
|---|---|---|---|
| Figures of Merit (FoM) | Weight | Gate Method | Friction Method |
| Simplicity | 2 | 1 | 1 |
| Load Speed | 4 | 1 | 1 |
| Volume Consumption | 3 | 1 | 0 |
| Total Score | | 9 | 6 |

The following design matrix demonstrates three methods that were considered to maintain the banner in an upright position and keep it from fluttering so much that it became impossible to read. During research of real advertisement banners towed behind airplanes, several traditional methods of managing this were found: fringes on the trailing edge, a parachute on the top trailing corner, and a tubular structure on the top edge. Cutting fringes into the trailing edge of the banner requires some additional length to the banner, in order to maintain the aspect ratio, but it proves to smooth out banners effectively during testing and was the easiest to implement. Another consideration was a small parachute on the top trailing edge corner of the banner but that would result in a significant amount of added drag. Finally, a tunnel created by folding the top edge of the banner over and sewing it to itself was considered to inflate the top of the banner and stiffen it during flight resembling a wind sock. While this may have worked well, it required more work to apply to the banner than simply cutting fringes on the banner.
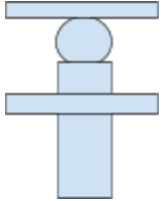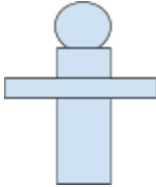
**Table 3.8 Banner Straightening Method**

| Banner Straightening Method | |  |  |  |
|---|---|---|---|---|
| **Figures of Merit (FoM)** | **Weight** | **Fringes** | **Parachutes** | **Wind Sock** |
| **Simplicity** | 2 | 2 | 0 | 1 |
| **Speed** | 5 | 1 | 0 | 1 |
| **Volume Consumption** | 3 | 2 | 0 | 1 |
| **Weight** | 4 | 0 | 1 | 1 |
| **Total Score** | | **15** | 4 | 14 |

The final design consideration for the components required by the competition was a means to secure the passengers during flight. Two methods were considered: active and passive retention. Active retention would require the use of a bar or other mechanism to hold them in place and was too difficult to manufacture and connect into the electronic system so passive retention was favored.

**Table 3.9 Passenger Holders**

| Passenger Holder | |  |  |
|---|---|---|---|
| **Figures of Merit (FoM)** | **Weight** | **Active Retention** | **Passive Retention** |
| **Simplicity** | 2 | 0 | 1 |
| **Loading Speed** | 5 | 1 | 0 |
| **Volume Consumption** | 3 | 0 | 1 |
| **Weight** | 4 | 0 | 1 |
| **Total Score** | | 5 | **9** |

# 4.0 Preliminary Design

## 4.1 Design / Analysis Methodology

After the conceptual design portion of the project was complete, more specific aspects were analyzed using experimental testing and computational parametric studies. To complete these analyses, several test rigs were assembled including a motor mount to test different propellers and a stand to measure banner drag from the top of a moving vehicle. The load data from these experimental tests was plotted and interpolated / extrapolated to obtain a correlation between thrust and amperage as well as speed of the aircraft and drag due to the banner (section 4.2.4). These correlations were then used to optimize the propeller choice and ideal amperage and banner size for the different missions (section 4.2.6). To choose an airfoil and control surface sizes, a combination of computational and experimental techniques were used. XFLR5 and AVL were used to obtain lift and drag data to characterize different designs. Two considerations for airfoil, Clark Y and Joukowski 12% were constructed out of balsa wood and foam board to be tested on the test plane for a measure of pilot's handling of the plane with each airfoil. Ultimately the Clark Y airfoil was chosen because of its superior handling and its aerodynamic properties (section 4.2.2).

## 4.2 Design / Sizing Trade Studies

To optimize the performance of the plane, several of its properties were tested in trade studies to determine the best design option for the aircraft. Several materials were considered for the sandwich structure of the composite fuselage and wings; various airfoils were studied in XFLR5 along with control surface sizes; finally, different lengths and configurations of banners were tested. The results from these trade studies were used to choose the optimal parameters of the final aircraft.

### 4.2.1 Material Selection

To construct a structurally sound aircraft, composite materials were chosen for this project. Various carbon fibers, fiberglass, and Kevlar fabrics were considered in the manufacturing of the aircraft. For added structural strength and minimized total weight, a composite sandwich structure was desired. To choose the core material, three-point bending tests were performed on several test specimens with four layers of twill carbon fiber material separated by varying core materials including various foam board, aramid honeycomb, and different woods. The specimens were roughly 4"x1" and 0.25" thick with an uncertainty of +/-0.00003 in. An example of each type of specimen is shown below demonstrating, from left to right, the core materials of white foam, blue foam, purple foam, pine, balsa, and honeycomb. MDF (medium density fiberboard) was also a core material considered.
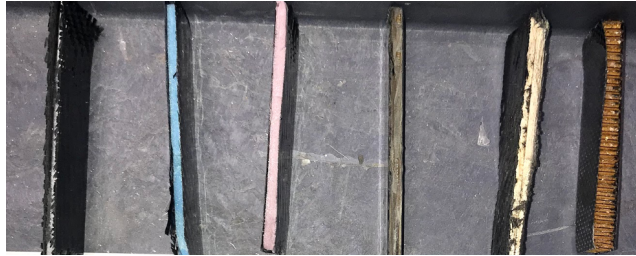
**Figure 4.1 Three-point bend test specimens**

Three to four specimens of each core material were created and tested and the results averaged. The results were used to plot the three-point bending curves for each material and find the corresponding stiffness and strength from the slope and peak of the plots, respectively. Figure 4.2 indicates that the MDF specimens demonstrated both the highest stiffness and strength values of all the specimens while the foam materials demonstrate the weakest properties.
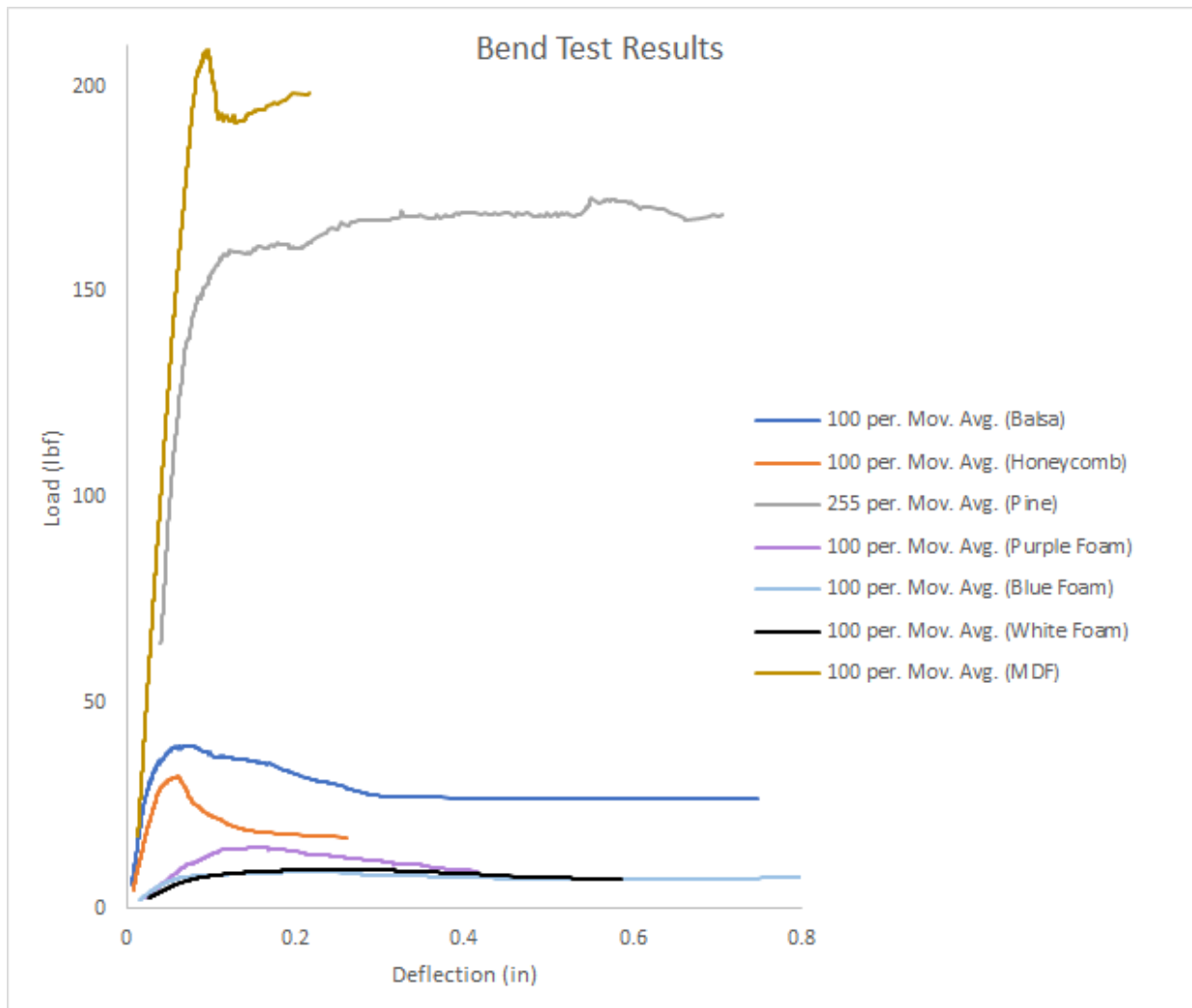


**Figure 4.2 Three-point bending data**

Since the strongest and stiffest materials were also the heaviest materials, they were not selected as the core material. Instead of using the raw data from the bending tests, the specific stiffness and strength values were found for each specimen by dividing the raw values by the specific weight of each specimen as shown in the equations below. The mass uncertainty was +/-0.005 g.

$$\text{Specific Stiffness} = E / (m \cdot g/V)$$
$$\text{Specific Strength} = UTS / (m \cdot g/V)$$

This property gives the most desirable material because the strength is maximized while weight is simultaneously minimized, an essential value in aerospace design.

**Table 4.1 Specific Stiffnesses and Strengths of 3-Point Bending Test Specimens**

| Material | Average Specific Stiffness (in) | Average Specific Strength (in) |
|---|---|---|
| Aramid Honeycomb | 1.74E+07 | 1.67E+05 |
| Balsa | 3.72E+07 | 1.94E+05 |
| Pine | 4.89E+07 | 5.43E+05 |
| Purple Foam | 8.42E+06 | 1.01E+05 |
| White Foam | 1.52E+07 | 1.24E+05 |
| MDF | 3.78E+07 | 4.95E+05 |

Furthermore, the values were normalized to clearly show which specimen was the strongest and stiffest. The results are shown below and indicate that the pine material is actually the most beneficial for the project. Even then, the wood specimens were still rather heavy. As a result, the honeycomb material was selected as the primary core material used on the aircraft.
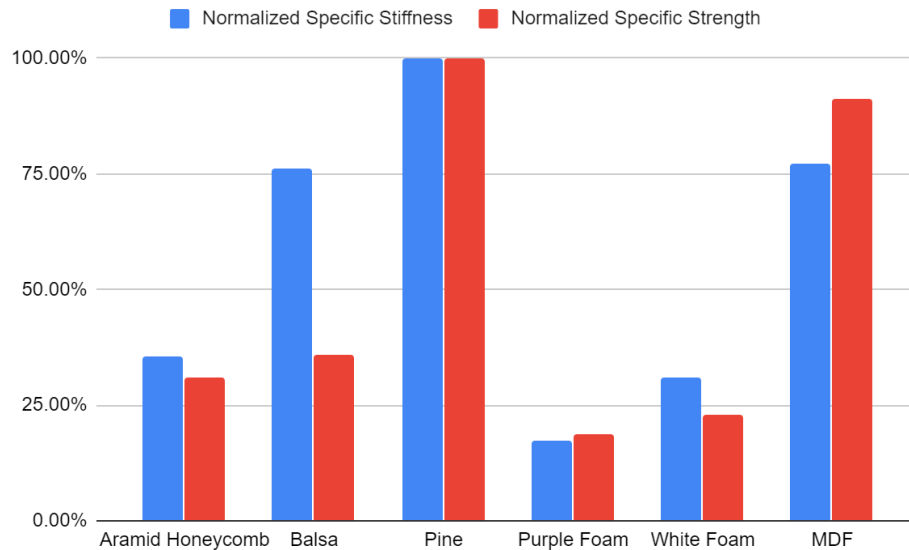
**Figure 4.3 Normalized Specific Stiffnesses and Strengths**

### 4.2.2 Airfoil Selection

Various airfoils were considered that would fulfill the mission requirements. The aerodynamic characteristics of each airfoil were analyzed using XFLR5, an analysis software for airfoils, wing and planes at low-Reynold number flows [7]. XFLR5 operates on Mark Drela's XFOIL program [6], a panel method airfoil analysis tool. Using XFLR5 the aerodynamic properties of each airfoil were compared for takeoff and cruise conditions. Considering the expected aircraft weight and size, the airfoil comparison was considered for Reynolds number 100,000 to 600,000.

The airfoils compared were the Joukowski 12%, Clark Y, AG 35 and SD7080. The airfoil sections were obtained from Airfoil tools. The compared airfoil polars from XFLR5 are displayed below in figures 4.4 and 4.5.
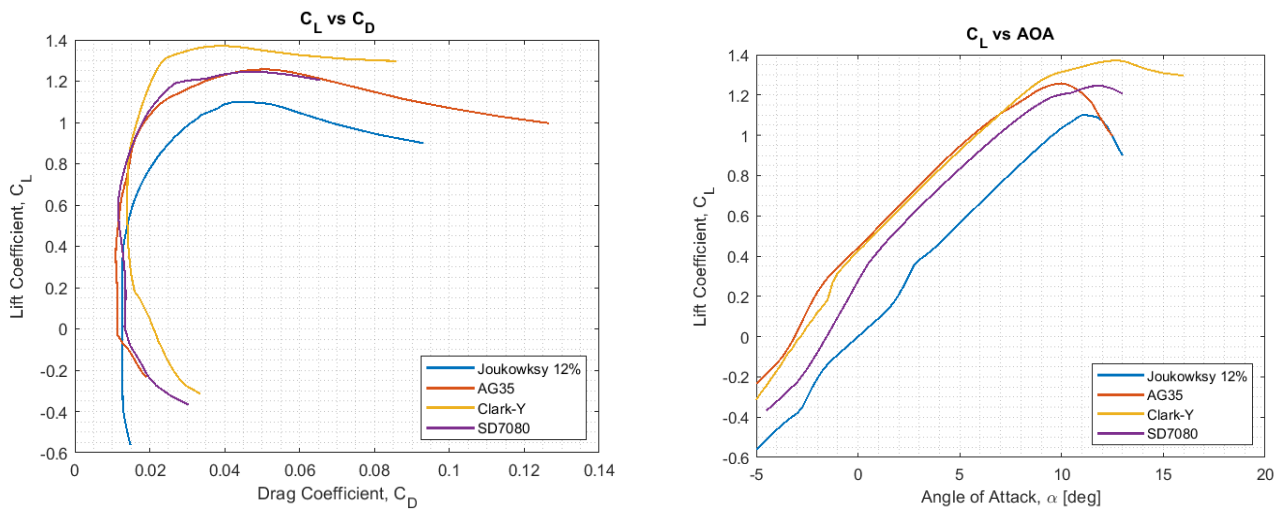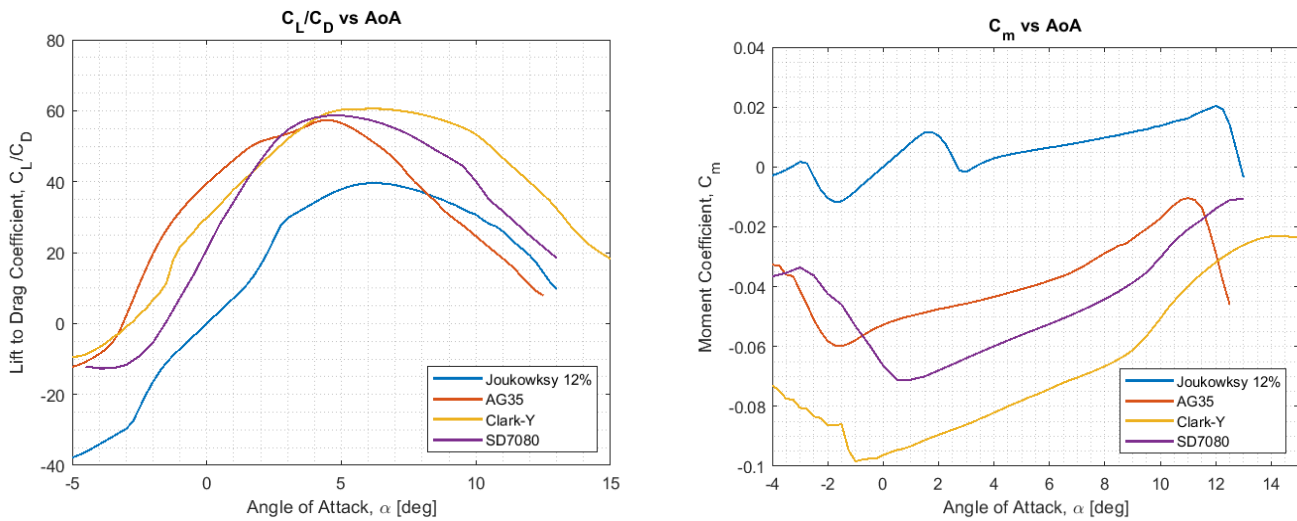


**Figure 4.4 Airfoil Polars**

**Figure 4.5 Airfoil Polars Continued**

To accommodate the spar chosen to structurally support the wing, the airfoil section at the root was required to have a minimum percent thickness of 11.5% in the vicinity of the quarter chord. This was based on the root chord of 18 inches. The maximum airfoil thickness is tabulated in Table 4.2. This requirement removed the SD7080 and the AG35 from consideration at the root section of the wing. Varying airfoils at sections of the wing were originally considered, but due to increased complexity in manufacturing it was decided to use a single airfoil profile with varying chord length throughout the wing. The Clark-Y and Joukowski 12% were the two airfoils ultimately chosen for further consideration for the final aircraft. With a root chord of 18" and a tip chord of 10", the maximum thickness of various airfoils are given below. This must be accounted for fitting the spar in the middle of the wing.

**Table 4.2 Airfoil Root Thickness Comparison**

| Airfoil | Airfoil Maximum Thickness at Root (in) |
|---|---|
| Joukowsky 12% | 2.160 |
| AG35 8.7% | 1.566 |
| Clark-Y 11.7% | 2.106 |
| SD7080 9.2% | 1.656 |

### 4.2.3 Control Surface Sizing

The size of the control surfaces was determined using traditional design practices and accepted conventions from the aviation and RC plane community. These designs were further verified to be adequate based on the numerical flow simulations and stability analysis. The ailerons and flaps each share 50% of the span of the wings and their chord lengths are 20% of the wing chord; following the acrobatic wing design, the flaps and ailerons taper towards the wing tips. The elevators range from 10 to 60% averaging about 50% of the horizontal fin including the horn aerodynamic balance at the tips. The horn reduces the force exerted on the servo for better maneuverability during flight; the addition of the balance

horn also prevents flutter of the surface. The rudder, shown below, comprises 50% of the vertical fin on average and is balanced for the same reasons as the elevator.

      The volume coefficients of the tail surfaces were determined by the equations below where $S$ is the area of the Horizontal tail, Vertical tail, and Wing and $l$ is the lever arm between the ¼ chord positions of the tail and the wing, $c$ is the chord, and $b$ is the wing span. The coefficient of the horizontal tail is 0.546 and the coefficient of the vertical tail is 0.0534; these values are typical for aerobatic planes.

$$C_H = \frac{S_H \cdot l_H}{S_W \cdot c_{MAC}}$$

$$C_V = \frac{S_V \cdot l_V}{S_W \cdot b}$$

The geometry of the vertical and horizontal tail as well as the wing are shown below. All dimensions given are in inches. The rudder is shown from the port side of the aircraft, the horizontal tail is shown from the bottom view, and the wing is shown from the top view.
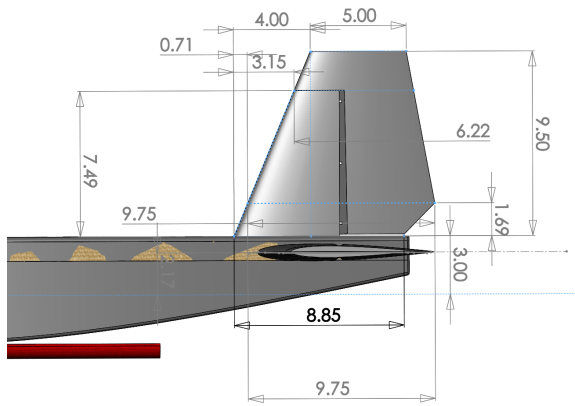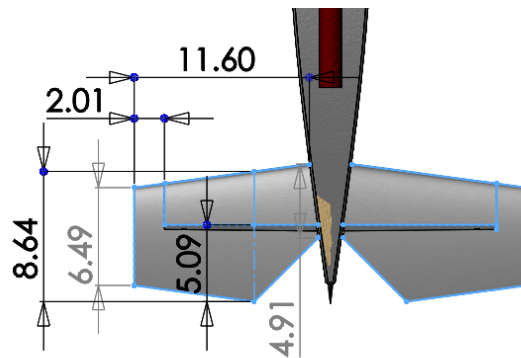


**Figure 4.6 Vertical Tail Rudder**



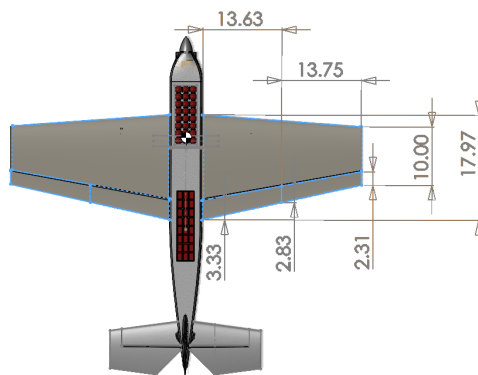**Figure 4.7 Horizontal Tail Elevators**



**Figure 4.8 Wing Control Surfaces**

The analysis of the selected airfoils considered the aerodynamic characteristics of flapped airfoils to increase the maximum lift coefficient due to takeoff requirements in Missions 1 and 3. The analysis was performed on XFLR5 at the expected takeoff Reynolds Number.
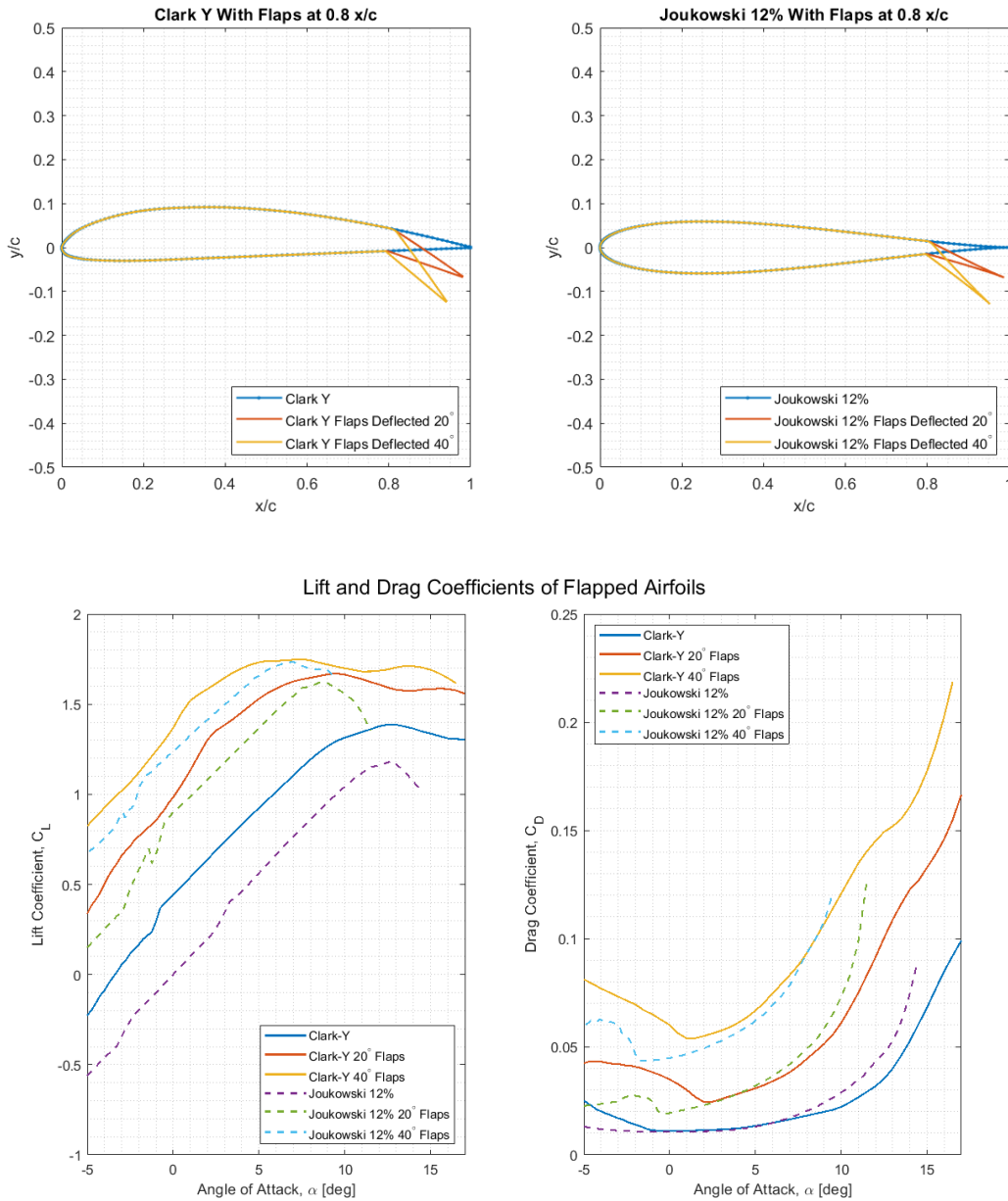


**Figure 4.9 Flapped Airfoil Polars**

### 4.2.4 CFD Analysis

In order to better predict the aerodynamic performance of the wing design, a numerical simulation was performed using computational fluid dynamics (CFD) software. The CFD simulations were performed using ANSYS Fluent. The primary

objectives of the CFD analysis were to have a more detailed comparison of the wing sections where the panel methods failed and to determine the expected loadings on the control surfaces to optimally size the actuators.

ANSYS Fluent was used to solve the steady Reynolds Averaged Navier-Stokes (RANS) equations. The RANS equations were solved using a fully coupled scheme. The convective terms were approximated using a second order upwind scheme. For turbulence closure, Menter's K-$\omega$ Shear Stress Transport (SST) eddy viscosity turbulence model was used [8]. The K-$\omega$ SST turbulence model was preferred as it is a robust turbulence model that is widely used. The use of the K-$\omega$ SST model required a sufficiently fine mesh near the surface of the wing to resolve the viscous sublayer of the boundary layer such that the non-dimensional wall distance, y+ was on the order of 1. The boundary layer refinement and y+ distribution on the wing is shown below.
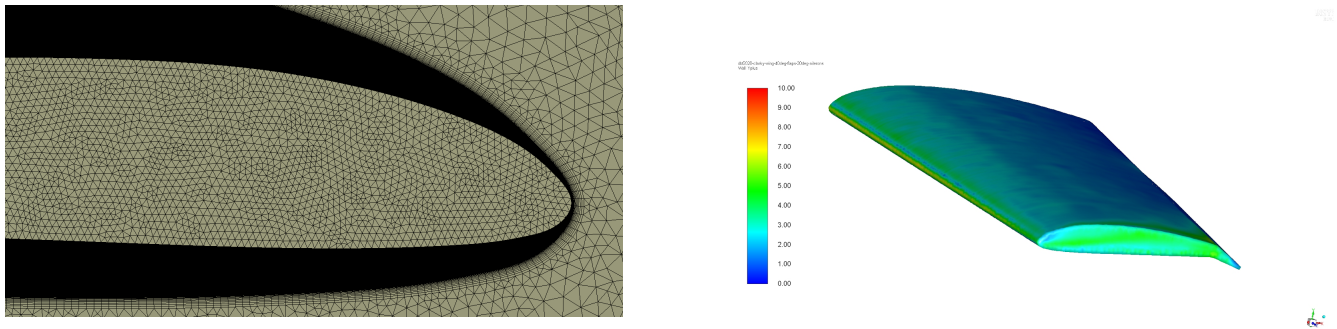


**Figure 4.10 Boundary Layer Mesh and Wing Y+ at Takeoff Conditions**

The flow domain consisted of a velocity inlet, pressure outlet and a symmetry plane. A hybrid mesh shown below was implemented where the unstructured portion discretized the inlet and near wing domain while the structured portion was used to capture the wake in the remainder of the flow domain downstream of the main wing.



**Figure 4.11 CFD Mesh**

A visual representation of the pressure distribution for the wing during ideal cruise conditions where the control surfaces are retracted is shown below followed by the wing during takeoff conditions with the flap deflected 30 degrees.

**Figure 4.12 Pressure Distribution on Clark-Y Wing**
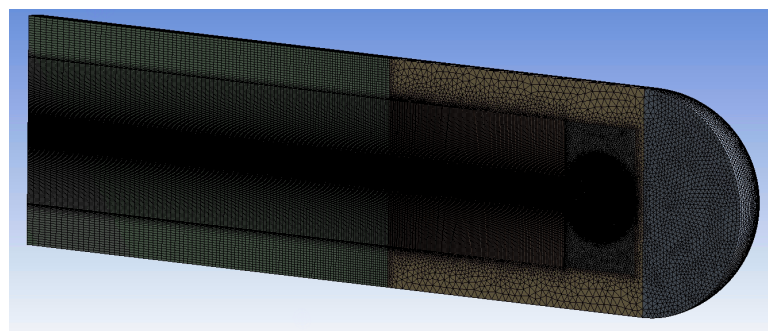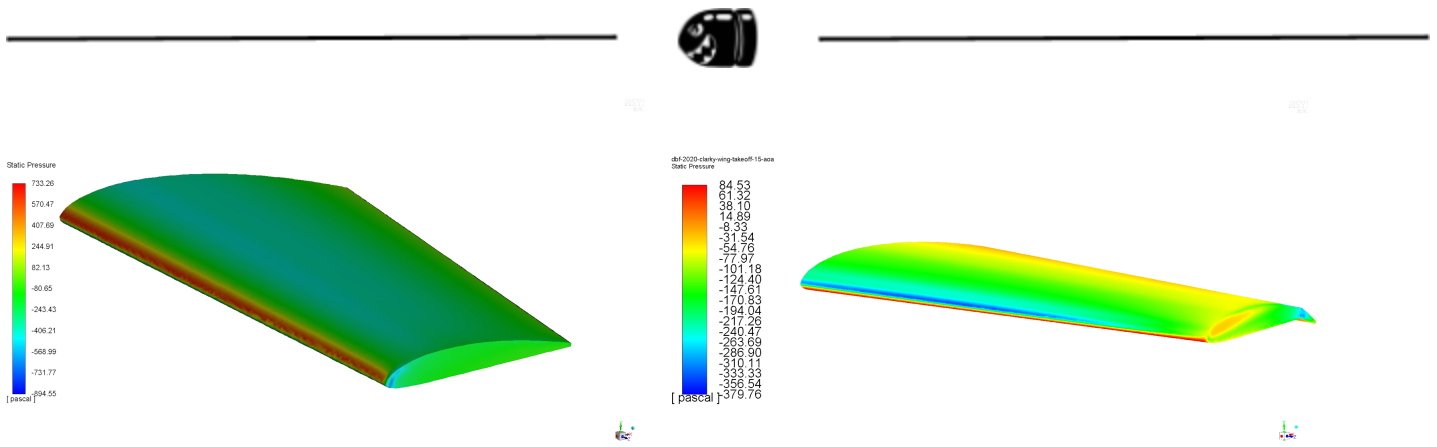
Lift and drag coefficients on the lifting wing and flaps are tabulated in the table below.

**Table 4.3 Lift and Drag Coefficients and Flap Loading from CFD Simulation**

| Case | Speed [mph] | AoA [deg] | Flap Deflection [deg] | Cl Wing | Cd Wing | Flap Hinge Moment [lbf-in] |
|------|-------------|-----------|------------------------|---------|---------|----------------------------|
| Take Off | 20 | 10 | 30 | 1.118 | 0.239 | 0.2691 |
| Take Off | 20 | 12 | 30 | 1.366 | 0.296 | 0.2811 |
| Cruise | 70 | -1.5 | 0 | 0.8 | 0.015 | 0.7553 |
| Cruise | 70 | -3 | 0 | 0.1 | 0.026 | 0.5368 |

### 4.2.5 Banner Sizing

From the Banner Drag ground tests, values for the drag load induced by banners of different dimensions were recorded from a load cell with +/-0.03% uncertainty at various speeds. The results are analyzed in Figures 4.13 and 4.14. For more information on the test setup, see Section 7.1.

The coefficient of drag was calculated for each test and was found to be close to the theoretical value of 0.3. While the drag coefficient decreased slightly as the size of the banner was increased, it remained close enough that a quadratic curve fit was used to extrapolate drag values at other speeds.
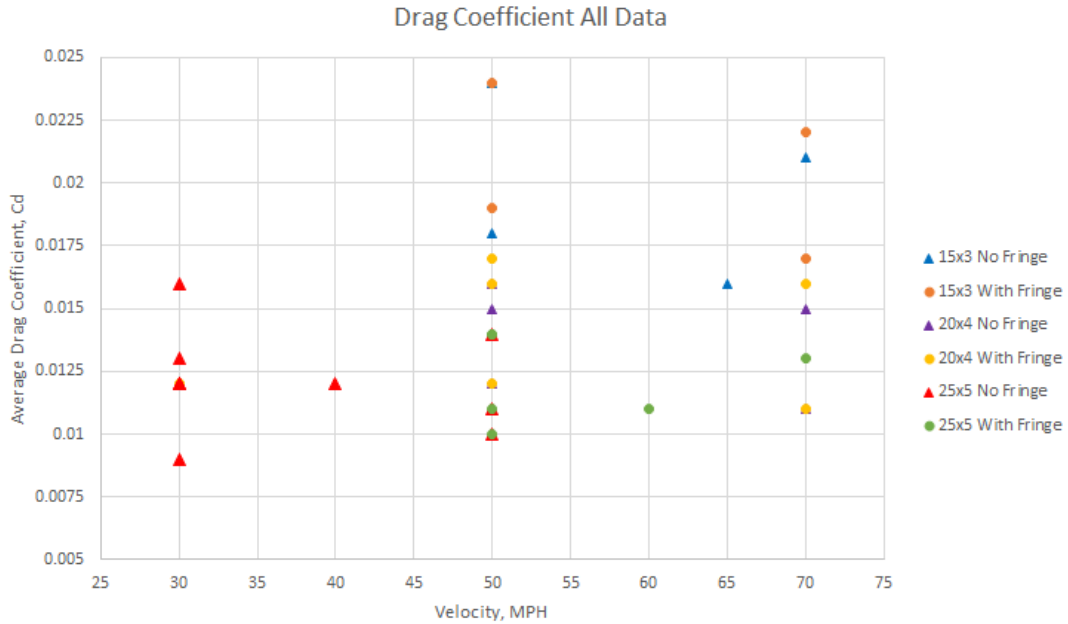
**Figure 4.13 Banner drag coefficients from experimental tests**

The relationship between drag and velocity is quadratic according to the drag equation in which drag is proportional to the square of velocity. Assuming that Cd is constant and that drag is zero when velocity is zero, the curves shown in Figure 4.14 are produced. The equations are used to extrapolate data to find drag at the desired velocity at which the aircraft will fly during Mission 3. For instance, if the aircraft is expected to fly at 60 MPH during Mission 3, the drag for each banner is predicted as shown below.

**Table 4.4 Predicted Banner Drag (lb) at 60 MPH**

| Banner Dimensions | No fringe | With fringe |
|---|---|---|
| 15'x3' | 7.5645 | 7.86 |
| 20'x4' | 9.342 | 9.7471 |
| 25'x5' | 12.739 | 13.1456 |

The resulting graph from the curve fittings is shown below; it indicates that the addition of the fringe adds a slight increase in drag to the banner. Conversely, the fringe significantly improves the legibility of the banner as it reduces the amplitude of the oscillations of the banners shape. The benefit of the fringe in maintaining the shape and position of the banner during flight outweighs the minimal cost of drag introduced. As predicted, the bigger banner results in more drag on the aircraft. For that reason, the medium and small banners might be preferable to take to competition to obtain a higher score due to the increased speed of the aircraft based on the conclusions of the sensitivity analysis completed previously.
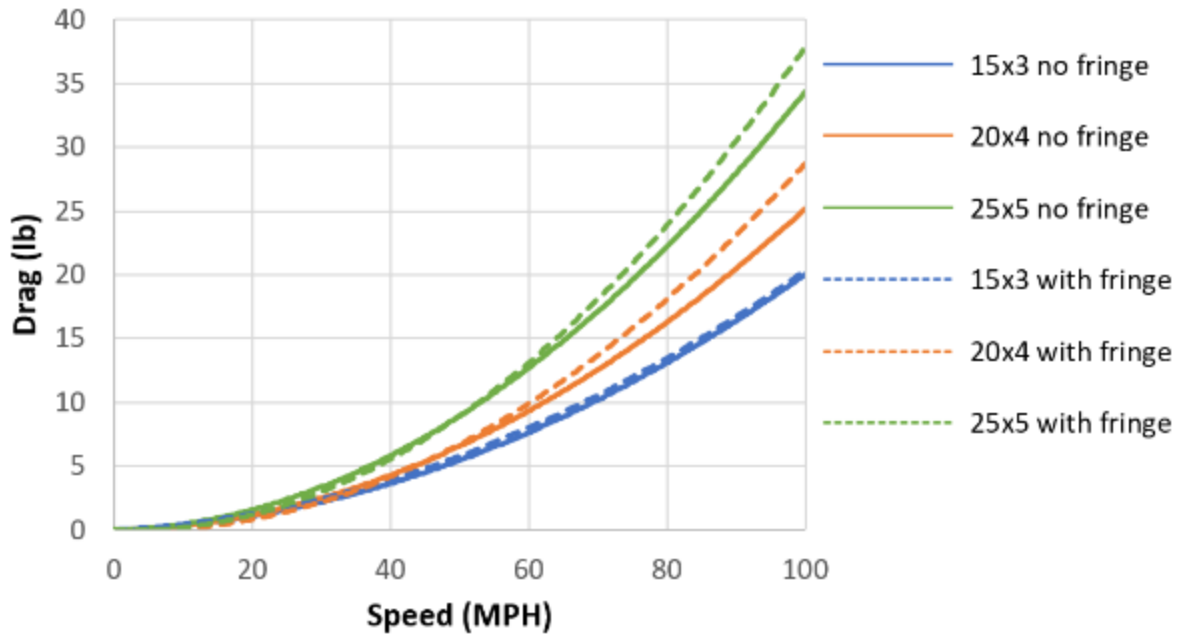
**Figure 4.14 Drag versus speed curves from experimental tests**

### 4.2.6 Propeller Selection

Several propellers were tested on a motor mount for their static thrust and corresponding amperage draw. From static tests using the motor mount shown in Figure 7.2, several propellers were tested and the results are summarized below. The most thrust came from the 15 and 16 inch diameter propellers. Propellers of greater diameters were not tested because full throttle with those propellers would likely surpass the maximum current recommended by the motor, 90 amps, and the maximum allowed before the ESC brings it to a soft stop, 125 amps. The 15" x 8" propeller was selected for Missions 1 and 2 since it has a high thrust but low current draw. For Mission 3, more thrust is required to counteract the additional drag due to the banner but changing of propellers is not allowed so the 15" x 8" propeller is also selected for that mission.

**Table 4.5 Propulsion Tests**

| Propeller | Pitch (in) | Diameter (in) | Max Thrust (lb) | Max Current (amp) |
|-----------|------------|---------------|-----------------|-------------------|
| 14 x 8.5 | 8.5 | 14 | 8.175 | 56.9 |
| 14 x 10 | 10 | 14 | 8.540 | 82.7 |
| 14 x 12 | 12 | 14 | 9.060 | 89.2 |
| 14 x 14 | 14 | 14 | 7.773 | 102.1 |
| 15 x 8 | 8 | 15 | 11.03 | 76.3 |
| 15 x 10 | 10 | 15 | 11.34 | 93.2 |
| 16 x 10 | 10 | 16 | 11.20 | 89.2 |

## 4.3 Methodology for Aircraft Performance Predictions

Aircraft performance predictions were obtained through simple aerodynamic calculations with lift and drag, CFD analysis in ANSYS and XFLR5, as well as by putting the weight and control surface sizes into a flight simulator and flying it. Since these are strictly theoretical predictions, there is a lot of uncertainty due to gusts of wind, or discrepancies in weight or sizing due to manufacturing processes, etc.
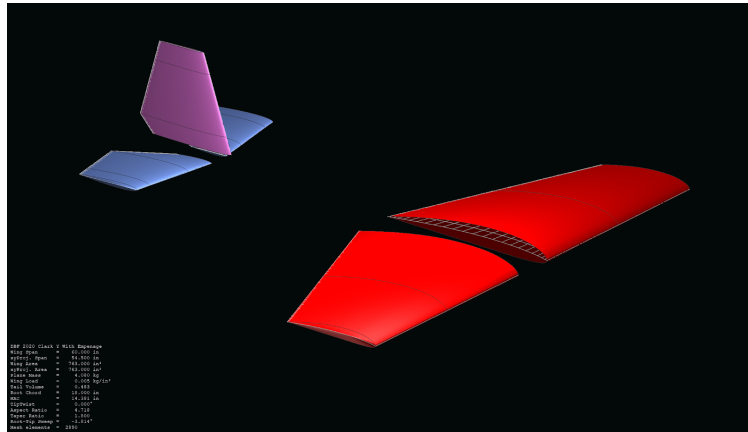


**Figure 4.15 Lifting and Control Surfaces Modeled on XFLR5**

## 4.4 Flight Characteristics Predictions

A majority of the initial aircraft data was obtained through XFLR5 as well as additional calculations of known aerodynamic formulas for the Clark Y airfoil. This particular airfoil will contain flaps that are 20% of the chord that are at an angle of attack of 20 degrees and also contain half span ailerons. The aircraft is also estimated to travel at about 80 mph while in flight. With these design specifications in addition to the Clark Y airfoil design the following aerodynamic properties are obtained. At an estimated flight speed of roughly 80 mph, the predicted lift and drag due to the Clark Y airfoil on the aircraft is 17.71 lb and 0.953 lb respectively.

The stability of the aircraft was initially analyzed using Athena Vortex Lattice (AVL), a vortex lattice code developed by Mark Drela. The analysis was done to ensure that the aircraft could successfully accomplish the missions. The aircraft main wing and empennage section were modeled in AVL while neglecting the fuselage. This model is shown in figure 4.16.
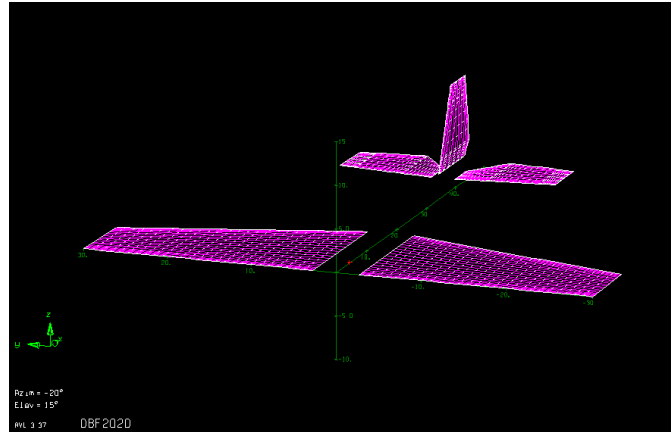
**Figure 4.16 AVL Model**

Through an iterative process of modifying the CG location, wing/tail placement, sizing and test flights on the test plane, a sufficiently stable aircraft design was generated. Through initial analysis in AVL and experimental test flights, the trim conditions of the aircraft were obtained. The most critical point was determined to be during mission 2 at take off conditions due to the increased weight of the aircraft. The stability derivatives for these conditions were obtained from AVL and are shown below. The obtained stability derivatives agreed with the handling of the test plane and based on the results, there was no concern regarding the static stability.

**Table 4.6 Stability Derivatives for Mission 2 at Takeoff**

| $C_{l\alpha}$ | 2.299 | $C_{l\beta}$ | -0.012 | $C_{lp}$ | 0.00 | $C_{lq}$ | 4.625 | $C_{lr}$ | -0.00 |
|---|---|---|---|---|---|---|---|---|---|
| $C_{m\alpha}$ | -.961 | $C_{m\beta}$ | 0 | $C_{mp}$ | 0.00 | $C_{mq}$ | -15.89 | $C_{mr}$ | 0.000 |
| $C_{n\alpha}$ | 0 | $C_{n\beta}$ | 0.136 | $C_{np}$ | -0.117 | $C_{nq}$ | -0.001 | $C_{nr}$ | -0.6792 |

Once the static stability and trim conditions were determined, the dynamic stability for the three missions were analyzed using AVL. From the static stability derivatives obtained in AVL and the aircraft's mass moments of inertia, the dynamic stability characteristics for 5 dynamic modes were designed to be stable based on the negative real components. These parameters are tabulated below in table 4.7 and plotted in a Root Locus plot in figure 4.17 for all three missions.

**Table 4.7 AVL Results**

| Mission | Parameter | Longitudinal Modes | | Lateral Modes | | |
|---|---|---|---|---|---|---|
| | | Short Period (1) | Phugoid (2) | Dutch Roll (3) | Roll (4) | Spiral (5) |
| Mission 1 | Damping Ratio, [-] | 0.52 | 0.21 | 0.32 | - | - |
| | Damped Natural Frequency [Hz] | 3.018 | 2.473 | 3.9 | - | - |
| | Time Constant [s] | 0.26 | 21.25 | 0.27 | 0.045 | 1.512 |
| Mission 2 | Damping Ratio [-] | 0.46 | 0.15 | 0.32 | - | - |
| | Damped Natural Frequency [Hz | 3.78 | 2.473 | 4.3 | - | - |
| | Time Constant [s] | 0.32 | 25.31 | 0.38 | 0.076 | 1.016 |
| Mission 3 | Damping Ratio [-] | 0.52 | 0.17 | 0.32 | - | - |
| | Damped Natural Frequency [Hz | 3.56 | 2.47 | 4.0 | - | - |
| | Time Constant [s] | 0.37 | 23.251 | 0.31 | 0.052 | 1.121 |
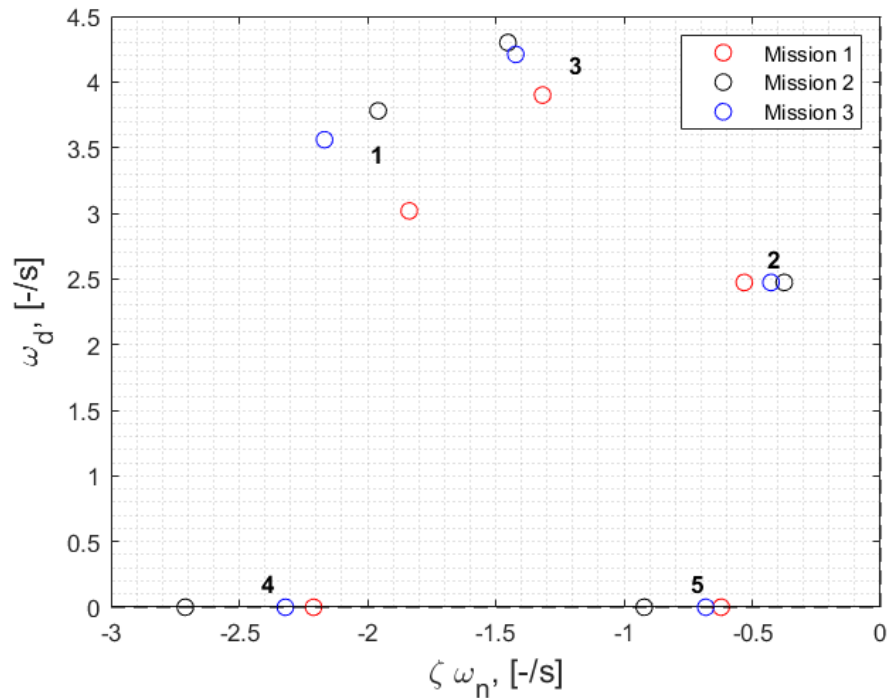
**Figure 4.17 Root Locus Plot**

### *4.5 Mission Performance Predictions*

For the Demonstration flight, the performance of the aircraft was summarized in Section 4.4. With the additional weight of the passengers and their luggage and additional drag due to the banner, the following predictions were developed using interpolation and extrapolation of the data obtained in Section 4.3.

### 4.5.1 Banner Mission Performance

For Mission 3, estimations of banner drag with respect to speed were computed using the trend lines shown in Figure 4.14. From the trendline equations from this chart, the aircraft cruise speed can be found for various drag values for each of the three banner lengths. Additionally, drag was related to the amperage pulled by the motor in the following extrapolation of some experimental data for the Scorpion SII 4035 450KV motor [1]. While in reality this relationship is not always linear, it can be assumed linear for the range in which the aircraft will operate and the experimental data below can be used.
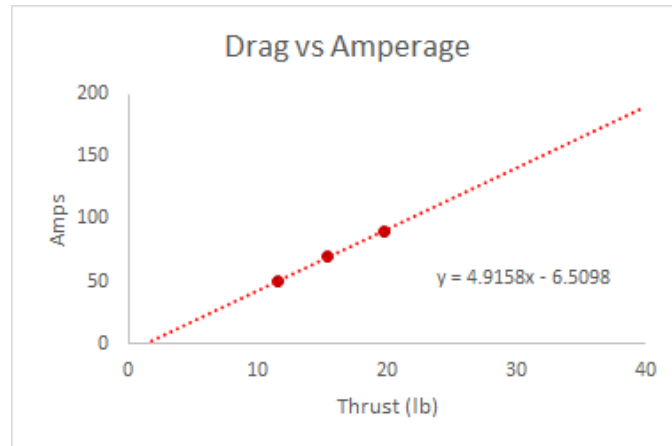
**Figure 4.18 Drag vs amperage curve from experimental tests**

From the trendline equation in 4.8, the amps pulled by the motor can be estimated at various drag values (assuming drag and thrust are equal at cruise speeds). Using two 3300 mAh 29.6 V LiPo batteries, the time until the batteries run out of energy can be approximated based on the amperage draw. From the time to failure and the cruise speed of the aircraft, the number of laps completed in Mission 3 can be estimated. The aircraft's score is either limited by the failure time of the batteries or, if the time to failure exceeds 10 minutes, the number of laps given by the Mission 3 rules. By multiplying the estimated number of laps completed and the length of the banner can be multiplied in a score prediction model shown below.
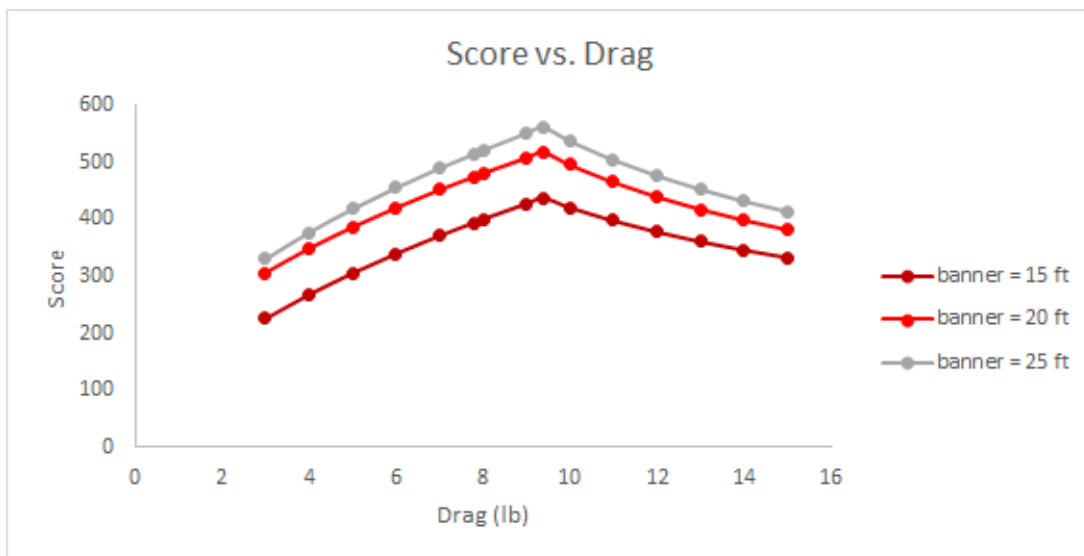


**Figure 4.19 Score vs Drag**

This figure indicates that the Mission 3 score is optimized with the 25 ft banner when drag is 9.39 lb. However, this corresponds to the batteries dying at 10 minutes which would incur damage to the batteries. A rule of thumb requires that

only 80% of battery capacity should be used to prevent damage to the cells. This parameter is achieved at a drag of 7.78 lb which, in turn, corresponds to a cruise speed of 47 MPH. A projection of banner length and score supports the use of a 25 ft banner as it is fairly close to optimal. However, in the event of high winds, a 25 ft banner might significantly hinder the flight performance of the aircraft.
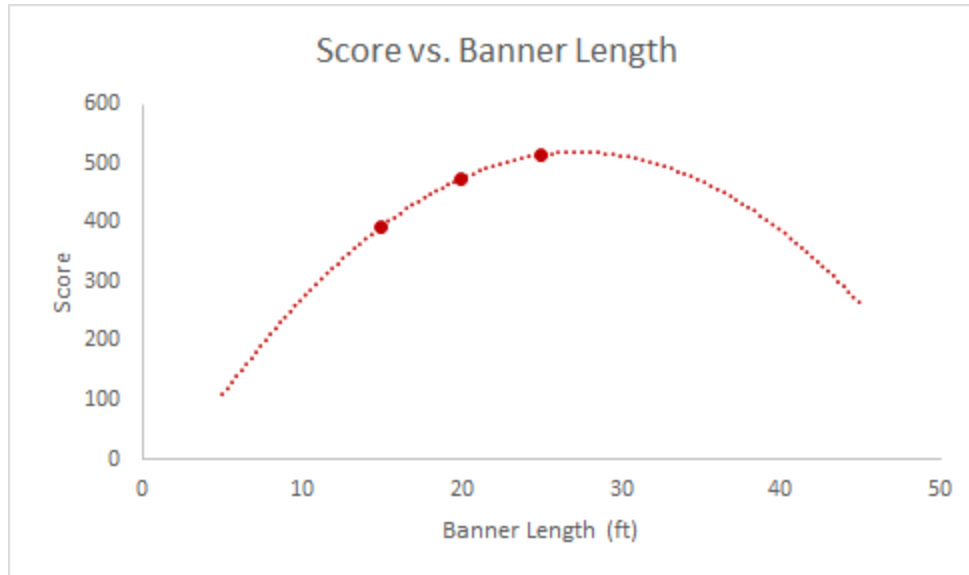


**Figure 4.15 Score vs Banner Length**

Based on the conclusions drawn from Mission 3 performance predictions and the experimental drag study on the banner, three banners will be taken to competition: a 25' x 5' banner which theoretically gives us a higher score, a 15' x 3' banner which is more manageable in gusts of wind, and a 5' x 1' banner which is the most manageable and contributes the least drag and would also be the fastest to load and deploy during the Ground Mission. In the following sections of the design report, it can be assumed that predictions, data, etc. refer to the 25' x 5' banner unless specified otherwise.

## 5.0 Detail Design

### *5.1 Dimensional Parameters*

The dimensions and characteristics of the final competition aircraft are provided in the table below.

**Table 5.1 *Bullitt* Dimensional Parameters**

| Wing (AR=4.037) | | Horizontal Stabilizer | | Vertical Stabilizer | | Fuselage | |
|---|---|---|---|---|---|---|---|
| **Airfoil** | Clark Y | **Airfoil** | NACA 0009 | **Airfoil** | NACA 0009 | **Total Length** | 56.74 in |
| **Wingspan** | 60.5 in (5 ft) | **Volume Coefficient** | 0.546 | **Volume Coefficient** | 0.0534 | **Nose Length** | 7.74 in |
| **Chord Length** | Max: 18 in Min: 9 in | | | | | | |
| **Area** | 774.38 in$^2$ | **Area w/ Elevators** | 169.2 in$^2$ | **Area w/ Rudder** | 71.48 in$^2$ | **Tail Length** | 18.41 in |
| **Ailerons** | Chord: 20% Area: 70.8in$^2$ Takeoff: 20 deg | **Elevator Chord** | 7.5 in | **Rudder Chord** | 7.5 in | **Width** | 5.0 in |
| **Flaps** | Chord: 20% Area: 85.12 in$^2$ Takeoff: 40 deg | **Elevator Area** | 101.44 in$^2$ | **Rudder Area** | 41.29 in$^2$ | **Height** | 5.1 in |
| **Taper Ratio** | 0.50 | **Taper Ratio** | 0.76 | **Taper Ratio** | 0.90 | **Distance from Ground** | 6.12 in |
| **Angle of Attack** | Takeoff: 15 deg Cruise: -1.5° | **Angle of Attack** | 0 deg | **Angle of Attack** | N/A | **Taper Ratio** | 0.32 |
| **Material** | Carbon FIber | **Material** | Carbon Fiber | **Material** | Carbon Fiber | **Material** | Carbon Fiber |
| Controls | | Motor | | Propeller | | Banner | |
| **Receiver** | Spektrum AR12310T | **Model** | Scorpion SII-4035-450KV | **Manufacturer** | APC | **Dimensions** | 25'x5' 15'x3' 5'x1' |
| **Servos** | Savox SV-1250MG | **No-Load Current** | 3A | **Diameter** | 15 in | **Material** | Ripstop Nylon |
| **Motor Batteries** | Thunder Power 3300 mAh | **Power Rating** | 2960W | **Pitch** | 8 in | **Leading Edge** | Carbon Fiber Rod |
| **Batt. Volume** | 3.336 in$^3$ | **kV** | 450 | Passengers | | **Trailing Edge** | 12" Fringe |
| **Cell Count** | 8 | **Resistance** | 0.026Ω | **Maximum #** | 24 | **String** | Braided Spectra |
| **Pack Voltage** | 29.6V | **Weight** | 435g | **Passenger Weight** | 0.25 lb | **Deployed Dist. from Plane** | 120" |
| **Pack Weight** | 1.46 lb | **Outer Diameter** | 1.9 in | **Luggage Weight** | 0.06 lb | **Stowed Dist. from Plane** | 0.5" |

### *5.2 Structural Characteristics / Capabilities*

### 5.2.1 Fuselage

The fuselage structure is comprised of a 5 layer composite sandwich construction where the outermost layers consists of 0.030 psf spread tow carbon fiber and 0.032 psf unidirectional carbon fiber, the middle layer consists of 0.25 in thick aramid 3 pcf honeycomb, and finally, the innermost layers consist of 0.025 psf kevlar mesh and 0.032 psf unidirectional carbon fiber. This sandwich makes for a strong yet light structure that resists bending and mitigates high stresses.

Servo mounts were reinforced with 0.25 in birch plywood to ensure firm hold of servo screws and to dissipate loads from servo torque on the surface. FIlm adhesive was laid in areas identified as high stress or on exposed ends of aramid honeycomb to encourage resistance to peeling and honeycomb delamination.

Reinforcements were added to high stress areas and areas of stress concentrations such as bolt holes, spar slots, and screw mounts. Hole stress concentrations were estimated with standard stress concentration equations and figures were for axial loads.

$$\sigma_{avg} = \frac{P}{A} = \frac{P}{(b-d)h}$$

Corner stress concentrations were found through Finite Element Analyses of the fuselage. The resulting plots were used to inform decisions on where to reinforce the underlying carbon fiber skin with extra unidirectional carbon fiber doublers.
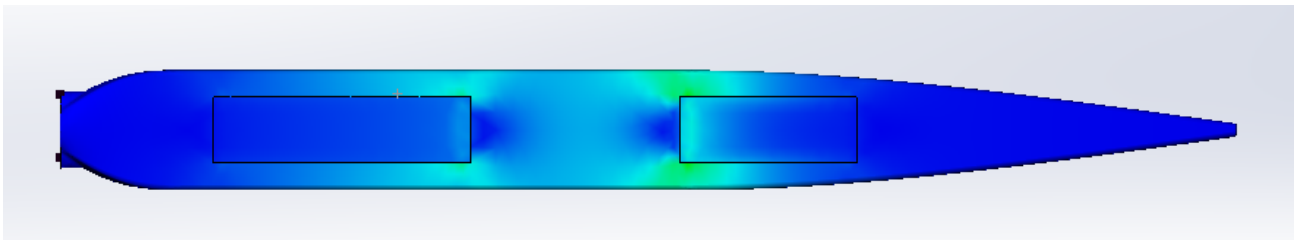


**Figure 5.1 Finite Element Analysis of the Fuselage**

### 5.2.2 Wing

The wing implements a single layer of 0.030 psf spread tow carbon fiber for the skin which is assumed to carry all torsional loading. The spar of the wing is assumed to carry all bending loads and is constructed with a symmetrical layup of four 0.030 psf spread tow carbon fiber lamina sandwiching a 0.25 in thick aramid 3 pcf honeycomb core. The innermost ⅓ of the wing's length also implements a double spar. In this section of wing, where the loading is highest, a commercially available round carbon fiber wing tube is added. This second spar carries through the fuselage of the aircraft allowing easy removal and stowing of the wings for transportation. The ribbing of the wing is also created from the same sandwich honeycomb structure as the main spar. These ribs support the carbon skin of the aircraft and transfer bending loads from the extremities of the wing to the spar.

Servo mounting slots are reinforced with 0.25 in birch plywood to ensure firm hold of servo screws and to dissipate loads from servo torque on the surface. Ribs and spars are adhered to both wing surfaces with epoxy ensuring maximum adhesive contact between wing surface and carbon fiber spar plies. A thin 0.015 psf fiberglass sleeve ensures loading is transferred between spars effectively and allows for effortless alignment of the wings upon assembly.
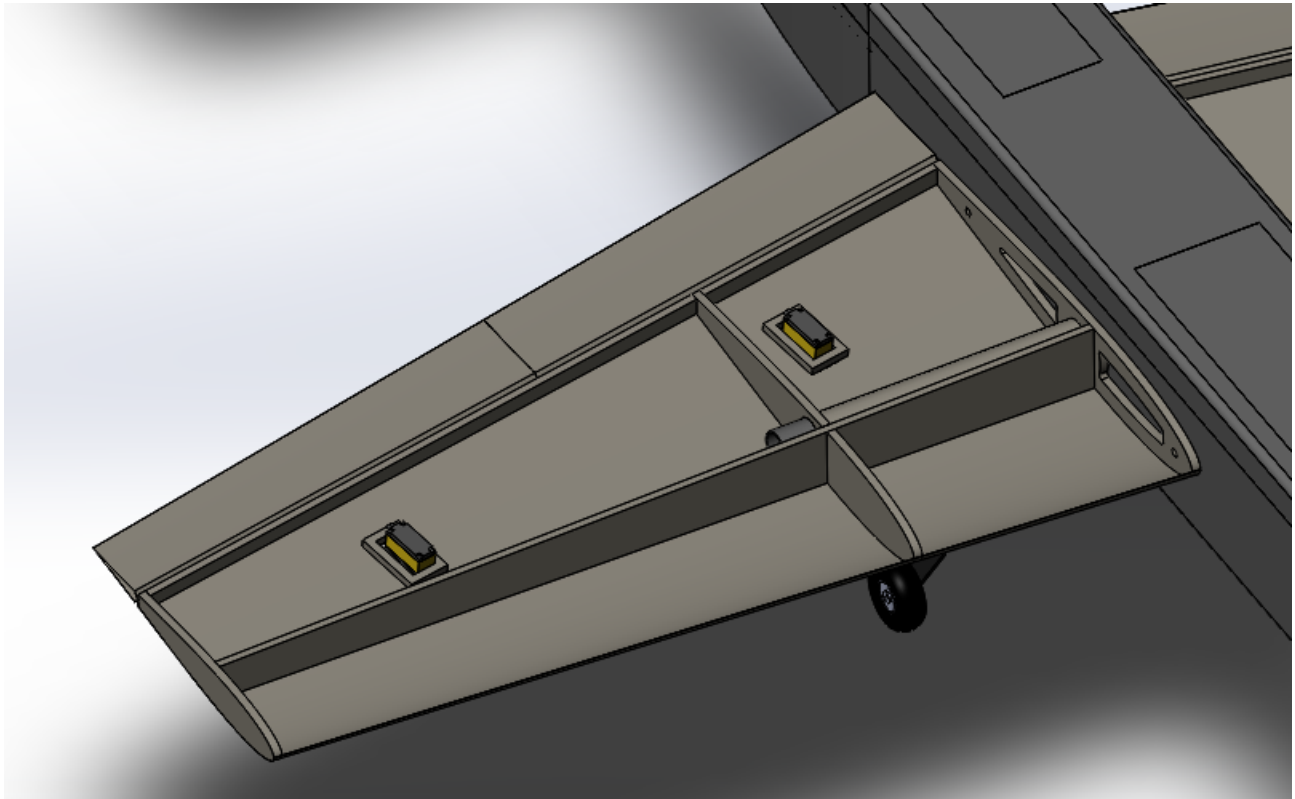
**Figure 5.2 Wing Spar and Ribbing**

### 5.2.2 Empennage

The empennage is constructed in much the same manner as the wings. A carbon skin encompases sandwich structure ribbing allowing for a light yet strong construction. A continuous spar connects the horizontal stabilizers to ensure that load is spread evenly. A spar also runs through the vertical stabilizer and connects to the horizontal stabilizer in a T configuration. From this, each empennage spar gains two points of internal contact with the fuselage increasing the moment arm that resists control surface bending forces. Control surface mating faces are chamfered to allow deflection. Hinges are placed halfway inside the chamfer and half way inside the stabilizer face for hinge pivot point alignment.
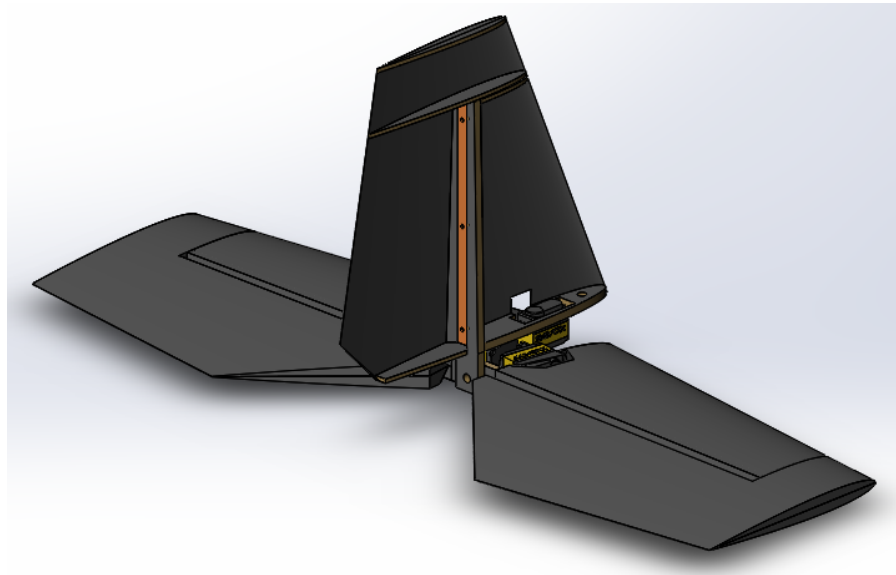
**Figure 5.3 Vertical Stabilizer Spar and Ribbing**

### 5.2.3 Landing Gear

The landing gear of this aircraft is in the tricycle configuration. This allows banner lengths to be variable and unrestricted as long as the CG of the banner does not fall outside of the banner deployment mechanism. One wheel is located forward of the CG. Two main landing gear are located aft of the CG where the axle of the main wheel is located 11.2 degrees behind the CG envelope. This feature allows for smooth rotation upon climb out as it was found that landing gear further aft created a tendency for the aircraft to jump into the air. The 11.2 degree landing gear position also creates conditions favorable for gentle landings as landing AOA places the CG fairly close to vertically aligned with the axles. The rotation of the aircraft forward can then be managed slowly in a controlled manner by the pilot.  It was determined that a steerable nose wheel was not necessary for accurate take off and landing from the prototype aircraft.
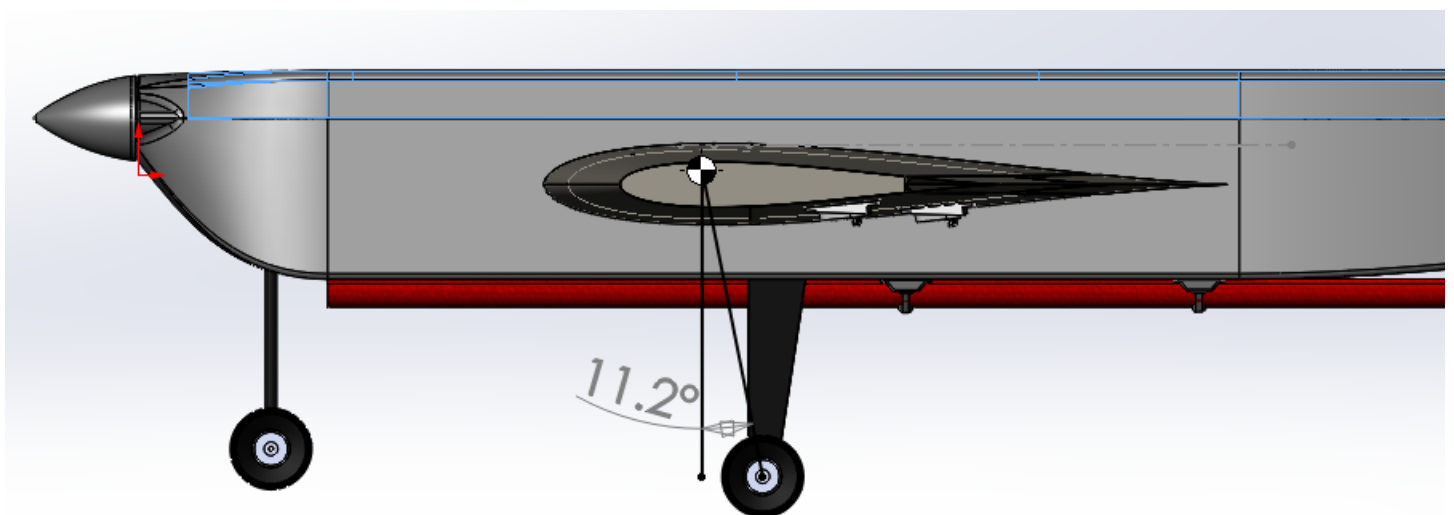


**Figure 5.4 Undercarriage**

## 5.2.5 Operating Envelope

The operating envelope of the aircraft is shown in the figure below. The values for maximum and minimum load factor for Mission 1 were taken from the Yak 54 RC airplane to be +9g and -7g [2]. The Yak 54 is an aerobatic aircraft similar in performance capabilities to *Bulittt*. The load factor limits were decreased for Missions 2 and 3 due to the higher gross weight of the aircraft during those missions. The maximum speeds for each operating envelope were determined during flight testing. For Mission 3, the maximum speed is significantly less due to the drag generated by the banner. The values for maximum speed were confirmed during experimental flight testing of the aircraft. Finally, the curved limits were found using the following equation with the maximum coefficient of lift for the Clark Y airfoil.

$$n = L / W = (\tfrac{1}{2} * CL\_max * \rho * v^2 * S) / W$$

From Figure 5.5, The operating flight envelope of the aircraft can be described. The stall speed can be found where the curve intersects with n = 1. Additionally, the maximum bank angle can be found from the equation:

$$n = 1 / \cos(\text{bank angle})$$

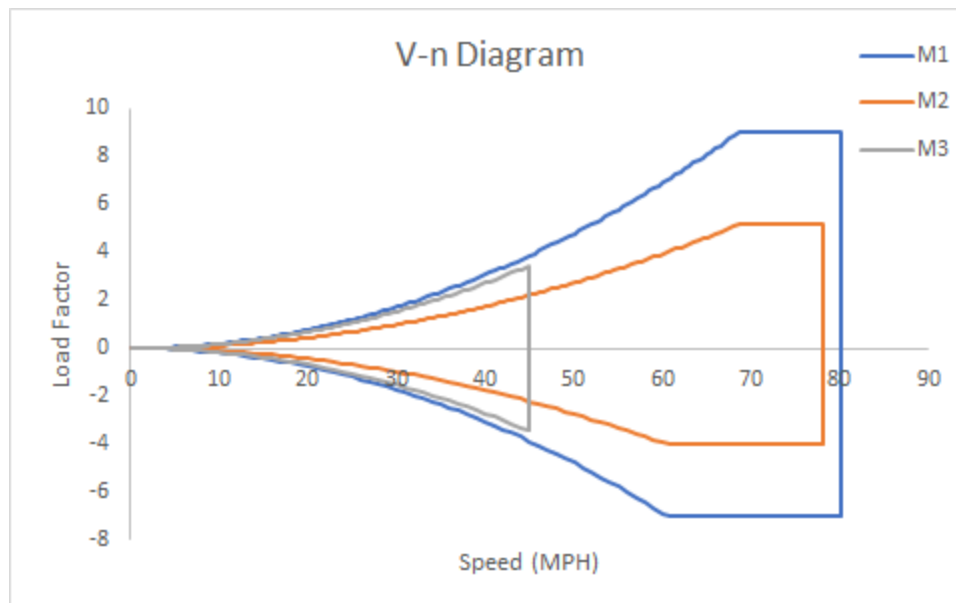

**Figure 5.5 Operating Envelope**

## 5.3 Systems Integration

### 5.3.1 Servos

*Bullitt* has seven total servo motors controlling the control surfaces to have ample maneuverability and stability in demanding situations in Missions 2 and 3. To accommodate high speeds and torques required for control surfaces, high

voltage 7.4 volt servos were chosen. Each wing has two servos. The wing-root end servos control the flaps to provide more drag and more lift for both landing and takeoff, respectively. The wing-tip end servos control the ailerons to keep lateral stability. The tail of *Bullitt* has three servos; the elevator surface has two servos that control each half of the elevator surfaces, while the rudder is controlled by a single servo. The remaining three servos in *Bullitt* contribute to the banner deployment and release mechanism.

### 5.3.2 Passengers/Luggage

For Mission 2, the passengers and luggage are placed completely within the fuselage that would optimize space amongst the other critical components. The passengers and luggage are placed in front and behind the carbon fiber wing spar, respectively to balance both sets of weighted components about the calculated CG. The passengers are positioned on top of batteries to have ease of accessibility for the Ground Mission, similarly so on the other side of the spar for the luggage. The passengers have passive shoulder retentions that prevent them from sliding upwards from their restraints in inverted maneuvers.
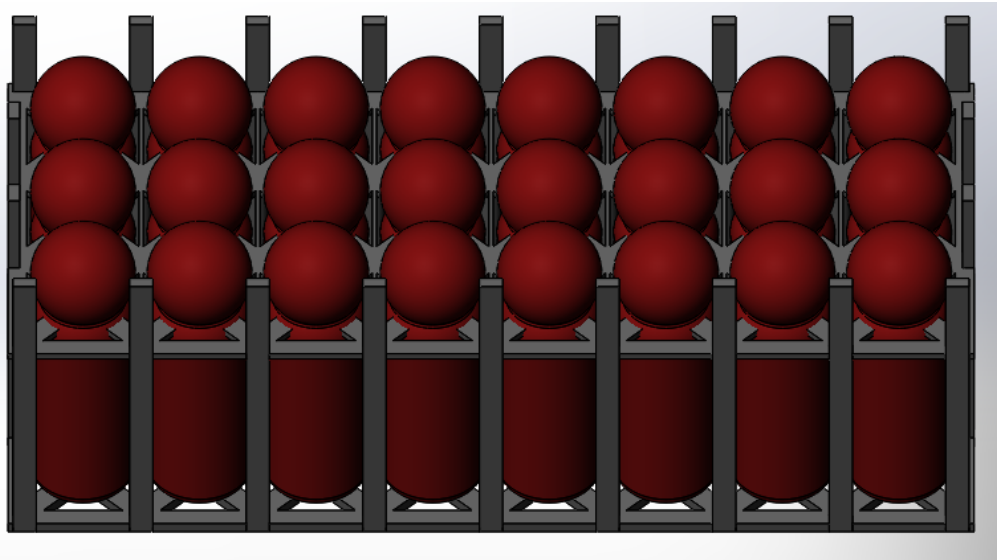


**Figure 5.6 Passenger Retention**

### 5.3.3 Banner Deploy/Release

For Mission 3, the banner is recessed in free-flow airstream underneath the fuselage. It is secured with two latch mechanisms that are controlled by a servo each to release the banner spool. The banner is rolled into a spool with all harnessing also wrapped neatly around the banners surface. The combined actions of the weighted leading edge of the spool and the tensioning of the banner string cause the whole spool to swing downwards about the tailend, having the leading edge now hanging down and the tailend pointing upwards. The banner unspools itself into the flight configuration slowly to avoid shock or sudden jolting. To release the banner from *Bullitt,* a servo located underneath the empennage is holding the banner string via a gate which is actuated by the transmitter.
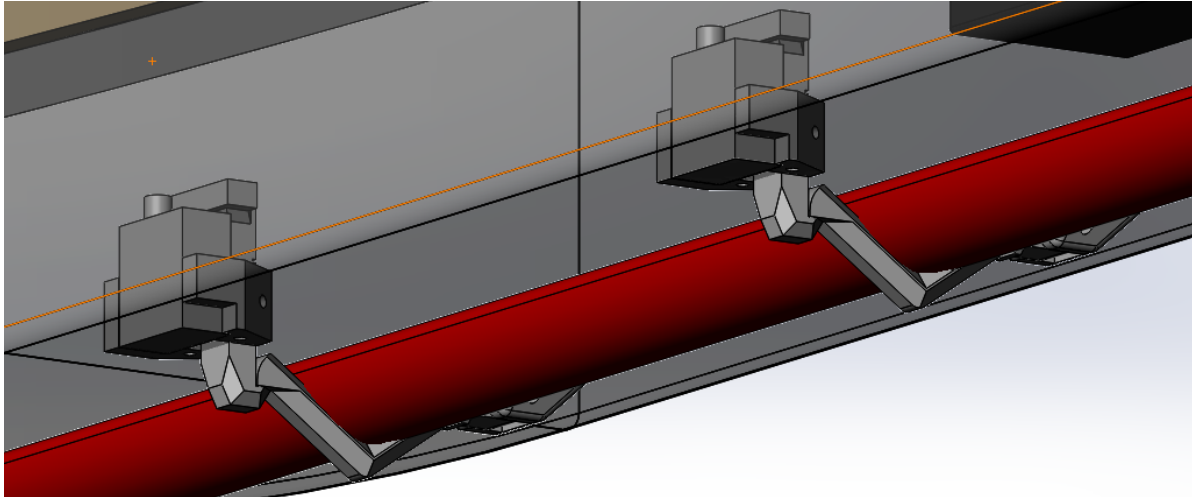
**Figure 5.7 Stowed Banner Position and Hook Mechanism**

### 5.3.4 Receiver, ESC, and Telemetry

The Spektrum AR12310T receiver contains 12 channels to control each servo and an integrated telemetry system which is capable of transmitting valuable flight information to a supporting transmitter. The receiver comes with three additional remote receivers to ensure a strong connection to a transmitter. In addition to integrated telemetry, the receiver also contains an X-bus and sensor port to expand the standard telemetry for a wider log of information. An AS3000 AS3X Flight Stabilization Module was added to the sensor port, giving the aircraft easily programmable gyroscopic capabilities and Roll/Pitch/Yaw logging data. The Castle Creations Phoenix Edge 100 ESC also contains logging capabilities which records information on the motor and batteries, such as current draw, motor power and Amp-Hour drain. With a Telemetry Link module, the ESC data can be live fed to the receiver through the X-bus port, and the data may be logged on the transmitter.

### *5.4 Weight and Balance*

The center of gravity was verified for the aircraft by performing a weight and balance investigation on the aircraft model in SolidWorks. Several of the key components and parts of the aircraft were measured for their mass and location from a fixed point one inch forward of the nose. All measurements were taken from the center of gravity of each respective part or from the centroid of multiple parts. The mass and moment arm were then multiplied to find the moment due to that part. The sum of the moments was taken for each mission. The results are shown in Table 5.2 below.
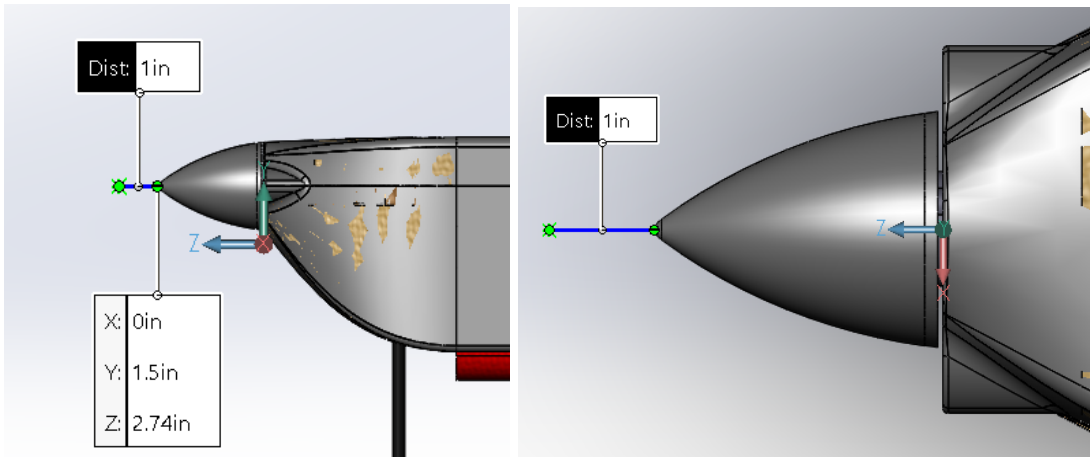
**Figure 5.8 Side and Top View of Reference Point, 1 in. in Front of Nose Cose**

**Table 5.2 Weight and Balance**

| Component | Location (inches from fixed location) | Weight (lb) | Moment (in-lb) |
|---|---|---|---|
| Fuselage | 22.3 | 1.53 | 34.12 |
| Wing(s) | 20.96 | 0.42 (Multiplied by 2) | 8.803 |
| Motor | 5.67 | 0.96 | 5.443 |
| Propeller | 3.69 | 0.09 | 0.332 |
| Batteries and Hardware | 13.83 | 3.25 | 44.95 |
| Horizontal Stabilizer | 54.24 | 0.10 | 5.424 |
| Vertical Stabilizer | 54.18 | 0.049 | 2.65 |
| Landing Gear (Front) | 7.25 | 0.03 | 0.218 |
| Landing Gear (Rear) | 21.93 | 0.12 (Multiplied by 2) | 2.632 |
| Aileron Servos | 22.32 | 0.13 (Multiplied by 2) | 2.902 |
| Flap Servos | 24.77 | 0.13 (Multiplied by 2) | 3.220 |
| Elevator Servos | 52.39 | 0.13 (Multiplied by 2) | 6.811 |
| Rudder Servo | 50.88 | 0.065 | 3.307 |
| Deploy Mechanisms | 27.79 | 0.10 (Multiplied by 2) | 2.779 |
| Release Mechanism | 57.3 | 0.03 | 1.719 |
| Release Mechanism Servo | 51.82 | 0.028 | 1.451 |
| **Mission 1: Empty** | | | |
| Passengers | 14.46 | 6 | 86.76 |
| Baggage | 27.6 | 1.5 | 41.40 |
| **Mission 2: Passengers** | | | |
| Banner (Stowed/Deployed) | 26.74 / 120 | 0.6 | 16.04 / 72.0 |
| **Mission 3: Banner** | | | |
| **Calculated CG** | | | |
| **Mission** | **1** | **2** | **3 (Stowed/Deployed)** |
| CG from Reference Point (Inches) | **18.80** | **17.90** | **19.45 / 27.07** |

## 5.5 Flight Performance Parameters and Mission Performance

To obtain flight performance information, the data logs generated in several flights by the Spektrum IX12 transmitter and Castle Creations Phoenix Edge 100 ESC were analyzed. The results are summarized in the table below.

**Table 5.3 Performance Capabilities**

| Parameter | Mission 1: Empty | Mission 2: Passengers & Luggage | Mission 3: Banner |
|---|---|---|---|
| Weight (lbm) | 8 | 14 | 9 |
| W/S (lbm/ft^2) | 1.36 | 2.74 | 1.76 |
| V_min (ft/s) | 11.09 (7.6 MPH) | 22 (15 MPH) | 29.3 (20 MPH) |
| V_max (ft/s) | 134.79 (91.9 MPH) | 114.4 (78 MPH) | 66 (45 MPH) |
| Takeoff Distance (ft) | 12 | 20+ | 13 |
| Turn Radius (ft) | 9.045 | 10.3 | 20 |
| Rate of Turn (°/s) | 72 | 60 | 36 |
| 360° Turn Time (s) | 5 | 6 | 10 |
| Lap Time (s) | 26 | 26 | 45 |
| Max Current (amp) | 76.3 | 76.3 | 93.2 |
| Voltage Consumed (%) | 50 | 80 | 80 |
| Static Thrust (lbf) | 11.03 | 11.03 | 11.34 |
| Mission Score | 1.0 | 2.07 passengers/s | 200 ft*laps |

Dimensions shown: 58.08, 17.91, 26.00, 5.49, 10.00, 27.13, 59.74, 15.00, 9.50, 15.00, 5.49
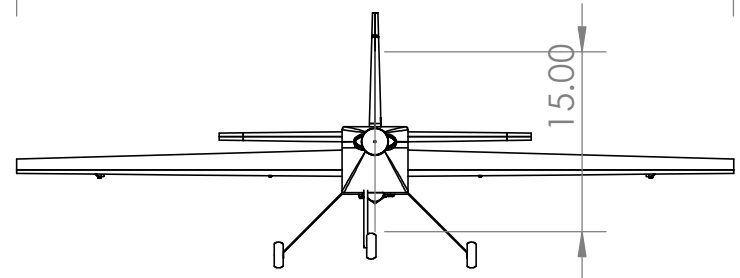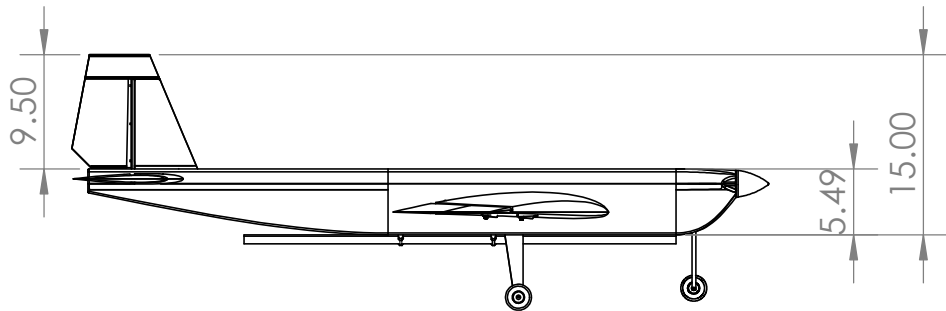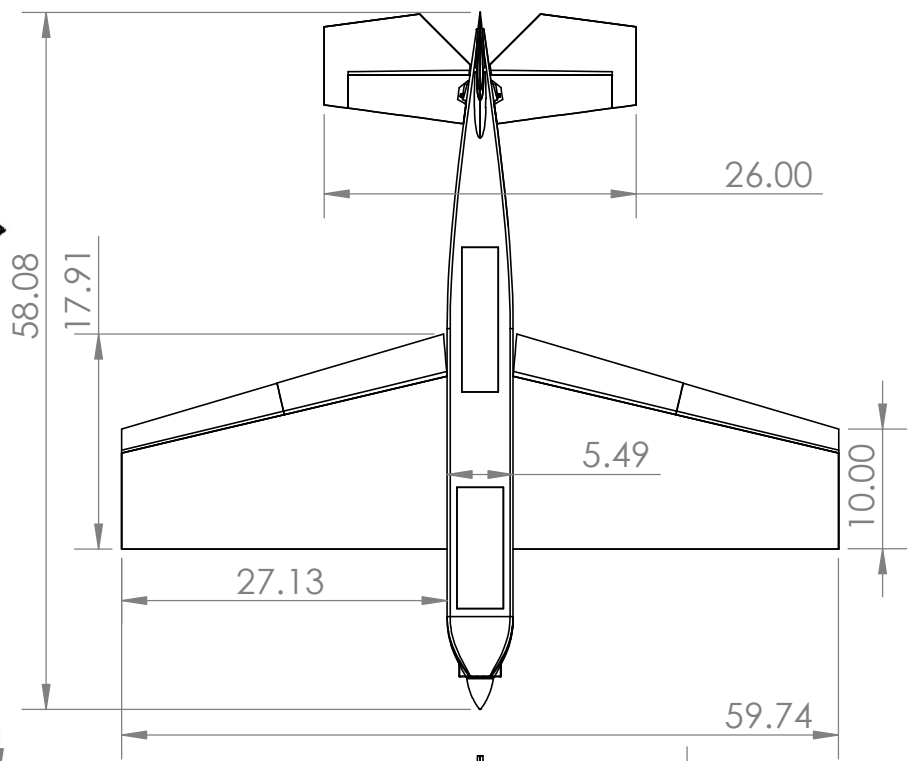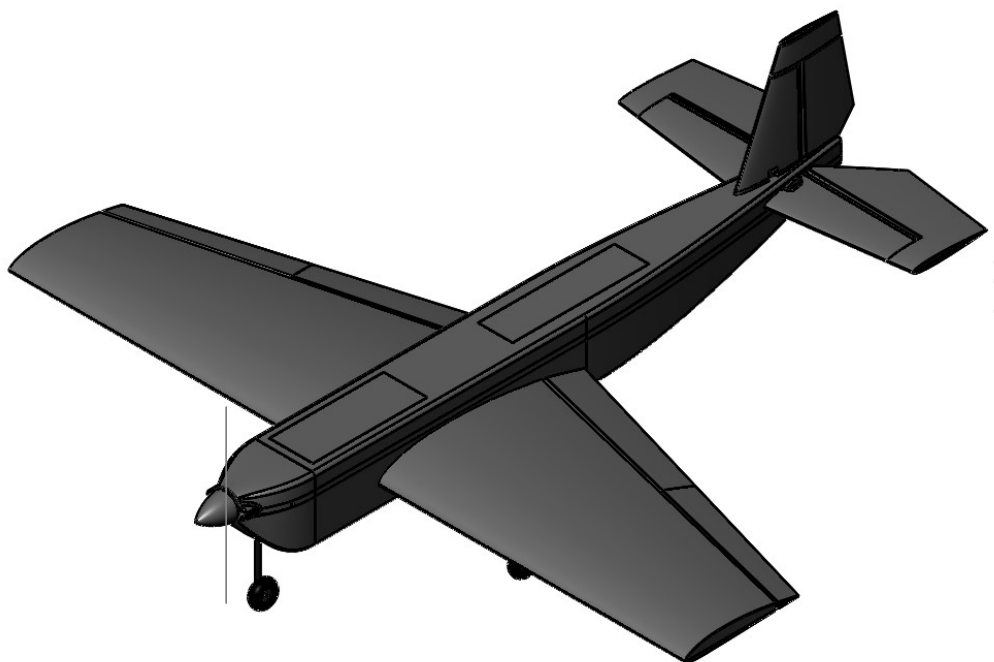
| TITLE: | | | |
|---|---|---|---|
| 3 View | | | |
| University of Nevada Las Vegas Bullitt Bill | | | |

| Drawn by: Sophia Leon | Size **B** | DWG NO. DBF_2020_UNLV_DRW_01 | Rev |
|---|---|---|---|
| | Scale 1:16 | | 1 of 5 |

| ITEM NO. | PART NUMBER | DESCRIPTION | QTY. |
|---|---|---|---|
| 1 | Fuselage | Carbon Fiber honeycomb | 1 |
| 2 | Motor | Scorpion sii 4035 450KB | 1 |
| 3 | Nose Cone | Carbon Fiber | 1 |
| 4 | Front Landing Gear | Carbon Fiber | 1 |
| 5 | Aft Landing Gear Strut | Carbon Fiber | 2 |
| 6 | Wheel | Lightweight Foam | 3 |
| 7 | Horizontal Stabilizer | Carbon Fiber | 1 |
| 8 | Left Wing | Carbon Fiber | 1 |
| 9 | Right Wing | Carbon Fiber | 1 |
| 10 | Vertical Stabilizer | Carbon Fiber | 1 |
| 11 | Firewall | Balsa Wood | 1 |
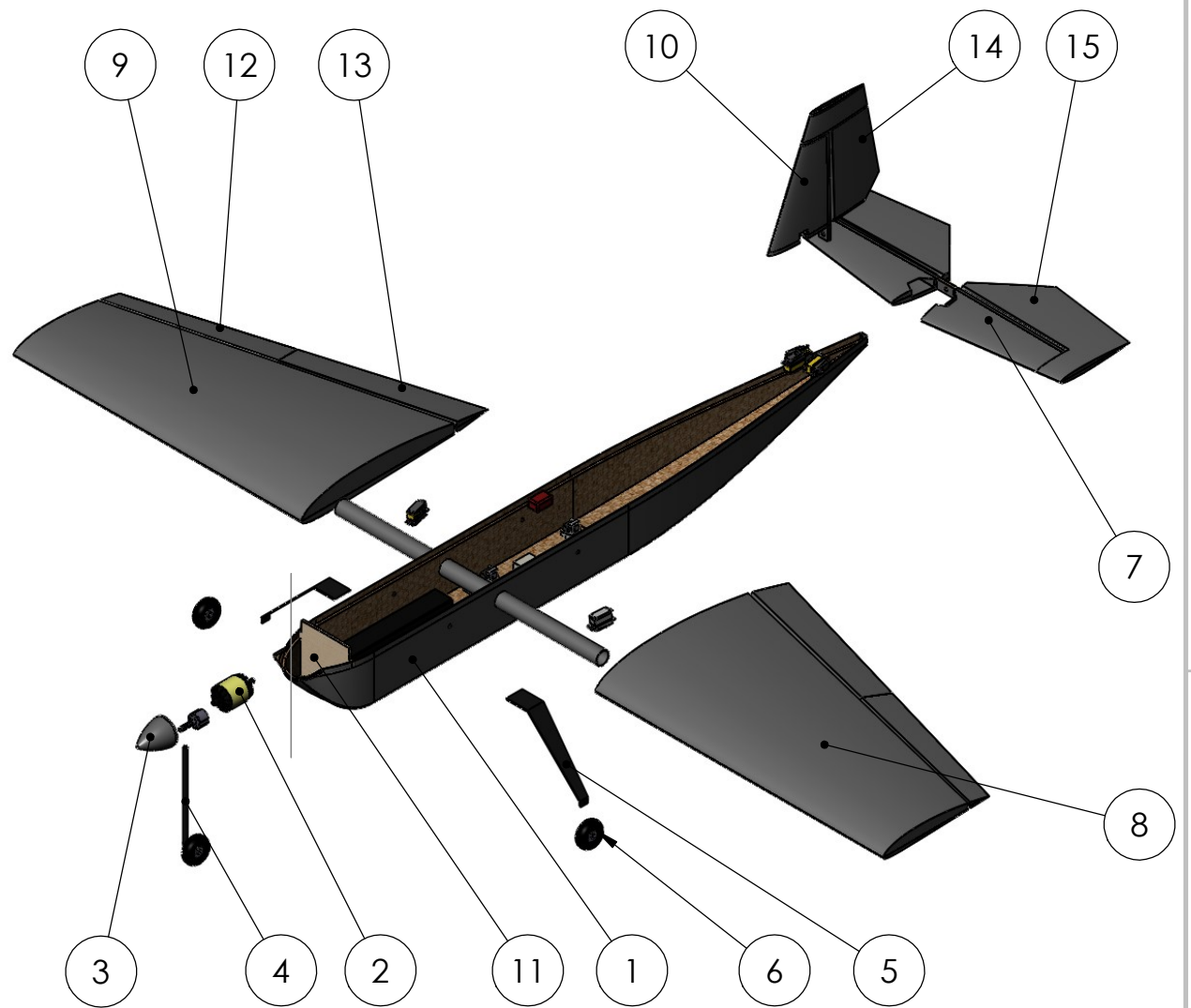
TITLE:
Structural Arrangement

University of Nevada Las Vegas
Bullitt Bill

Drawn by:
Sophia Leon

Size
B

DWG NO.
DBF_2020_UNLV_DRW_02

Rev

Scale 1:12

2 of 5

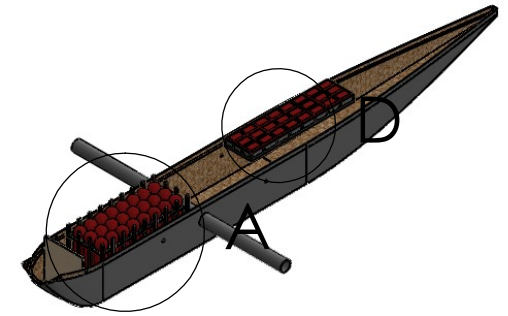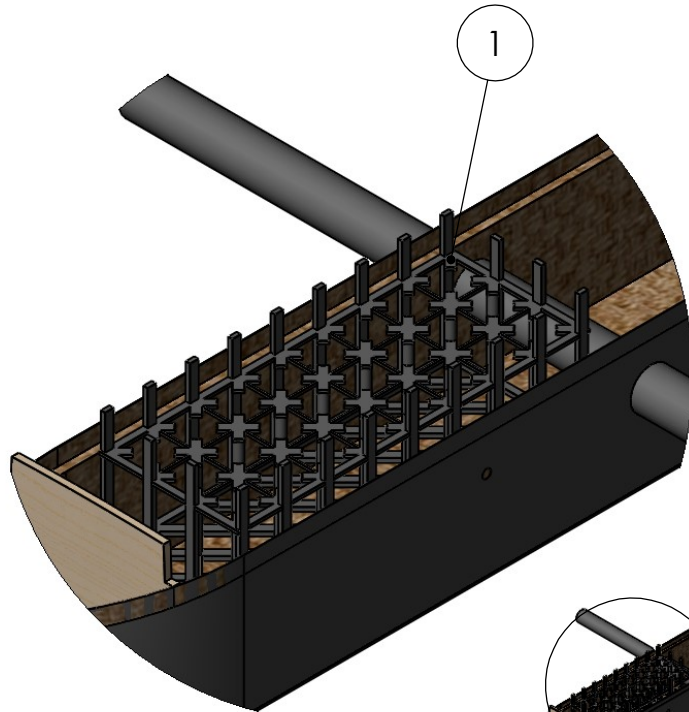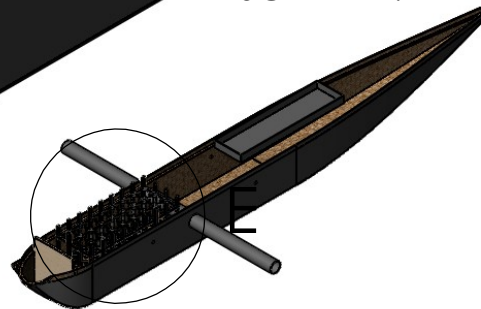| ITEM NO. | PART NUMBER | DESCRIPTION | QTY. |
|---|---|---|---|
| 1 | Passenger Restraint | TPU & 0.25 in plywood | 1 |
| 2 | Passenger | PLA & Lead Weight | 24 |
| 3 | Luggage | PLA & Lead Weight | 24 |

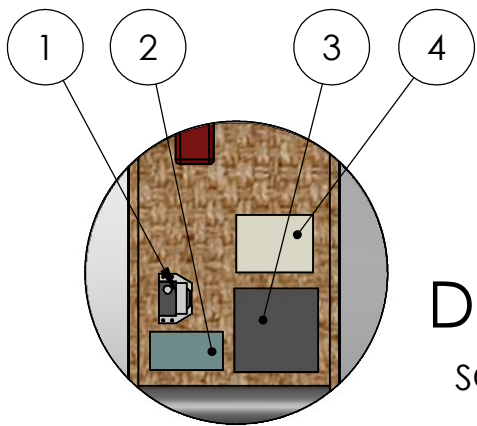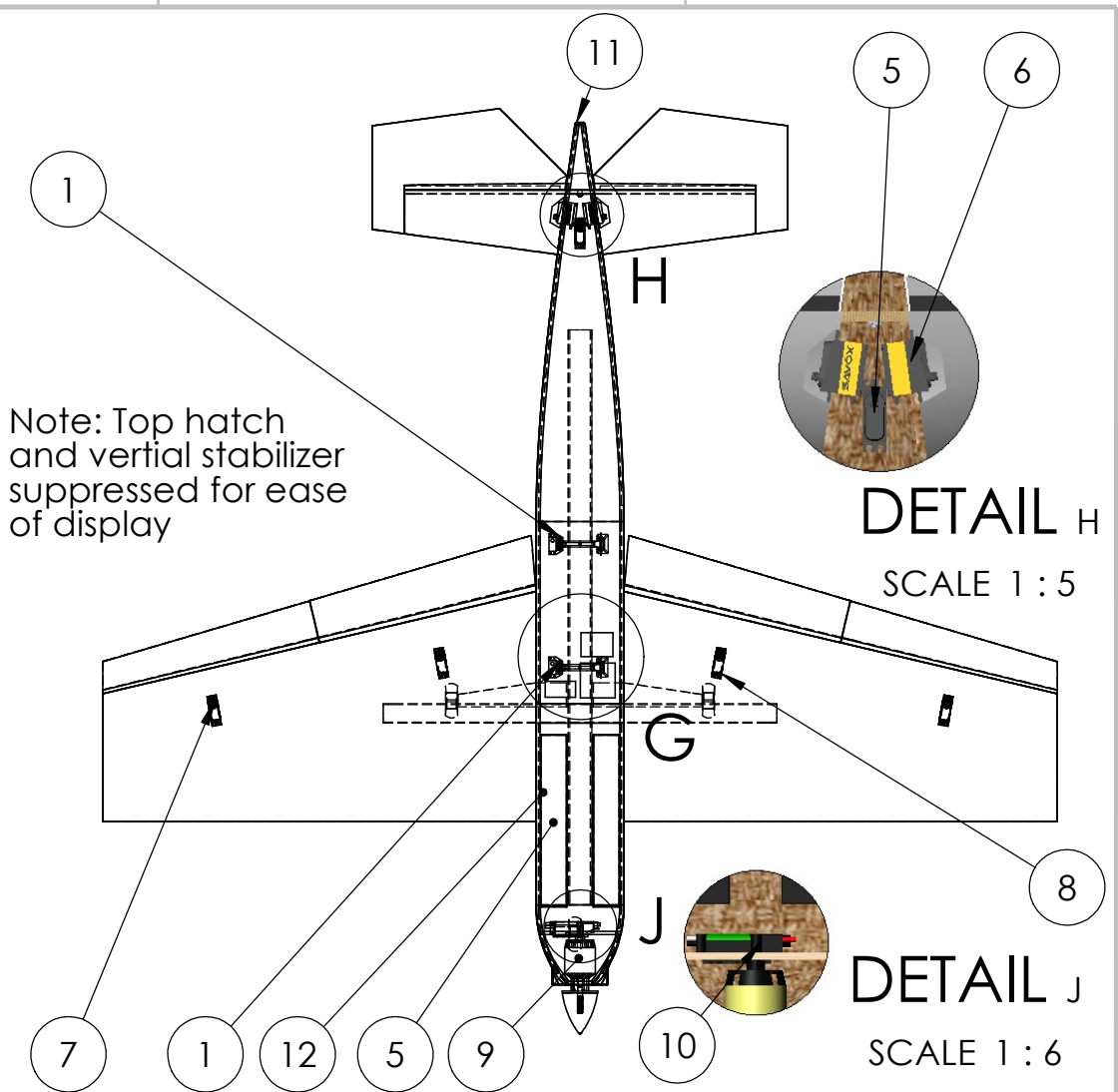DETAIL D
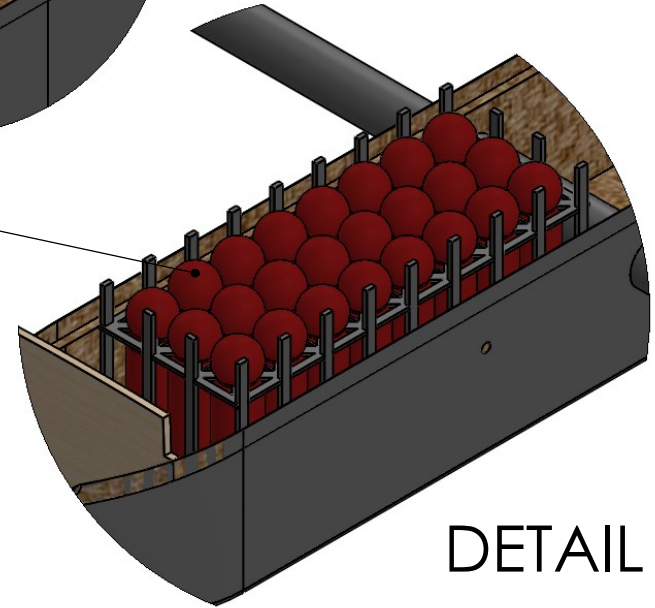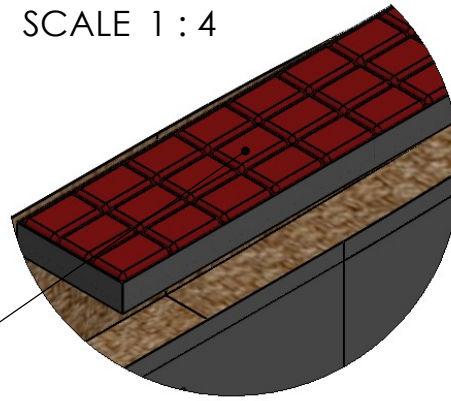
SCALE 1 : 4



DETAIL E

SCALE 1 : 4

DETAIL A

SCALE 1 : 4

TITLE:
Payload Arrangement

University of Nevada Las Vegas
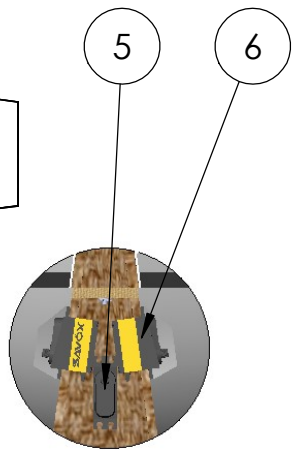Bullitt Bill

Drawn by:
Sophia Leon

Size
B

DWG NO.
DBF_2020_UNLV_DRW_03

Rev

3 of 5

| ITEM NO. | PART NUMBER | DESCRIPTION | QTY. |
|---|---|---|---|
| 1 | Banner Mechanism Servo | Hitech HS-5070 MH | 2 |
| 2 | BEC | regulates receiver voltage | 1 |
| 3 | Receiver | Spektrum AR 20310T | 1 |
| 4 | Receiver Battery | 3S 1300 mAh LiPo | 1 |
| 5 | Rudder Servo | Savox SV-1250MG | 1 |
| 6 | Elevator Servo | Savox SV-1250MG | 2 |
| 7 | Aileron Servo | Savox SV-1250MG | 2 |
| 8 | Flap Servo | Savox SV-1250MG | 2 |
| 9 | Motor | Scorpion SII 4035 450KV | 1 |
| 10 | ESC | Castle Phoenix Edge 100 | 1 |
| 11 | Banner Release Servo | Savox SV-1250MG | 5 |
| 12 | Aircraft Batteries | Thunder Power 8S 3300 mAh | 2 |

Note: Top hatch and vertial stabilizer suppressed for ease of display

DETAIL H
SCALE 1 : 5
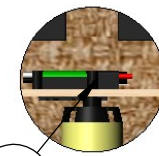
DETAIL J
SCALE 1 : 6

DETAIL G
SCALE 1 : 5

TITLE:
Systems Layout

University of Nevada Las Vegas Bullitt Bill

Drawn by:
Sophia Leon

Size: B

DWG NO. DBF_2020_UNLV_DRW_04

Rev

4 of 5

M

N
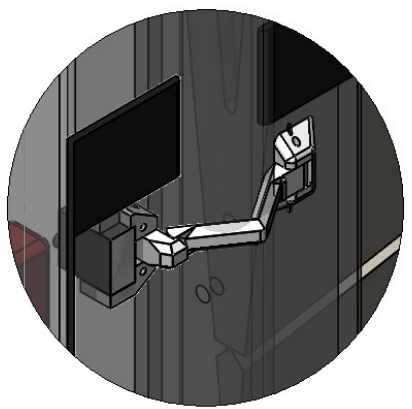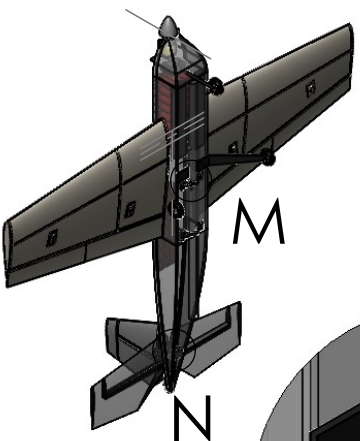
DETAIL M

SCALE 1 : 2.5

Release Pin

Release Sear

Actuation Bar
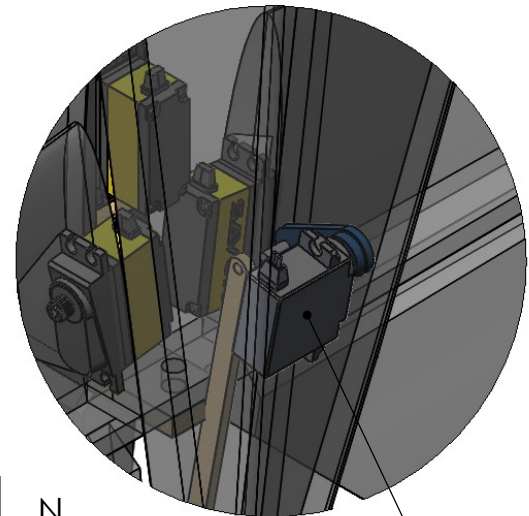
Release Hinge Body

DETAIL N

Banner Deploy Servo

Banner Release Servo

Release Latch

Latch Hinge Body

TITLE:
Banner Deploy & Release Mechanism

University of Nevada Las Vegas
Bullitt Bill

| Drawn by: | Size | DWG NO. | Rev |
|---|---|---|---|
| Sophia Leon | B | DBF_2020_UNLV_DRW_05 | |
| | | | 5 of 5 |

# 6.0 Manufacturing Plan

## 6.1 Selection of Manufacturing Process

The manufacturing processes investigated and the reasoning behind the ultimate selection are summarized below. The option that was chosen because the benefits outweighed the costs is highlighted in light red for each category.

**Table 6.1 Manufacturing Selection Process**

| | Option | Pros | Cons |
|---|---|---|---|
| **Types of Molds** | **Female** | ● Greater control over the appearance of the exterior surface<br>● When combined with vacuum-bagging, the dimensions of the final product better match the design | ● Because skirts are required for vacuum-bagging, this mold necessitates more material<br>● Creating the mold with the CNC machine is time-consuming |
| | **Male** | ● When laying up it is easier to control the external appearance because it is visible<br>● Uses less material | ● The part will grow during lamination so there is difficulty in controlling size |
| **Mold Material** | **MDF** | ● Affordable<br>● Readily available<br>● Easy to form to desired shape | ● Requires additional surface treatments such as sanding, priming, and painting to achieve a smooth impermeable surface |
| | **Foam** | ● Requires little to no surface treatment | ● Weak material leaves little room for error when it comes to testing<br>● May not be able to stand cure temperatures |
| | **Aluminum** | ● Best finish<br>● Robust, few replacements needed | ● Too expensive |
| **Surface Treatment** | **B-I-N Shellac Primer and Sealer** | ● Affordable<br>● Easy to use | ● Long dry time, this adds up especially because the MDF needs multiple coats |
| | **Krylon Epoxy Paint** | ● Readily available<br>● Affordable | ● This epoxy paint dries clumpy, rendering the surface on which it dries unusable (but there is a way to circumvent this with primer) |
| | **Duratec Surfacing Primer** | ● One member has experience with this primer and can attest to its good reviews | ● Expensive |
| **Mold Release** | **Paste Wax & PVA parting release** | ● Readily available | ● Because there are no other options to compare this parting release to the limitations of this parting release are not known |

## 6.2 Manufacturing Process

A manufacturing flow chart displaying a general overview of the process transitioning from designing to building the competition aircraft is shown in the figure below. Details specific to the final manufacturing process selected are provided in the following section.
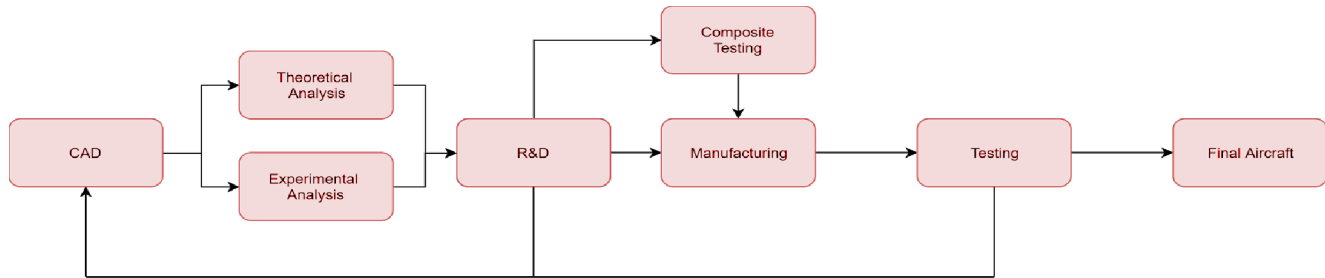


**Figure 6.1 Manufacturing Flow**

Parts production for the competition aircraft can be separated into two categories: the aircraft's skin and its support structures.

Pre-impregnated carbon fiber will function as the skin of the aircraft and it is cured into shape using female molds. Each part of the skin is done in halves to be able to epoxy the support structures in later. The molds for the skin will be composed of ¾" layers of MDF because the CNC mill has a maximum plunge depth of 2"; this constraint requires each layer of MDF to have keyed slots in order to be able to jigsaw the layers together to produce the final mold.

After assembling each of the MDF molds, the surfaces are primed with B-I-N Shellac. The primer fills the pores of the MDF mold and allows the Krylon Epoxy Paint to set on the surface evenly instead of swelling the wood. Between each coat of epoxy paint, wet sanding is performed on the mold to create a smooth, impermeable surface for the aircraft skin to be vacuum-bagged and cured on. Before vacuum-bagging, the now-prepped MDF mold is buffed with five coats of Partall Paste Wax and a coat of PVA release film to prevent the prepreg part from sticking to the mold. After undergoing all preparations the prepreg part is now ready to be heat-cured.

As for the support structures, these are to be constructed by sandwiching ¼" honeycomb in between plain weave carbon fiber. This composite support structure is manufactured by wet layup. Only one layer of carbon fiber is adhered to the honeycomb at a time. This method does increase layup time, but it allows for greater control over resin-content of the part by taking advantage of gravity and making sure no unnecessary extra resin cures inside of the honeycomb structure. Once the carbon fiber honeycomb sandwich cures it is then cut into structured ribbing with a water jet.

The final competition aircraft is then assembled by epoxying the honeycomb carbon fiber between the two halves of the pre-impregnated carbon fiber skin. After the support structure is in place the skin itself is sealed with epoxy as well.

The manufacturing milestones are listed in the chart below. The planned timeline for each milestone is indicated by a colored bar while the actual timeline is indicated by a black, dashed line.
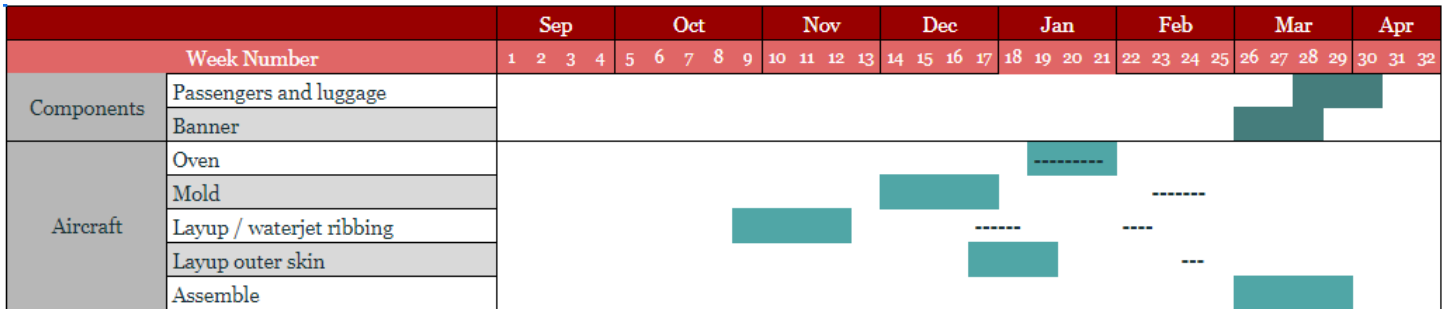
| Components | | Sep | | | | Oct | | | | | Nov | | | | Dec | | | | Jan | | | | Feb | | | | Mar | | | | Apr | | |
|---|---|---|---|---|---|---|---|---|---|---|---|---|---|---|---|---|---|---|---|---|---|---|---|---|---|---|---|---|---|---|---|---|---|
| **Week Number** | | 1 | 2 | 3 | 4 | 5 | 6 | 7 | 8 | 9 | 10 | 11 | 12 | 13 | 14 | 15 | 16 | 17 | 18 | 19 | 20 | 21 | 22 | 23 | 24 | 25 | 26 | 27 | 28 | 29 | 30 | 31 | 32 |

Figure 6.2 Manufacturing Gantt Chart

# 7.0 Testing Plan

## *7.1 Ground Tests*

The ground tests planned for this project include testing of the drag due to the banner, static thrust from different propellers, and testing of the banner deployment and release mechanism to ensure that it functions reliably at competition. The objectives and applications of each are summarized in the table below.

**Table 7.1 Ground Test Summary**

| Test | Objective | Data Collected | Application |
|---|---|---|---|
| **Banner Drag** | Characterize banner drag relative to airspeed and banner length | ● Drag<br>● Speed | Interpolate / extrapolate data to find drag at various speeds and banner sizes |
| **Static Thrust** | Measure thrust and amperage of propellers of various pitches and diameters | ● Thrust<br>● Amperage | Select propeller with ideal thrust for each mission |
| **Banner Deployment and Release** | Practice operation of banner deployment and release mechanisms | ● Observations<br>● Familiarity | Use consistency and repeatability of results to justify mechanism reliability |

### 7.1.1 Banner Drag Tests

Experimental data was found for the banner drag by mounting banners of varying sizes with a load cell on the roof of a car as shown below. The car was brought up to a steady speed and the speed was recorded. Meanwhile, data was gathered from the load cell every second. From this data, the average drag measured when the car was at a constant speed was obtained and plotted against its corresponding speed. From each data point, the coefficient of drag and a drag curve were determined.

**Figure 7.1 Experimental Banner Drag Test Rig**

### 7.1.2 Propulsion Tests

A motor mount was constructed using a low friction sliding rail to which the motor is securely attached. When the propeller is turned on by the radio controller, the component slides back and pushes against a single point load cell. An Arduino records the output voltage on the load cell, which is translated to motor thrust. Simultaneously, the Phoenix Edge ESC records the the amperage drawn by the motor while the tests on the mount are conducted. These two values, thrust and amperage draw, are then stored and analyzed for each propeller size tested. The results are shown in Table 4.4. These can be applied to select which combination of propeller and airspeed should be used for maximum efficiency and score during each mission.
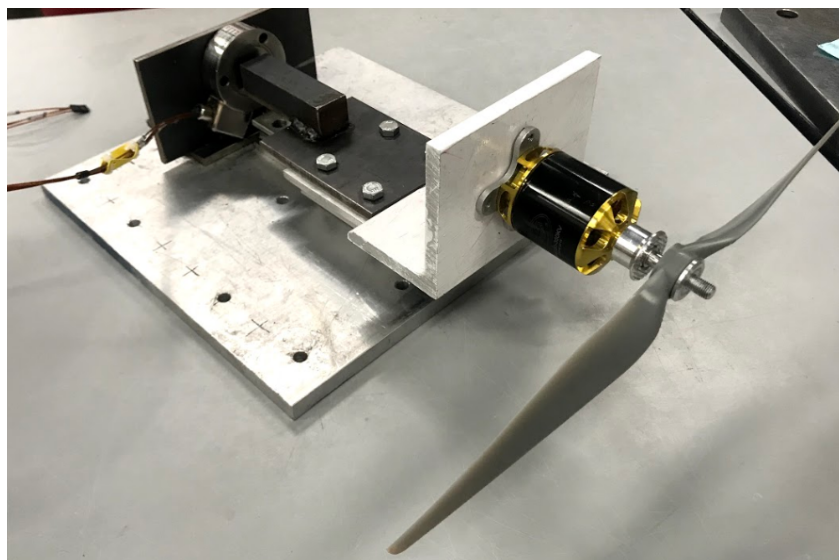


**Figure 7.2 Motor Mount for Static Thrust Tests**

## 7.2 Flight Tests

The flight tests are summarized in the table below. More flight tests are planned once the manufacturing phase of the aircraft is complete and the carbon fiber version of the aircraft can be tested.

**Table 7.2 Flight Test Summary**

| Test | Objective | Data Collected | Application |
|---|---|---|---|
| **Flight Demonstration** | Complete a successful maiden flight of plane | <ul><li>Visual feedback</li><li>Tactile feedback</li></ul> | Use observations from flight to modify aircraft control surface sizes, etc. based on pilot's previous knowledge |
| **In-Flight Data Collection** | Quantify flight performance capabilities and run through Missions | <ul><li>Speed</li><li>Takeoff distance</li><li>Turn radius</li></ul> | Compare predictions of mission and flight performance with real data |
| **Competition Aircraft** | Confirm that the final composite aircraft flies as predicted | <ul><li>Lap times</li><li>Mission scores</li></ul> | Predict performance at the competition for each mission and overall score |

The first flight test was a simple maiden flight of the aircraft without any passengers or the banner to make sure the aircraft is designed well enough to sustain stable and controlled flight. Flight characteristics like thrust and maneuverability were qualitatively assessed by the student pilots. The flight was recorded on video for visual analysis and observations.

The second flight test was designed to gather numerical data such as Mission scores, lap times, maximum speed, takeoff distance (Figure 7.4), stall speed, and more. This flight test also included the insertion of passengers and luggage and the attachment of a small banner. The aircraft used during flight tests was a foam board version of the competition aircraft. This aircraft used a 15" x 8" propeller and a PixHawk flight controller. The Pixhawk flight controller not only acts as a receiver, but it was also utilized to use hardware to log measurements such as airspeed, GPS location, etc. The ESC also provided current draw and battery life information. Finally, traditional means such as using a timer and measurement devices were used to measure 360° turn time, lap time, etc. Figure 7.3 shows lines marked on the ground 5 feet apart to approximate the takeoff distance of the aircraft. The total weight is similar to the weight of the competition plane to obtain applicable flight data. The test plane is shown below. It has the same dimensional parameters as the final aircraft though it is not made of composite materials.



**Figure 7.3 Takeoff Distance Measurements**

**Figure 7.4 Flight Test Aircraft**

<span style="color:red">7.2.1 Checklists</span>

The following checklists were used before flight testing and will be used during the competition to ensure safety procedures are followed when operating the aircraft to protect both the plane and the people operating the aircraft.

**Table 7.3 Pre-Flight Checklist**

| | Task |
|---|---|
| **Fuselage** | ❏ Charge all batteries<br>❏ Connect receiver to ESC and ESC to batteries<br>❏ Check location of CG<br>❏ Close all hatches |
| **Components** | ❏ Insert and secure passengers and luggage (Mission 2)<br>❏ Attach banner (Mission 3) |
| **Pilot Checklist** | ❏ Connect fuse and arm ESC<br>❏ Check control surfaces<br>❏ Run-up motor<br>❏ Go-No-Go decision |

**Table 7.4 Aircraft Inspection Checklist**

| | Task |
|---|---|
| **Motor** | ❏ Motor mount is securely fastened and there is no obvious damage to the mount or surrounding fuselage<br>❏ Propeller is securely fastened<br>❏ Propeller is balanced<br>❏ Propeller and shaft are free of obvious damage |
| **Fuselage** | ❏ Receiver is secured to the fuselage and connected<br>❏ Servo wires are secured to the fuselage and connected<br>❏ ESC is secured to the fuselage and connected<br>❏ Batteries are secured to the fuselage and connected<br>❏ There are no visible cracks<br>❏ Components are secured and connected (if applicable) |
| **Wing And Tail** | ❏ There is no visible damage<br>❏ Servo arms are secure<br>❏ Control surfaces move freely<br>❏ Wing is secured to fuselage and free to rotate |
| **Landing Gear** | ❏ Landing gear is secured<br>❏ There is no damage to landing gear and surrounding fuselage<br>❏ Wheels spin freely |

### 7.3 Testing Schedule

A Gantt Chart demonstrating the predicted and actual test schedules are shown below. All tests have been completed at the time of this report submission besides the testing of the banner release mechanism and testing of the final competition aircraft which is scheduled for the month of March.
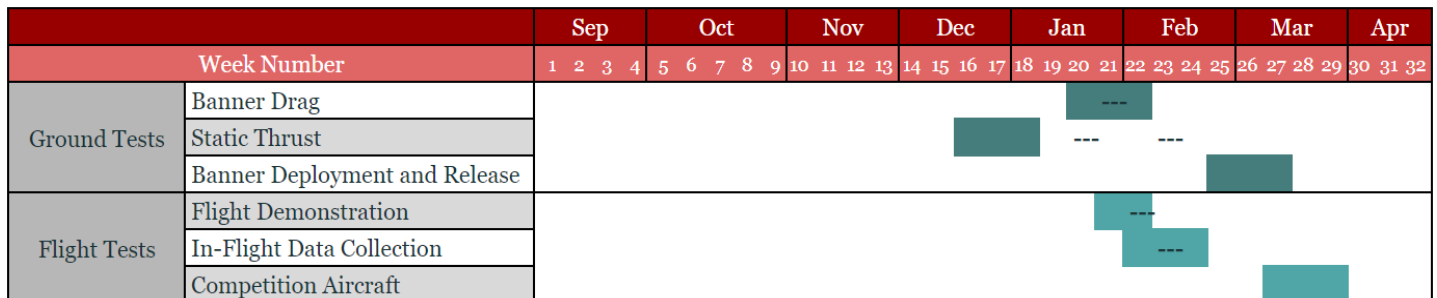


**Figure 7.5 Testing Gantt Chart**

## 8.0 Performance Results

### 8.1 Subsystem Performance

Servos and the avionics suite in the aircraft were tested by simply connecting the receiver and motor to the battery and using the remote to check the proper movement of the control surfaces and propeller behavior. For the selected propellers

used for the competition, their static thrust and corresponding amperage were measured using the motor mount and recorded below.

**Table 8.1 Propulsion Performance Results**

| Mission | Propeller | Pitch (in) | Diameter (in) | Static Testing | | Flight Testing |
| --- | --- | --- | --- | --- | --- | --- |
| | | | | Max Thrust (lb) | Max Current (amp) | Max Current (amp) |
| 1 | 15 x 8 | 8 | 15 | 11.03 | 76.3 | 90.0 |
| 2 | 15 x 8 | 8 | 15 | 11.03 | 76.3 | 91.6 |
| 3 | 15 x 10 | 10 | 16 | 11.34 | 93.2 | - |

To test the components required by the competition, the Ground Mission was simulated to practice loading and unloading both the passengers/luggage and the banner. The resulting times required are summarized in the table below. An approximate Ground Mission time can be approximated as 90 seconds with the largest banner. Note that the banner release time was measured under the effects of gravity and by suspending the banner from a handheld position several feet above the ground. The banner load and release times are given in seconds per foot as the time will increase depending on which banner is used during the Ground Mission.

**Table 8.2 Components Ground Performance Results**

| Mission Parameter | Predicted Time | Average Time |
| --- | --- | --- |
| Passenger Load Time (s) | 7.5 | 90 |
| Banner Release Time (s/ft) | 0.6 | 0.463 |
| Banner Load Time (s/ft) | 7 | 6.5 |

The initial passenger load time was initially predicted to be much lower, assuming the use of a tool was designed to very quickly load and unload the passengers. Unfortunately, after rule clarifications, the tool was determined illegal and the time to load the passengers was increased sixfold. On the other hand, the banner release time was significantly faster than our predictions.

## *8.2 Aircraft Performance*

Estimates for aircraft's flight performance during the competition were obtained during flight testing with the foamboard test plane. Table 8.3 summarizes the differences found between Mission 1 and the payload missions, Mission 2 with the passengers and luggage and Mission 3 with the banner.

**Table 8.3 Components Flight Performance Results**

| Component | | Speed Reduction (MPH) | Added Weight (lb) | Added Drag (lb) |
| --- | --- | --- | --- | --- |
| Passengers and Luggage | | 2 | 6 | 0 |
| Banner | 25'x5' | 35 | 0.6 | 23 |
| | 15'x3' | 18 | 0.5 | 13 |
| | 5'x1' | 6 | 0.4 | 5 |

Other parameters such as gross weight of the aircraft and its components, the wing loading on the aircraft during cruise, the average lap time, maximum flight speed, and number of laps completed in the allotted time frame were measured during flight tests and are recorded below alongside their predicted value.

**Table 8.4 Flight Test Results**

| Mission Parameter | Mission 1 | | Mission 2 | | Mission 3 | |
|---|---|---|---|---|---|---|
| | Predicted | Measured | Predicted | Measured | Predicted | Measured |
| **Weight (lb)** | 8 | 7.83 | 14 | 13.83 | 9 | 8.26 |
| **W/S (lb/in$^2$)*10$^{-3}$** | 10.87 | 10.6 | 19.03 | 18.79 | 12.23 | 16.6 |
| **Average Lap Time (s)** | 30 | 26 | 30 | 27 | 30 | 45 |
| **Flight Speed (ft/s)** | 117.3 (80 MPH) | 116.96 (79.7 MPH) | 117.3 (80 MPH) | 114.4 (78 MPH) | 66 (45 MPH) | 55.5 (37.9 MPH) |
| **Number of Laps** | 3 | 3 | 3 | 3 | 20 | 13 |

The results obtained during flight testing agree with the predictions from the design process. *Bullit* is expected to perform well at the AIAA DBF 2020 competition based on the performance of the aircraft and its components during flight testing. Because the performance of the other teams' airplanes is unpredictable, an estimate for the total score at the competition cannot be obtained at this time.

## Bibliography

[1] Motor Thrust Chart, Scorpion System, https://www.scorpionsystem.com/files/i3,100_data_chart.pdf

[2] Aeroconcept, (n.d.). Retrieved February 12, 2020, from http://www.aero-concept.com/fiches/54.html

[3] Raymer, D., "Aircraft Design: A Conceptual Approach," Second edition, Education Series, AIAA, Washington, DC, 1992.

[4] "Basic Aircraft Design Rules," *MIT Opencourseware* [online], ocw.mit.edu/courses/aeronautics-and-astronautics.

[5] "Airfoil database", Airfoil tools [online database], http://airfoiltools.com/ [retrieved 15 October 2019].

[6] Drela, M., and Youngren, H., "XFOIL", Massachusetts Institute of Technology [online], 2013, https://web.mit.edu/drela/Public/web/xfoil/ [retrieved 11 September 2019]

[7] Deperrois, A., "XFLR5," Website, [online], Available at: https://xflr5.com/xflr5.htm [Accessed November 2019]

[8] Menter, F. R. "Two-equation eddy-viscosity turbulence models for engineering applications," *AIAA Journal,* Vol.32, No.8, 1994, pp. 1598-1605.
https://doi.org/10.2514/3.12149

[9] Drela, M., and Youngren, H., "AVL Overview", Massachusetts Institute of Technology [online], 2008, http://web.mit.edu/drela/Public/web/avl/. [retrieved 5 January 2020],

[10] "NACA 2412 Airfoil." *Airfoil Tools* [online], airfoiltools.com/airfoil/details?airfoil=naca2412-il [accessed November 2018].

[11] "Solutions for Students," *Solidworks* [online], solidworks.com. [accessed September 2018].

[12] Baker, A., "Composite Materials for Aircraft Structures," Second edition, Education Series, AIAA, Virginia, 2004.

[13]Mallick, P.K., "Fiber-Reinforced Composites," Materials, Manufacturing, and Design, 3rd ed., Taylor & Francis Group, Florida, 2008,.

[14] Nomex Honeycomb Material Properties, Core Composites, https://www.corecomposites.com/products/honeycomb/nomex-honeycomb.html

[15] Carruthers, A.C., Filipone, A., "Aerodynamic Drag of Streamers and Flags," Journal of Aircraft, Vol.42, No. 4, 2005, pp. 976-982.

[16] Anderson, John. "Fundamentals of Aerodynamics," 6th ed., McGraw-Hill Education, New York, 2017.